Offshore wind power plants with VSC-HVDC transmission

Grid code compliance optimization and the effect on high voltage ac transmission system

Ndreko, Mario

DOI
10.4233/uuid:2d2cbe51-12fc-4162-aaf2-044c6bc5e15b

Publication date
2017

Document Version
Final published version

Citation (APA)
Ndreko, M. (2017). *Offshore wind power plants with VSC-HVDC transmission: Grid code compliance optimization and the effect on high voltage ac transmission system*. [Dissertation (TU Delft), Delft University of Technology]. https://doi.org/10.4233/uuid:2d2cbe51-12fc-4162-aaf2-044c6bc5e15b

OFFSHORE WIND POWER PLANTS WITH VSC-HVDC TRANSMISSION

GRID CODE COMPLIANCE OPTIMIZATION AND THE EFFECT ON HIGH VOLTAGE AC TRANSMISSION SYSTEM

OFFSHORE WIND POWER PLANTS WITH VSC-HVDC TRANSMISSION

GRID CODE COMPLIANCE OPTIMIZATION AND THE EFFECT ON HIGH VOLTAGE AC TRANSMISSION SYSTEM

Proefschrift

ter verkrijging van de graad van doctor
aan de Technische Universiteit Delft,
op gezag van de Rector Magnificus prof.ir. K. C. A. M. Luyben,
voorzitter van het College voor Promoties,
in het openbaar te verdedigen op dinsdag 19 december 2017 om 10:00 uur

door

Mario Ndreko

Diploma in Electrical and Computer Engineering,
The National Technical University of Athens, Griekenland,
Master of Science in Sustainable Energy Technology,
Technische Universiteit Delft,
geboren te Albania

Dit proefschrift is goedgekeurd door de

promotor: prof. ir. Mart A.M.M van der Meijden
copromotor: dr.Dip.Ing Marjan Popov

Samenstelling promotiecommissie:

Rector Magnificus,	voorzitter
Prof. ir. M. A. M. M van der Meijden	Technische Universiteit Delft
Dr. Dip.Ing M. Popov	Technische Universiteit Delft
Onafhankelijke leden:	
Prof. dr. D. Jovcic	University of Aberdeen
Prof.dr. L. Söder	KTH Royal Institute of Technology
Prof. dr. ir. J. A Ferreira	Technische Universiteit Delft
Prof. dr. P. Palensky	Technische Universiteit Delft
ir. J. Bos,	TenneT TSO B.V.

This research is financially supported by the Far and Large Offshore Wind (FLOW) project in the Netherlands.

ISBN 978-94-6299-804-9

An electronic version of this dissertation is available at
http://repository.tudelft.nl/.

to Violeta and Viron

SUMMARY

Wind Power is an important enabler of future sustainable energy development. Besides onshore wind power, offshore wind power has huge potential to be an abundant resource for Europe. The development of large offshore wind power generation in the North Sea has been significantly accelerated in the last years. The large distance from shore in combination with the need for large transmission capacity has raised the interest for the voltage source converter high voltage direct current technology (VSC-HVDC). In that direction, proposals have been recently made for the construction of an offshore multi-terminal HVDC grid in the North Sea which could facilitate the grid integration of bulk offshore wind power.

Transmission system operators in order to ensure high degree of the power system security of supply, impose strict grid connection requirements to offshore wind power plants and their HVDC transmission. These set of grid connection rules include technical specifications for the normal operation as well as for grid fault conditions. Grid code compliance technical solutions should consider the complementary view point of all players: turbine manufacturers, offshore project developers, transmission technology suppliers and system operators. Based on these boundary conditions, the overall research objectives that have been assessed in the context of this thesis include the following points:

- Assessment of the state of the art coordinated fault-ride through strategies for offshore wind power plants with VSC-HVDC transmission.
- Analysis of unbalanced grid faults for wind power plants with VSC-HVDC transmission.
- Investigation of the effect of negative sequence current control for onshore and offshore AC faults.
- Analysis of the effect of typical grid codes on the power system voltage and rotor angle stability.

Based on these boundary conditions, the main achievements of this thesis are summarized as follows:

- Modeling and analysis of negative sequence current control schemes for offshore wind power plants with VSC-HVDC connection. Assessment of the effect of different negative sequence current control options on the unbalanced fault response of the onshore transmission grid as well as the offshore collector system. Cases between negative sequence current suppression and negative sequence current injection are investigated thoroughly. In addition, new control schemes are proposed which enhance the unbalanced fault response while at the same time respecting the physical limits of the converter station.

- Formulation of an iterative procedure which utilizes heuristic optimization algorithms for achieving the optimal tuning of fault-ride through compliance strategies for offshore wind power plant with VSC-HVDC transmission. The methodology addresses the state of the art coordinated fault ride through strategies which eliminate the use of DC-chopper. The optimal tuning is achieved using a sequence of electromagnetic transient (EMT) type simulation runs of the plant driven by meta-heuristic optimization algorithms. The method has been tested for the point-to-point and the multi-terminal HVDC connection case of the offshore wind power plants.

- Proposal of an enhanced grid forming control scheme for the offshore VSC-HVDC station which enables robust fault ride though compliance and injection of reactive current for a three phase to ground faults at the terminals of the offshore VSC-HVDC station.

From the analysis presented within the context of this thesis, the most striking conclusions which could be drawn are summarized as follows:

The injection of negative sequence current from the VSC-HVDC station proportionally to the negative sequence voltage amplitude during unbalanced AC grid faults has a two-fold benefit. First, it increases in amplitude the negative sequence fault current component at the connection point during line-to-line faults. Second, it increases in amplitude the zero sequence current component during single-line to ground faults. Moreover, the reduction of the positive sequence active current component and the injection of only negative sequence reactive current during AC grid unbalanced faults is considered to be the best approach for implementation in future grid codes for VSC-HVDC systems.

With the enhanced grid forming control scheme for the offshore VSC-HVDC station, it is possible both for the wind plants and the HVDC station to provide positive sequence reactive fault current injection during offshore AC grid faults. This would sustain the voltage at the offshore island grid (during offshore grid faults) and ensure adequate fault current levels for the protection schemes to detect and isolate permanent faults.

In the case of three phase onshore faults, the increased AC fault current capacity of the onshore VSC-HVDC station (above the 1.1p.u) followed by increased positive sequence reactive current boosting gain (k) and reactive current limiting priority, would improve the rotor angle and short term voltage stability in the transmission system. The later is more visible for grid connection points with relevantly low short circuit ratio (below 10). In additional, during severe AC voltage drops, the combined active and reactive current injection by VSC-HVDC stations could lead to voltage angle instability.

Finally, the developed methodologies, models and control schemes proposed within the context of this thesis could facilitate the analysis of transmission systems with HVDC connected offshore wind power plants. Moreover, it provides insights on the application and the effect on typical grid codes requirements.

SAMENVATTING

Windenergie is een belangrijke drijfveer voor toekomstige ontwikkeling van duurzame energie. Behalve wind op land heeft ook wind op zee een enorm potentieel als overvloedige hulpbron voor Europa, die bovendien in overvloed aanwezig is. De ontwikkeling van grootschalige opwekking van wind op zee is de laatste jaren in een stroomversnelling terecht gekomen. De grote afstand van de kustlijn in combinatie met de noodzaak tot schaalverschroting voedde de belangstelling voor voltage sourced converter hogegelijkspanning (VSC-HVDC) als transmissietechnologie. Om de netintegratie van grootschalige wind op zee te bevorderen is er in die richting recentelijk een aantal plannen beraamd voor de installatie van een multi-terminal net op zee gebaseerd op HVDC.

Om de hoge betrouwbaarheid van het elektriciteitsvoorzieningssysteem te waarborgen stellen netbeheerders eisen aan de netverbinding van offshore windparken en hun HVDC-steekverbindingen. Deze verzameling regels omhelst de technische specificaties voor zowel normaalbedrijf als tijdens verstoringen. Technische oplossingen om aan netcodes te voldoen moeten rekening houden met de aanvullende standpunten van alle partijen zoals turbinefabrikanten, offshore projectontwikkelaars, technische leveranciers en netbeheerders. Op basis van deze randvoorwaarden omvatten de overkoepelende onderzoeksvragen die worden beschouwd in dit proefschrift de volgende punten:

- De Bepaling van de huidige stand van zaken omtrent zgn. fault-ride through (FRT)-strategieën van offshore windparken verbonden door middel van VSC-HVDC
- De Analyse van asymmetrische kortsluitingen en de ontwikkeling van nieuwe regeltechnische concepten voor VSC-HVDC-verbonden windparken.
- Het onderzoeken van het effect van het regelen van de inverse stroomcomponent voor on- en offshore netverstoringen.
- Analyse van het effect van gangbare netcodes en hun invloed op de spannings- en rotorhoekstabiliteit.

Op basis van bovengenoemde randvoorwaarden zijn de hoofdresultaten van dit proefschrift als volgt samen te vatten:

- De modellering en analyse van regeltechnische concepten voor inverse stroomcomponenten van VSC-HVDC-verbonden offshore windparken. Het bestuderen van het effect van verschillende regelopties op de foutrespons van het zowel het onshore transmissiesysteem als het collectienetwerk van het windpark zelf. De onderdrukking alsook de injectie van een inverse stroomcomponent zijn hierbij uitvoerig onderzocht. Aanvullend worden er nieuwe regeltechnische schema's voorgesteld die enerzijds de foutrespons tijdens asymmetrische fouten verbetert en anderzijds de fysische (technische) grenzen van het converterstation respecteert.

- De bepaling van een nieuwe iteratieve procedure die gebruikt maakt van heuristische optimalisatiealgoritmes om een optimale afstelling van FRT-strategieën voor VSC-HVDC-verbonden windparken te bewerkstelligen. Deze methode behandelt gecoördineerde FRT-strategieën, wat de inpassing van een DC-chopper overbodig maakt. De optimale afstelling wordt gerealiseerd door het uitvoeren van een serie elektromagnetische-transientensimulaties van het offshore windpark, waarvan de variaties bepaald worden door de metaheuristische optimalisatiealgoritmes. De methode is getest voor zowel enkelvoudige (punt-punt) als voor multi-terminal-HVDC verbindingen .

- Het voorstel van een verbeterd netvormend regeltechnisch concept voor het offshore converterstation. Dit stelt ons in staat een robuuste naleving van de vereisten voor FRT en blindstroominjectie voor een driefasen kortsluitingen aan de klemmen van het offshore VSC-HVDC-station te realiseren.

Vanuit de analyse die is voorgedragen in de context van dit proefschrift kunnen de meest in het oog springende conclusies als volgt worden samengevat: De effectieve afstemming van gecoördineerde FRT-strategieën kunnen de elektrische stress op de HVDC-verbinding en de offshore windparken die plaatsvindt gedurende onshore verstoringen verlagen.

De injectie van een inverse stroomcomponent door het VSC-HVDC-station evenredig aan de inverse spanningscomponent heeft twee voordelen. Ten eerste garandeert het voldoende foutstroom op het verbindingspunt gedurende fase-fasefouten. Ten tweede veroorzaakt het een verhoogde homopolaire stroom gedurende enkelfase aardfouten. Voor toekomstige netcode-vereisten met betrekking tot asymmetrische fouten in het AC net blijkt het bovendien de beste optie om de normale, actieve stroomcomponent te reduceren terwijl de inverse, reactieve stroomcomponent ondersteund wordt.

Met de juiste, verbeterde netvormende regelstrategie voor het offshore VSC-station is het voor zowel het windpark als het HVDC-station mogelijk reactieve stroom te leveren gedurende netverstoringen in het kabelnetwerk van het offshore windpark. Dit ondersteunt de spanning in het eilandsysteem van het offshore windpark (gedurende verstoringen aldaar), de gerelateerde stabiliteit en verzekert voldoende foutstroom voor de geassocieerde netbeveiligingssystemen om kortsluitingen te detecteren en af te schakelen.

In het geval van onshore driefasensluitingen zorgt een verhoogde doorlaatstroom van de onshore VSC (hoger dan 1.1 pu) samen met een verhoogde proportionele versterkingsfactor voor de blindvermogensregeling (k) en de gerelateerde stroombegrenzingsmethode voor een verbetering van de rotorhoek- en spanningsstabiliteit in het transmissiesysteem. De verbetering in spanningsstabiliteit is het beste waarneembaar bij aansluitpunten met een lage kortsluitvastheid (factor lager dan 10). Daarnaast kan gedurende diepe spanningsdips een gecombineerde actieve en reactieve stroomondersteuning door VSC-stations leiden tot spanningshoekinstabiliteit en het verlies van hun synchronisatiekoppeling. In dit geval wordt de begrenzing van actieve stroom aanbevolen ten behoeve van de reactieve stroom.

Tenslotte kunnen de voorgestelde methodes, modellen en regelstrategieën die zijn aangedragen in dit proefschrift de analyse van transmissiesystemen met wind op zee

verbonden door HVDC faciliteren. Dit proefschrift biedt waardevolle inzichten in de toepassing en het effect van typische eisen die gesteld worden in netcodes, zowel offshore (windparken) als onshore (transmissiesysteem)

CONTENTS

1

INTRODUCTION

1.1. BACKGROUND

Modern societies require abundant energy resources to meet social and economic development [1–4]. Electricity, gas, coal and oil belong to the class of energy commodities [5]. Electricity has the unique characteristic that it is uneconomical to be stored, hence it must be consumed as soon as it is generated. The generation of electricity for the past century has been based on fossil fuel oriented technology. Greenhouse gas emission from power generation processes has contributed significantly to the global warming [6]. Environmental concerns related to climate change and the binding targets prescribed in international protocols [7, 8] have transformed the global energy landscape demanding for the utilization of renewable energy technologies in the electricity generation. The use of renewable energy resources will change not only the way that electricity is generated but also transmitted and distributed [9, 10].

The grid integration of large scale wind and solar power has already started in many European countries [10, 11]. Wind power is supposed to boast the edge, as it is technologically mature and it can be deployed on a massive scale [12]. Next to onshore wind, offshore wind power has a very dynamic potential for the North Sea countries [13, 14]. Specifically Europe is the pioneer of offshore wind technology development with Denmark, Germany and the UK leading the path. As a matter of fact, the installed offshore wind power capacity in Europe has increased from 50MW in 2000 to about 11GW by the end of 2016 (Wind Europe, 2016).

The associated high cost of offshore wind power has been a major barrier towards its large scale deployment [15, 16]. Major cost contributors are the wind turbine technology (blades, nacelle and generator), the foundation structures and the grid connection infrastucture [17, 18]. Significant cost reduction has been recently achieved compared to the previous years due to the advances of the wind turbines design and the standardization of the grid connection equipment. Furthermore, synergies with other marine industries such as oil and gas could contribute additionally to a further cost reduction in the following years [19].

Offshore wind power plants located close to shore usually utilize high voltage alternative current (AC) grid connection cable technology. High voltage direct current (HVDC) cable technology is justified from cost perspective in far from shore and large in size offshore wind power plants [20], [21]. The voltage source converter HVDC technology (VSC-HVDC) is nowadays the state of the art for the grid connection of remote offshore wind power plants. There are well proved advantages that a VSC-HVDC system preserves. Namely, the capability to energize and supply passive networks with controlled voltage and frequency. The inherent advantage to operate in weak power systems (with very low short circuit power levels and even zero power system total inertia). The capability to damp resonances and of course the independent control of the active and reactive power exchange with the grid are only a few to mention.

Moreover, offshore VSC-HVDC links, primarily installed for the grid connection of offshore wind power plants, can be expanded to multi-terminal HVDC connections between countries. In that direction, recent proposals have been made for the construction of an over-lay HVDC grid. The latter would boost the interconnection capacity between European countries [22], while at the same time it would facilitate the large scale integration of offshore wind power and other renewable energy technologies (i.e hydro and PV) [10].

In addition, the inherent controlability of VSC-HVDC systems could enhance the voltage and frequency stability (short and long term). Frequency stability challenges caused by the massive grid connection of power electronic interfaced renewable generation units have been already observed in the Irish transmission system [23] as well as in the United States [24]. Provision of ancillary services such as the fast active power control (commonly referred in literature as synthetic inertia response), primary frequency control and damping of power system electromechancial oscillations can be facilitated by VSC-HVDC systems [25].

1.2. PROBLEM DEFINITION

Transmission system operators (TSOs) with the goal to ensure a certain level of the power system security of supply impose grid connection requirements to offshore wind power plants and their HVDC transmission system [26]. Current grid connection codes for offshore wind power plants are written based on the relevant power systems needs and system operators experience. In some cases the connection codes are adopted from other jurisdictions without an analysis of their effect on the power system security. Different connection codes impose different compliance costs as no standard technical compliance solutions prevail. Harmonized grid codes, would reduce the grid connection cost as standard compliance solutions might prevail.

The European Network of Transmission system Operators for Electricity(ENTSO-E) has contributed significantly in the recent years to the development of European grid connection requirements. Initially, grid code requirements for generation units (known as RfG) have been published. Lately, new network code requirements for high voltage direct current (HVDC) transmission systems and HVDC connected offshore wind power plants are released. While the approach of national driven grid code development is simpler, it might lead to non-optimal compliance. Grid code compliance technical solutions should consider the complementary viewpoints of all players: turbine manufacturers,

offshore project developers, transmission technology suppliers, and transmission system operators. These challenges has led to specific topics that will be investigated in the context of this thesis:

Optimization of the coordinated fault ride through compliance strategies - Offshore wind power plants utilizing voltage source converter (VSC)-HVDC technology shall be capable to present fault ride through capability during onshore and offshore collector grid faults and support to power system stability. For onshore faults, the technical challenge is the protection of the HVDC link from direct over-voltages which impose high electrical stresses to the fragile HVDC system switches. The conventional compliance method used by vendors today is by the installation of a DC chopper controller resistor which is installed at the onshore DC terminal. In order to reduce the grid code compliance cost, state of the art, communication free coordinated control strategies have been documented in the literature [27]. The most known is the voltage drop and the frequency modulation method. These methods use the inherent controllability of the VSC-HVDC system and the offshore wind plants in order to ensure fault ride through compliance (for the onshore station). The disadvantage of such coordinated fault ride through schemes is that an effective tuning of the associated controllers is needed in order to avoid unwanted interactions between the wind plants and the VSC-HVDC system. The selection of these control variables should be performed on case by case project since different offshore island grid configurations appear (i.e cable length, wind turbine types and offshore collector grid layouts etc). Hence, a methodology to select the best set of the control variables is needed.

Assessment of the effect of fault ride through compliance of VSC-HVDC systems on the power system short term voltage and rotor angle stability - The reactive current injection during grid faults by wind and solar power plants is nowadays a mandatory requirement in most of the national level connection codes. It is typically described by the reactive current boosting profiles which link the injected reactive current to the residual voltage at the point of common coupling. The shape of the reactive current boosting profiles shall be effectively selected such as the VSC-HVDC link is not over-engineered while the provided voltage support is optimized. The power system operators shall define and if possible quantify analytically the derived technical benefits from the grid code compliance of the VSC-HVDC link during AC faults. In addition, it is important to effectively control the active and reactive current injection of the VSC-HVDC system during AC faults since it influences the voltage and rotor angle stability of the AC power system. Hence, clear insights proven by time domain simulations and recommendations on how VSC-HVDC systems can support the power system stability with grid connection code as boundary condition are needed.

Control of an offshore VSC-HVDC link during unbalanced AC grid faults. Although three phase faults affect mostly power system stability, unbalanced AC grid faults are more commonly observed in power systems and their analysis becomes relevant for protection system design. In addition, the increased penetration of power converters in the transmission grid has raised research questions on the control of VSC-HVDC systems during unbalanced faults and their effect on transmission grid response. In that direction new grid code articles have been introduced in connection codes which describe the behavior of the converter stations.

During unbalanced faults, it is possible to control the VSC-HVDC link current injection in the positive and in the negative sequence. Commonly, the negative sequence current component is suppressed in order to avoid high unbalanced fault currents and protect the sensitive IGBTs of the converter station. Hence, it becomes relevant to study the expected fault response of the VSC-HVDC link for various applied control schemes in the positive and in the negative sequence so as to design effective fault detection and protection schemes in AC transmission systems where VSC-HVDC links feed in. The same applies for the offshore AC island grid although the control layout is significantly different. In that context, the design of control schemes which enhance the unbalanced fault behavior of the onshore and the offshore station needs to be investigated.

1.3. THESIS OBJECTIVES

The main research goal of this thesis is the analysis and optimization of mandatory grid code compliance control strategies during AC fault conditions for offshore wind power plants with VSC-HVDC connection.

The first research objective addresses the development of a new optimal iterative procedure which optimizes the mandatory fault ride through compliance of offshore wind power plants that use VSC-HVDC transmission. Both point-to-point and multi-terminal connections are explicitly addressed. The method aims to tune the controllers in order to achieve minimal electrical stresses in the combined wind power plant and VSC-HVDC system taking into account the non-linear dynamic behavior of the control modules. The reduction of the electrical stresses at the offshore wind power plants and the HVDC system during AC faults can lead to the increase in the life expectancy of the equipment. Moreover, it reduces the impact that grid code requirements impose to hardware while at the same time ensures power system voltage and transient stability support.

The second objective of this thesis, is to quantify the effect of the fault ride thought grid connection requirements applied to HVDC connected wind power plants on the voltage and rotor angle stability of the mainland AC transmission system. The goal is to present by analytical methods augmented by stability type, time domain simulations, the achieved improvement on the power system voltage and rotor angle stability metrics as a result of grid code compliance. Both point-to-point and the multi-terminal HVDC connections are addressed in order to derive general conclusions.

As a third objective, the thesis studies the unbalanced fault ride through response of VSC-HVDC links connecting large offshore wind power plants. Unbalanced grid faults are simulated at the onshore and the offshore AC terminals of the VSC-HVDC link. The importance of the negative sequence current control is defined. Two level VSC-HVDC technology is assumed for the offshore wind connection case. The aim is to demonstrate how the negative sequence current control of VSC-HVDC systems affects the unbalanced fault response of AC-DC transmission grids.

1.4. RESEARCH QUESTIONS

The formulated research questions in the context of this thesis address the main problem of how technical capabilities, system functionality and grid code requirements for off-

shore wind power plants and their VSC-HVDC system delivery can lead to the improvement of power system faulted dynamic response. It is important that wind power plants and HVDC systems are not over-engineered from the electrical engineering perspective, yet system operators are assured of stable grid operation under all circumstances. The thesis research questions are summarized and grouped as follows:

1. Which control parameters affect the fault ride through (FRT) compliance of offshore wind power plants in VSC-HVDC grid connection during balanced onshore AC grid faults? What are the experienced electrical stresses at the VSC-HVDC system and/or the wind plants? Are there any negative interactions, undesired dynamics and risks when coordinated FRT strategies are applied? Could a point-to-point HVDC connection be FRT compliant when expanded to meshed HVDC grid connection? What are the observed differences with respect to the power system response between the point to point and the multi-terminal HVDC grid connection of the offshore wind power plants? How can we reduce the cost of FRT grid code compliance while respecting the technical limitations of the offshore wind power plants in VSC-HVDC connection?

2. Is it possible to optimize the dynamic response of the offshore wind power plants and the VSC-HVDC system while at the same time minimizing the imposed electrical stresses as a result of fault ride through compliance? How to estimate the optimal grid code related control parameters in a generic way which can be applied on a case by case basis per project?

3. Which control blocks in the VSC-HVDC system affect the unbalanced fault behavior of the AC transmission system? What are the imposed electrical stresses in the VSC-HVDC equipment and how to mitigate them? What are the associated risks for the AC power system during the fault response and how the AC-DC transmission system can be optimized from the power system protection perspective? What are the needs in a future power system with high penetration of power electronic interfaced generation units?

4. How does the choice of the grid code variables affect the short term voltage and the rotor angle stability of the onshore transmission system during AC grid faulted conditions? How does the sizing of the onshore VSC-HVDC transmission system affects the power system voltage and rotor angle stability? Is it possible to quantify the benefits from power system perspective?

5. Offshore wind power plants with VSC-HVDC connection are isolated AC systems with very low short circuit power levels. How does such an island grid behave during balanced and unbalanced AC faults? What are the available control options for the FRT grid code compliance? What are the benefits for imposing grid codes at the offshore island grid? What is the additional control functionality needed?

1.5. APPROACH

The analysis in this thesis is performed using time domain dynamic simulations for well defined test systems. Three types of dynamic models have been developed. First, a detailed electromagnetic transient (EMT) type model in PSCAD/EMTDC environment. It represents an offshore wind power plant with a VSC-HVDC system. All the associated control loops for the offshore wind power plant, the onshore and the offshore VSC-HVDC converter station are represented in detail. Control interactions during AC faults are observed and new control schemes for improving the grid code compliance of mandatory requirements are proposed.

Next, average value EMT type models have been developed in the Matlab/Simulink environment. The models are modular, parametric and can be easily extended from the point-to-point VSC-HVDC connection to the multi-terminal HVDC case. The choice of Matlab/Simulink simulation platform is performed with the goal to couple iterations of the EMT type simulations to the optimization toolbox, developed in the Matlab environment. Using the EMT Matlab/Simulink model and state of the art stochastic optimization algorithms, an iterative procedure is formulated for the optimal tuning of the coordinated fault-ride through strategies.

Finally, RMS value time domain simulations have been used in order to demonstrate the effect of the FRT grid code compliance on the power system rotor angle and voltage stability. The rms models used are simplified, under the main assumptions taken for stability type studies. The models include a VSC-HVDC system model and wind power plant models in point-to-point as well as in multi-terminal DC connection. Using the model, sensitivity analysis is performed in order to show the effect of grid code and grid code compliance control parameters on the power system transient stability.

1.6. THESIS OUTLINE

Chapter 2 provides a literature review on offshore wind development, technical challenges for sustainable power systems and VSC-HVDC technology. A overview is given of general grid connection requirements for offshore wind power plants with VSC-HVDC transmission. Furthermore, a discussion is presented on the state of the art technology for the fault-ride-through compliance.

Chapter 3 introduces three novel control modules for offshore wind power plants with a point-to-point VSC-HVDC connection. The goal is to enhance the fault ride through (FRT) capability of the HVDC system and the connected offshore wind power plants during unbalanced AC faults. Firstly, a positive-sequence-voltage-dependent (PSVD) active current reduction control loop is proposed for the offshore wind turbines. The method enhances the performance of the offshore AC voltage drop FRT compliance strategy. Secondly, an enhanced current limiting control module which operates simultaneously on the positive and the negative sequence current is discussed. It enables negative sequence current injection, while at the same time respecting the maximum fault current capacity of the HVDC converter station. Finally, the chapter introduces a novel enhanced control strategy for the offshore VSC-HVDC station. It enables improved FRT compliance for balanced and unbalanced AC faults at the remote island offshore grid. Simulation results with a detailed EMT type model in PSCAD/EMTDC environment are

presented for onshore and offshore faults. The test system consists of a two level VSC-HVDC link, rated at ±250 kV, connecting an offshore wind power plant with 700 MW generation capacity.

Chapter 4, presents a new iterative procedure augmented by electromagnetic transient (EMT) type simulations and the state of the art mean variance mapping optimization (MVMO) algorithm. It enables the optimal tuning of coordinated fault ride through (FRT) compliance strategies for offshore wind power plants with VSC-HVDC transmission. The formulated optimization task minimizes the electrical stresses experienced by the VSC-HVDC system and the offshore wind power plants during the FRT and post-FRT period. Moreover, it ensures that the onshore and offshore grid code profiles are not violated due to unwanted dynamics associated with the combined response of the VSC-HVDC system and its wind power plant. Two different state of the art coordinated FRT strategies are optimized for the first time in this work using the iterative procedure. The first FRT strategy is the controlled offshore AC voltage drop method. Two sub-cases of the latter are addressed. In the first sub-case, the offshore wind turbines provide reactive current support to the onshore island grid during the controlled offshore AC voltage drop period. In the second sub-case, a new alternative technique is tested which uses a voltage dependent active current reduction controller at the offshore wind power plants. The second optimized FRT strategy is the frequency modulation technique supported here by a wind turbine level controller. The wind turbine controller modulates adequately the active current for a given offshore frequency. The combined VSC-HVDC system and wind plant dynamic response is compared by means of time domain simulations. Recommendations on the best solution are provided.

Chapter 5 extends the applied iterative procedure for the optimization of the coordinated fault ride through compliance strategies to an offshore multi-terminal HVDC grid case used for grid connection of far and large offshore wind power plants during AC system failures. The chapter initially discusses control modules and parameter sensitivities which affect the combined dynamic response of the MTDC grid and the connected offshore wind power plants. Then it presents the improvements achieved when the control parameters are optimally selected.

Chapter 6 presents the improvement in the short term voltage and rotor angle stability of an AC transmission system as a result of the fault ride through and reactive current injection compliance of VSC-HVDC systems used for the grid connection of offshore wind power plants. The analysis is performed by analytical equations on equivalent linear circuits, augmented by time domain dynamic simulations on the modified IEEE 39-bus test system. The benchmark AC-DC transmission system consists of point-to-point and multi-terminal HVDC connections. Different control strategies and parameter sensitivities are evaluated in order to draw conclusions and provide recommendations about the dynamic response of future AC-DC transmission systems.

Chapter 7 provides the overall conclusions of the thesis and answers to the research questions while providing recommendation and future work.

1

1.7. CONTRIBUTION OF THIS THESIS TO THE FLOW PROJECT IN THE NETHERLANDS

The grid code compliance certification process for offshore wind plants is a tedious procedure. It initially requires practical field tests, where critical parameters for the wind turbine models need to be defined. Next, offline simulation studies are required by system operators in order to prove that the wind plant is grid code compliant and does not jeopardize the power system security of supply.

In that prospect, steady-state and dynamic models for wind plants are needed by the project developers and power system operators. From the project developers and TSOs perspective, building such models is a time consuming process, which involves additional costs and delays. Obtaining black box dynamic models from wind turbine and HVDC system manufacturers is a common practice. However, it is not always sufficient as there are confidentiality and intellectual property concerns. Let alone the black box models do not always provide deep insights due to their restricted in use nature.

The primary contribution of this thesis to the Far and Large Offshore Wind (FLOW) project is development of offline simulation tools. Secondary, the simulation tools are used within the project in order to perform control parameters trade-off analysis. In that prospect the system stability impact of far and large offshore wind (FLOW) power plants on the interconnected power system is demonstrated for a variety of grid connection studies. In addition, an optimal iterative methodology is proposed for the grid code compliance. It reduces the cost of grid code compliance, as it eliminates the use of hardware, and optimizes the dynamic behaviour of the FLOW plants from technical perspective.

The simulations models and methodologies for optimal grid code compliance documented in this project deliverables, cover all the spectrum of the needed grid connection simulation studies including namely: power flows, detailed transient and dynamic stability models. It can be used to define transient stability metrics and design grid codes for the Dutch power system and evaluate its stability for various scenarios of wind power penetration levels.

It is also shown that by using the grid code compliance optimal trade-off tool, along with adequate analysis on technical compliance options, it is possible to achieve a cost reduction of 0.5% according to the FLOW cost model, mainly due to the contributions in capital expenditude (CAPEX), development expenditure (DEVEX) and operation expenditure (OPEX). The substitution of hardware equipment (as the HVDC DC-chopper) by coordinated software based control schemes for fault ride through compliance, would decrease the CAPEX for the HVDC link. Furthermore, clearly defined offshore grid codes at national level, harmonized to the European grid codes released by ENTSO-E, and confidence that the offshore HVDC networks can be safely operated will encourage the development of offshore wind resources. Finally, the project provides insights into technical risks associated with the grid code compliance of HVDC connected FLOW power plants during AC grid faults. Risks arise from badly tuned control loops installed in order to support the system during AC fault conditions.

2

REVIEW OF TECHNOLOGIES FOR SUSTAINABLE POWER SYSTEMS AND THE ROLE OF OFFSHORE WIND POWER

2.1. TECHNICAL CHALLENGES

2.1.1. ENERGY SECTOR TRANSITION

The environmental concerns about the global warming have promoted the transformation of the European energy sector [6, 9, 28]. In that context, the European Union has set the binding target of 27% renewable energy utilization in its final energy consumption. This translates to about 47% of electricity generated explicitly by renewable energy sources [29]. Moreover, the need to make Europe independent on foreign energy resources (imported coal, gas and oil) has further boosted this initiative [30–32]. The emerging renewable energy markets would strengthen the European economy [1, 33], promote innovation technology and open new oppurtunities for member states [34]. Renewable energy accounted for 77% of all new installed power generation plants in 2016 [35]. The falling costs of renewable energy technologies has made them a competitive option for new installed power generation [36, 37]. Onshore wind and photovoltaic (PV) technology have become today an affordable source of electricity generation in many parts of the world.

Wind, solar, biomass, geothermal and hydro power resources are abundant through Europe [38]. Wind energy is supposed to take the Lions share in the future renewable electricity generation mix [39]. Based on the "Wind-Europe" association central development scenario, about 320GW wind power capacity will be installed in EU by 2030 [40, 41]. This is twice as big as the installed wind power capacity in 2014 (129GW). Wind is estimated to contribute 24% in the total energy share in the EU (778TWh). Up to date

wind sector covers about 12% of the European energy demand.

2.1.2. INNOVATION TECHNOLOGY

The development of sustainable energy systems requires innovation technology in two main topics. First is the cost reduction for renewable energy technologies including the manufacturing,[42, 43] installation and supply chain [15, 44–46]. Reducing offshore wind energy costs has been a major focus of research and development activities through the past decade [47]. Up to date, the record for the lowest reported cost has been observed in the Netherlards, for the Borselle I project with a strike price of 72.7Euros/MWh (not including the grid connection costs). Only in the past five years, wind energy sector has featured the largest number of EU registered technology patents clearly reflecting research and development activities. These breaking points boost the anticipation and confidence for investors that offshore wind industry will be fully competitive with gas, coal and nuclear energy in the future [15].

The second topic for innovation technology is the need to ensure the power system security of supply for future sustainable electrical grids. The development of grid friendly renewable energy technologies is currently at the spot of research activities [48–51]. The future replacement of large conventional power plants units by power electronic based renewable energy technologies has brought into the spot new challenges for grid operators (both at the distribution and transmission level). Ensuring power system security of supply and certain levels of power quality would not be an easy task mainly due to lack of experience with future sustainable power grids [52–56]. Nonetheless, these challenges present a clear will from the European industry and power system society to promote innovation and the development of new power system technology.

2.1.3. POWER SYSTEMS DOMINATED BY CONVERTERS

The majority of renewable energy sources (PV, wind and battery storage) are grid connected via power electronic converters. So far the power electronic modules have been designed and optimized from the component perspective. Since, less conventional power plant units will be available in future grids, renewable sources need to provide grid support services [48, 57]. Moreover, new challenges arise which will be briefly discussed below.

FREQUENCY STABILITY

An important technical concern for future sustainable power systems is frequency stability. Frequency stability challenges with large penetration of wind and solar have been identified in Ireland [23] and the United States [24]. These real grid cases have provided an indication of challenges that interconnected systems will meet due to the reduction of conventional generation units, and as a consequence of the rotating kinetic energy in the grid.

VOLTAGE CONTROL AND RESTORATION

The majority of power converters used for the grid connection of renewable generation units are current controlled voltage sources. Their association with voltage control is referred as their ability to provide reactive current in normal and fault conditions. In future

grids, with very high penetration of power converters in the transmission, distribution and low voltage level, the ability of power converters to build the voltage applying grid forming control schemes would be important. Although 100% power converter generation is not realist scenario during normal operation, it could potentially happen in cases of system split where part of the transmission system will contain only power converter based generation and loads. In that case, grid forming schemes would enable stable operation while current control converters would simply lead to system black-out. Hence, voltage control and restoration in power electronic based grids shall be regarded as the ability of forming the voltage in similar manner as conventional generation units do.

HARMONIC STABILITY OF AC-DC TRANSMISSION AND DISTRIBUTION SYSTEMS

The high penetration of power converters in the grid (tranmission and distribution level) would affect the delivered power quality due to harmonic emitions [58]. Furthermore, the applied control strategy and parameters of the converter affect additionally the dynamic interaction with the grid resonance. Challenges with harmonic instability have been already identified in large wind power plants with HVDC connection [59–61]. Similarly, when a large number of HVDC converters are connected to the transmission grid in close electrical proximity, similar phenomena might be observed as a result of bad tuning of controlers [62]. Generic assessment methods and harmonic stability criteria are needed in order to ensure power quality and robustness in a converter dominated power system [63, 64].

SYSTEM RESTORATION SERVICES

In a future sustainable grid, wind turbines and HVDC systems should be capable to provide black start or operate completely in island grids without the presence of conventional machines. Until today system restoration services from wind plants have remained unexplored [65, 66]. Detailed requirements or technical specifications does not exist in grid codes. Moreover, the stochastic nature of wind generation units, makes system operators reluctant to rely on wind plants for system restoration. Sufficient information about wind conditions and highly advanced wind forecasting techniques will be demanded. The integration of storage at wind turbines would be a potential solution to provide voltage restoration via the power electronic modules.

STORAGE

Storage is a key element for sustainable energy systems. The witnessed cost reduction in battery storage, has opened new business opportunities for the provision of system support services (i.e frequency response and local balancing) from local consumers. In that context, consumers have been turned into prosumers which could potentially play a major role in the operation of future grids. Large scale storage is also key for the vast geographic integration of sustainable energy throughout Europe. Pumped-Hydro power remains still the most efficient and cost effective mean of applying large system storage.

SHORT CIRCUIT CURRENTS

Adequate short circuit power levels are important for the power system in order to ensure the effective operation of its protection schemes [67, 68]. In a future power system dominated by power converters, protection would be an additional challenge [69–71]. The

limited overcurrent capacity of power converters during the fault period would make fault current detection and isolation hard [72, 73]. Over-dimensioning power converters with purpose to provide high fault currents could be an option but it would mean additional costs for the components. When considering unbalanced faults, the increased fault current capacity would enable the injection of negative sequence currents which would boost the fault detection capability during unbalanced grid faults.

WEAK CONNECTION POINTS

In future sustainable power systems, wind plants will be connected to remote sites, with long transmission systems, electrically far from stiff grid connection points. This brings additional challenges for the the stability of the plant and the power system. Instabilities for power converters have been already observed for weak grid connection points. Defining challenges of such connections and linking them to the grid codes applied would limit risks related to stability of the grid [74–78].

2.1.4. WIND POWER PLANT TECHNOLOGY TODAY

Wind tubine technology has experienced a rapid development during the past 10 years [79, 80]. The demand for power system support services and the strict grid code requirements [81] have motivated wind turbine vendors to build machines which are highly sophisticated devices. Having as starting point the fixed speed wind turbine, the state of the art technology today incorporates variable speed technology [82] augmented by power electronic actuators which are capable to provide high degree of controllability and flexibility during normal operation and faulted conditions [83].

Two types of variable speed technology have dominated the market. First is the full converter interfaced wind turbine (type 4) which uses an AC/DC/AC conversion rated at the generator capacity of the wind turbine [84–87]. The second, is the double fed asynchronous generator wind turbine with a slip ring rotor with the converter rating being only 25% of the machine rating [88–94]. The main advantages of using such machines are namely: the high delivered power quality, the limited filter requirements, the capability to withstand grid faults up to zero voltage level providing limited short circuit current injection, the capability to change the power set points with purpose to contribute in the power system load frequency control and finally the ability to handle unbalanced grid faults with high efficiency are only a few to mention.

Offshore wind turbines need to withstand the very unfriendly offshore environment, placing additional stresses to the applied materials [95]. Also, another important concern is the limited space available at the offshore platforms which demands for the optimization of the substation layout[96–99]. In principle in order to reduce the cost of the offshore wind farms, higher capacity factors are required which means that the size of the generator and the blades lengths have been significantly increased [100]. Furthermore, with a goal to minimize the turbulence and wake effect, offshore wind turbines are adequately placed and their distances between each other are optimized [101, 102].

GRID FRIENDLY WIND PLANT TECHNOLOGY

Grid system services and enhanced control functionality are key aspects in order to ensure the stable integration of large scale renewable resources [103, 104]. Since wind

farms have grown in size forming big wind power plants, system services are more and more requested by system operators [105–109]. Some of these services are grid codes nowadays. Voltage and frequency control are functions that modern wind plants could provide [85, 110–123].

Technical enhancement of future grid support services by wind plants would demand for faster and reliable communication technology which would enable data exchange between grid operators and wind plant owners [124, 125]. Sophisticated wind forecasting techniques and dedicated applied control schemes are needed in order to estimate the available system services and enhance power system stability. Specifically for offshore wind power plants, grid support services need to consider the applied transmission system technology (HVAC vs HVDC). Offshore wind plants for example with HVAC connection can provide relevantly easier frequency support services compared to HVDC connected wind power plants where there is need either for enhanced communication technology or advanced coordinated control schemes. Implementing enhanced grid support services for voltage and frequency control would involve additional investments that would be translated to additional costs.

2.2. STATE OF THE ART OFFSHORE WIND PLANTS WITH HVDC CONNECTION

The development of far from shore and large in size offshore wind power plants demand for alternative grid transmission system solutions which would make these projects economically and technically feasible [126–128]. VSC-HVDC transmission is a cost effective solution for distances above 120km. The use of VSC-HVDC links for offshore wind plants would provide advantages [20, 129] but it would introduce additional challenges with respect to the design, the control and the operation of such new schemes.

The connection of the offshore wind plants via VSC-HVDC transmission [130] provides the technical feasibility to create large offshore clusters by connecting large offshore wind plants to certain offshore hubs. The rated capacity of the state of the art VSC-HVDC technology is currently around 1200MW which enables the connection of power plant modules of different sizes. With VSC-HVDC connection the offshore electrical grid becomes completely decoupled from the onshore power system. If adequately controlled, the VSC-HVDC system and the offshore wind plants could be operated as power plant unit or a virtual plant which provides controllable active and reactive power at its onshore grid connection point.

The main engineering challenges for offshore wind plants with VSC-HVDC transmission takes place at the offshore side. The limited space at the offshore platform and the exposure to sault, water and wind conditions demands for reliable components with appropriate sealing and insulation. Important are also the auxiliary supplies which need to ensure power supply availability even at no zero wind speed conditions. Normally, the auxiliary power supply is provided by the wind turbines, however, during no wind conditions either a diesel generator is used, or a parallel AC cable embedded in the HVDC cable. Reverse power flow from the onshore HVDC station to the offshore station is also possible.

Another important concern, beside the component design, is control robustness and

stability. The offshore island grid shall be stable both during steady state operation and offshore grid fault conditions. For steady state operation, the so called harmonic stability has been recently identified as a potential risk. Harmonic stability refers to the ability of the offshore island grid to ensure that high frequency interactions between the power converters and the offshore AC cables will be always damped with reasonable time constants and not get amplified by the power converter modules.

The offshore island AC grid is basically using high voltage cables which reduces the risks of faults. However, when such faults occur the AC island grid shall remain stable while the fault be effectively cleared. As a result, the protection schemes shall be capable to selectively detect and isolate parts of the offshore AC grid while the un-faulted part does not trip. The fault ride through capability of the wind power plants and the offshore HVDC station shall be ensured. The nature of the fault ride through is not the same as in the onshore side since there are no connected consumers. Keeping the voltage high at the island grid is essential for the wind turbines power converters to remain grid tied and recover during the post-fault period. Moreover, beside the need for fault ride through compliance, challenges have been lately identified in the case that the offshore VSC-HVDC station blocks for a couple of cycles. Blocking of the offshore HVDC converter might lead to trip of the hub and loss of significant amount of wind generation. The wind turbines should be capable to withstand this disturbance. From this discussion one can foresee that the components design, the optimization of the substation layout, the design of the control modules and the optimization of the intra-array cables in conjugation with the control and the operation of such offshore islands has become very relevant.

The onshore VSC-HVDC station provides the grid interface with the high voltage transmission grid. Its functionality is to control the DC link voltage, ensuring the power balanced between the onshore and offshore stations. Moreover, the onshore station should provide grid support services including reactive power and voltage control during normal voltage conditions, fault current injection during AC grid faults, synthetic inertia response (in coordination with the offshore wind plants), emergency power control especially for ramping down the power and damping of electromechanical oscillations. Finally, the onshore station, has the ability to ensure that its operation does not interact with the grid resonance neither shift the grid resonance not create sub-synchronous interactions with generators in the close electrical vicinity. The above mentioned challenges have been identified by transmission system operators and HVDC system vendors.

2.2.1. HVDC SYSTEM TOPOLOGIES

HVDC systems can be built in many configurations depending on the power rating and the system needs. The most simple HVDC system configuration is the mono-polar. Depending on the grounding configuration in the DC side, mono-polar configurations are termed as mono-polar with metalic return, mono-polar with grounded midpoint and mono-polar with ground return. In order to increase the transmission capacity and reliability of the delivered power, bipolar configurations are applied either with metalic return or with ground return. For AC grid disturbances, the effect of the HVDC circuit configuration does not affect significantly the HVDC stations response.

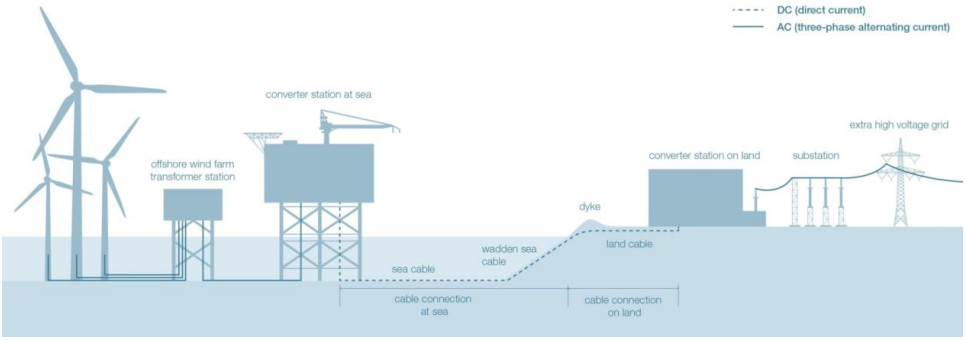

Figure 2.1: An offshore wind power plant with VSC-HVDC tranmission system.

2.2.2. VOLTAGE SOURCE CONVERTER TOPOLOGY

Voltage source converter technology is the current state of the art technology for HVDC systems. The first generation of VSC-HVDC systems utilized two level converter technology based on IGBT. The IGBT technology enables controlled switching on and off enabling self commutation and energization of passive networks. The switching frequency of the IGBTs shall be kept high in order to reduce the current ripple, without at the same time increasing significantly the switching losses. The two level VSC technology produces voltage wave-forms with the fundamental frequency and higher harmonics appearing at multiples of the carrier frequency. Hence, passive filters are installed in order to improve the delivered power quality of the voltage and current reducing the total harmonic distortion. As an improvement of the two level VSC, the three level technology has been used. This configuration is derived by clamping the neutral point of the DC link. Its main advantage is the lower harmonic distortion and the reduction in the size of the needed passive filters.

The modular multi-level converter technology is today the state of the art HVDC technology. This topology is capable to built the sinusoidal voltage waveform by a large number of step voltages which are inserted and removed from the circuit in a controlled way. The biggest advantage is the very low harmonic distortion which reduces the size of the passive filters. The main drawback for the MMC-HVDC is the switching losses due to the large number of components.

2.2.3. TYPICAL CONNECTION LAYOUT

The main components of an offshore wind plant with VSC-HVDC tranmission is presented in figure 2.1. As it can be observed, the onshore sub-station which operates as inverter provides connection to the high voltage AC transmission system. At the sub-station are located AC filters, DC filters, switching devices and the converter modules. At the offshore terminal, the offshore HVDC station, operates as tectifier and provides AC voltage to the offshore hub. Additionally, every wind plant connected to the hub, contains its own platform where the medium voltage to high voltage transformers are

located. Usually, the wind turbines are connected at 33kV medium voltage level.

2.2.4. Control functionality

Reactive power and voltage control in offshore HVDC links

VSC-HVDC technology enables voltage and reactive power control in high voltage transmission systems. The size of the onshore HVDC converter station is considerable and should be utilized as a source for controlled active and reactive power. The latter provides flexibility to the system operators to handle congestion in the grid. The converter is capable either of providing a fixed amount of reactive power (ordered by the system operator) or controlling the voltage levels at its grid connection point. Moreover, it is possible to integrate the reactive power control capability of the onshore HVDC station to the secondary voltage control level of the onshore power system, based on optimal load flow algorithms.

At the offshore AC island grid, the voltage is formed by the offshore station. The wind turbines can further contribute in the reactive power and voltage control by regulating the amount of reactive power injected by each individual turbine. Over-all, it is the combined operation of the offshore station as a slack bus and the wind turbines as reactive power sources which ensure adequate voltage and reactive power flows in the offshore AC island. Recent research has presented an integrated approach where the reactive power set-points per each individual wind turbine in the farm are optimally selected in order to minimize losses and reduce the plant operation costs.

Active power and frequency control of offshore wind plants with HVDC connection

A typical offshore VSC-HVDC link for offshore wind power grid connection could provide active power control in order to support the power system frequency stability. The onshore converter station, varies its active current in such a way that the DC voltage at its terminal is controlled at its reference set point. The offshore station, provides the voltage at the offshore island grid and controls the frequency of the voltage via the internal voltage angle. So the control philosophy does not have a "direct" active power set point, but rather as slack bus that absorbs the generated offshore wind power to the onshore terminals. Hence, in the case that active power control functionality is needed (i.e frequency control), either a communication link is needed or other coordinated control schemes have to be applied. The disadvantage of using communication is the dependency of the provided service to measurements and communication infrastructure latency.

Capability to enhance harmonic stability

A future challenge for power systems with high penetration of power electronic converters is high frequency harmonic interactions. Offshore VSC-HVDC links shall be capable to utilize adequate control blocks which can shape their output impedance in such a way that it does not interact with the grid resonance. The grid resonance frequencies depend on many factors, as the system configuration and the grid operating point. For VSC-HVDC links, it is important to be able to detect these changes and adopt its control modules or parameters if needed in order to avoid harmonic interactions. So self-adopting controllers for mitigating harmonic interactions would be very important both for onshore and the offshore terminals of the VSC-HVDC station.

FAULT RIDE THROUGH

The capability of the offshore wind plants and their VSC-HVDC system delivery to onshore and offshore faults is important. For onshore faults, the challenge for the VSC-HVDC link is to avoid very high direct over-voltage in the HVDC link during the fault period while injecting reactive fault current. Different FRT schemes have been proposed in the literature, using either hardware as the DC chopper solution or coordinated control schemes. The DC chopper is a very straight forward approach which uses controlled resistances to dissipate the power that is not flowing to the grid during the fault period. Its limitation is the size of the substation and the its costs. With respect to the coordinated schemes, two categories can be defined. Those who act on the offshore AC voltage and those who act on the offshore island frequency. Both aim to reduce the generated offshore wind power.

2.3. MULTI-TERMINAL HVDC NETWORKS

The connection of several HVDC terminals from the DC side would enhance the power system operation [131, 132]. It would reduce grid connection costs as the same HVDC station could be used to transfer power to different control zones. Moreover, the outage of one terminal (i.e onshore HVDC station) would not interrupt the utilization of wind power generation in the system [133]. Similar to offshore connections, the expansion of embedded HVDC links or links connecting asynchronous zones to a transnational overlay multi-terminal HVDC grid, would enable more effective power flow in the AC transmission grid, efficient congestion management, effective cross border power flows and enhancement of the rotor angle stability (both large and small signal).

The development of HVDC grids is not new as a concept. In the 70s and 80s research efforts mainly using line commutated converter (LCC) HVDC technology have proven the feasibility of HVDC grids. The HVDC grid real world application were limited to only three terminals. LCC-HVDC converter technology is very well proven, mature and cost efficient for bulk power transmission capacity. However, it has certain disadvantages for the development of offshore HVDC grids as it does not provide fast power reversal and demands for communication technology, reactive power compensation and stiff grid connection points. Moreover, it cannot energize passive offshore networks neither it can operate to weak grids. LCC-HVDC is used in Brasil and China up to date for Bulk power transmission in very long distances and it has achieved rating of up to 6000MW. Recent advances in HVDC technology, and the new modular multilevel converter (MMC) topology has revived the scientific interest for HVDC grids.

2.3.1. HVDC CIRCUIT BREAKER

The protection of the DC circuit and the interruption of the DC fault current is a key element in order to realize fully operational meshed HVDC grids. The high costs of converters demand for sophisticated DC protection schemes and advanced DC circuit breaker technology in order to detect and effectively isolate the fault from the rest of the HVDC grid. HVDC breakers shall provide sufficient fault current interruption capability, fast operation, minimum on state losses, capability to withstand over-voltages, bidirectional current flow, lightness, compactness, modular design and reliability.

DC faults shall be selectively cleared and allow post-fault direct voltage recovery in the HVDC grid while ensuring robustness and stability of HVDC station control schemes. The small time constants and the DC capacitive behaviour of HVDC circuit (and converter station), requires for very fast circuit interruption time, typically between 5-10 ms. HVDC breakers are very large in size and very expensive compared to AC breakers. One of the main difference with respect to AC breakers is the absence of natural zero current crossing point in DC circuits. Hence, the HVDC breaker needs to create a zero crossing in order to interrupt the current. This is done by posing a counter voltage of the adequate amplitude. Moreover, due to the large DC fault current, the energy stored in the inductance needs to be dissipated by the breaker. The larger the counter voltage, the higher the dissipated energy in the device. The breaker has to withstand the voltage generated (during fault at the healthy poles and post-fault) and comply with the insulation and coordination of the HVDC system.

Two DC circuit breakers types can be identified, namely the electromechanical and solid-state. The Electromechanical type can be categorized into three sets based on the method used. First is the inverse voltage generating method, second the divergent current oscillating method, and third the inverse current injecting method. Only the inverse current injecting method can be used in high voltage and current ratings. In this type of breaker, a current zero point can be achieved by superimposing a high frequency inverse current on the input current by dis-charging a capacitor (that was pre-charged) through an inductor.

The Solid-state circuit breaker is the second type of HVDC breaker particularly effective for use in VSC-HVDC grids. The main advantage of these breakers compared to the previous category is that they can interrupt the fault current much faster than the electromechanical circuit breakers. They are based on Integrated Gate Commutated Thyristors (IGCT), which compared to IGBT (bipolar thyristors) have lower on-state losses. The current flows through the IGCT and when it has to interrupt it, the IGCT is turned off. Once that occurs, the voltage quickly increases. A varistor which is designed to block voltages above the voltage level of the system (that is in parallel to the thyristor) is conducting. The main disadvantage of these types of circuit breakers are the high on-state losses and the capital costs.

Finally, the utilization of HVDC breakers can be enhanced by the new generation of full bridge MMC-HVDC topology which is capable to block the fault current and enhance the fault interruption capability. The later provides the ground for new fault detection and isolation strategies in meshed HVDC grids.

2.3.2. DIRECT VOLTAGE AND CONTROL OF HVDC GRIDS

In a fully operational HVDC grid (offshore or embedded in the power system), the direct voltage at the DC nodes, shall be maintained at strictly defined range during normal and fault conditions. During faults (AC or DC), emergency actions are taken in order to limit the deviation from these operation ranges.

The direct voltage control in an HVDC grid has two main targets. First, enabling the normal operation of the power electronic components of the HVDC stations. Second, the affective and robust of power flow control in an HVDC grid [134].

2.3.3. SYSTEM SUPPORT SERVICES FROM HVDC GRIDS

The high active and reactive power controllability of the HVDC grid terminals could be used for system support services in the transmission level. The fast independent control of active and reactive power enables frequency support and damping of rotor angle oscillations in the AC grid. When embedded in the transmission network, HVDC grids can effectively damp inter-area oscillations by means of active power modulation. If the HVDC grid is connecting offshore wind power or coupling two control areas (synchronous or asynchronous), the active power control can significantly enhance the frequency stability of the system.

With respect to the reactive power and voltage control, HVDC stations can be regarded as independent sources of reactive power as long as normal conditions exist in the DC side. Even with zero active power, HVDC stations can operate as STATCOM and enhance locally the voltage stability. The same applies for fast reactive current injection during AC grid faults. The injection of reactive current from the HVDC stations could support short term voltage stability in the close vicinity of the connection point. Moreover, HVDC stations feeding power to a grid connection point can be used as active harmonic filters.

2.4. REVIEW OF GENERAL GRID CONNECTION REQUIREMENTS APPLIED TO OFFSHORE WIND PLANTS AND HVDC SYSTEMS

2.4.1. FREQUENCY AND ACTIVE POWER CONTROL

An HVDC converter station, irrelevant of its technology, shall remain grid connected for a predefined frequency range. Each TSO is responsible to define these frequency boundaries for its system. The typical frequency range in Europe is 49.0-51.0 Hz. Furthermore, the HVDC station shall withstand a rate of change of frequency of 2.5Hz/s.

Within these boundaries, the HVDC system shall be capable to control its active power (ramping up or down). Furthermore, the HVDC system shall be capable to provide synthetic inertia response. Synthetic inertia (or artificial inertia as it is else referred in literature) is defined as the fast active power response of the HVDC station as a function of the rate of change of the power system frequency measured at the grid connection point. This functionality could be activated both during high and and during low frequency regimes by withdrawing or by injecting a fast active power to the AC system. The delay for the inertia response provision shall be as small as possible.

2.4.2. FAULT RIDE THROUGH

In the case of AC grid faults, the HVDC converter station shall stay grid connected for a predefined period of time. Typical grid connection requirements include a well defined voltage against time envelope. This profile clearly defines pre-fault, fault and post-fault voltage levels associated with time. Figure 2.2 presents a generic low voltage ride through curve. The fault duration period is normally defined by the critical clearing times in the power system.

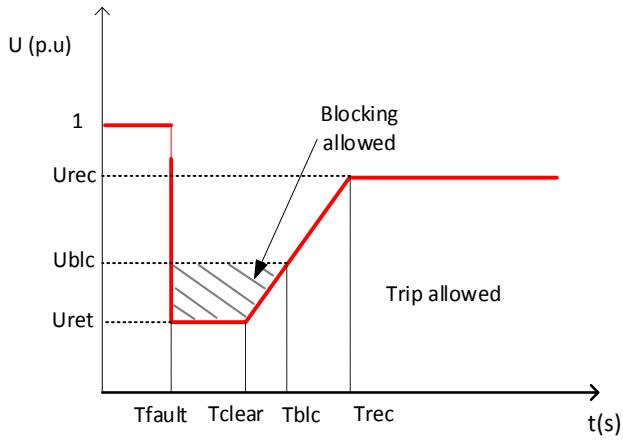

Figure 2.2: A typical low voltage ride through curve. In the x-axis are defined namely the fault time (Tfault), the fault clearing time (Tclear), the blocking time (Tblc) and the recovery time (Trec). This time instances correspond to the relevant voltage levels.

2.4.3. SHORT CIRCUIT CURRENT INJECTION

Beside remaining grid connected for the fault and the post-fault period, HVDC systems are required to provide a fast fault current injection at the grid connection point [135]. Grid connection HVDC codes define this injection as mandatory only for three phase faults. Hence, it is mainly a positive sequence current injection. It is in the responsibility of the TSO to define whether the fault current will be reactive, active or a combination of both. This choice has to do mainly with the power system needs. Additionally, when the maximum fault current capacity is reached, the TSO specifies which current priority is applied. Figure 2.3 presents a typical reactive current boosting curve.

Usually the fault current injection by the HVDC system should be provided to the grid as a function of the phase-to-phase voltage deviation at the grid connection point. For wind power generation units, there is an explicit description of this value. The slope of the curve is a control parameter which the relevant TSO needs to specify and it is termed as 'k' gain or "k-factor" in the literature. It is usually provided as a proportional gain applied at the outer control loops which relates the reactive current injection to the per unit voltage deviation of the phase to phase voltage. A voltage operating point U_o is needed in order to cover specific operating ranges. Finally, a dead band could be potentially selected in the range of nominal network voltage in order to avoid triggering reactive current injection during slow voltage variations. Following changes in voltage, the HVDC converter shall be capable of achieving 90 per cent change in reactive power, in a predefined by the relevant TSO rise time. Typical values of this rise time would be less than 20ms.

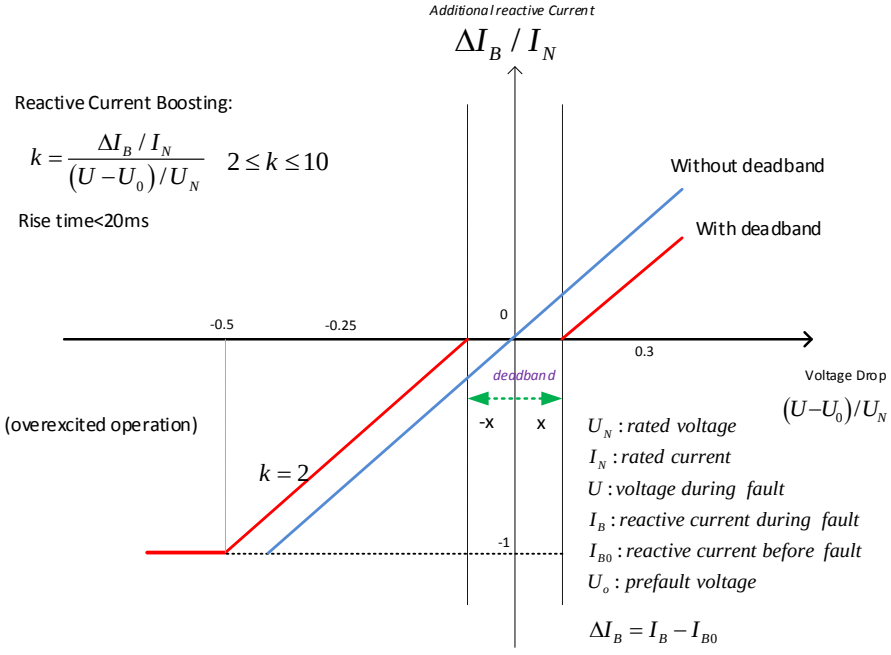

Figure 2.3: A typical reactive current boosting curve which quantifies the injection of reactive current proportionally to the voltage variation during AC grid faults.

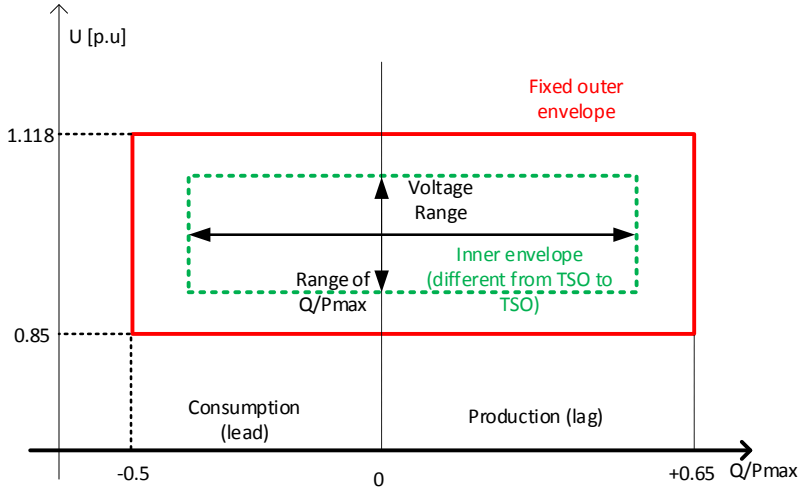

Figure 2.4: A typical profile which describes the steady state operation of an HVDC station with regard to its reactive power capability.

2.4.4. VOLTAGE AND REACTIVE POWER CONTROL

State of the art grid codes require for HVDC systems and wind power plants to remain grid connected for a wide range of voltage levels [135]. Within these voltage ranges the HVDC station needs to prove its capability to control active and reactive power exchange with the grid.

The reactive power capability of the HVDC converter station is commonly defined from the relevant TSO by a given U-Q/Pmax profile as presented in figure 2.4. These profiles describe the boundaries of reactive power injection that each HVDC converter station shall provide at its maximum active power capacity.

2.4.5. ROBUSTNESS, INTERACTIONS WITH THE GRID AND OTHER PROVIDED SERVICES BY HVDC SYSTEMS

The design of the HVDC link control modules shall ensure robustness. The HVDC system must be always stable during large system contingencies (i.e AC transient faults, trip of AC lines and transmission system reconfiguration). In addition, the HVDC system shall not interact with other plant controllers in the close electrical proximity in an unstable manner.

Finally, the high controlabillity of the HVDC system could be potentially used for the enhancement of small signal stability of AC grids. The implementation of power system oscillations damping is not a mandatory requirement as given in the NC-HVDC. In that frame it can be applied only if system operators require for it. The power oscillation damping (POD) controllers tuning for HVDC systems is a time consuming process which requires adequate identification of the active modes in the power grid.

2.4.6. REQUIREMENTS RELATED TO THE FREQUENCY CONTROL

The network Code HVDC (NC-HVDC) [135] stipulates that an HVDC connected offshore wind power plant shall have access to the measured onshore power system frequency measured at the onshore grid connection point. Fiber-optic is the most commonly used and proven communication technology nowadays. It is commonly embedded in the offshore HVDC cable which connects the onshore and the offshore converters without placing additional equipment costs. A maximum time delay of 0.1s is allowed between the time of the measurement to the activation of the fast active power response. The NC-HVDC defines the frequency ranges between 49.0-51.Hz for normal variations in the island AC offshore grid connected to the HVDC station.

3

Fault Ride Through Compliance for Balanced and Unbalanced Faults

3.1. Introduction

Voltage source AC/DC converters experience double synchronous frequency ripples visible in the active power and DC voltage when exposed to unbalanced AC grid voltages [136]. A variety of control techniques to mitigate this phenomenon have been proposed initially for low power converters [137], [138] and later expanded to wind turbine applications [139], [140], [141]. Next to the design of such negative sequence current control schemes, their effect on the protection of AC transmission systems is stressed in [142] for the case of AC connected wind power plants.

For VSC-HVDC applications, an analysis on negative sequence current control for the particular case of embedded in the power system VSC-HVDC link is presented in [143]. In [144], the unbalanced fault response of the offshore wind power plants with VSC-HVDC connection is investigated for the first time during offshore AC faults. The emphasis is placed on the double frequency harmonic mitigation for single-line-to ground faults applied at the offshore collector grid. However, it is not investigated how the VSC-HVDC system and the offshore wind turbines connected ensure that their over-current capacity is not violated during the combined positive and the negative sequence current injections. In that prospect, a step-wise adaptive positive and negative sequence current limiting control scheme is discussed in [145]. The method demonstrates satisfactory results, however, the over-current capacity of the VSC-HVDC station is over-sized compared to what it is commonly used in real system applications.

The fault ride through (FRT) capability is nowadays a mandatory requirement for VSC-HVDC systems [135]. A variety of FRT strategies for offshore VSC-HVDC systems have been documented in the literature, using either offline simulations [146], [27], [147], [148] or real time digital simulators (RTDS) [149]. In vast majority of these papers, the

offshore island AC system is aggregated by an equivalent wind turbine model which is directly connected to the HVDC station, neglecting the potential effect of the offshore AC island grid. Furthermore, the voltage drop FRT strategy is studied in [27], [147],[148] only for balanced faults using very simple control schemes at the offshore HVDC converter station and not the state of the art cascaded current-controller that manufacturers utilize today. Although, recently a lot of research effort is spent on the new generation of HVDC transmission, the MMC-HVDC [150], [151], [152], [153] yet a number of issues related to the two-level HVDC links need to be addressed.

This chapter proposes an improved voltage drop FRT control strategy which enables the offshore wind turbines to participate in the overall FRT compliance of the VSC-HVDC link during onshore AC grid faults. The voltage drop FRT strategy is enhanced here by applying an active current reduction control loop to the offshore wind turbines. The latter is implemented as a function of the imposed AC voltage drop by the offshore HVDC station without communication resources. When unbalanced onshore AC grid faults are applied, a current limiting control module with positive sequence current priority is applied at the onshore VSC-HVDC station. Furthermore, this current limiter is supported by a negative-sequence-voltage-dependent (NSVD) active current reduction module which enables a higher injection of the negative sequence current while at the same time respecting the over-current capacity of the HVDC station. For the case of offshore AC grid faults, an enhanced control scheme is presented which enables FRT compliance of the offshore VSC-HVDC station for faults at its terminals. The proposed controllers are tested for balanced and for unbalanced AC grid faults (namely for line-line and single-line-to-ground) at the onshore and offshore AC terminals where FRT compliance need to be demonstrated.

3.2. OFFSHORE VSC-HVDC TEST SYSTEM

A 200km VSC-HVDC link is used in this chapter with rated direct voltage at +/-250kV. It provides grid connection to a 700MW offshore wind power plant. Two-level VSC-HVDC technology is assumed. The grid side VSC-HVDC station (GSVSC) is interfaced to the infinite grid through a 30km transmission line at 380kV as it is presented in figure 3.1. The offshore AC island grid consists of two HVAC cables at the 150kV voltage level. A pair of three-winding transformers are used to interface the 150kV cables to the 33kV feeders. Detailed models are used for the three winding transformers including their saturation effect. The offshore AC island HVAC cables are represented with a pi-equivalent model with 7.5km and 4.5km length respectively. The group of the wind turbines connected per each feeder are aggregated to an equivalent full converter permanent magnet wind turbine EMT-model connected at the 33kV terminal.

3.3. UNIFIED VSC DYNAMIC MODEL

3.3.1. POSITIVE AND NEGATIVE SEQUENCE DQ REFERENCE FRAMES

Any unbalanced three phase variable, under the assumption of no zero sequence component, can be described mathematically as the sum of the positive and the negative sequence signal as it is shown in 3.1.

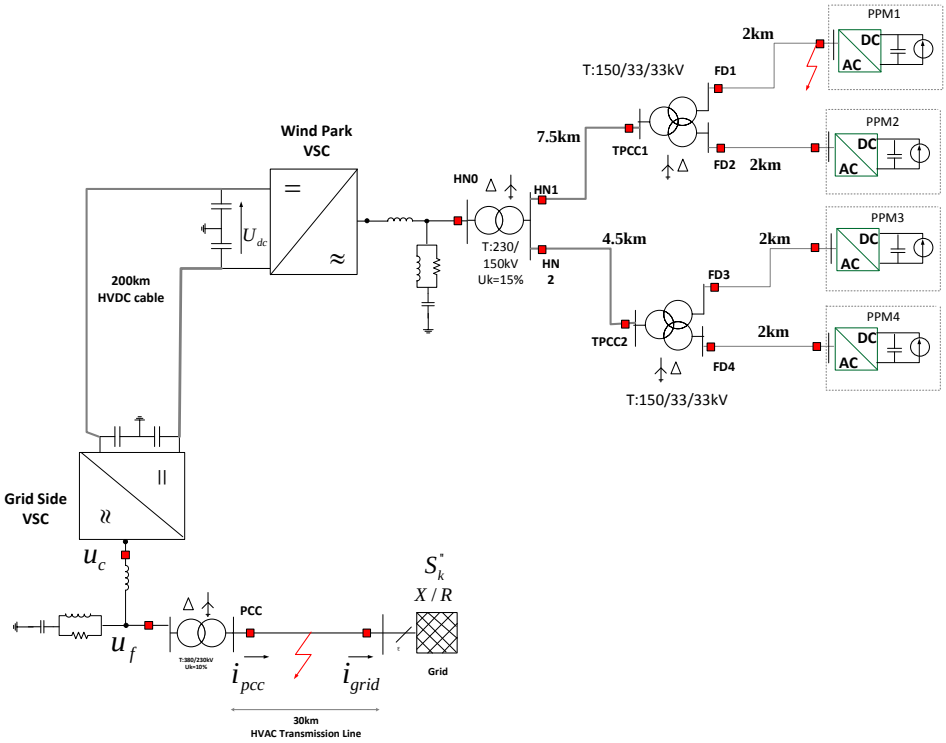

Figure 3.1: The VSC-HVDC transmission system and the connected offshore wind power plant as it is used in this chapter.

$$f_{abc}(t) = f^{+}_{abc}(t) + f^{-}_{abc}(t) \tag{3.1}$$

Let assume a positive sequence dq^{+} reference frame rotating with the synchronous frequency and a negative sequence dq^{-} frame rotating in the counterclockwise direction. The variables in the positive and the negative rotating dq reference frames are defined as:

$$f^{+}_{dq} = T(\theta) f^{+}_{abc}(t) \tag{3.2}$$

$$f^{-}_{dq} = T(-\theta) f^{-}_{abc}(t) \tag{3.3}$$

where $\theta = \omega t$ and $T(\theta)$ is given as:

$$T(\theta) = \frac{2}{3} \begin{pmatrix} cos(\theta) & cos(\theta - 2\pi/3) & cos(\theta - 4\pi/3) \\ -sin(\theta) & -sin(\theta - 2\pi/3) & -sin(\theta - 4\pi/3) \end{pmatrix}$$

Similarly the time domain instantaneous signal can be recovered from the positive and the negative sequence dq components by the equation 3.4.

$$f_{abc} = T^{-1}(\theta) f_{dq}^{+} + T^{-1}(-\theta) f_{dq}^{-} \tag{3.4}$$

where:

$$T^{-1}(\theta) = \begin{pmatrix} cos(\theta) & -sin(\theta) \\ cos(\theta - 2\pi/3) & -sin(\theta - 2\pi/3) \\ -cos(\theta - 4\pi/3) & -sin(\theta - 4\pi/3) \end{pmatrix}$$

Let us define as u_c the internal voltage of the onshore converter station, u_f the filter voltage and i the current flowing in the AC reactor. The differential equations of the converter model in the positive sequence dq frame are given by equations 3.5 and 3.6. In these equations, u_{fd+} and u_{fq+} are the positive sequence dq components of the filter voltage, u_{cd+} and u_{cq+} are the dq components of the internal voltage of the converter and i_{d+} and i_{q+} are the phase reactor dq current components. Similarly, the differential equations which describe the converter negative sequence components in the dq frame are given in 3.7 and 3.8. In the same way as for the positive sequence components, u_{fd-} and u_{fq-} are the negative sequence components of the dq filter voltage, u_{cd-} and u_{cq-} are the negative sequence dq components of the internal voltage of the converter and i_{d-} and i_{q-} are the phase reactor dq negative sequence current components. R is the resistance of the phase reactor and L the inductance. The system described by 3.5 to 3.8 can be visualized as the composition of the "positive-sequence subsystem" and the "negative-sequence subsystem" . In next sections the control of the sequence subsystems will be discussed.

$$\frac{di_{d+}}{dt} = -\frac{R}{L} i_{d+} + \omega i_{q+} + \frac{u_{cd+}}{L} - \frac{u_{fd+}}{L} \tag{3.5}$$

$$\frac{di_{q+}}{dt} = -\frac{R}{L} i_{q+} - \omega i_{d+} + \frac{u_{cq+}}{L} - \frac{u_{fq+}}{L} \tag{3.6}$$

$$\frac{di_{d-}}{dt} = -\frac{R}{L} i_{d-} - \omega i_{q-} + \frac{u_{cd-}}{L} - \frac{u_{fd-}}{L} \tag{3.7}$$

$$\frac{di_{q-}}{dt} = -\frac{R}{L} i_{q-} + \omega i_{d-} + \frac{u_{cq-}}{L} - \frac{u_{fq-}}{L} \tag{3.8}$$

3.3.2. SEPARATION OF THE INSTANTANEOUS SIGNAL TO POSITIVE AND NEGATIVE SEQUENCE COMPONENTS

In the decoupled control of positive and negative sequence current, the Park transformation uses the instantaneous positive and negative sequence values of the voltages and currents. The later are calculated online with the control block of figure 3.2.

As it can be observed, the simplified Clark transformation is used in order to derive the alpha-beta variables from the instantaneous variables. Then the positive and negative sequence components of the alpha-beta variables are defined as shown in figure 3.2. At the last stage, the inverse simplified Clark is performed for obtaining the positive and the negative sequence components. The Simplified Clark transformation as used are presented as follows:

$$C = \frac{2}{3}\begin{pmatrix} 1 & -\frac{1}{2} & -\frac{1}{2} \\ 0 & \frac{\sqrt{3}}{2} & -\frac{\sqrt{3}}{3} \end{pmatrix}$$

while the inverse Clark is defined as:

$$C^{-1} = \frac{3}{2}\begin{pmatrix} \frac{2}{3} & 0 \\ -\frac{1}{3} & \frac{\sqrt{3}}{3} \\ -\frac{1}{3} & -\frac{\sqrt{3}}{3} \end{pmatrix}$$

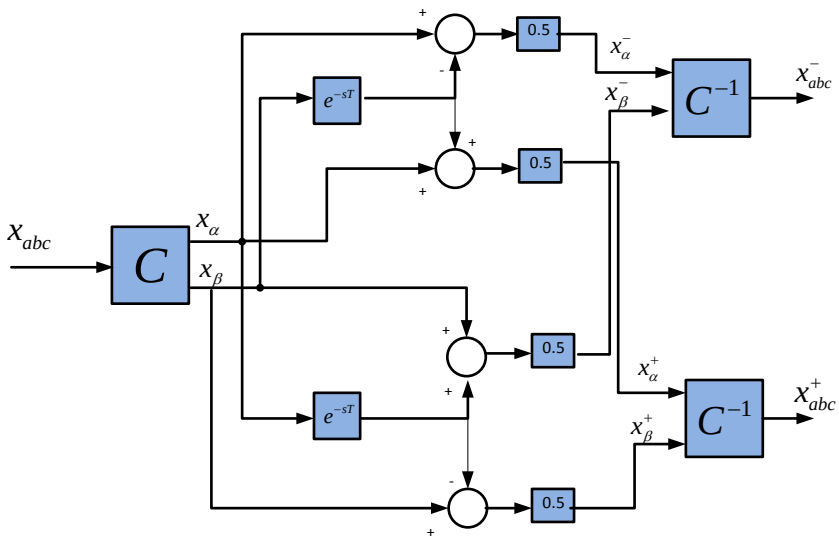

Figure 3.2: Control block for the separation of the positive and the negative instantaneous values of current and voltage.

3.3.3. GENERIC PHASE-LOCKED LOOP MODEL

A very important task for the successful control of the voltage source converter station during unbalanced grid faults is the extraction of the positive and negative sequence dq components. This task has been performed in this chapter by making use of the phase-lock loop (PLL) presented in figure 3.3. The PLL uses equations 3.2 and 3.3 in order to transform the instantaneous voltage of the filter u_f to its dq components. It should be noted that the positive and the negative instantaneous values of the voltage are used, derived from the block of figure 3.2. In addition, the angle θ is regulated by a PI-regulator such as u_{fq+} is zero in steady state . By controlling the u_{fq+} to zero, the u_{fd+} is allied with the vector of the u_f. The latter is rotating with the synchronous speed, which means that in steady state $\theta = \omega t$. The angle θ is multiplied by -1 in order to define the negative sequence dq-components given that the negative sequence voltage vector rotates in the opposite direction to the positive sequence voltage.

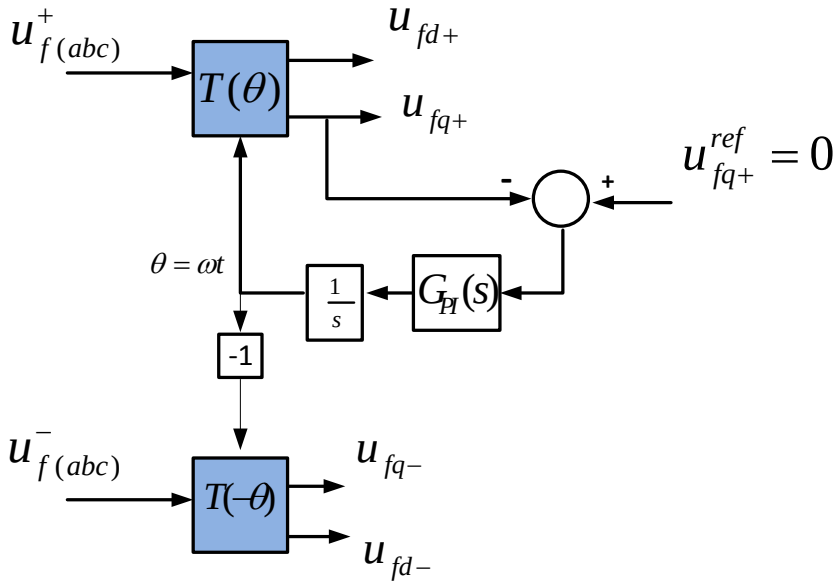

Figure 3.3: Block diagram of the PLL used to extract the positive and negative sequence dq components of the voltage and the angle theta.

This type of PLL is ofter called synchronous reference frame PLL (SRF-PLL). It is worth to mention that the selection of the PI-regulator parameters in the SRF-PLL is a tedious process which needs to take into account the stiffness of the grid connection point. In this chapter, the focus is placed mainly on a stiff grid connection points.

3.4. MODEL AND CONTROL OF THE ONSHORE VSC-HVDC STATION

The differential equation 3.5 to 3.8 stipulate that the postive and negative sequence current injections of the converter station can be controlled independently in the positive and negative rotating dq frames. In this context, the dual synchronous reference frame (SRF) control scheme, is utilized at the onshore HVDC converter station [136]. Figure 3.4 presents the control system layout of the onshore converter HVDC station. A SRF-PLL (Phase Lock Loop) is utilized both for the positive and for the negative sequence current control modules. Notch filters, adequately tuned have been applied in order to filter out the double synchronous frequency oscillations which appear in the measured dq-voltages and currents components during unbalanced fault conditions.

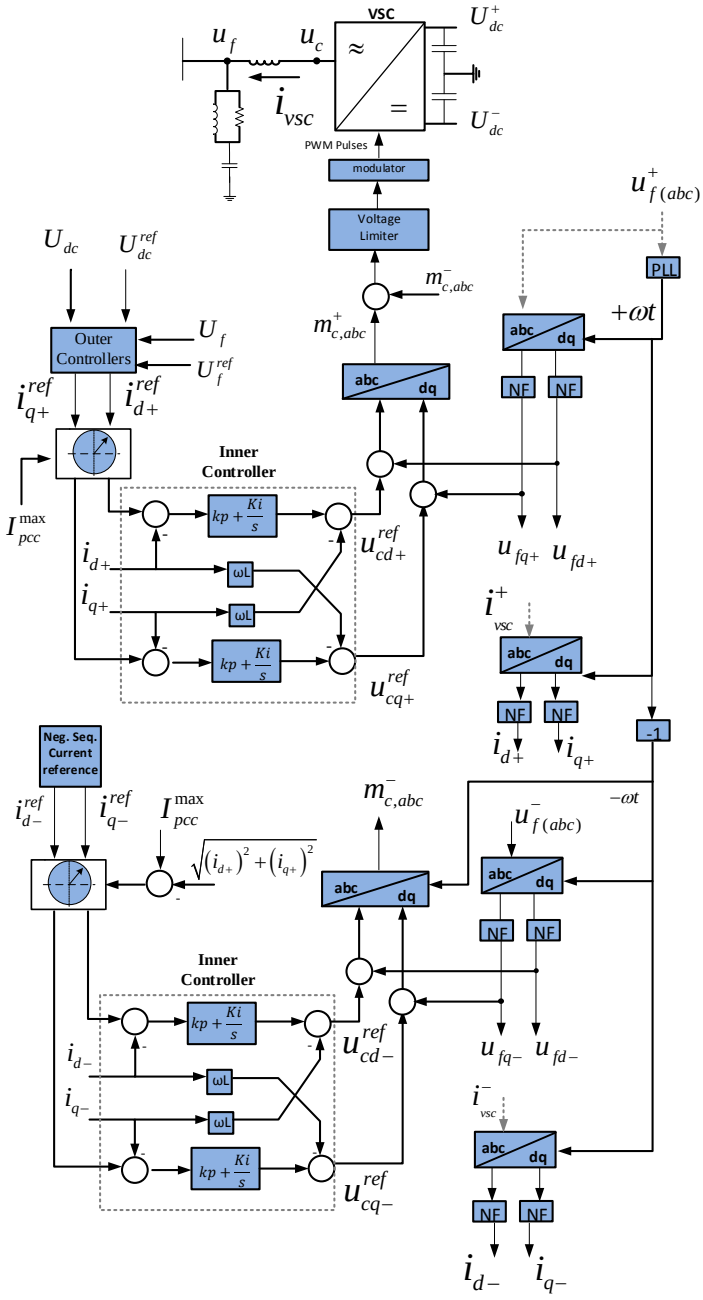

Figure 3.4: Positive and negative sequence current control loops as implemented at the onshore HVDC converter station. Positive sequence variables are denoted with "+" while negative sequence variables are denoted with "–".

3.4.1. POSITIVE SEQUENCE OUTER CURRENT CONTROL LOOP

The positive sequence active current component (d+ axis) of the onshore converter station is assigned to control the direct voltage of the VSC-HVDC link. The controller is mathematically defined in time domain by (equation 3.9), where $K_{p,U_{dc}}$, is the proportional gain, $T_{i,U_{dc}}$ is the time constant of the PI regulator and U_{dc} is the pole-to-pole measured direct voltage of the HVDC link at the onshore DC terminals.

$$i_{d+}^{ref} = K_{p,U_{dc}}(U_{dc}^{ref} - U_{dc}) + \int \frac{(U_{dc}^{ref} - U_{dc})}{T_{i,U_{dc}}} dt \tag{3.9}$$

The reactive current control loop provides continuous AC voltage control during normal voltage conditions (with time constants in seconds range) and a fast reactive short circuit current injection during AC system falts (with time constants of milliseconds range). The reactive current control loop is defined by the equation (3.10) where $K_{p,U_{ac}}$ is the proportional gain of the AC voltage PI controller while $T_{i,U_{ac}}$ is the PI-regulator time constant. Furthermore, i_q^{LVRT} accounts for the short circuit current injection of the converter station which is provided additionally during the FRT period.

$$i_{q+}^{ref} = i_{q+}^{LVRT} + K_{p,U_{ac}}(U_f^{ref} - U_f) + \int \frac{(U_f^{ref} - U_f)}{T_{i,U_{ac}}} dt \tag{3.10}$$

The positive sequence reactive short-circuit current injection i_q^{LVRT} is provided with a proportional gain k_1 added to the slow in its response PI-Based AC voltage controller. The description of the reactive short circuit current injection is given by equation (3.11), where, k_1 is the reactive current boosting gain (with values between 2 and 10 in per unit) and $U_f^{th,min}$ and $U_f^{th,max}$ is the lower and upper boundary of the voltage dead-band where the reactive current injection is inactive.

$$i_{q+}^{LVRT} = \begin{cases} k_1(U_f^{ref} - U_f), 0 \le U_f \le U_f^{th,min} \\ 0, U_f^{th,min} \le U_f \le U_f^{th,max} \end{cases} \tag{3.11}$$

Beside the slow AC voltage control loop, it is possible to control the reactive power of the VSC by substituting equation (3.10) by the equation (3.12).

$$i_{q+}^{ref} = i_{q+}^{LVRT} + K_{p,Q_{ac}}(Q^{ref} - Q) + \int \frac{(Q^{ref} - Q)}{T_{i,Q_{ac}}} dt \tag{3.12}$$

The time constant $T_{i,Q_{ac}}$ defines the response of the slow controller and can be adequately selected in order to achieve the anticipated response. Q and Q_{ref} is the measured and reference reactive power the PCC terminal.

3.4.2. NEGATIVE SEQUENCE OUTER CURRENT CONTROL LOOPS

Grid codes require for HVDC power converters to be able to withstand negative sequence voltage and current components during unbalanced faults. However, grid codes do not make explicit the control strategy to be applied with respect to the negative sequece current control [135]. This shall be decided based on the grid connection point needs per

each project. It is the responsibility of the relevant TSO to define the behaviour of the VSC-HVDC link during unbalanced faults.

Normally, vendors apply negative sequence current suppression, as it ensures that the converter does not experience large unbalanced fault currents. The motivation for negative sequence current injection is derived from the need to enhance the fault detection capability in combined AC-DC transmission systems during the case of line-to-line AC faults.

SUPPRESSION OF THE NEGATIVE SEQUENCE CURRENT

The negative sequence current of the onshore converter station can be suppressed to the zero value during unbalanced voltages by applying the control references in (3.13). The dual SRF control scheme enables decoupled control of positive and negative sequence current of the VSC under the condition that the total current capacity of the VSC-HVDC station is respected.

$$i_{q-}^{ref} = i_{d-}^{ref} = 0 \tag{3.13}$$

NEGATIVE SEQUENCE CURRENT INJECTION

The second approach which is studied in this chapter is the injection of the negative sequence current proportionally to the negative sequence voltage measured measured at the filter. This is a fast injection of the negative sequence reactive current only happening during unbalanced AC grid faults. A proportional controller is used, with proportional gain equal to k_2. This follows the same principle as the injection of the positive sequence reactive current. The application of proportional controller is robust and stable in its response. During balanced grid voltage conditions, the dq-voltage components in the negative SRF are zero while during unbalanced faults they increase. These variables are already available and there is no need for additional measurement. In this way the amplitude of the negative sequence voltage can be used in order to inject proportionally a negative sequence reactive current. The applied negative sequence current references are:

$$i_{d-}^{ref} = 0 \tag{3.14}$$

$$i_{q-}^{ref} = k_2 \sqrt{(u_{fd-}{}^2) + (u_{fq-}{}^2)} \tag{3.15}$$

3.4.3. STATE MACHINE FOR THE ONSHORE VSC-HVDC STATION

The FRT and post-FRT response of the onshore VSC-HVDC station during balanced AC grid faults is managed by the proposed state machine presented in figure 3.5. The use of this state machine provides a clear distinction of different operating states of the onshore converter while at the same time it defines the expected behaviour of VSC-HVDC station. The input of the state machine is the positive sequence d+ axis voltage component. In the range between 0.9-1.1 p.u, the onshore HVDC converter station operates in normal condition (state S1). In the sate S1, the converter utilizes the controller 3.9 or the controller 3.10.

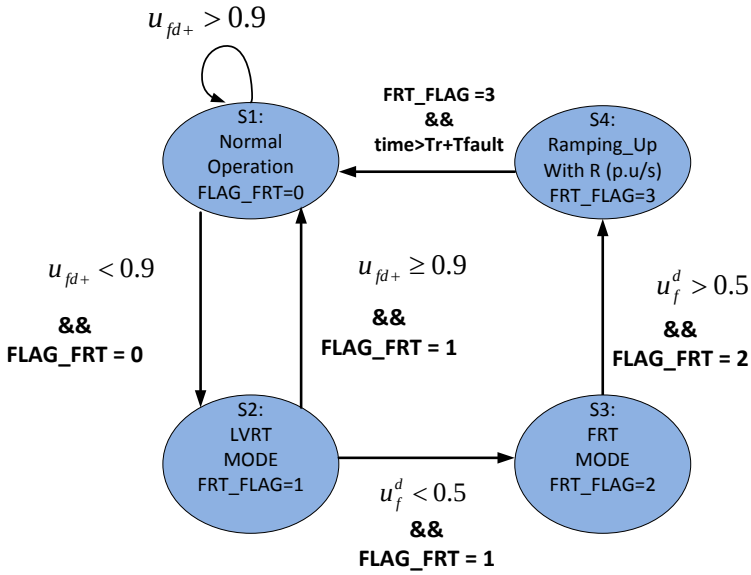

Figure 3.5: State machine for the LVRT, FRT and post-FRT control logic which allows the implementation of the ramp-up function during the post-fault period (Tr is the ramping time calculated based on the ramping rate R, while Tfault is the time that the fault is applied).

When u_{fd+} drops below the 0.9 p.u threshold, the onshore HVDC station operation shifts towards the LVRT state (S2). In the state (S2), the controller (3.11) is applied, and the converter injects positive sequence reactive current. Reactive current limiting priority is applied when the over-current capacity of the VSC station is reached. The converter supports the AC system voltage by injecting reactive current activating the i_{q+}^{LVRT} whilst the PI-regulator of the slow AC voltage controller (equation 3.10) is set to freeze. Similarly, the PI-regulator of the direct voltage controller (equation 3.9) of the HVDC link is set to the freeze mode and the duty of the HVDC link power balancing is explicitly managed by the FRT control scheme. The selection of the value u_{fd+} is done such as the state machine could operate both during balanced and unbalanced grid faults.

When u_{fd+} voltage drops below the 0.5 p.u threshold, the converter enters the FRT mode (S3). In the FRT mode (S3) given that at least a reactive current boosting gain 2 p.u is used (as it is commonly required by most of grid codes), the positive sequence reactive current is taking all the fault current capacity, whilst the active current is reduced to zero. Again in state (S3), equation 3.11 is applied. The choice of the 0.5p.u voltage threshold is based on the fact that for AC voltages below 0.5 p.u, the reactive current injection leads to active current reduction to the zero value by the positive sequence current limiter. Consequently, post-fault as soon as the voltage recovers, the converter shall move to state (S4), where a smooth ramping is ensured.

For the case of voltage drops which are above the 0.5p.u threshold, the converter returns from (S2) back to state (S1) without applying any ramping. In the ramp-up state (S4), the active current is ramped following a predefined ramping rate R (pu/s). The

selected ramping rate is a trade-off which affects the dynamic response of the AC system, as presented in [147]. The converter remains in the ramping state for a period T_r which ensures that the active current is ramped to the pre-fault level. Throughout the LVRT, FRT and ramp-up states of the HVDC link, the direct voltage controller (3.9) and the slow AC voltage controller (controller 3.10) are blocked.

3.4.4. CURRENT LIMITATION WITH POSITIVE SEQUENCE CURRENT PRIORITY

The injection of combined positive and negative sequence current during unbalanced faults shall respect the total fault current capability of the converter station. For that purpose, the limitation strategy applies here a positive sequence current limitation priority, as it is presented in figure 3.4. The positive sequence maximum current limit is constant and it is equal to the over-current capacity of the converter (1.1 p.u). The negative sequence current limit I_{max2} is regulated based on the available over-current capacity. It uses as input signal the measured positive sequence current injection of the converter station. The module then calculates on line the available over-current capacity left for the negative sequence current injection during unbalanced faults.

3.5. EMT MODEL AND CONTROL SCHEMES OF THE OFFSHORE VSC-HVDC STATION

The voltage and the frequency of the offshore AC island grid is provided completely by the offshore VSC-HVDC station. It applies a grid forming control scheme. The control scheme of the offshore VSC station is presented in figure 3.6. In this control approach, an oscillator is used at the offshore converter station. The angle of the oscillator is corrected by the PI regulator in order to ensure the 50 Hz frequency in the island system. Although the oscillator provides a fixed frequency, the angle has to be regulated such as the offshore HVDC station operates as a power sink. If the internal converter voltage angle is not regulated, the system will be unstable to the wind power variations. The most important elements of the offshore HVDC station are namely the frequency regulator, the current controller, the controller reference block and the dq to abc Park Transformation blocks.

It is worth to observe that the total inertia of the island grid is negligible, depending on the type of the installed wind turbines. For example, in the case of full converter wind power plant, the rotating inertia directly connected to the island grid is zero. Hence, the frequency control of the island grid is driven mainly by the VSC-HVDC station.

3.5.1. FREQUENCY REGULATOR

The frequency regulator controls the offshore AC island grid frequency. This is performed by providing the adequate phase angle to the oscillator block as presented in figure 3.6. It is important to stress that the control scheme used here is similar to the power synchronization control. The difference in this chapter approach lies on the fact that the frequency is regulated and not the active power. No PLL is used in this case since the angle is provided by the frequency regulator. However, although such an approach is very efficient and provides a stable response during normal conditions, it cannot limit

the fault current during faults applied electrically close to the VSC terminals. In that case a PLL is needed in order to shift the operation of the VSC station from voltage controlled to current controlled model. In the following paragraph, a control scheme will be presented which enables fault ride through for the offshore VSC-HVDC station.

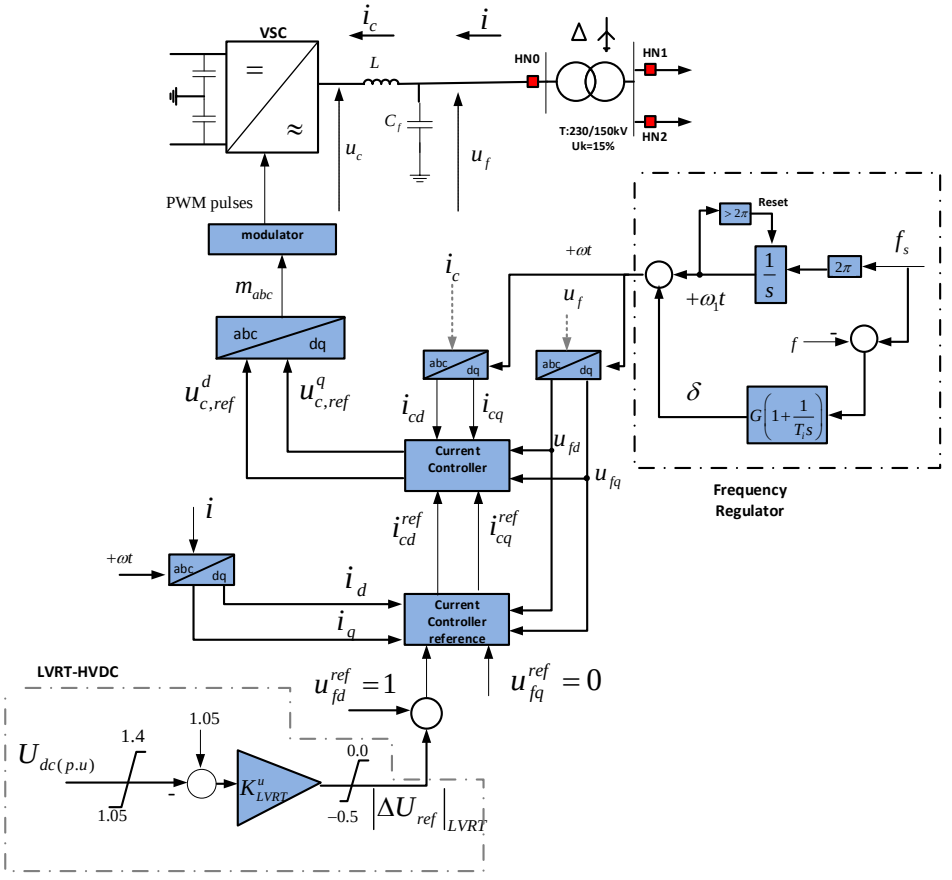

Figure 3.6: Offshore converter station model and its control loops. In the figure with dashed lines is the frequency regulator control loop and the control block for voltage drop FRT strategy.

3.5.2. CURRENT CONTROLLER

The control of the offshore HVDC station consists of a cascaded scheme with an inner current controller which sets the inner voltage reference of the converter and an outer current controller reference block, which provides current references.

The equations which describe the inner current controller are given in (3.16) and (3.17) where L is the inductance of the phase reactor and R its resistance. In addition, k_{p3} and k_{p4} are the proportional gains and T_{I3} and T_{I4} the time constants of the integral part of the PI-regulator. The output of the equations (3.18) and (3.19)are used to define

the internal dq-voltage of the converter station.

$$u^{d}_{c,ref} = i_{cd}R - \omega L i_{cq} - k_{p3}(i^{ref}_{cd} - i_{cd}) + \int \frac{i^{ref}_{cd} - i_{cd}}{T_{i3}}\, dt \tag{3.16}$$

$$u^{q}_{c,ref} = i_{cq}R + \omega L i_{cq} - k_{p4}(i^{ref}_{cq} - i_{cq}) + \int \frac{i^{ref}_{cq} - i_{cq}}{T_{i4}}\, dt \tag{3.17}$$

3.5.3. CURRENT CONTROLLER REFERENCE

The equations which describe the calculation of the inner current control loop references are given in 3.18 and 3.19. In these equations, id is the d-axis current flowing of the fliter, k_{p1} and k_{p2} the proportional gains and T_{I1} and T_{I2} the time constants of the integral part of the PI-regulator. The current controller reference block, defines the reference of offshore HVDC station current in the dq-frame such as the the dq-components of the filter voltage is regulated at the desired reference. The dq-reference current is then applied to the current controller. u_{fd} and u_{fq} are the filter voltage and C_f is the filter capacitance.

$$i^{ref}_{cd} = i_d - \omega C_f u_{fq} + k_{p1}(u^{ref}_{fd} - u_{fd}) + \int \frac{u^{ref}_{fd} - u_{fd}}{T_{i1}}\, dt \tag{3.18}$$

$$i^{ref}_{cq} = i_q - \omega C_f u_{fq} + k_{p2}(u^{ref}_{fq} - u_{fq}) + \int \frac{u^{ref}_{fq} - u_{fq}}{T_{i2}}\, dt \tag{3.19}$$

3.5.4. CONTROLLED AC VOLTAGE DROP FRT STRATEGY FOR THE HVDC LINK

When faults are applied at the terminals of the onshore VSC-HVDC station, the active power of the onshore station is zero (since voltage is zero) while at the same time the power in-feed in the HVDC link from the offshore HVDC station does not change. This results in a power imbalance between the onshore and the offshore station which creates direct over-voltages in the HVDC link since the energy is stored in the DC capacitors. Beside the classical chopper based strategy to limit the over-voltage, the coordinated offshore AC voltage drop FRT compliance strategy is assessed in this chapter.

The controlled offshore AC voltage drop FRT strategy is applied as presented in figure 3.6 (termed here as "LVRT-HVDC" module). The voltage drop is applied proportionally to the HVDC link direct voltage when the voltage exceeds the 1.05p.u threshold as it is measured at the offshore DC terminal. The benefit from the reduction of the internal converter voltage is the reduction of the active power at offshore HVDC converter during AC grid onshore faults. This provides a balancing effect in the DC link and ensures controlled over-voltage levels.

In this chapter the "LVRT-HVDC" controller is designed so that the applied AC voltage does not drop below the 0.5 p.u threshold, for the case of faults at the onshore AC terminal. This threshold is set in order to limit the electrical stresses imposed at the island grid. Furthermore, in order to enhance the FRT compliance of the onshore HVDC converter

station, an additional control loop is proposed here at the wind turbines. This control loop applies a positive-sequence-voltage-dependent (PSVD) active current reduction at the wind turbines as it will be discussed in following paragraph. Detailed description is provided in following section o of this chapter. The reason for the participation of the wind turbines in the FRT compliance of the onshore station is twofold. First it reduces the delivered active power, bringing power balance to the HVDC link while at the same time enabling the power to be dissipated in the wind turbine choppers. Secondly, it reduces the currents in the offshore island as will be shown in the next paragraph. No communication resources is needed in this case.

3.5.5. THEORETICAL DISCUSSION ON THE GRID FORMING CONTROL SCHEME

The grid forming control scheme presented in figure 3.6 uses an oscillator in order to provide the reference frequency (50Hz). The dq-frame that the control scheme is developed is corrected by the angle δ. Figure 3.7 presents the phasor diagram and the dq-frame that the control is implemented. The grid forming scheme is capable of regulating the angle δ_{cf} between $\underline{U}_f$ and $\underline{U}_c$, via the current adjustment of the converter station. By controlling the amplitude of $\underline{U}_f$ at 1 p.u and by regulating the angle δ, the offshore HVDC station operates as a slack bus for the offshore AC island grid.

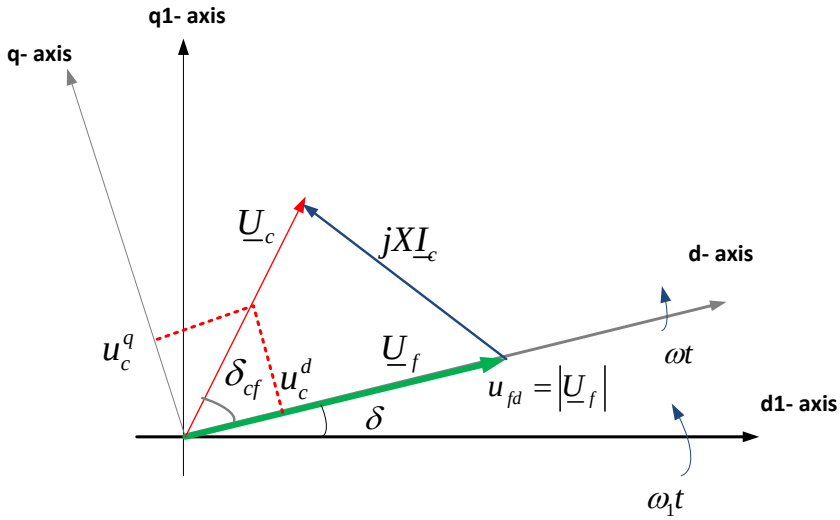

Figure 3.7: Phasor diagram explaining the operation of the grid forming control scheme applied at the offshore HVDC station for resistance of the phase reactor (R) equal to zero. X is the reactance of the phase reactor.

3.6. FAULT RIDE THROUGH CONTROL SCHEME FOR THE OFFSHORE VSC-HVDC CONVERTER STATION

There is a fundamental difference between the onshore and the offshore VSC-HVDC station with respect to their fault response. The onshore VSC-HVDC station using typical PLL techniques applies a current controlled approach. During AC grid faults, the onshore HVDC station remains grid connected providing short circuit current injection. As soon as the fault is cleared, the voltage recovers in the grid and the onshore station returns to its normal operation. The voltage recovery during the post-fault period is an inherent characteristic of the power systems, itself, affected by the short circuit power level and the reactive power flows in the grid.

At the remote offshore AC island grid, the voltage is provided explicitly by the VSC-HVDC station (using a grid forming control scheme). Hence, when a fault is applied at the remote offshore AC island grid, the HVDC converter shall be capable to perform three tasks. First, remain connected to the island grid providing its fault current capacity as reactive current injection. Second, ensure that the fault current is bounded by the converters fault current capacity. Third, restore the voltage in the island grid to the pre-fault value during the post-fault period. The challenge is that unlike the current controlled voltage source converters, the grid forming control is weak at performing the task of limiting the current, especially for faults electrical close to it. The problem with the grid forming control scheme of figure 3.6 is that it does not provide current limiting capability during AC grid faults in the offshore AC island. The frequency regulator does not remain stable during the fault and especially, during post-fault period. In addition, the current controller could ensure rated current only during normal operation but not during grid faults.

So far, there is not much work done with respect to the fault ride though behaviour of the remote offhsore AC island network during faults at the offshore VSC-HVDC station terminal (HV Cable side). Commonly, in grid connection studies the offshore island grid is represented by a voltage source with very low short circuit ratio, typically one. However, this very simplified approach does not take into account the actual dynamic behavior of the offshore station neither the possible control interactions between the wind turbines. An intersting study for the FRT capability of a weak island grid is presented in [78] for the power synchronization control strategy. This study presents the response of the power synchronization control for the case of an offshore fault. However, no detail description was given on the way that the offshore station deals with the offshore fault at its terminal.

In this paragraph, an improved grid forming control strategy for the offshore VSC-HVDC is defined. It has the advantage that it allows the offshore VSC-HVDC station to remain connected to the island grid during offshore AC faults at its terminal. Moreover, it is capable to provide the rated fault current capacity as a reactive current injection, which supports the island grid short term voltage stability during offshore faults. Figure 3.8 presents the complete control block of the enhanced offshore VSC-HVDC station strategy. The main principle of the proposed strategy is the shift from grid forming operation to current controlled mode during the fault period.

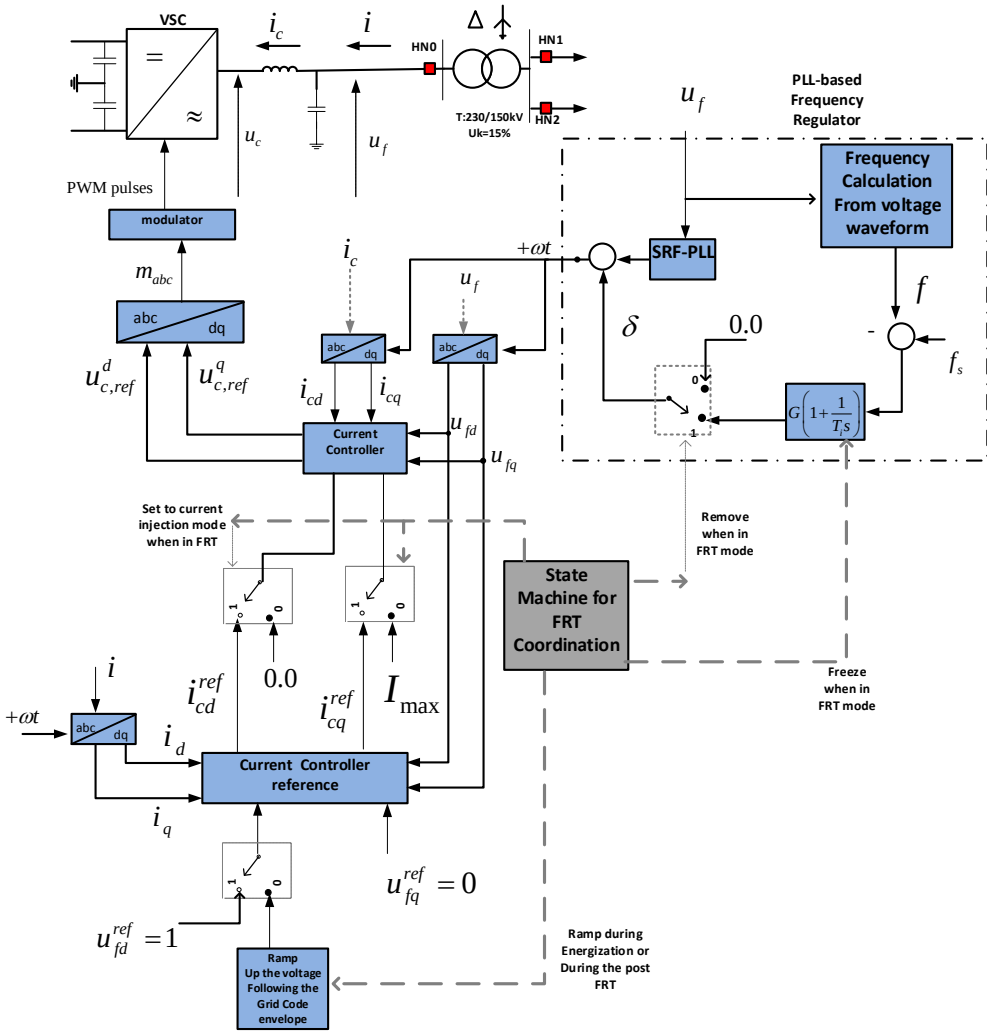

Figure 3.8: Offshore converter station model and its control loops. In the figure with dashed lines is the PLL-Based frequency regulator control loop.

3.6.1. PLL-BASED FREQUENCY REGULATOR

Compared to the conventional approach, the enhanced control scheme for the offshore converter station does not utilize an oscillator but a PLL. As already discussed, the oscillator provides the $\omega_1 t$. In the alternative approach presented in figure 3.8, a SRF-PLL is used. The angle in this case is ($\omega_{pll} t$) and not ($\omega_1 t$). It is provided by the PLL and regulated by the frequency regulator before it is passed directly to the Park transformation. The PLL is always online and its angle is available at any time. The phasor diagram of the proposed control is the same as with figure 3.7, with only difference that $\omega_1 = \omega_{pll}$. During normal voltage conditions, the offshore station operates in the grid forming control scheme using the PLL angle. However, during offshore faults close to the offshore station the control shifts to current control mode. The latter has the advantage of limiting the fault current of the offshore HVDC converter station.

As soon as a fault occurs close to the offshore VSC-HVDC station the voltage drops to almost zero value in the offshore island. The state machine control block sends a signal in order to instantly freeze and remove the frequency regulator from the control loop. The converter enters in typical current controlled mode. At the same time the state machine sets the current reference controller to freeze state and the i_{cq}^{ref} reference of the inner current controller is set to the maximum current of the HVDC station, provided as purely reactive current and the i_{cd}^{ref} to zero. The converter, remains in the fault current injection state till the fault is cleared. Here we assume a typical grid code fault ride through duration, which is 150ms. Once the fault is cleared, the converter shifts back to the grid forming operation mode and the offshore voltage is restored. At the same time, the frequency regulator and the current controller reference module is de-blocked.

3.6.2. OFFSHORE VSC CURRENT LIMITATION BY REDUCTION OF THE MODULATION INDEX

As discussed in the previous paragraph, it is only during AC faults close to the offshore VSC-HVDC station terminal that the voltage drops close to zero and the control shifts to current control mode in order to limit the fault currents experienced by the station.

However, when the voltage drop is not big (i.e for faults in the 33kV grid), the classical control approach of the figure 3.6 can provide limiting current capability in an effective way by means of modulation control. The reduction of the fault current experienced by the offshore VSC-HVDC station can be performed by the control block presented in figure 3.9.

As it can be seen, as soon as the maximum current is surpassed, the over-current detection and limitation block reduces the amplitude of the modulation index. The latter reduces the internal voltage of the converter leading eventually to lower fault currents.

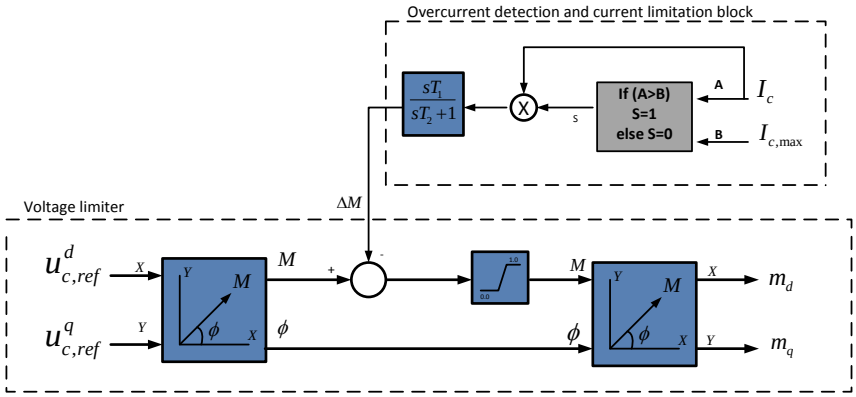

Figure 3.9: Limitation of the fault current experienced by the offshore station via internal converter voltage reduction.

As it can be seen in figure 3.9 the voltage limiter ensures that the modulation index of the converter is between the value zero and one. In addition, the overcurrent detection and current limitation block acts acts on the voltage limiter in order to reduce the modulation index. The reduction of the modulation index, would lead to the reduction of the converter's internal voltage which limits the current of the converter. This strategy is efficient for faults which occur in the 33kV feeders where the voltage at the converter does not drop to very low values due to the impedance of the HVAC cables and transformers.

3.7. MODEL AND CONTROL OF THE OFFSHORE WIND POWER PLANTS

3.7.1. FULL CONVERTER TYPE WIND TURBINE EMT-MODEL

The offshore wind power plant consists of full converter interfaced permanent magnet wind turbine generators (commonly referred as type-4 in the IEC-61400 standard). The aggregation of the power plant is performed per each feeder at the 33kV voltage level. An EMT type, average value model is utilized, presented in the figure 3.10.

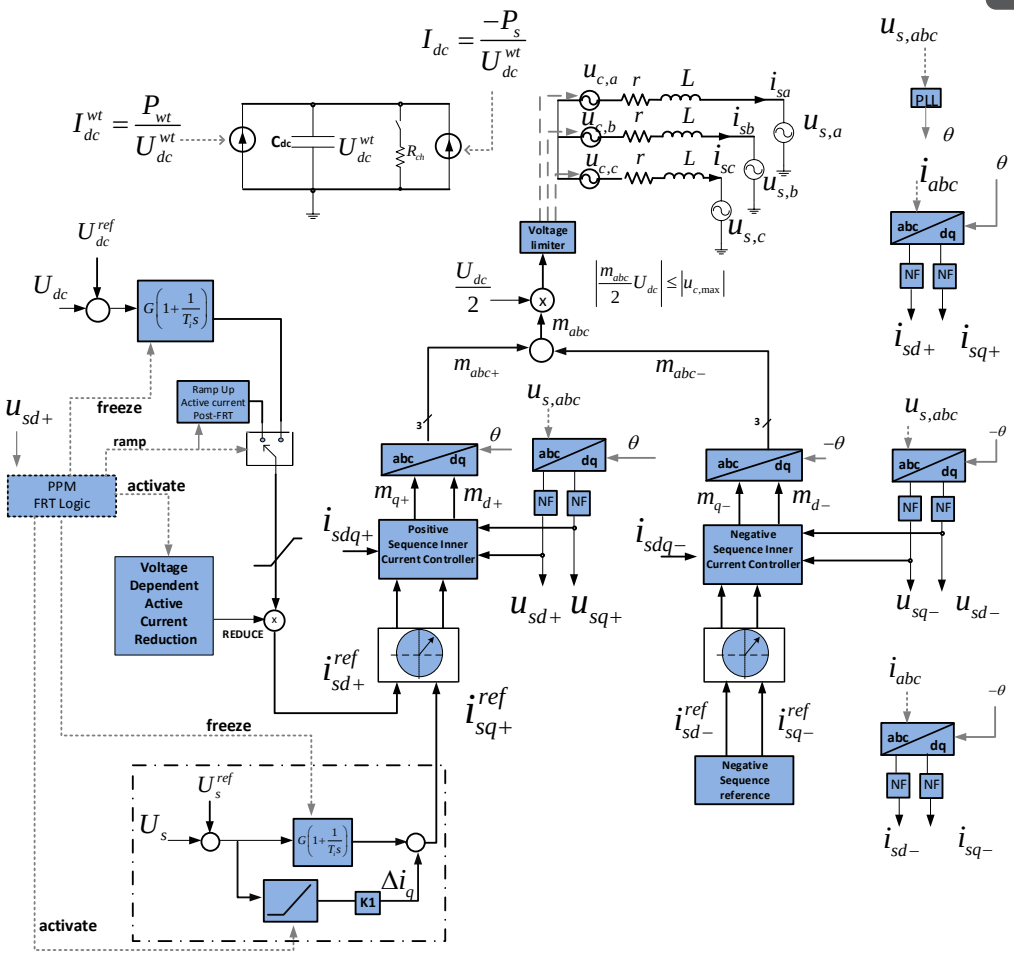

Figure 3.10: Positive and negative sequence current control loops of the type 4 offshore wind power plant model.

The inverter model of the wind turbine consists of positive and negative sequence current control loops. The permanent magnet generator and the generator side AC-DC rectifier are modelled here by a DC current injection. Since permanent magnet wind turbines utilize a DC chopper based FRT strategy, the electrical torque of the permanent magnet machine is completely decoupled from the AC grid voltage during AC grid faults. The later ensures that the speed of the permanent magnet generator is not affected through the FRT process.

3.7.2. WIND TURBINE POSITIVE SEQUENCE CURRENT CONTROL LOOPS

The positive sequence current control loop of the equivalent wind turbine model enables decoupled active and reactive power control. The inverter regulates the DC link voltage and the reactive power exchange with the AC island grid during normal operation. The reactive current control loop applies a PI regulator. It is capable to control the amplitude of the AC voltage at a given set point. During offshore grid faults, the wind turbines inject short circuit current. In figure 3.10, it can be seen that the outer controllers are set to the freeze state by the wind turbines during the FRT period. Furthermore, a ramp-up linear function is used for ramping the active current during the post fault period of the wind turbine. The coordination of different states is performed using a state machine. The next paragraph describes the states of the FRT logic for the wind turbine.

3.7.3. FRT LOGIC FOR THE WIND TURBINES

The FRT and post-FRT response of the wind power plants is guided by the state machine of figure 3.11. Similar to the onshore HVDC station, the state machine of the wind turbine is separated in four different operating states (S1-S4). The normal operating point state (S1) is defined for voltage values above 0.8 p.u. In this zone the wind turbine provides continuous AC voltage control (or reactive power control) to the island offshore AC collector grid. As soon as the AC voltage measured at the wind turbine terminals drops below the 0.8 p.u threshold, it enters in the state (S2).

There are two possible reasons for entering state (S2). First, due to the activation of the offshore VSC-HVDC station "LVRT-HVDC" block in figure 3.6. This basically occurs due to an onshore AC grid fault and the activation of the voltage drop FRT strategy. The second reason is an AC fault in the offshore AC island. In the state (S2), the wind turbine applies the positive-sequence-voltage-dependent (PSVD) active current reduction controller presented in figure 3.12. By means of design here, the wind turbines do not inject reactive current in the state (S2) since there is no presence of an offshore fault. The wind turbines only reduce their active current applying controller of figure 3.12.

Hence, this proposed approach enhances the voltage drop FRT strategy of the HVDC link during onshore AC grid faults since the wind turbines reduce the generated power. The reduced wind turbines active power is dissipated in the wind turbines choppers which are present by default in their DC bus. Only during physical faults in the offshore AC island grid would enter the wind turbines the state (S3). Only in the state (S3) will reactive current be injected. The slow AC voltage controller in the wind turbines is set to freeze mode for states (S2) to (S4).

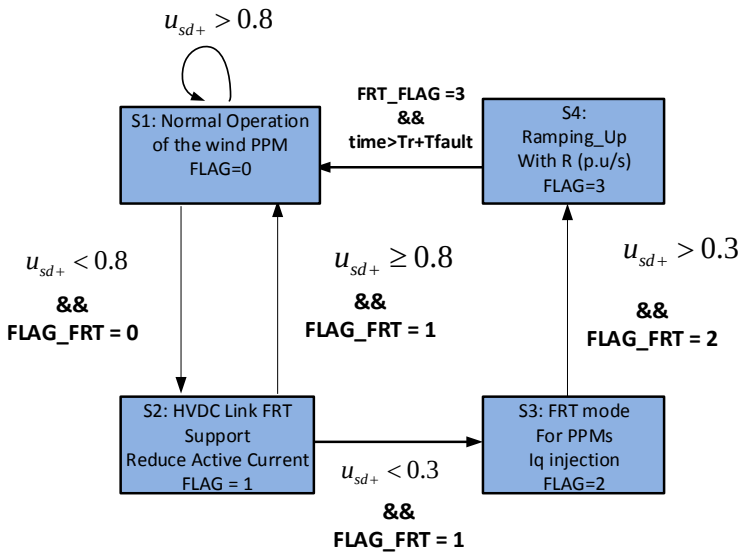

Figure 3.11: State machine for the full converter interfaced wind turbine average EMT-models.

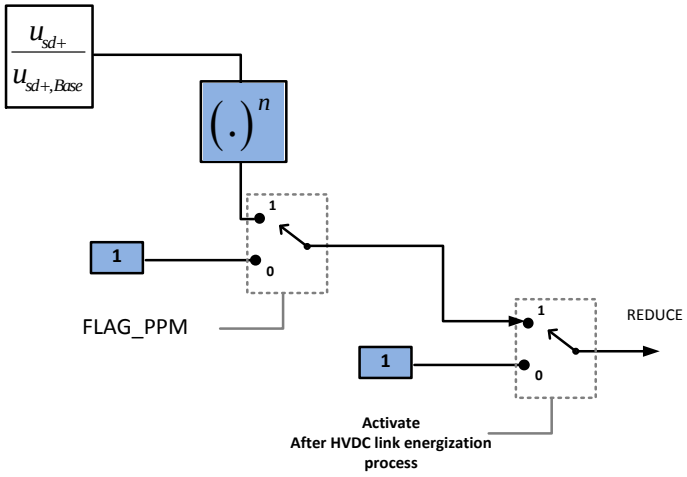

Figure 3.12: Positive-sequence-voltage-dependent (PSVD) active current reduction module for the offshore wind turbines with VSC-HVDC connection. The output of the controller is applied to the active current reference of the wind turbine.

In the case of an AC fault in the offshore AC island, the wind turbine enters the state (S3). In (S3), a fast reactive current injection takes place proportionally to the residual voltage. In this state, since a fault occurs in the offshore AC island, the wind turbines support the voltage and provide reactive fault current for the protection schemes to detect and clear the fault. Finally, being already in the state (S3), as soon as the wind turbines AC terminal voltage recovers, the wind turbines enter state (S4). Their active current is ramped-up, following a predefined ramp-up rate (p.u/s).

3.7.4. NEGATIVE SEQUENCE CURRENT CONTROL LOOPS

Modern wind turbines are equipped with negative sequence current control loops which enhance their dynamic performance during unbalanced AC faults. In this paper, a negative sequence current control loop as it is presented in figure 3.10 is applied. A variety of negative sequence current control strategies can be followed for the control of the negative sequence current during unbalanced grid faults. Similar to the onshore HVDC station case, two strategies are tested here for offshore AC grid unbalanced faults. The first strategy applies negative sequence current suppression and the second strategy negative sequence current injection proportionally to the negative sequence offshore voltage.

3.8. NEGATIVE SEQUENCE VOLTAGE DEPENDENT ACTIVE CURRENT REDUCTION

During unbalanced faults at the mainland AC transmission grid, the onshore converter HVDC station is loaded with positive and with negative sequence currents. The negative sequence current depends on the applied negative sequence current control strategy, as discussed in the previous section. The zero sequence current does not flow in the phase reactor due the delta side of the step-up transformer. It has been discussed, that positive sequence current priority is applied as current limitation strategy. In order to increase the share of the negative sequence current in the total onshore converter fault current injection, the positive sequence active current is reduced using the module in figure 3.13. We call it negative-sequence-voltage-dependent (NSVD) active current reduction.

This control module is used especially in case when the reactive positive sequence current injection is active during unbalanced faults. The negative sequence voltage component is an incremental quantity, typically zero or very small under normal conditions, producing no pre-fault restraining bias. With purpose to avoid unnecessary active current reduction during switching transients, a dead-band of 0.3 p.u is used. A quadratic function is applied to reduce the active current component. Hence, when the negative sequence current injection is selected as an option, the reduction of the positive sequence active current (id+), enables the share of the VSC current capacity only by the positive and the negative sequence reactive currents. It is worth to mention that if the grid code does not require for reactive positive sequence current injection during unbalanced faults, only the negative sequence current is injected following 3.14 and 3.15.

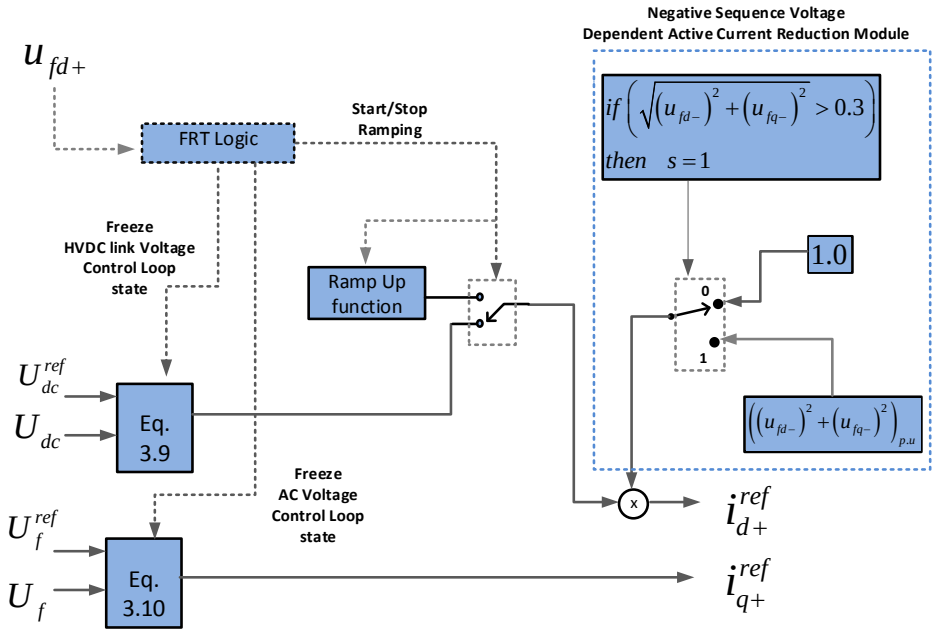

Figure 3.13: Negative sequence voltage dependent active current reduction for the onshore VSC-HVDC station.

3.9. SIMULATION RESULTS FOR ONSHORE FAULTS

The response of the enhanced FRT control strategy and the negative sequence current control loops are demonstrated for balanced as well as for unbalanced onshore faults. The benchmark test system as presented in chapter 3 is used. The response of the VSC-HVDC system and the connected wind power plants will be observed for three fault cases, namely:

1. A three phase fault in the middle of the 380kV transmission line onshore.
2. A line-to-line fault at the mid of the 380kV transmission line onshore.
3. Line-to-ground fault at the mid of the 380kV transmission line onshore.

3.9.1. THREE PHASE FAULT AT THE ONSHORE TRANSMISSION LINE

A 250ms, self-cleared, three-phase-to-ground fault is applied at the mid-point of the 380kV-HVAC transmission line. The fault duration represents the stricter FRT period observed in typical grid connection requirements. During the fault period, the onshore VSC-HVDC station provides a fast positive sequence reactive (i_{q+}) current injection, utilizing a reactive current boosting gain k_1 equal to 2. The voltage-drop FRT strategy, presented in figure 3.6 is applied in order to protect the HVDC link from high direct overvoltages. The onshore HVDC converter station utilizes its maximum fault current capacity as positive sequence reactive current (i_{q+}) injection during the fault period. The latter leads to the reduction of the active current (i_{d+}) to the zero value by the current limitation strategy. During the post-fault period, as soon as the fault is cleared and the voltage has recovered, the active current is ramped up following a pre-selected ramping rate as presented in figure 3.14 and figure 3.15 (defined as in the state S4).

The ramping of the active current ensures a smooth recovery of the VSC during the post-fault period. As it can be observed in figure 3.14, the disadvantage of the active current current ramping is the delay of the direct voltage (U_{dc}) recovery to its pre-fault steady state value. Furthermore, it prolongs the duration of the imposed offshore island voltage drop beyond the duration of the onshore fault, as it can be seen in figure 3.16. With regard to the negative sequence current control loop, it can be observed in figure 3.15 that it does not affect significantly the positive sequence current injection. The oscillation observed at the instant of time the fault is applied and the fault is cleared is due to the notch filters response.

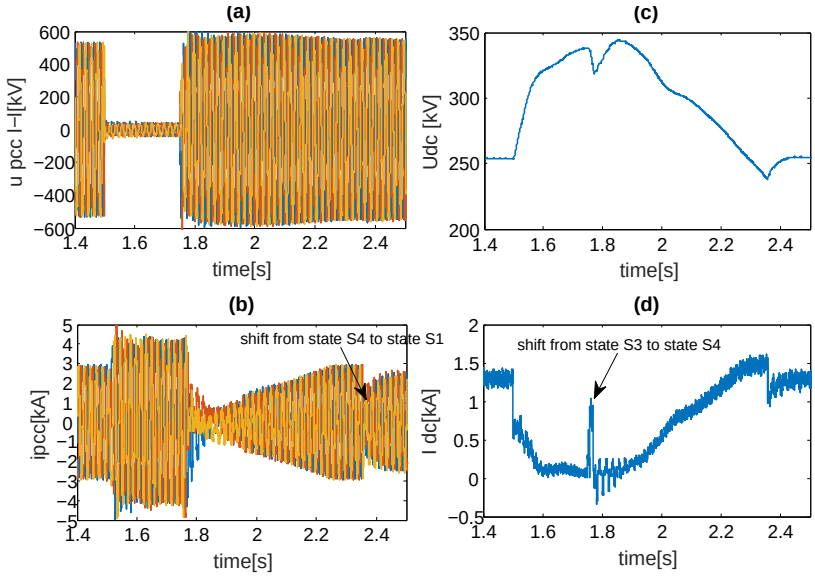

Figure 3.14: (a) Instantaneous voltage at PCC, (b) instantaneous current of the onshore VSC-HVDC station. (c) Offshore DC terminal direct voltage, (d) HVDC link direct current, for the case of balanced three phase fault onshore.

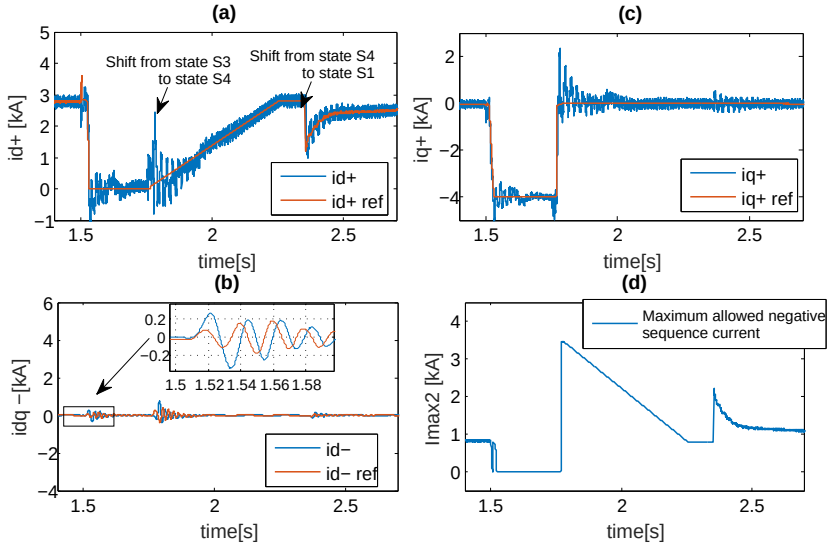

Figure 3.15: (a) positive sequence active current, (b) negative sequence dq-currents. (c) positive sequence reactive current, (d) maximum allowed negative sequence current given by the current limiter.

The low voltage ride-through HVDC controller (LVRT-HVDC) presented in figure 3.6 reduces the d-axis component of the filter voltage of the offshore HVDC converter station, while the q-axis component is controlled to be zero. In this way the amplitude of the instantaneous voltage at the offshore VSC-HVDC station terminal is reduced as presented in figure 3.16. In addition, a positive sequence active current reduction is performed by the offshore wind turbines as it is presented in figure 3.17. This supports the power balance in the HVDC link, hence reduces the observed over-voltage. During the LVRT period, no reactive current injection is provided from the wind turbines to the island grid as the wind turbines operate in the state S2. Figure 3.17 presents the response of the active and reactive current of the wind turbine model which represents the dynamic response of PPM1.

It is worth observing, that the voltage drop strategy using the control block "LVRT-HVDC" does not reduce the voltage at the offshore HVDC station terminal below the 0.5p.u value. This is intentionally selected so as the offshore HVDC converter station does enter its FRT mode. This is a design property of the enhanced scheme proposed in this chapter. It distinguishes from the case where a fault is applied in the offshore island grid from the case that the voltage is reduced as a result of coordinated FRT strategy. The case of three phase offshore faults is especially covered in the next paragraph.

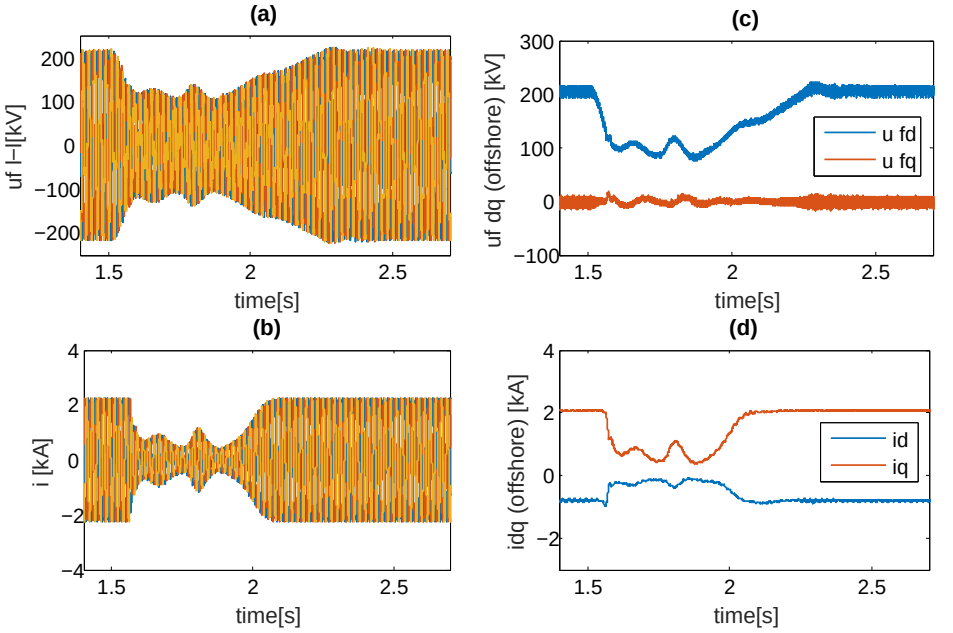

Figure 3.16: Response of the wind plant side HVDC station during balanced fault at the onshore HVDC converter AC terminals. (a) instantaneous voltage at the offshore filter, (b) instantaneous current at HN0 breaker,(c) dq-voltages of the offshore converter station, (d) dq-currents of the offshore converter station.

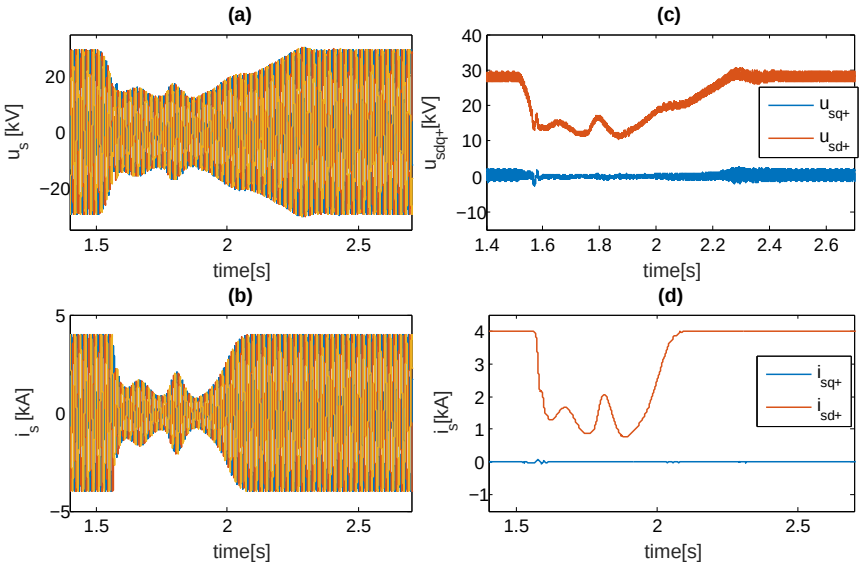

Figure 3.17: The response of the offshore wind PPM1 after the reduction of the AC island grid voltage triggered by a fault in the onshore converter station terminals. (a) the instantaneous voltage of the wind plant, (b) the instantaneous current, (c) the dq components of the voltage (d) the dq component of the PPM1 current.

3.9.2. SELECTED SIMULATION CASES FOR UNBALANCED FAULTS

Five different control options which influence the response of the onshore VSC-HVDC station and the external HVAC transmission line are tested. Namely:

1. Negative sequence current suppression at the onshore station (reflected with $k_2 = 0$, in figure 3.18) without the positive sequence reactive current boosting ($k_1 = 0$). This represents a situation where the grid code does not require for reactive current injection during unbalanced faults.

2. The VSC provides positive sequence reactive current boosting ($k_1 = 2$,) similar to the balanced fault case. At the same time, the negative sequence current is suppressed ($k_2 = 0$).

3. Activation of simultaneous positive and negative sequence current injections ($k_1 = k_2 = 2$). The bottlenecks of this approach are addressed.

4. As a solution to the previous bottlenecks, the proposed negative-sequence-voltage-dependent (NSVD) active current reduction control module at the onshore converter station is illustrated. Similarly the applied gains are ($k_1 = k_2 = 2$).

3.9.3. LINE-TO-LINE ONSHORE FAULTS

The first case for a line-to-line fault applied at the AC transmission system are studied. The equivalent circuit of the onshore transmission system is discussed in order to explain the selected control options.

EQUIVALENT CIRCUIT FOR LINE-TO-LINE (LL) ONSHORE FAULTS

The equivalent circuit of the external 380kV transmission line including the onshore VSC-HVDC converter station is presented in figure 3.18. When the negative sequence current is suppressed (reflected with $k_2 = 0$ in figure 3.18), the fault current contribution of the VSC station consists of the positive sequence current component. This term includes the steady state value positive sequence current and the positive sequence reactive current boosting term provided by equation (3.10).

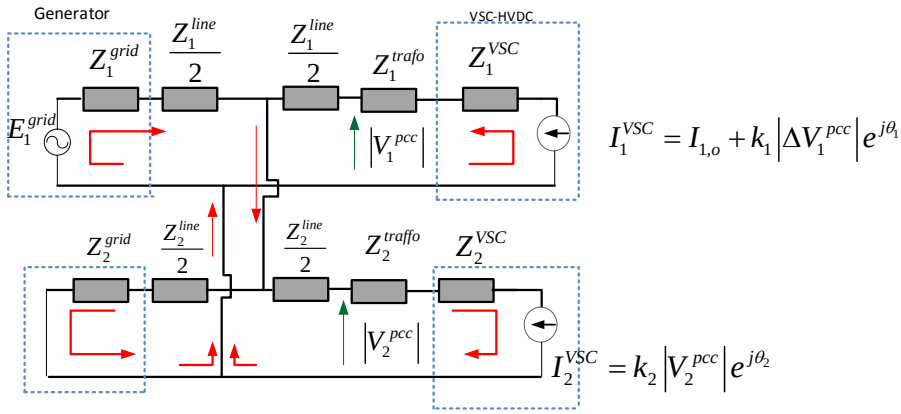

Figure 3.18: Positive, negative and zero sequence equivalent circuits of the onshore converter station and the external grid for the line-line fault case study. The circuit helps to understand the EMT simulations presented below.

During unbalanced faults, when the reactive current boosting gain (k_1) is selected to be zero, the fault current injection of the VSC consists only of the steady state value current. The later depends on the operating point of the VSC. Some national level grid codes require for positive sequence reactive current injection (i_{q+}) using equation (**??**) explicitly during balanced faults. Other grid codes does not differentiate the balanced from the unbalanced fault conditions.

In any of these two cases, the fault current contribution of the onshore VSC station during line-to-line faults can be increased by the injection of a negative sequence current. The latter choice enables the converter to behave as a current source both in the positive as well as in the negative sequence circuit. Finally, the presence of negative sequence current in the AC transmission line terminals, enhances the unbalanced fault detection capability at the VSC side terminals of the AC line, especially during line-to-line faults.

CASE 1

Figure 3.19 presents the simulation results for a 250ms self-cleared line-to-line fault at the mid-point of the 380kV transmission line. As it can be observed, the negative sequence dq-current components (i_{dq-}) are suppressed to zero while, the positive sequence dq-currents (i_{dq+}) are kept constant during the fault period given that the active and reactive current control loops are set to freeze state. Observing the instantaneous value of the current at the PPC point, it can be seen that the fault current injection of the VSC station is equal to the steady-state value current. It consists mainly of the positive sequence current component. The negative sequence current is suppressed while there is no zero sequence current in the external grid during line-to-line faults.

CASE 2

The next selected option is the injection of a positive sequence reactive current (i_{q+}), while simultaneously suppressing the negative sequence current of the onshore HVDC station ($k_2 = 0$). The simulation result is presented in figure 3.20. The positive sequence reactive current is provided proportionally to the rms value of the line-line voltage as it is measured at the filter of the VSC. It is performed in a similar way as for balanced faults utilizing a gain (k_1) equal to 2.

CASE 3

With the purpose to increase the negative sequence fault current measured at the onshore HVDC station terminal, we utilize a combined positive and negative sequence current injection. The negative sequence current is injected during the unbalanced fault period proportionally to the negative sequence voltage following the equations (3.14) and (3.15). This negative sequence current injection is bounded by the limited fault current capacity of the HVDC station. One such case is simulated and presented in figure 3.21. Due to the limited over-current capacity of the HVDC station, a combined positive and negative sequence reactive current boosting cannot be achieved. Since the current priority is given to the positive sequence current, there is no available fault current for negative sequence although the fault is line-to-line fault. Hence, a negative sequence current injection by the onshore converter station cannot be achieved unless the positive sequence current (either the active or the reactive current component) is reduced. The latter explains the need for the proposed control module of figure 3.13.

CASE 4

In this paragraph, the active current reduction based on the negative sequence voltage is presented. Figure 3.22, shows the response of the system for the same disturbance. As it can be seen, the reduction of active current as a function of the negative sequence voltage, provides additional space for the negative sequence current to be injected into the grid.

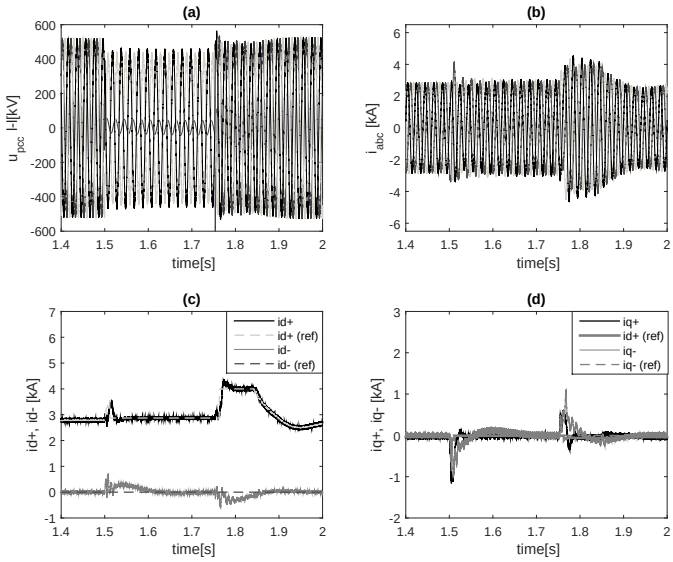

Figure 3.19: Response of the VSC-HVDC link during a line-to-line fault at the onshore 380kV transmission system (Case 1). (a) the instantaneous value of the onshore PCC voltage, (b) the instantaneous value of the onshore PCC current, (c) the active positive and negative sequence d-axis currents, (d) the reactive positive and negative sequence currents (iq) of the onshore station.

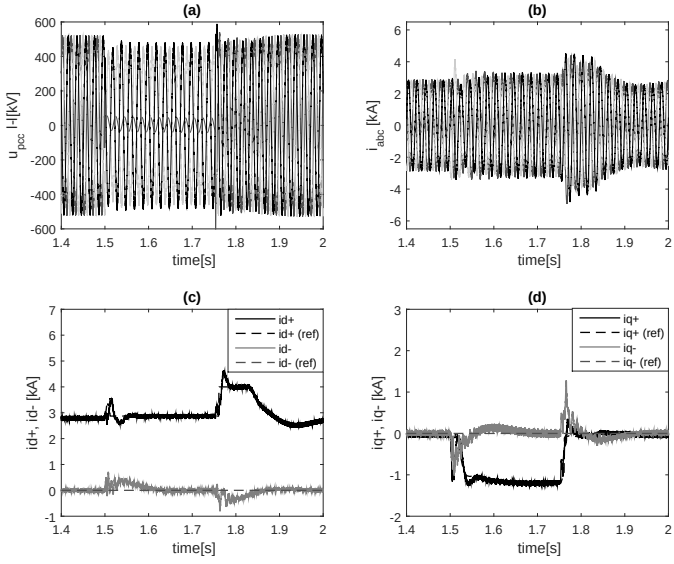

Figure 3.20: The response of the VSC-HVDC link during a line-to-line fault at the onshore 380kV transmission system (Case 2). (a) the instantaneous value of the onshore PCC voltage, (b) the instantaneous value of the onshore PCC current, (c) the active positive and negative sequence d-axis currents, (d) the reactive positive and negative sequence currents (iq) of the onshore station.

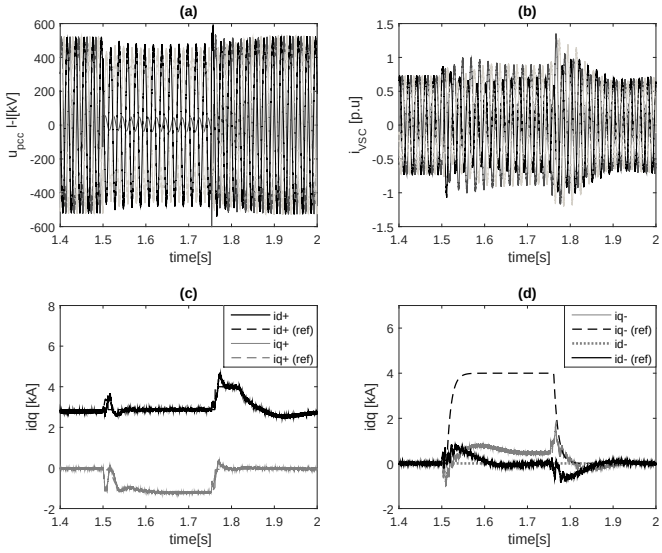

Figure 3.21: The response of the GSVSC during unbalanced fault for case 3. (a) the instantaneous value of the onshore PCC voltage, (b) the instantaneous value of the onshore PCC current, (c) the positive sequence dq-currents (d) negative sequence currents dq currents.

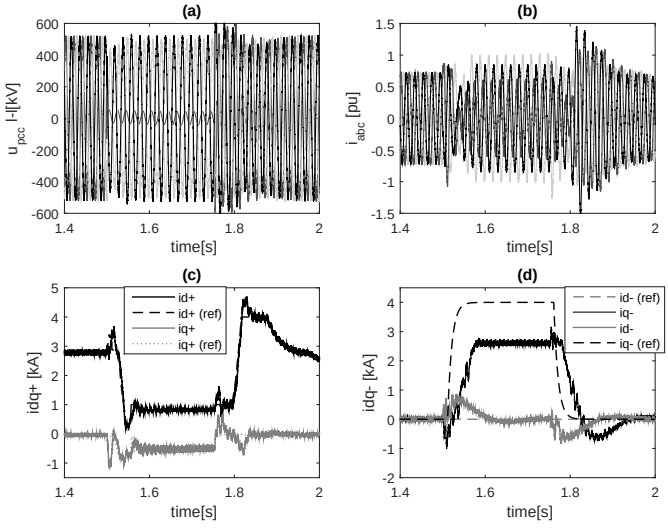

Figure 3.22: The response of the GSVSC during balanced fault for case 4. (a) positive sequence active current, (b) negative sequence reactive current, (c) the positive sequence dq-currents (d) negative sequence currents dq currents.

THE EFFECT OF THE STUDIED CASES ON THE VOLTAGE AND CURRENT SEQUENCE COMPONENTS

The response of the positive and the negative sequence components of the current and the voltage at the PCC as defined in figure 3.18 are presented in figure 3.23 for the different examined cases. Comparing these simulation results, it can be observed that the case 4 presents a better response in terms of the positive sequence voltage drop. In the case 4, the positive sequence active current of the HVDC station is reduced as can be seen in figure 3.22. In addition, positive sequence reactive current is injected. The later two actions, have resulted in a higher positive sequence voltage at PCC as it is observed in figure 3.23. Observing the response of the negative sequence voltage component in figure 3.23, a higher negative sequence voltage is observed at the PCC for the case 4. Since in line to line faults, positive and negative sequence voltages are very close (see the circuit of figure 3.18), the increase of the positive sequence voltage has increased the negative sequence voltage components as it shown in figure 3.23. The combined positive and negative sequence voltage component constitute the total voltage amplitude at the PCC. The instantaneous value of the latter is shown in figure 3.22 a.

From these results, it can be concluded that the injection of negative sequence reactive current by the onshore HVDC station followed by the reduction of the positive sequence active current as performed in the case 4, enables negative sequence current flow in negative sequence circuit while supporting also the positive sequence voltage at the PCC. From the instantaneous value of the PCC voltage, no significant over-voltages are observed during the fault period.

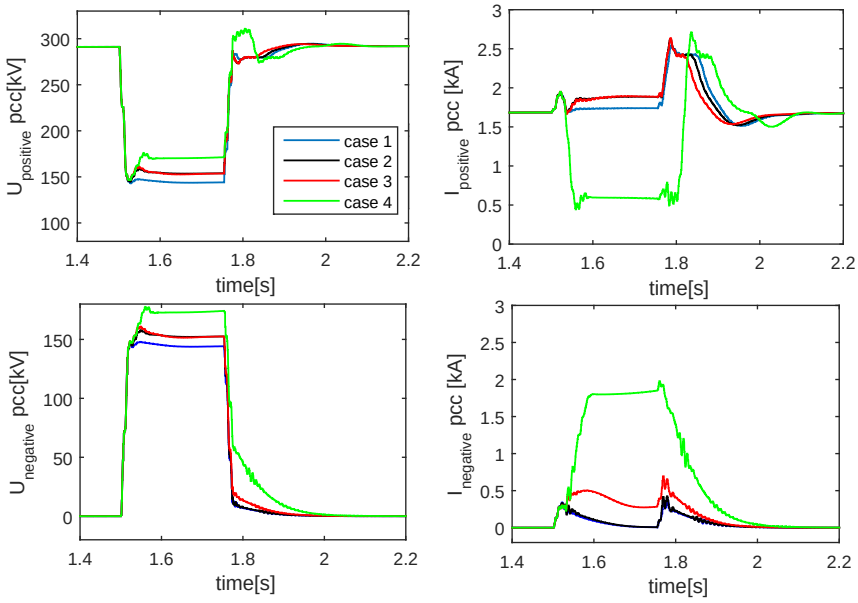

Figure 3.23: Response of the external HVAC network for the different simulation cases of section 3.9.3.

3.9.4. SINGLE-LINE-TO-GROUND ONSHORE FAULTS

EQUIVALENT CIRCUIT

Figure 3.24 presents the positive, negative and the zero sequence circuits of the onshore transmission grid for the case of SLG fault as applied as in figure 3.1. The step up transformer of the onshore converter station, which is a star/grounded-delta configuration, decouples the zero sequence current component between the external AC transmission system circuit and the phase reactor. Hence, the onshore VSC-HVDC station is capable to control only the positive and the negative sequence currents between the converter and the externals circuit (380kV line and the infinite grid). The positive sequence fault current is determined primarily by the positive sequence reactive current boosting gain, k1. However, from the equivalent circuit, the control of positive and negative sequence current affects the zero sequence current in the external HVAC transmission line. In order to study and evaluate the effect of different negative sequence current control applied at the GSVSC, the same cases (as for the LL fault) are now tested for the SLG fault.

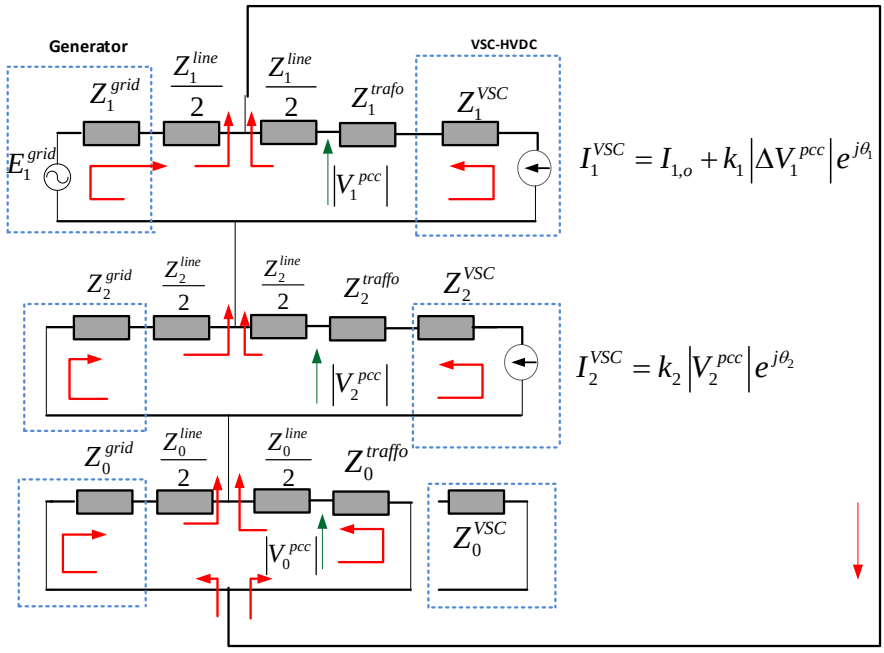

Figure 3.24: Positive, negative and zero sequence equivalent circuits of the onshore converter station and the external grid for the single-line-to-ground fault case study. The circuit helps to understand the EMT simulations presented below.

THE EFFECT OF THE STUDIED CASES ON THE VOLTAGE AND CURRENT SEQUENCE COMPONENTS

For the same evaluated cases as in section 3.9.3, the response of the sequence voltage and current components is presented in figure 3.25 and figure 3.26. From these results, it can be observed that the injection of the negative sequence current by the GSVSC station proportionally to the negative sequence voltage leads to an increased zero sequence current component. Observing the negative sequence voltage profiles, a reduced negative sequence voltage is observed in the case 4, when negative sequence current is injected. The increased zero sequence current flowing in the external grid, increases the amplitude of the zero sequence voltage at the PCC. So between the cases 1 and 4, there is a lower negative sequence voltage in case 4, an a higher zero sequence voltage. Of course, the variation of the sequence components depends strongly on the sequence circuit impedance (positive, negative and zero).

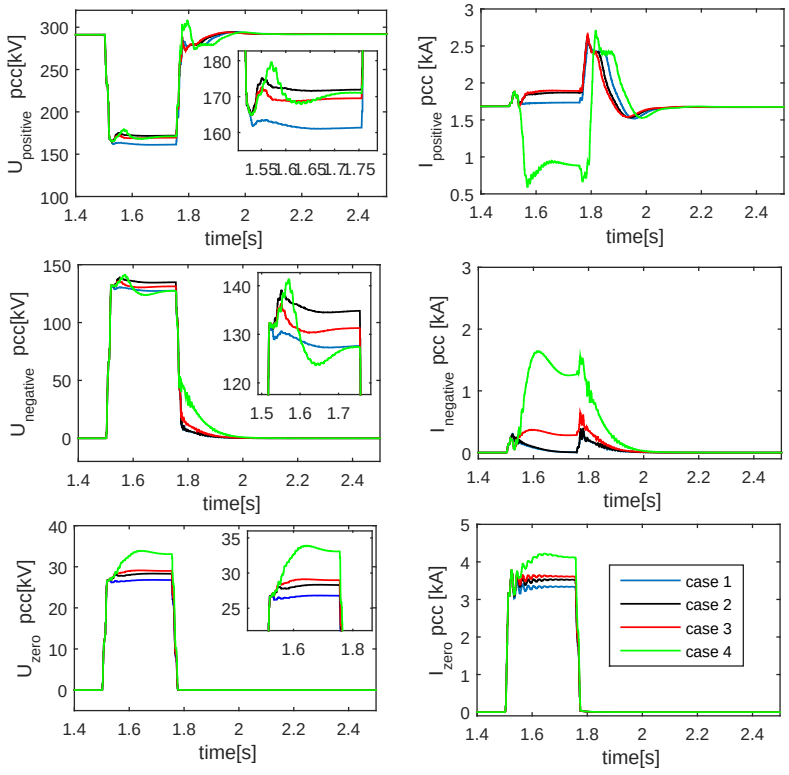

Figure 3.25: The response of the onshore converter station sequence voltage and current components for the SLG fault at the middle of the AC line.

Observing the simulation result for the sequence components of voltage after the Z_{grid} in figure 3.24 it can be concluded that the zero sequence current component at the infinite grid is increased when the negative sequence current is provided by the VSC-HVDC station. The presence of zero sequence current component could facilitate the detection and isolation of SLG faults.

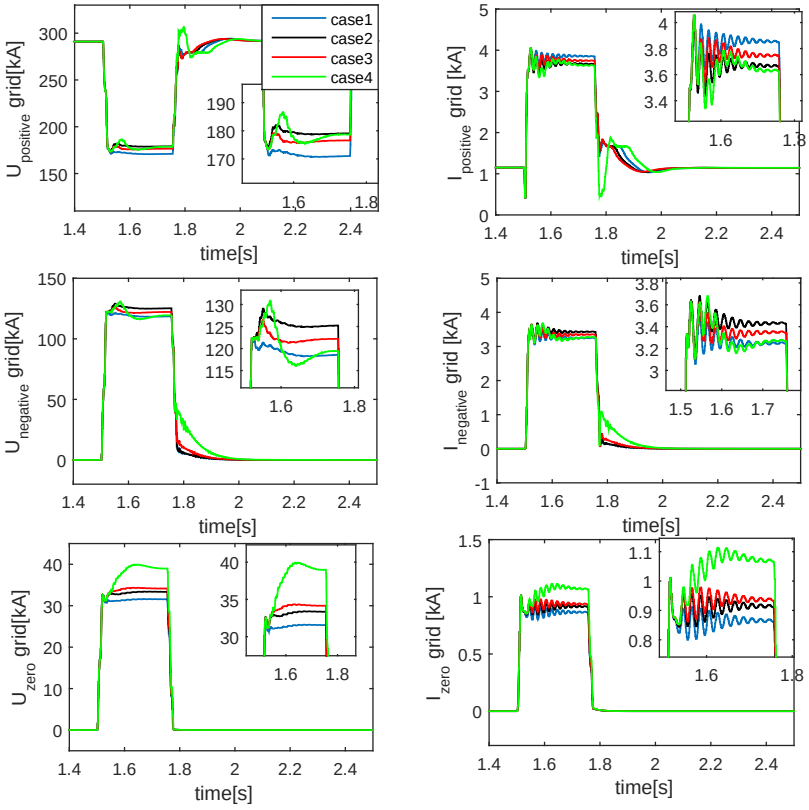

Figure 3.26: The response of the VSC-HVDC link for the SLG onshore fault at the middle of the AC line.

Finally, it could be concluded that both for line-to-line and single-line-to-ground faults at the onshore HVDC converter station terminals, the injection of negative sequence current as in the case 4 has shown the best results for the unbalanced response of the external HVAC transmission system.

3.10. SIMULATION RESULTS FOR OFFSHORE FAULTS

3.10.1. THREE PHASE FAULT AT THE OFFSHORE VSC-HVDC STATION TERMINALS

The response of the offshore island grid is presented in figure 3.27 for a three phase to ground fault at the 150kV offshore transformer terminal. The active current reduction block is activated at the wind turbines. As it can be be observed, the offshore converter station using the enhanced control scheme presented in figure 3.8 is capable of providing the fault current injection limited to the maximum current capacity off the offshore HVDC station. In these results, u_{wpvsc} is the instantaneous voltage of the converter and i_{wpvsc} its current. Moreover, the sequence voltage components of the VSC-HVDC offshore station, its modulation index and the dq voltage and current components are presented in figure 3.28. Finally, figure 3.29 presents the response of the PPM1 wind turbine equivalent model. As it can be seen, the positive sequence voltage of the offshore wind turbine terminal PPM1 u_{ppm1} drops during the fault period while the wind turbines provide reactive fault current injection. During the post-fault period, the voltage is recovered to its pre-fault value. From these results it can be seen that the proposed enhanced control scheme is capable to ensure FRT and fault current injection for a three phase fault at the 150kV terminal.

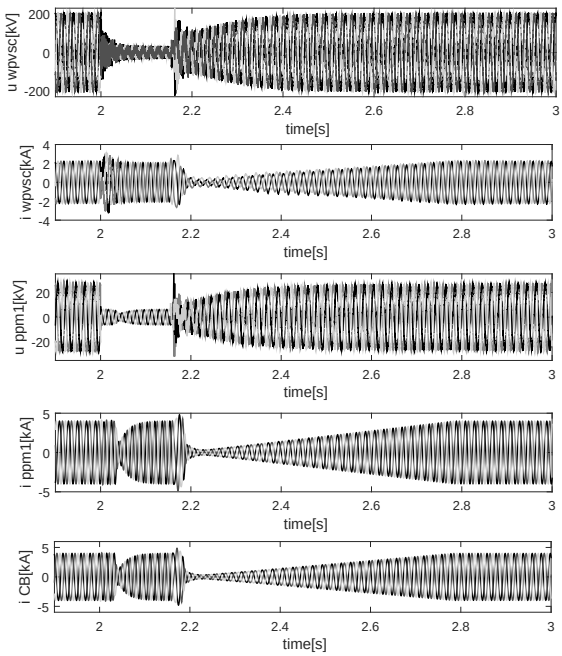

Figure 3.27: The instantaneous value of (from top to bottom): the WPVSC voltage, WPVSC current, PPM voltage, PPM current, and circuit breaker CB current a point FD1.

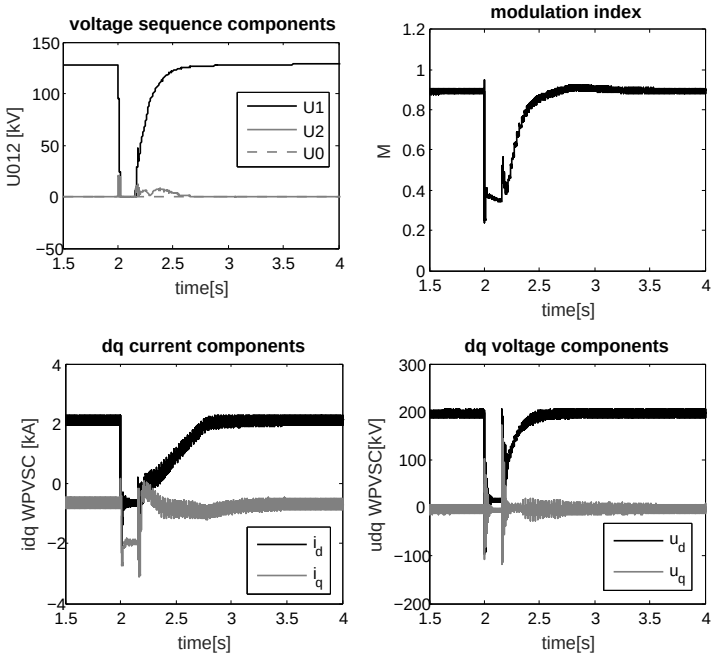

Figure 3.28: The positive (1), negative (2) and zero sequence (0) voltage components, the modulation index, the dq-currents and the dq-voltages of the offshore VSC-HVDC station.

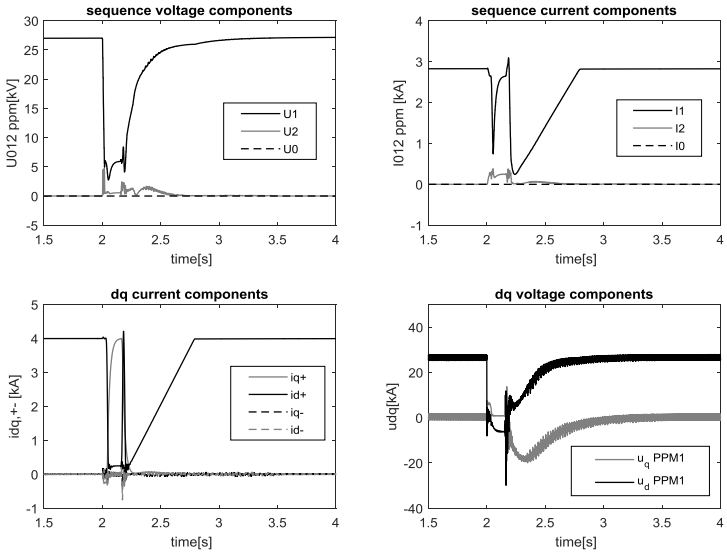

Figure 3.29: The positive (1), negative (2) and zero sequence (0) voltage and current components, the dq-currents and the dq-voltages of the offshore wind PPM1.

RESPONSE OF THE ISLAND GRID WITHOUT REACTIVE CURRENT INJECTION FROM PPMS

In this section, the response of the island grid is assessed for the same fault under the condition that no reactive current is injected from the wind power plants during the fault. The active current reduction block is also activated as in the previous case. From the results in figure 3.30 it can be seen, that only the offshore VSC-HVDC station provides fault current injection. The wind turbines do not inject reactive current while their active current is reduced from the active current reduction block.

Comparing figure 3.29 and figure 3.30 its worth to observe the voltage boosting achieved in the case the wind turbines provide reactive current injection. Furthermore, the current observed at the circuit breaker CB is zero in the second case. From these results it can be concluded that the proposed enhanced fault ride through strategy at the offshore VSC-HVDC station in combination with the reactive fault current injection from the wind power plants during offshore faults ensures improved voltage response and adequate fault current levels at the offshore island grid. Finally, figure 3.31 and figure 3.32 provide the remaining results for completeness.

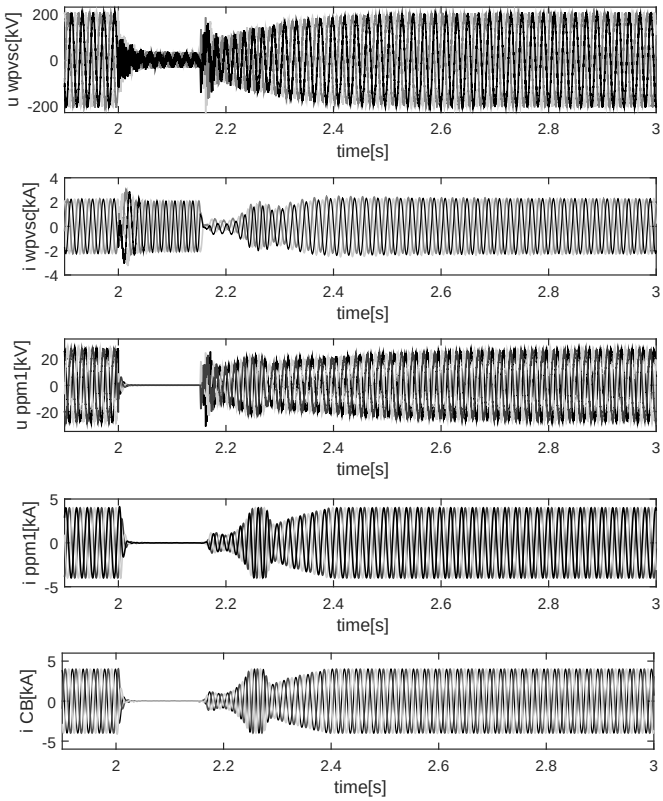

Figure 3.30: From top to bottom the instantaneous value of: the WPVSC voltage, WPVSC current, PPM voltage, PPM current, and circuit breaker CB current (FD1 point). Case without reactive current injection from the wind turines.

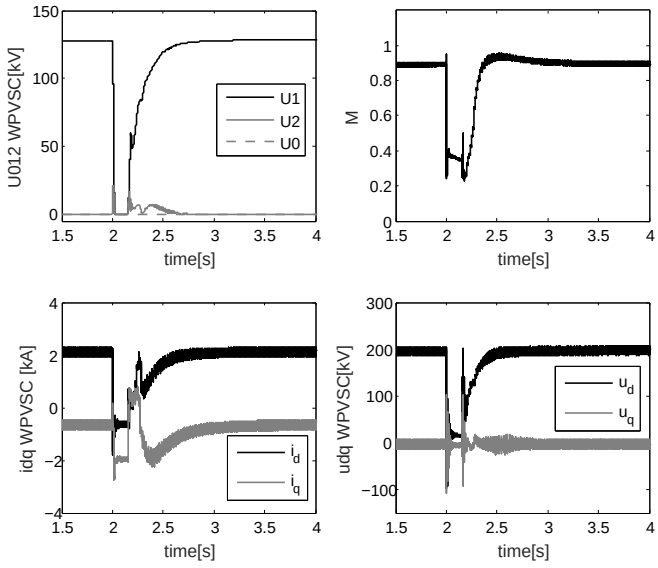

Figure 3.31: The positive (1), negative(2) and zero (0) sequence voltage components, the modulation index, the dq-currents and the dq-voltages of the offshore VSC-HVDC station. Case without reactive current injection from wind turbines.

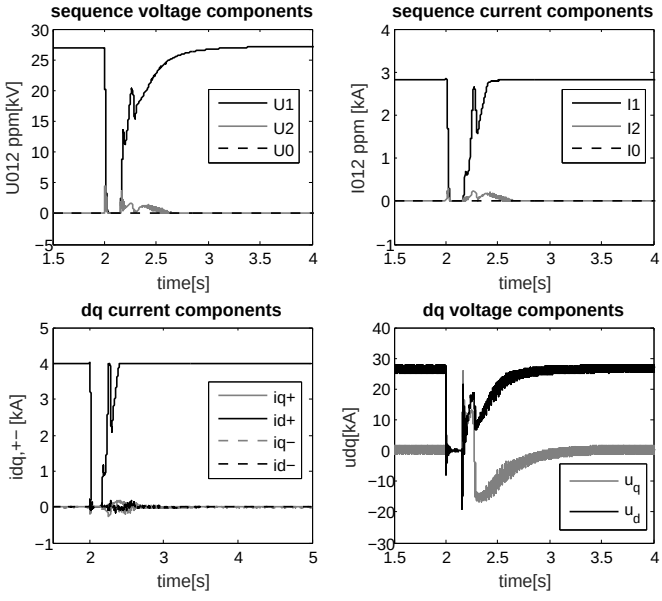

Figure 3.32: The positive (1), negative (2) and zero (0) sequence voltage and current components, the dq-currents and the dq-voltages of the offshore wind PPM1. Case without reactive current injection from wind turbines.

3.10.2. THREE PHASE FAULT AT THE 33KV SYSTEM

Next, a three phase fault is applied at the offshore wind turbine PPM1 terminal. Figure 3.33 presents the instantaneous values of voltages and currents in the offshore island. The voltage drop at the terminal of the offshore VSC-HVDC station is not big enough so that the HVDC station do not enter the fault current injection state. Hence, the block of figure 3.9 only reduces the converter internal voltage in such a way that the fault current is limited to the maximum capacity.

From these result, it can be observed that for a three phase faults at the 33kV terminals, the VSC-HVDC station is capable to ensure FRT compliance without experiencing high fault currents. The wind turbines inject reactive current supporting locally the voltage. The active and reactive voltage and current components are presented in 3.34 and 3.35.

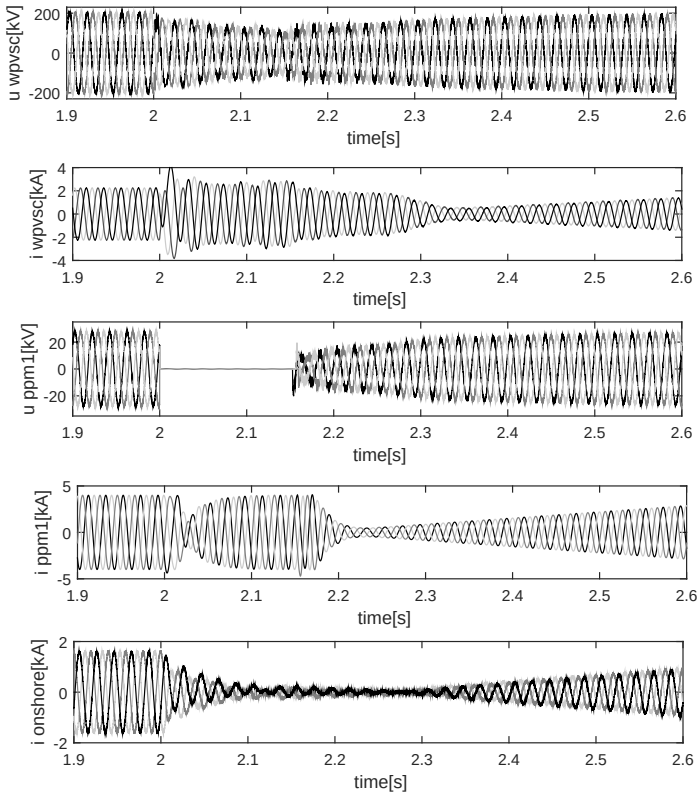

Figure 3.33: The instantaneous value of (from top to bottom): the WPVSC voltage, WPVSC current, PPM voltage, PPM current, and circuit breaker CB current.

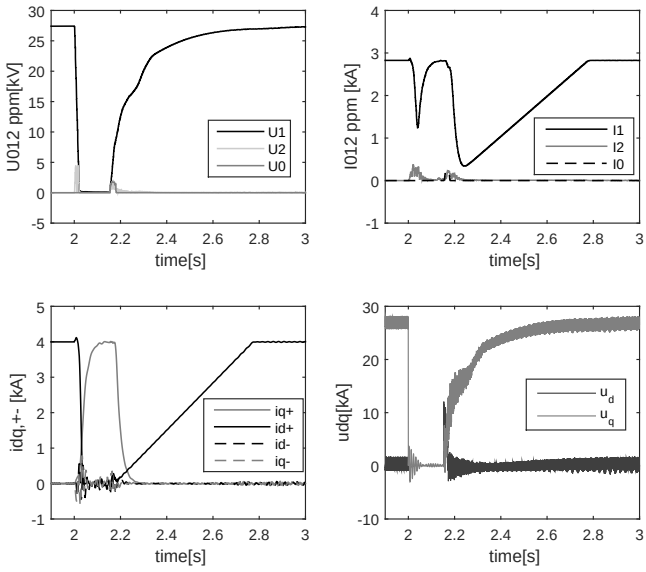

Figure 3.34: The positive (1), negative (2) and zero (0) sequence voltage and current components, the dq-currents and the dq-voltages of the offshore wind PPM1.

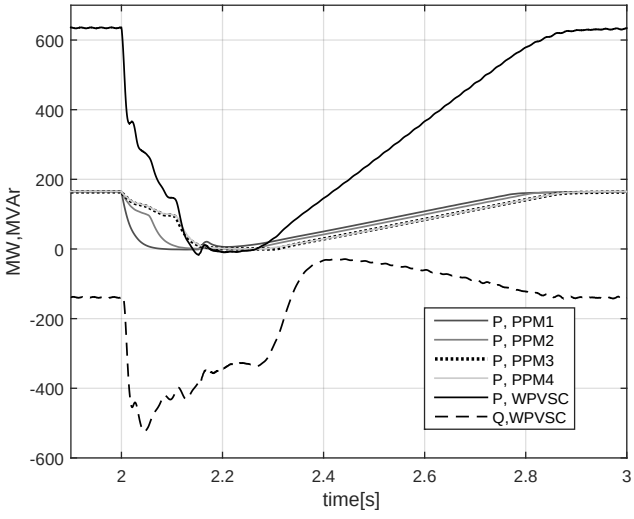

Figure 3.35: The active power measured at different points in the grid.

3.10.3. LINE-TO-LINE FAULT AT THE 33KV

Besides the assessment of three phase faults, this paragraph provides the analysis for line-to-line faults applied at the 33kV offshore collector grid. The effect of the negative sequence current control at the offshore wind turbines is assessed. In that content, three cases are addressed, reflecting different options for negative sequence current control.

CASE1: NEGATIVE SEQUENCE CURRENT SUPPRESSION AT THE WIND TURBINES

A line-to-line fault is applied at the 33kV terminal of the power plant module 1 (PPM1 in figure 3.1). The PPM1 utilizes the negative sequence current suppression control strategy. Furthermore, it is assumed that no positive sequence reactive current is injected into the island grid from the offshore PPMs during the unbalanced fault period. Figure 3.36 presents the instantaneous value of the voltage and the current at the PPM1 AC terminals, at the location FD1 of the circuit breaker (CB) and at the offshore HVDC converter station terminals (point of HN0).

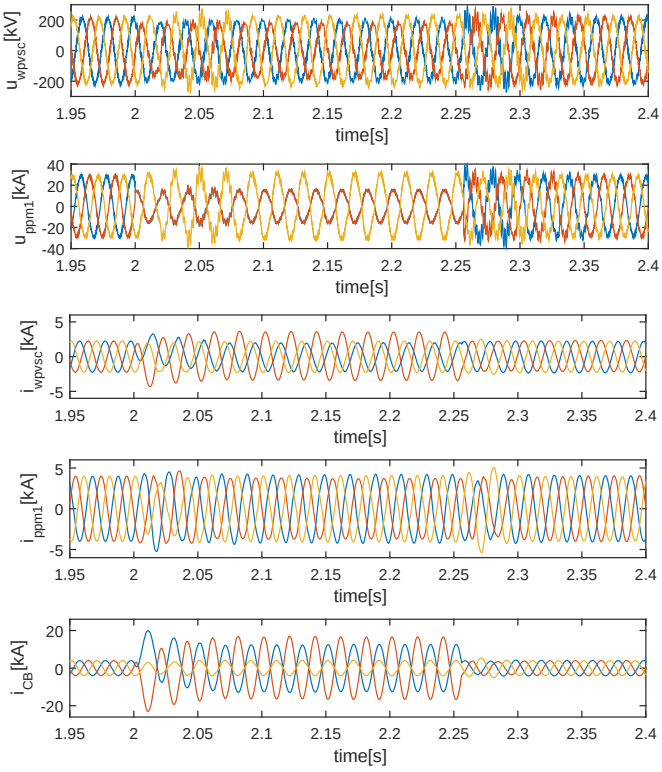

Figure 3.36: The response of the offshore AC island to a line-to-line fault in the PPM1 terminals. From top to bottom, the instantaneous voltage at the wind park VSC (WPVSC) HVDC converter terminal, the instantaneous voltage at PPM1 terminal, the current at WPVSC terminal, the current at the PPM1 and the current at the FD1, 33kV point.

The dq-components of the voltage and the currents of the PPM1 can be seen in figure 3.37. The wind turbines before the fault is applied provide their maximum power generation (with rated current 4kA per each PPM). As it can be observed in figures 3.36-3.37, the fault current injection of the wind turbine is equal to the steady state active current. This depends on the operating point of the wind turbine, hence on wind speed. Observing the sequence components of the voltage and the current at the offshore VSC-HVDC station (WPVSC), it can be seen that a positive and a negative sequence exist. In addition, an adequate fault current level is measured at the FD1 (CB) point, where the breaker is installed.

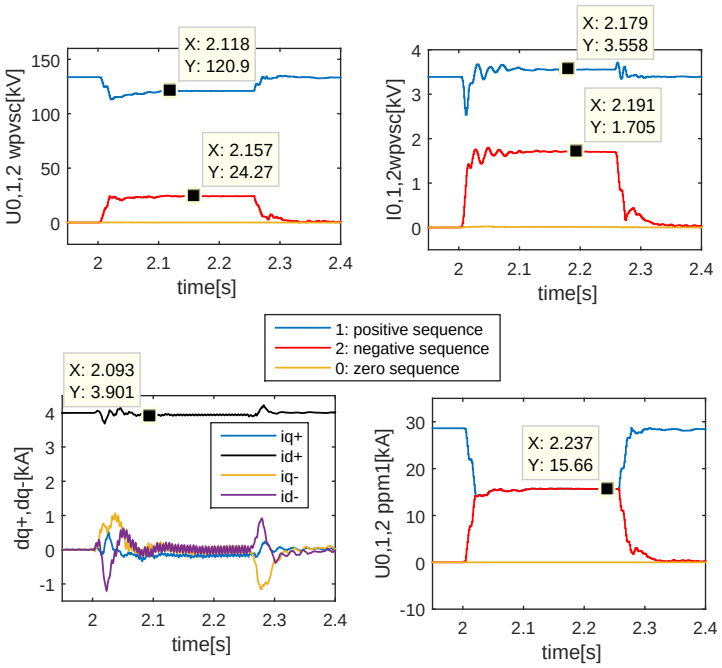

Figure 3.37: The response of the offshore AC island to a line-to-line fault in the PPM1 terminals. Upper subfigures: the sequence components of WPVSC terminal. Lower subfigures: the dq-positive, the dq-negative sequence currents of the PPM1, and the sequence voltages at the PPM1 terminal.

CASE 2: NEGATIVE SEQUENCE CURRENT SUPPRESSION WITH FRT ACTIVE CURRENT REDUCTION METHOD APPLIED

In this case, the proposed positive-sequence-voltage-dependent (PSVD) active current reduction at the offshore wind turbines is assumed to be in operation. The presented results aim to demonstrate that the PSVD loop in figure 3.12 does not jeopardize the fault detection capability at the FD1 point where the fault needs to be cleared. Similarly to the previous case, no reactive current injection is performed during the unbalanced fault period by the wind turbines.

As it can be observed in the figure 3.38 and 3.39, the total fault current injection from the offshore PPM1 is smaller in this case given that neither reactive positive sequence current is provided nor negative sequence current (see figure 3.38). Observing the fault current measured at FD1 (i_{CB}), it can be seen that the application of the proposed active current reduction module for the FRT enhancement of the HVDC link, does not affect the fault detection capability in the island grid. The fault current level at the FD1 is at the same value as in the previous case where the active current is not reduced. Furthermore, not much difference is observed compared to the base case, with regard to the positive and the negative sequence voltage profiles of the offshore island grid. From these results, it can be concluded that under unbalanced faults at the 33kV grid, the operation of the proposed enhanced FRT scheme for the HVDC link does not deteriorate the fault detection capability of the island grid nor the voltage profiles during the fault period.

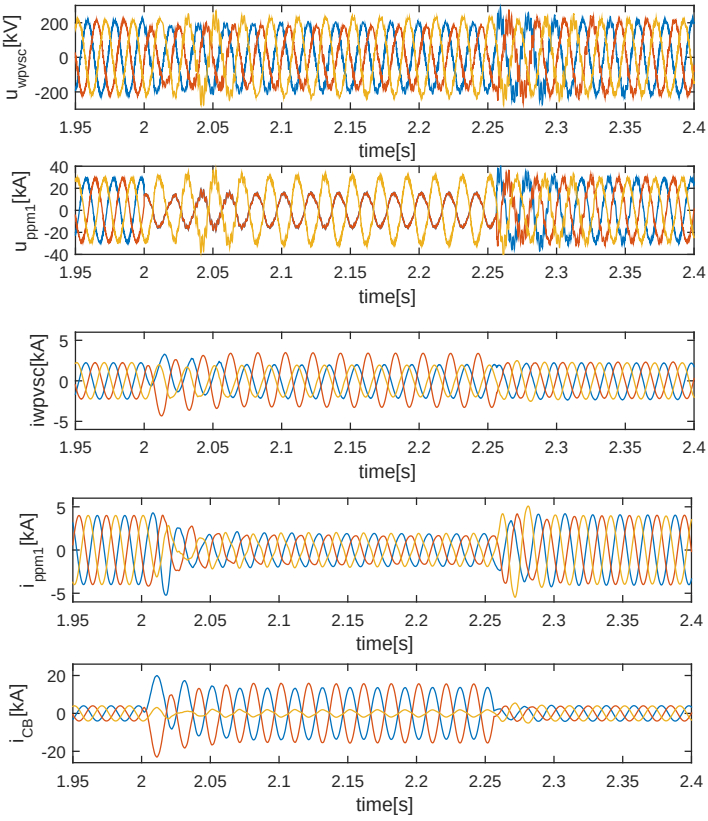

Figure 3.38: The response of the offshore AC island to a line-to-line fault in the PPM1 terminals. From top to bottom, the instantaneous voltage at the wind park VSC (WPVSC) HVDC converter terminal, the instantaneous voltage at PPM1, the current at WPVSC, the current at the PPM1 and the current at the FD1 point.

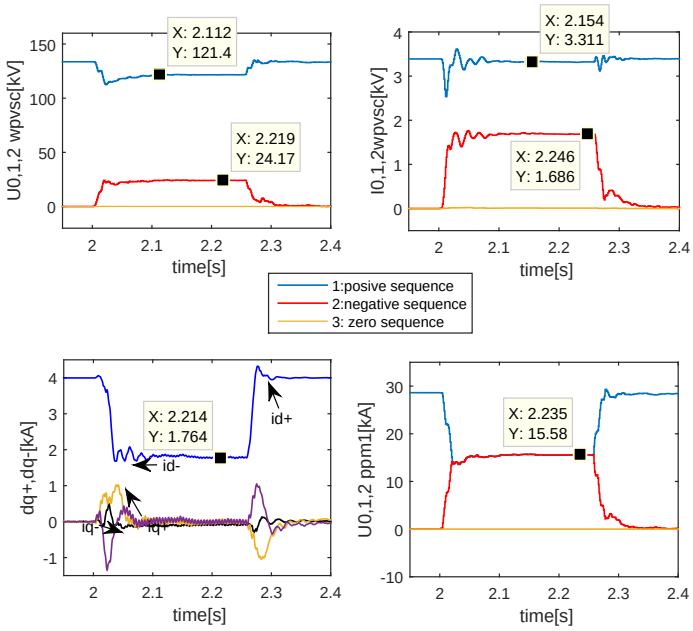

Figure 3.39: The response of the offshore AC island to a line-to-line fault in the PPM1 terminals. Up the sequence components of WPVSC terminal, down, the dq-positive and dq-negative sequence currents of the PPM1, and the sequence voltages at the PPM1 terminal.

CASE 3: NEGATIVE SEQUENCE CURRENT SUPPRESSION AND POSITIVE SEQUENCE REACTIVE CURRENT INJECTION

So far, it has been assumed that no positive sequence reactive current is provided to the offshore AC island. This paragraph addresses the effect of the reactive current injection during line-to-line faults on the unbalanced fault response of the offshore island AC collector grid. In that prospect, figures 3.40 - 3.41 present the line-to-line fault case, where the wind turbines suppress the negative sequence current and inject positive sequence reactive current proportionally to the positive sequence voltage.

As it can be seen in figure 3.40 - 3.41, the PPM1 fault current injection is symmetrical since only positive sequence is provided. The active current in the wind turbines is reduced to zero, because all the fault current capacity is provided as reactive current. The positive and the negative sequence voltage at the PPM1 is presented in 3.41. Compared to the case 2, in case 3 it can be seen that the reactive positive sequence current injection leads to lower positive sequence voltage levels at the PPM1 (12.1kV instead of 15.56kV). Hence, during unbalanced faults, the reactive positive sequence current injection for the power electronic based offshore island does not bring the expected benefits in the offshore system concerning the voltage support. It would have been expected that the injection of reactive current during unbalanced faults, would boost the positive sequence voltage. Finally, the same fault levels are measured at CB compared to the previous cases.

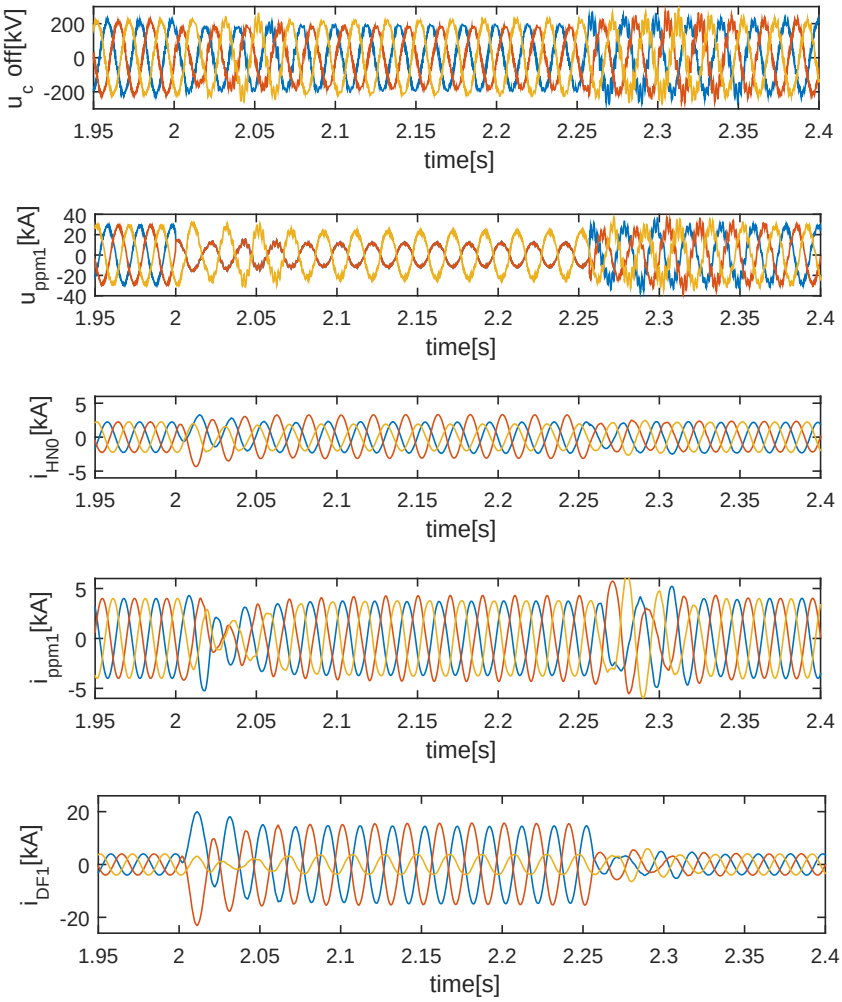

Figure 3.40: The response of the offshore AC island to a line-to-line fault in the PPM1 terminals. From top to bottom, the instantaneous voltage at the wind park VSC (WPVSC) HVDC converter terminal, the instantaneous voltage at PPM1, the current at WPVSC, the current at the PPM1 and the current at the FD1 point.

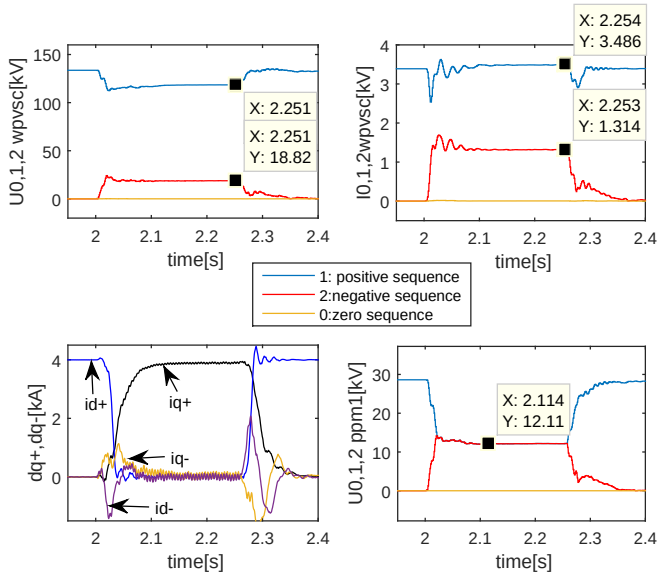

Figure 3.41: The response of the offshore AC island to a line-to-line fault in the PPM1 terminals. Up the sequence components of WPVSC terminal, down, the dq-postive and dq-negative sequence current of the PPM1, and the sequence voltages at the PPM1 terminal.

3.11. CONCLUSION

In this chapter the fault ride through response of offshore wind power plants with VSC-HVDC transmission is assessed for onshore and offshore AC faults. An enhanced voltage drop fault ride through control strategy is proposed and its response is presented by means of time domain simulations. The use of the new positive-sequence-voltage-dependent (PSVD) active current reduction control module at the offshore wind turbines, ensures improved fault ride through compliance for the HVDC link. Although during offshore AC grid faults the application of the active current reduction at the offshore wind turbines reduces their fault active current injections, it does not affect significantly the fault current levels at the 33kV feeder. The fault current is primary fed by the VSC-HVDC. The chapter presented also an improved control scheme which enables the fault ride through compliance of the offshore VSC-HVDC station during severe three phase faults at offshore HVDC station terminals. With respect to the reactive current injection from the wind turbines, it is recommended to be applied only during balanced offshore faults.

In addition, the chapter investigates the unbalanced fault response of the VSC-HVDC link during onshore transmission system faults. It is demonstrated that the suppression of the negative sequence reactive current by the onshore HVDC converter station leads to steady state value fault current levels. The latter depends on the operating point and does not always utilize all the fault current capacity of the HVDC converter station.

In that context, a variety of control strategies are tested for the onshore VSC-HVDC station. It is presented that due to the limited fault-current capacity of the onshore

HVDC station, the combined positive and negative sequence reactive current injection is not achievable when reactive positive sequence currents are provided simultaneously during unbalanced faults. With purpose to solve this bottleneck, a new control module is proposed which reduces the positive sequence active current during unbalanced faults proportionally to the negative sequence voltage. Since, the negative sequence current is provided proportionally to the negative sequence voltage, the injection of negative sequence substitutes the positive sequence active current. In this way, negative sequence reactive current next to positive sequence reactive current can be provided in order to enhance the protection of the AC transmission lines where VSC-HVDC systems are connected.

4

AN EMT-ENABLED ITERATIVE PROCEDURE FOR OPTIMAL FAULT RIDE THROUGH COMPLIANCE

4.1. INTRODUCTION

The majority of offshore HVDC connections up-to-date utilise the DC-Chopper method as fault ride-through (FRT) compliance strategy [154]. In order to use the high controllability of the HVDC link and the wind plant, various coordinated FRT control strategies are proposed in the literature [155], [27], [78], [156], [157]. Two are the most common techniques, the controlled offshore voltage drop method and the offshore frequency modulation technique. The controlled offshore AC voltage drop strategy is studied in [155], [27], [158] and further improved in [159] for the case of wind power plants with double fed induction generator type wind turbines. In chapter 3 of this thesis, the offshore AC voltage drop strategy has been enhanced with the participation of the wind turbines in the process. Moreover, it has been assessed for the case of balanced and unbalanced, offshore and onshore faults. Recently, the voltage drop method has been extended to the multi-terminal HVDC grid connection case of the offshore wind power plants in [133], [157], [160].

However, still research gaps exist in the literature. So far the compliance of the wind turbines with their own reactive current boosting requirements at the offshore AC island grid is neglected in the previous references. Furthermore, the post-FRT active current dynamic behavior of the wind turbines which is affected by the choice of the active current ramping rate, is omitted. The latter influences the power restoration in the HVDC link during the post-fault period.

Badly tuned control blocks would prolong the duration of the controlled AC voltage drop as a result of the extended direct over-voltage in the VSC-HVDC link. Furthermore, it could lead to the trip of the wind plant if the voltage profile at their terminals exceeds the offshore FRT envelopes given in the grid code. Currently, the calculation of the FRT

control parameters of HVDC link is carried out on a trial and error basis using detailed electromagnetic transient(EMT) type models which is a very time consuming process without always ensuring that the best values are selected. A methodology to effectively calculate the best control parameters for the coordinated FRT strategies has not been yet presented in the literature. The optimal tuning of the coordinated FRT control modules becomes challenging for two main reasons. Initially, the coordinated FRT strategy shall take into account the interactions among the offshore VSC-HVDC converter station and the wind turbine control modules. Furthermore, the non linear dynamic response of the associated current control limiters and state machines integrated in the control loops of the wind turbines and the VSC-HVDC system cannot be captured by linear models, making classical design methods non-applicable. In that frame, the concept of EMT-enabled tuning as introduced in [161] is adopted and further developed in this chapter. The problem will be formulated and solved in this chapter for various control schemes. The variables to be optimized are the control parameters of the coordinated FRT scheme of the offshore HVDC station, the control parameters of the wind turbine which assist the FRT compliance process and the post-fault ramping rate of the wind turbines. The FRT grid code profiles are considered in the process.

4.2. EMT-ENABLED ITERATIVE PROCEDURE FOR OPTIMAL FRT COMPLIANCE TUNING

4.2.1. ITERATIVE PROCEDURE

The EMT-enabled iterative procedure used in this chapter is based on a sequence of time domain simulation runs. It is driven by an evolutionary optimization algorithm which iterates the vector of control parameters in order to define the best set which satisfies a well defined objective function. The flow chart of the algorithm is presented in figure 4.1. The objective function is mathematically formulated with aim to reach the design goal (i.e minimize the direct over-voltage, hence the stresses in the HVDC link in conjugation with the imposed AC voltage drop at the offshore island). The iterative procedure begins with a set of random FRT control parameters. An EMT type simulation is executed for a given fault. The time-domain response of key metrics (AC and DC terminal variables) are used in order to define the fitness function. As long as the problem has not yet converged, new control variables are generated by the optimization algorithm. The EMT model is updated with the new control variables and a new simulation run is executed. The iterations are terminated either when the upper boundary limit of iteration numbers is reached or the acceptable tolerance in the error of the fitness function is found.

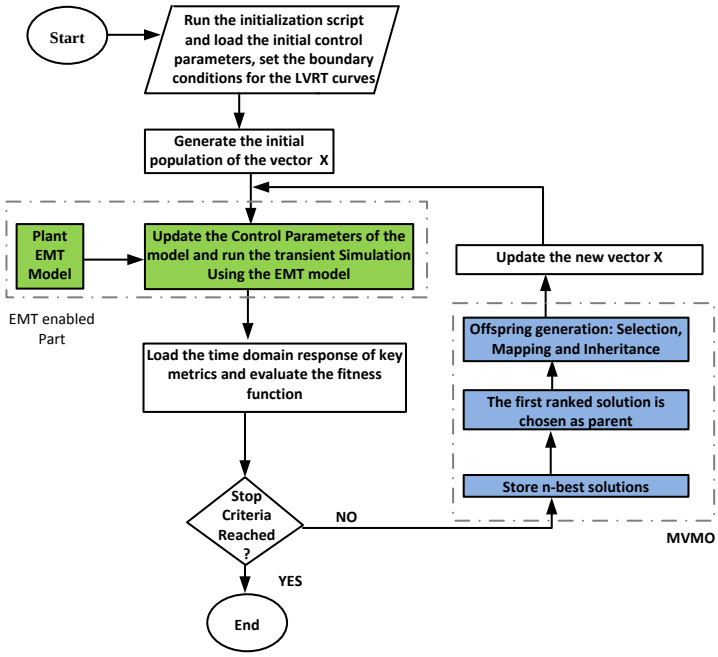

Figure 4.1: Iterative procedure for optimal FRT compliance tuning of the offshore wind plants with VSC-HVDC connection.

4.2.2. MEAN VARIANCE MAPPING OPTIMIZATION ALGORITHM FOR THE ITERATIVE PROCEDURE

The iterative procedure uses the mean variance mapping optimization (MVMO) algorithm [162]. Figure 4.1 presents the algorithmic steps of the MVMO. The blue blocks highlights the steps involved in the evolutionary mechanism. The procedure starts with the generation of an initial population, which constitutes a vector comprising random samples of the optimization variables, each one drawn within the corresponding [min, max] bounds. The sampled values are normalized to the range [0, 1]. The optimization variables are de-normalized only in the stage where the optimization problem is evaluated.

The core of the iterative procedure involves the inner loop of the flow diagram. In this loop the evaluation of the fitness function for a given solution is performed updating the solution archive (i.e. memory of the success achieved by evolving the solution throughout the search process) followed by the creation of a new solution. The later is based on the best ranked solution in the archive (i.e. parent) and by applying the mapping function to generate new values for a set of selected optimization variables. From the later a subset of optimization variables is sequentially selected throughout the optimization search and subsequently mutated to have new values by applying a map-

ping function, which accounts for the statistical performance measures derived from the solution archive. The procedure ends once the termination criterion, defined as a maximum number of function evaluations, is met. Remarkably, the mapping function allows to adaptively switch the search emphasis from exploration (greedy search across the search space) to exploitation (intensified search within an attractive region of the search space). A thorough comparison between MVMO and other types of optimization algorithms is out of scope of this chapter [162].

The ranking of the solutions in the archive is based on a fitness measure, which is defined based on the HVDC link performance and penalized due to violation of technical constraints (e.g. maximum allowed HVDC link over-voltage). The penalization is computed as the sum of a penalty factor, which is chosen as a high value (i.e 4 p.u). It is defined from a sensitivity based assessment of the quality of the solution as affected by considering penalty factors of different magnitudes, and the sum of the constraint violations. This kind of penalization is known as static penalty scheme.

4.3. AVERAGE VALUE EMT MODEL OF OFFSHORE WIND POWER PLANT AND VSC-HVDC SYSTEM

4.3.1. TEST SYSTEM CONFIGURATION

In order to test the formulation and solution of the optimization problem, a point-to-point offshore VSC-HVDC link connecting two offshore wind power plants is used as it is presented in the figure 4.2. The link is rated at +/-320kV, with a 200MW transmission capacity. The AC terminal voltage of the onshore converter station is 230kV. It is interfaced to the 380kV AC grid via a step-up transformer. The length of the HVDC cable is 100km. The AC terminal voltage of the offshore converter station is 150kV. It is connected to the 110 kV HVAC offshore cables with step-down transformer. The wind plant consist of two areas, power plant module 1 (PPM1) and power plant module 2 (PPM2) connected at the 33kV voltage level.

4.3.2. MODEL AND CONTROL OF THE GRID SIDE VSC-HVDC STATION

Compared to the model of chapter 3, where a detailed switch model was used in PSCAD, a time-average EMT model is used in this chapter for the HVDC link [27]. The model is developed in Matlab/Simulink in order to enable coupling of the simulations with the optimization algorithm. It includes full representation of the inner and the outer current control loops, synchronized to the AC grid voltage using a typical synchronous reference frame phase-lock-loop (SRF-PLL). The convention used here is that the d-axis voltage is aligned with the voltage vector at the PCC point while the q-axis grid voltage is controlled to the zero value. The outer loops utilize PI regulators for setting the inner controller current references. Figure 4.3 presents the onshore VSC-HVDC station model and its associated control modules as it is used in this work.

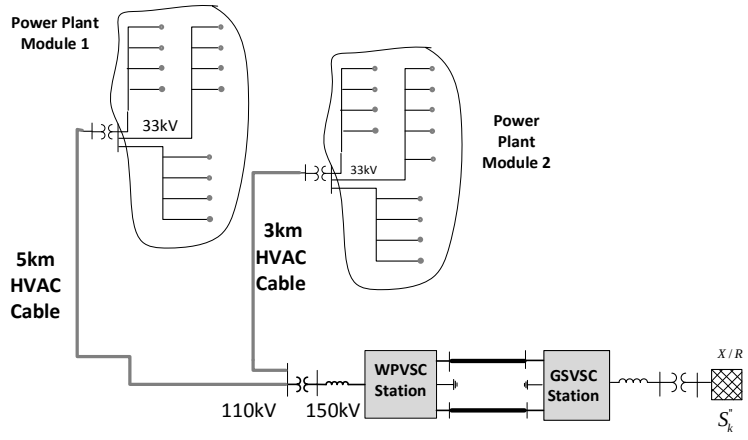

Figure 4.2: The point-to-point VSC-HVDC link and the connected offshore wind power plants as it is used in this chapter.

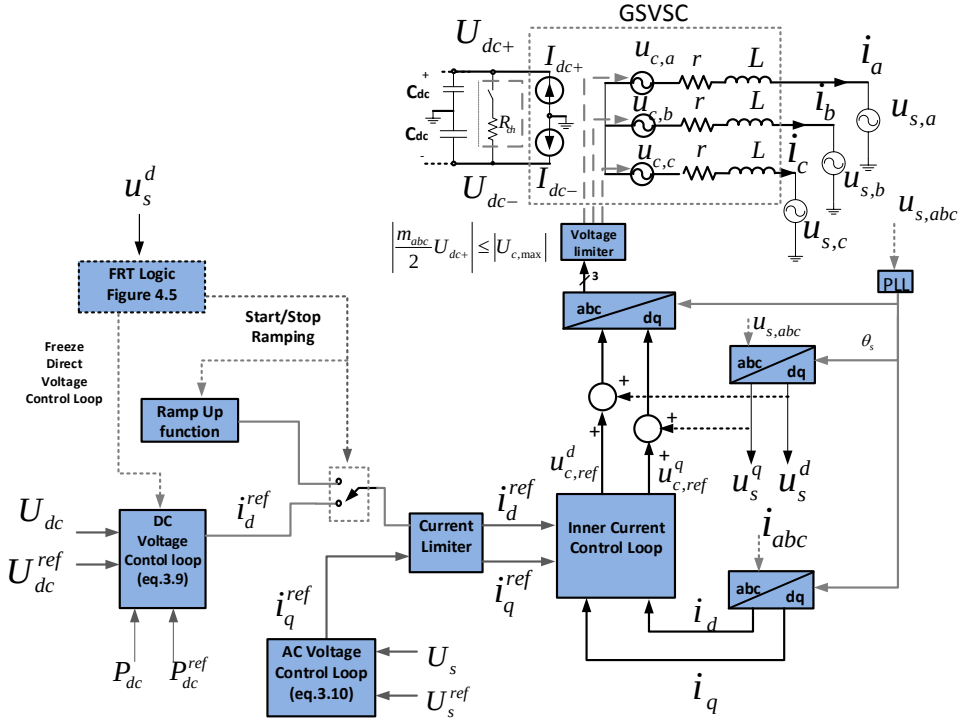

Figure 4.3: Average value EMT model of the onshore VSC-HVDC station. In the figure it can be seen the inner, the outer loop and the average value EMT modeling approach used.

4.3.3. MODEL AND CONTROL OF THE OFFSHORE VSC-HVDC STATION

The offshore wind power plant side VSC-HVDC (WPVSC) station is controlled as a power sink for the generated offshore wind power. The block diagram of the model is presented in figure 4.4 along with two FRT controllers. The per unit direct voltage value is used in order to impose a controlled voltage drop at the offshore AC island as first presented in [160]. In this way, it is ensured that the AC voltage drop will be applied only when the direct voltage rises above the U_{dc}^{th} threshold value. At the same time the offshore AC voltage reference is coupled proportionaly to the direct voltage variations. The advantage of such approach compared to the PI-based solution presented in [27] is that a simple controller is linking the direct over-voltage of the HVDC link to the offshore voltage control.

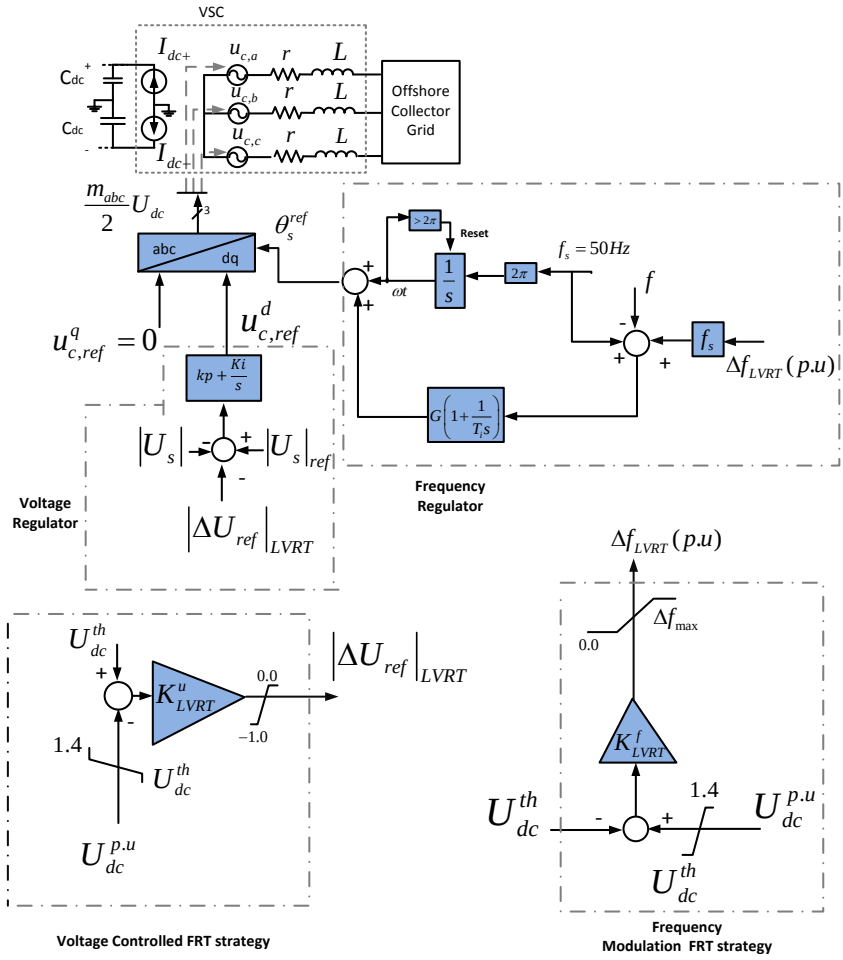

Figure 4.4: Time average model of the offshore VSC-HVDC station and its associated control loops. In the model it can be seen the two fault ride through strategies, namely the voltage drop method and the frequency modulation method. These two methods are applied separately at the offshore HVDC station.

The second FRT control module, uses similar approach in order to change the reference of the frequency controller as presented in figure 4.4. A proportional gain K_{LVRT}^{f} is used in order to link the direct voltage variation to frequency reference. The selection of these control parameters will be formulated and solved as an optimization task.

4.3.4. STATE MACHINE FOR FRT COORDINATION OF THE HVDC LINK

The coordination among the normal operation, the AC fault condition and the post-fault state of the onshore HVDC converter station is performed using the state machine presented in figure 4.5. The input variable is u_s^d which accounts for the positive sequence d-axis voltage at the onshore converter station in per unit value. As soon as the voltage drops below $U_s^{th,min}$ (which in our case we assume to be 0.9 p.u) the converter enters the low voltage ride through (LVRT) state. It shifts its current limitation priority from active to reactive current current priority. It also follows the equation 3.10 with the PI controller set to "freeze". If the voltage drops further below the 0.5 p.u threshold, the converter enters the FRT mode. In this mode of operation,the total current capacity is used as reactive current. Furthermore, the direct voltage control loop of equation 3.9 is set to the freeze state.

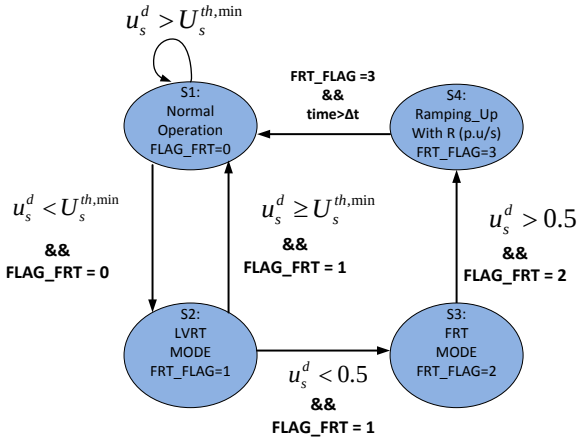

Figure 4.5: Proposed state machine for pre-fault, fault and post-fault period coordination for the onshore VSC-HVDC station.

In the FRT mode, the active current is reduced to zero as a result of reactive current injection given that the minimum reactive current boosting gain, k, is selected to be equal to 2. As soon as the voltage recovers above the 0.5 p.u threshold, the onshore converter enters the post-fault state (S4), where the active current i_d is ramped up from the zero value (during the state S3) to the pre-fault value i_{d0} with a predefined rate R given in p.u/s. The duration of the ramping period is calculated from equation (4.1) where T_{fault} is the time the fault is applied, T_r is the time the ramping is ended and i_d^{fault} is the value of the active current in the FRT mode, which is zero. During the states S3 and S4, the DC voltage control loop remains blocked.

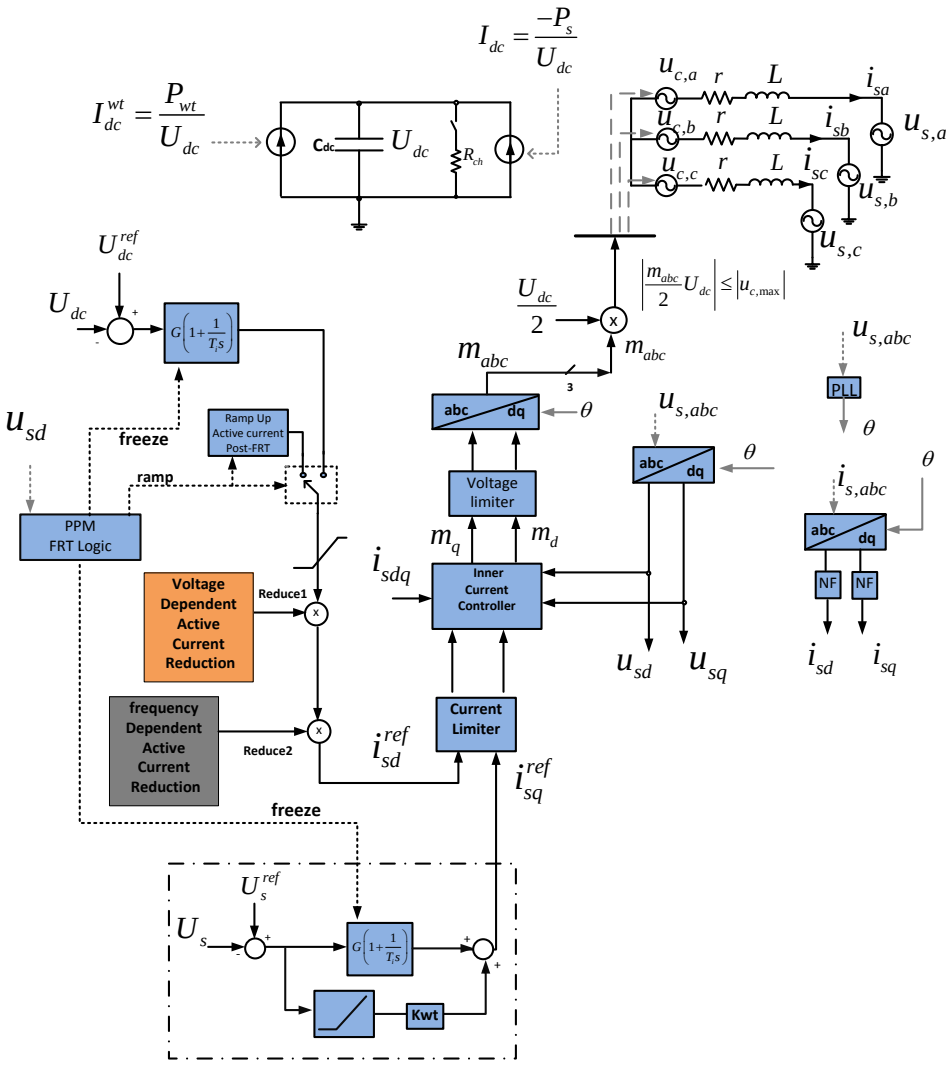

Figure 4.6: Type-4 aggregate offshore wind power plant model and the associated control modules. Namely in the diagram it can be seen the inner controller, the current limiter, the FRT logic, the ramp-up block and the active current reduction blocks.

$$R = \frac{\Delta i_d}{\Delta t} = \frac{i_{d0} - i_d^{fault}}{T_r - T_{fault}} \tag{4.1}$$

4.3.5. OFFSHORE WIND POWER PLANT AGGREGATE MODEL

The offshore wind power plants connected to the offshore VSC-HVDC station are modeled by an aggregate equivalent model connected to the 33kV terminal. Full converter interfaced wind turbine generator technology (type 4A) is assumed represented by an EMT average value model. Since the wind turbine generator is completely decoupled from the offshore AC grid voltage by means of the AC/DC/AC conversion, only the AC-DC converter at the offshore grid side is modeled considering its DC bus. The later model includes detailed representation of all the control loops as it can be seen in figure 4.6. The model presented here is different from the chapter 3 model, in the sense that it does not have negative sequence current control and it uses additional functions for reduction of the active current. In that context, for completeness it was considered necessary to present it in this section.

When faults occur in the AC offshore collector grid, the wind turbines as typical grid codes require provide reactive current injection to the isolated AC offshore collector system. This is performed proportionally to the reactive current boosting gain, K_{wt}. The control loop utilized is the same to the equation 3.10. A current limiter control module ensures that the injected currents do not exceed the over-current capacity, which is here 1.0 p.u.

4.3.6. STATE MACHINE FOR FRT COORDINATION OF THE WIND POWER PLANT

The operation of the offshore wind power plant module (PPM) is guided by the state machine presented in figure 4.7. The state machine follows the same approach as in the case of the GSVSC station with different thresholds. The normal operation is defined for voltage levels at the offshore terminals above the U_{offsh}^{lim1} value. Once, the voltage drops below U_{offsh}^{lim}, the wind turbine enters the LVRT range where it injects reactive current following reactive current priority. If the voltage drops below the level U_{offsh}^{lim2}, the wind turbine enters the FRT mode.

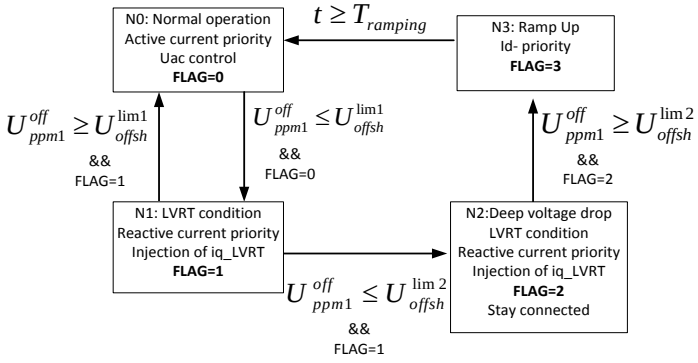

Figure 4.7: State machine that describes the operating modes of the type 4 wind turbine. The state machine is used to coordinate the fault and post-fault control loops of the PPM. The signals associated with state machine can be seen in figure 4.6.

The value of voltage theshold U_{offsh}^{lim1} is selected to be 0.8 p.u in order to ensure that the normal operation voltage variations are covered. The value of U_{offsh}^{lim2} is selected to be 0.5p.u. The choice is made assuming that the minimum reactive current boosting for the wind plants is 2. Hence, if the voltage is below 0.5 p.u, the PPM enters the state N2, providing all its current capacity as reactive fault current. Once, the voltage recovers, the PPM enters state N3 which enables the active current ramp up. If the voltage drop at the wind turbine is above the 0.5p.u, the wind turbine returns to state N1 without applying ramping.

4.3.7. CONTROL MODULES AT THE WIND PLANT FOR ENHANCEMENT OF THE VSC-HVDC LINK FRT COMPLIANCE

This paragraph introduces two control modules at the wind turbines for the enhancement of the coordinated FRT capability of the VSC-HVDC link. The first is a voltage dependent active current reduction block, presented in figure 4.8. It is used in the case that a controlled voltage drop is imposed by the offshore HVDC station. As it can be seen, the module utilizes the per unit d-axis voltage component in order to impose an active current reduction at the wind turbines. It is important to note that the block is activated when the wind turbine enters state N1 in figure 4.7. In this way it is ensured that the active current reduction is not performed during normal offshore voltage conditions.

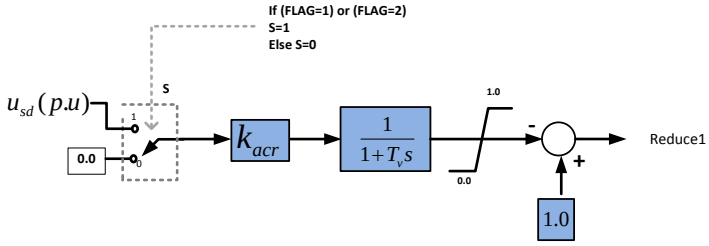

Figure 4.8: Block diagram of the voltage-dependent-active-current (VDAC) reduction method as it is used in the PPM model of figure 4.6.

The second control module which is installed at the offshore wind PPMs uses the available frequency by the PLL in order to impose an active current reduction at the wind turbines. The control block is given in figure 4.9. As it can be seen, the per unit frequency variation is used in order to impose the active current reduction. A lead-lag block with a proportional gain is used in order to provide flexibility in the tuning and ensure the best result without imposing instabilities. In both cases, the reduction is performed by multiplying the output signal of the control modules to the active current reference of the wind turbine as it can be seen in figure 4.6.

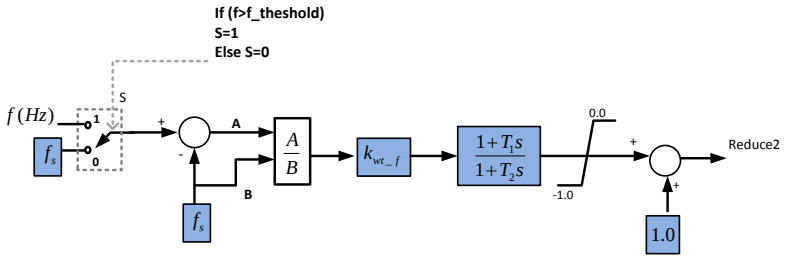

Figure 4.9: Block diagram which presents the control module used by the wind turbines to impose a frequency dependent active current reduction at the wind plant.

4

4.4. OBJECTIVE FUNCTION FOR THE STUDIED FRT COMPLIANCE STRATEGIES

4.4.1. OBJECTIVE FUNCTION FOR THE VOLTAGE DROP FRT STRATEGY FOLLOWED BY REACTIVE CURRENT INJECTION FROM PPMS

The optimal tuning problem is initially formulated for the voltage drop FRT strategy. The expected qualitative time domain response of the VSC-HVDC link and the connected offshore wind power plants during the FRT and the post-FRT period is illustrated in Figure 4.10. The direct voltage variation in the HVDC link is restricted by the U_{dc}^{min} and the U_{dc}^{max} values. These selected boundary conditions are defined based on the manufacturer specifications and depend on the electrical stresses that the components are allowed to withstand during the normal operation as well as during the FRT period. Within these dynamic limits, we define the (U_{dc}^{th}) threshold which is the offshore direct voltage value where the voltage drop FRT scheme is triggered. The green zone in figure 4.10 describes the normal operation zone while the orange zone the emergency situation zone. Direct voltage values below U_{dc}^{min} (red zone) indicates a DC fault condition and leads to the HVDC link tripping.

During a severe onshore AC grid fault, the onshore converter station provides additional reactive current injection following the equation 3.10. Due to the limited fault current capacity, the active current is reduced to zero by the current limiter control module in figure 4.3. The direct voltage rises as a result of surplus of power flowing in the HVDC link with respect to the power flowing out of the link. As soon as the U_{dc}^{th} is reached, the controlled voltage drop is applied at the offshore AC grid by the offshore HVDC converter station. In the presence of this voltage drop the wind turbines inject reactive current.

Let us at recall the two AC voltage thresholds defined in the state machine of figure 4.7 which are U_{off}^{lim1} and U_{off}^{lim2}. When the voltage amplitude shifts below the threshold U_{off}^{lim2}, the wind turbines enter the FRT state. In this case, since the voltage drop is very deep, all the wind turbines current capacity is provided as reactive current injection while the active current is reduced to the zero value by the current limitation control module .

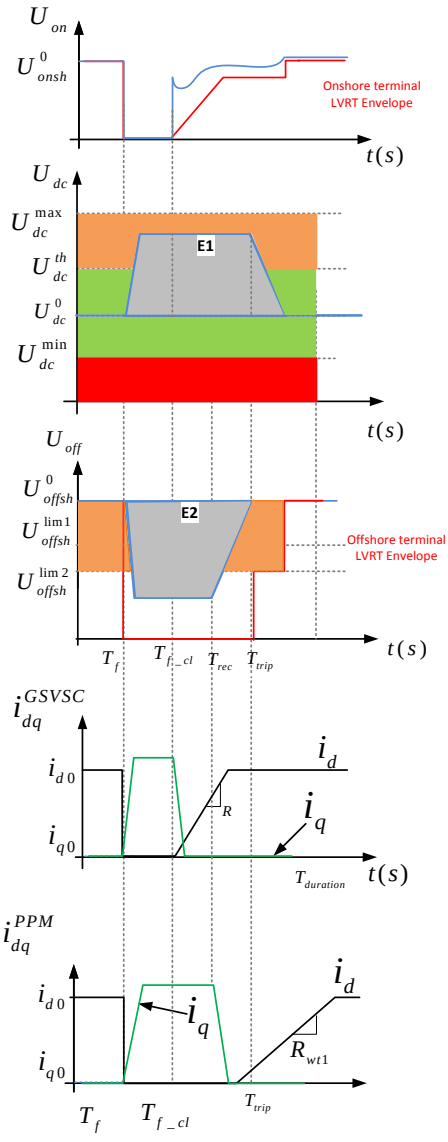

Figure 4.10: Qualitative expected time-domain response of the offshore wind power plant and the HVDC link for the onshore fault. From top to down, the direct voltage at the offshore DC terminal, the controlled offshore AC voltage drop, and the active and reactive currents at the onshore HVDC converter station and the offshore wind power plant.

As long as the wind turbines have entered their FRT state, their post-fault active current is ramped with a given rate defined as R_{wt}. In the case that the offshore voltage drop is such that the PPMs have not entered their FRT mode, the active current will be immediately recovered without ramping. The goal of the optimization task is to minimize the normalized HVDC link over-voltage defined here as the area E_1 in figure 4.10 in conjugation with the normalized offshore AC voltage drop area E2. The optimization problem is solved over the X vector control parameters given in (4.2) for the test system in figure 4.2 where K_{wt1} and K_{wt2} are the reactive current boosting gains of the two offshore wind power plants (PPM), R_{wt1} and R_{wt2} are the ramp up rates of the active current during the post-fault period of the PPMs and K_u^{LVRT} is the proportional gain of the voltage drop FRT method controller in figure 4.4.

$$X = [K_{wt1}, K_{wt2}, R_{wt1}, R_{wt2}, K_u^{LVRT}]. \tag{4.2}$$

The mathematical formulation of the optimization problem is given by the equations (4.3) to (4.7). The minimization of the areas E_1 and area E_2 is formulated as the weighted sum of the two integrals. The values for w_1 and w_2 can be selected so as priority is given to one of the two functions over the other. In this case, since we need to ensure that the direct over-voltage is always bounded within the limits with minimum offshore voltage drop, we select w1 to be equal to w2. The chosen value is 100 derived from sensitivity analysis. The calculation of the two integrals is performed using the time domain simulation plots of the direct voltage at the offshore DC terminal, $U_{dc}(t)$, and the AC voltage at the offshore 150kV terminal, $U_{ac,off}(t)$. Finally, $T_{duration}$ is the duration of the time domain simulation, and $U_{ac0,off}(t)$ and $U_{dc0}(t)$ is their time domain response without the fault being applied , which reflects the system normal operating condition.

$$minJ_1(X) = w1F_{dc}^{area}(X) + w2F_{ac}^{area}(X) \tag{4.3}$$

$$F_{dc}^{area}(X) = A1\int_{t=0}^{t=T_{duration}} (U_{dc}(t) - U_{dc0}(t))dt \tag{4.4}$$

$$F_{ac}^{area}(X) = A2\int_{t=0}^{t=T_{duration}} (U_{ac,off}(t) - U_{ac0,off}(t))dt \tag{4.5}$$

The constants A_1 and A_2 are given as:

$$A1 = \frac{1}{\int_{t=0}^{t=T_{duration}} U_{dc0}(t)dt} \tag{4.6}$$

$$A2 = \frac{1}{\int_{t=0}^{t=T_{duration}} U_{ac0,off}^{i}(t)dt} \tag{4.7}$$

The problem is solved subject to the inequality constraints (4.8) and (4.9). The constrain (4.8) ensures that the imposed offshore voltage drop by the offshore HVDC station will not surpass the FRT grid code voltage envelope, $H_{FRT}(t)$. This FRT envelope is provided as an input to the iterative procedure. The constrain (4.9) defines the boundaries that the control variables are allowed to vary. The constraint (11) is not included in the

static penalty scheme, because the normalized search space of MVMO always ensures the fulfillment of the min-max bounds.

$$U_{ac,off}(t) \geq H_{FRT}(t) \tag{4.8}$$

$$X_{min} \leq X \leq X_{max} \tag{4.9}$$

4.4.2. OBJECTIVE FUNCTION FOR VOLTAGE DROP FRT STRATEGY FOLLOWED BY ACTIVE CURRENT REDUCTION AT WIND PLANTS

The alternative control approach to the FRT compliance problem of the VSC-HVDC link is the use of the proposed voltage-dependent active current reduction control block presented in figure 4.8. In this scheme the wind turbines during the offshore voltage drop period reduce their active current in order to reduce the HVDC link overvoltage. In this case no reactive current is provided by the wind plants during the voltage drop period. The anticipated qualitative response of the PPMs on the imposed offshore voltage drop by the WPVSC is presented in figure 4.11.

The formulation of the optimization problem is similar to the previous case, given by equation (4.3) with the only difference that the vector X is given by (4.10). The time constant of the low pass filter, T_v in figure 4.8, is selected to be 20ms for both offshore wind plants. Hence, the optimization task targets only the best proportional control gains. The inequality constraints are the same as in (4.8) and (4.9). The weights w1 and w2 used are both equal to 100.

$$X = [K_{acr(wt1)}, K_{acr(wt2)}, K_u^{LVRT}] \tag{4.10}$$

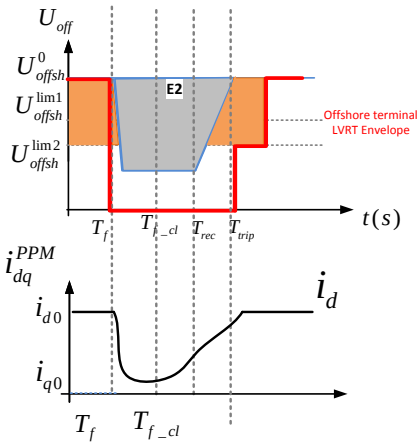

Figure 4.11: Qualitative response of the wind plant for an applied voltage drop when equipped with voltage-dependent-active-current reduction block.

4.4.3. OBJECTIVE FUNCTION FOR THE FREQUENCY MODULATION CONTROL STRATEGY

The last FRT strategy which is optimized in this chapter is the frequency modulation method. The control block used at the WPVSC is presented in figure 4.4. The frequency is allowed to vary between strictly defined boundaries. In addition, given that the plant consists of full-converter interfaced wind turbines, the dedicated control module in figure 4.9 is applied in order to impose a frequency dependent active current reduction. Figure 4.12 proposed the anticipated time domain response of the plant. Two operation zones are defined for the offshore frequency. The first zone is between f_{min} and $f_{threshold}$ where the frequency is allowed to vary during normal operation. This frequency band shall take into account the variations observed in the offshore plant during power set-point changes or other control actions.

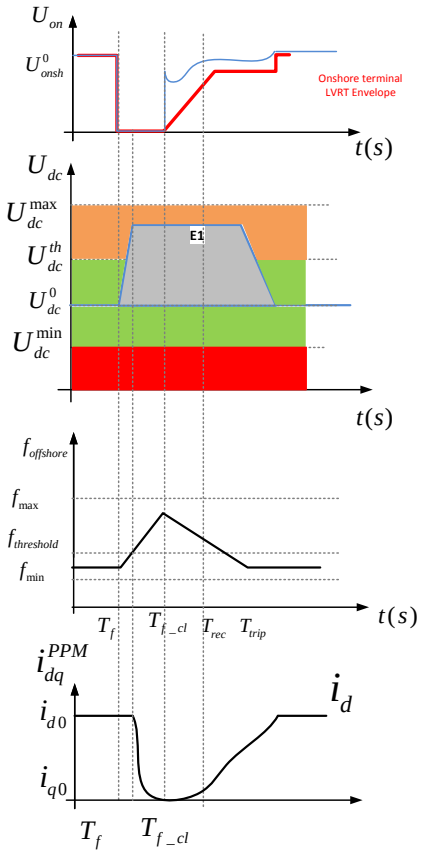

Figure 4.12: Qualitative result for the case where the frequency modulation is applied followed by active current reduction at the offshore wind power plants.

Once the offshore frequency reaches the threshold value $f_{threshold}$, the control block of figure 4.9 imposes an active current reduction to the wind turbines. The lead-lag block of the active current reduction controller can be used in order to compensate the delay that might occur in the active current reduction process or due to frequency measurement. The depth of the active current reduction is affected by the proportional controller gain K_{wtf} in figure 4.9. As soon as the fault is cleared at the onshore side and the direct voltage recovers, the frequency drops below its threshold value $f_{theshold}$ and the active current of the wind turbines returns to normal operation.

Given that the frequency variation is driven by the control module of figure 4.4, the mathematical formulation of the objective function targets the minimization of the area E_1 in figure 4.12. The objective function is given by (4.11).

$$minJ_3(X) = F_{dc}^{area}(X) \tag{4.11}$$

The vector of the optimization variables is given for the test system as in (4.12) subjected to max-min boundaries of the variables. It is worth to mention that since the frequency limits are set by the WPVSC controller itself as "hard" limits, it is not needed to impose them as constrains in the optimization problem.

$$X = [K_{f(wt1)}, T_{1(wt1)}, T_{2(wt1)}, K_{f(wt2)}, T_{1(wt2)}, T_{2(wt2)}, K_{LVRT}^{f}] \tag{4.12}$$

4.5. SIMULATION RESULTS

4.5.1. VOLTAGE DROP FRT WITH REACTIVE CURRENT FROM PPMS

This paragraph presents the results of the optimal tuning for the controlled offshore voltage drop method where the offshore wind power plants are assumed to comply with the reactive current injection requirements at the offshore AC island grid. The voltage drop control module of figure 4.4 is used. The number of the maximum iterations is selected to be 500 for this problem. Figure 4.13 presents the evolution of the best fitness function per iteration. In addition, figure 4.14 presents the control variable iterations.

As it can be seen, the MVMO algorithm converges to the optimal fitness value after 451 iterations. Additional experiments with higher number of iterations have been conducted and the same results are found. It can be seen that after 400 iterations the optimization variables are concentrated around the optimal values. The best results achieved for the particular case is given in (4.13).

The algorithm has converged to different reactive current boosting gains and post-fault active current ramping rates for the two plants. The latter is justified due to the different lengths of the cables. In addition, the solution of different ramp up rates reduces the DC link over-voltage during the post fault period compared to the default case.

$$X_{opt} = [2.02, 4.29, 2.44, 3.31, 71.94]. \tag{4.13}$$

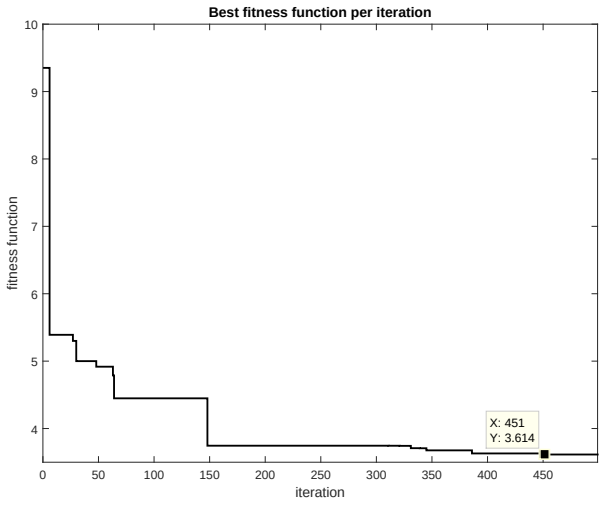

Figure 4.13: Evolution of the best fitness function for the case of the voltage drop followed with reactive current injection.

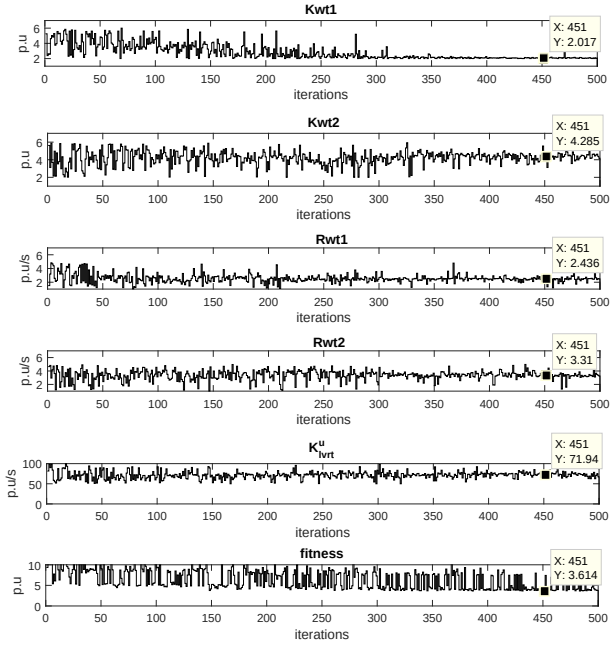

Figure 4.14: Control variable iterations for the optimization problem. The results are for the case with voltage drop and reactive current injection from the wind plants.

Finally, the best control parameters are validated against the default values in (4.14) which reflect typical grid code parameters. These default value reflect typical parameters. Figure 4.15 presents the comparison between the optimal and the default case. As it can be seen, the use of the optimally tuned control variables reduces the HVDC link over-voltage as well as its duration. The same is also observed for the imposed voltage drop at the offshore AC island.

$$X_{default} = [2.0, 2.0, 4.0, 4.0, 40]. \tag{4.14}$$

From the simulation results it can seen that the injection of the reactive current by the wind plants during the voltage drop period is beneficial for the total HVDC link FRT response. This benefit is mainly due to the inherent active current reduction achieved as a matter of the over-current limiters at the wind turbines.

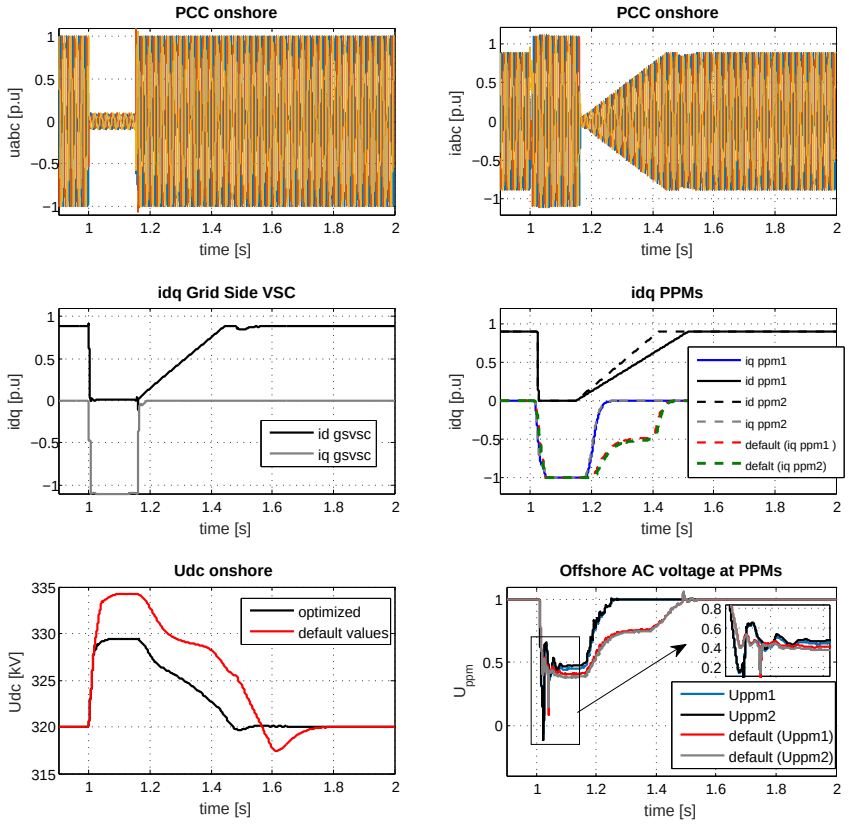

Figure 4.15: Time domain response of the wind power plants and VSC-HVDC link for two subcases of the voltage drop strategy followed by reactive current injection of the wind turbines during the voltage drop period. In the first subcase, default values are used at the controllers. In the second subcase, the optimized values of the control parameters are utilized.

4.5.2. VOLTAGE DROP FOLLOWED BY ACTIVE CURRENT REDUCTION FROM WIND POWER PLANTS

The optimization of the voltage-dependent-active-current (VDAC) reduction method is presented in this paragraph. Figure 4.16 presents the best fitness evolution per iteration of the MVMO algorithm. As it can be seen, the algorithm converges to the best solution for 300 iterations. For this particular case, the iterations of the control variables are presented in figure 4.17. From the results it can be observed that the algorithm has already defined the region of the proportional reductions gains $Kacr1$ and $Kacr2$ for approximately 200 iterations while the proportional gain of the voltage drop method is varied in order to define the best fitness. The optimization problem has been solved for 500 and 1000 iterations and nearly the same optimal values are defined.

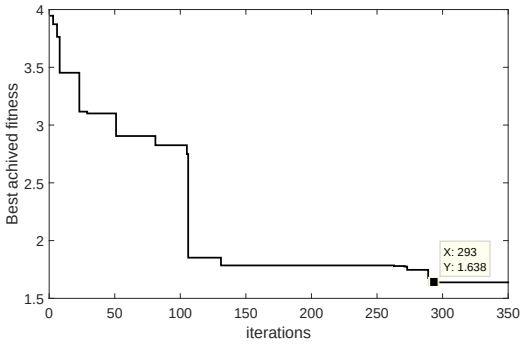

Figure 4.16: Best fitness for the case of voltage drop followed by active current reduction by wind plants.

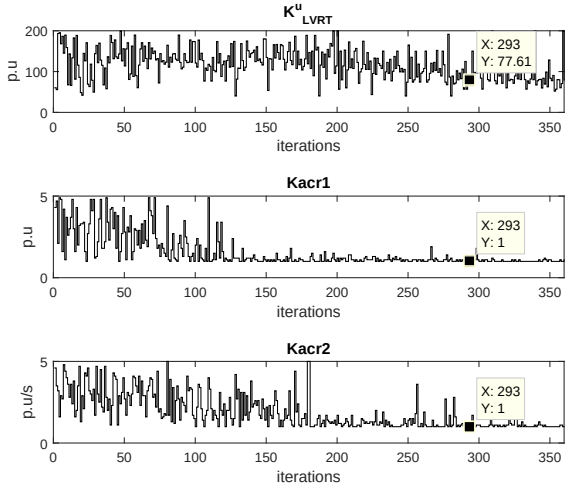

Figure 4.17: Evolution of the best solution for the case of the voltage drop with active current reduction from the wind plants.

The optimized voltage-dependent-active-current (VDAC) reduction strategy is compared in figure 4.18 to the base case as in [147] and [27] where the voltage drop is imposed without the wind turbines providing neither reactive current injection, nor active current reduction. Observing the time domain response of the system, it can be seen that the optimized by the proposed iterative procedure control variables improves significantly the HVDC link over-voltage. Additionally, it ensures that the over-voltage in the HVDC link is below the selected 330kV maximum value. This improvement is achieved mainly due to the active current reduction by the wind turbines.

Observing the optimized offshore AC voltage at WPVSC in figure 4.18 to the default parameters cases, it is observed that the voltage drops to values very close to zero. This is justified since first a voltage drop has to occur before the active current is reduced while in the previous paragraph case, in figure 4.15, even a small voltage drop would lead to injection of full current capacity as reactive current and reduction of the active current to zero. The later explains why the active current reduction methods contributes mainly in the HVDC link over-voltage and not much in the offshore voltage drop.

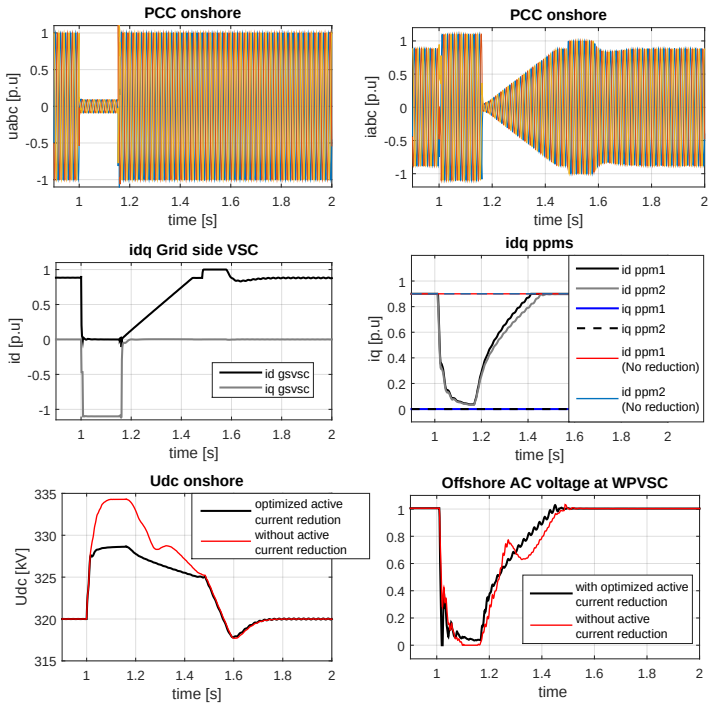

Figure 4.18: Time domain response of the offshore wind power plants and VSC-HVDC system for two subcases of the voltage drop strategy. In the first one the wind turbines do not contribute in the FRT of the HVDC link (neither by active current reduction nor by reactive current injection). In the second one the optimized voltage dependent active current reduction controller is applied at the offshore wind plants.

4.5.3. FREQUENCY MODULATION CONTROL STRATEGY

The evolution of the optimal tuning procedure for the frequency dependent FRT scheme is presented in figure 4.19. As it can be seen, the iterative procedure is terminated after 300 iterations and the optimal point has been detected for 100 iterations. The vector of the optimal control parameters is given by figure (4.15) while the time domain response of the system by figure 4.20.

$$X_{opt} = [-111.6, 0.06, 0.07, -167.7, 0.1, 0.05, 1.0]. \tag{4.15}$$

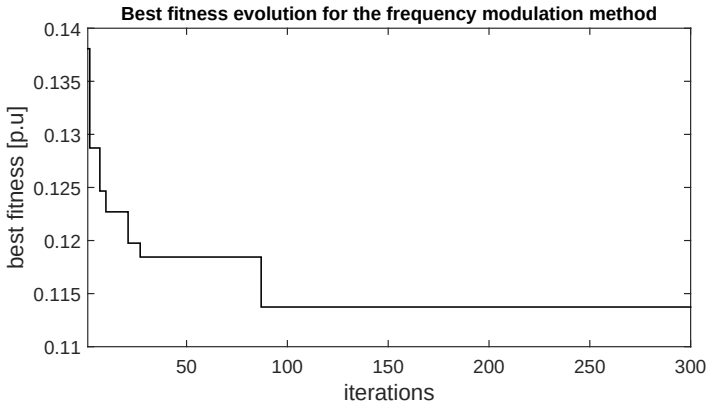

Figure 4.19: Evolution of the best fitness function for the frequency modulation FRT strategy.

4.5.4. COMPARISON OF THE OPTIMALLY TUNED STRATEGIES

Comparing the optimally tuned FRT strategies, the best response with reference to the HVDC link over-voltage is achieved in the case of the voltage drop method which is assisted by the reactive current injection by the wind turbines. The advantage is not derived directly from the reactive current injection itself but rather from the followed active current reduction which is achieved due to the limited fault current capacity of the wind turbines. Although, the voltage amplitude at the wind turbines PCC terminals is boosted, the resulted active current reduction enhances significantly the power balance in the HVDC link, thus reduces the direct over-voltage. Furthermore, since the wind turbines are forced to enter their FRT mode, their post-fault active current ramping when accurately tuned with respect to the active current ramping of the onshore VSC-HVDC station, improves the post-fault direct over-voltage at the HVDC link.

Finally, concerning the offshore frequency modulation FRT method, it does not present as good results as the other two strategies with reference to the achieved over-voltage. This is mainly attributed to the associated time constant of the frequency regulator of the WPVSC. Smaller time constant could not be applied in this cases as it resulted in the controller instability. As long as the best achieved direct over-voltage can be tolerated by the equipment, the frequency modulation FRT is suitable. In any case, by optimizing the control parameters of the three FRT strategies improves the dynamic response of the HVDC link.

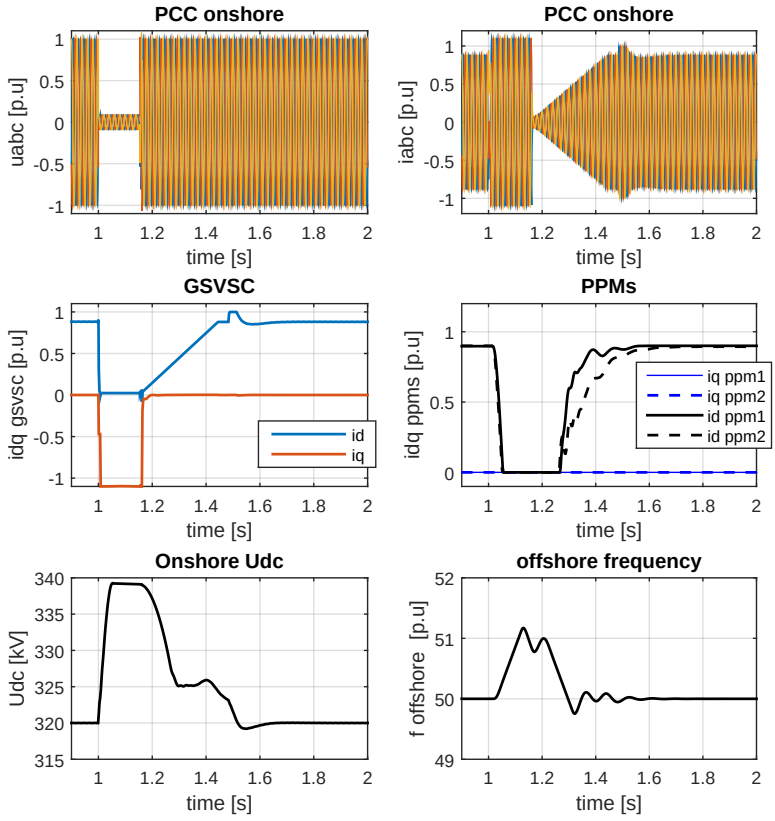

Figure 4.20: Time domain response of the system for the optimized frequency modulation case.

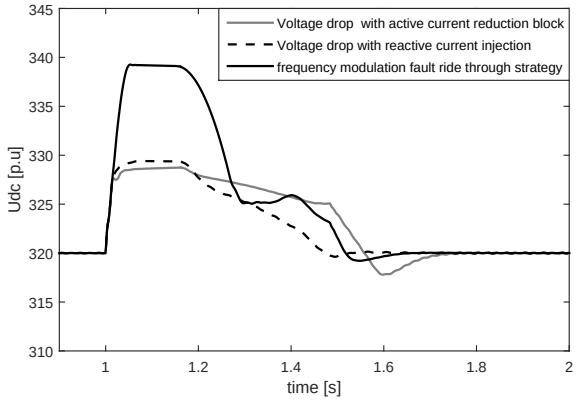

Figure 4.21: Comparison of the direct voltage response at the onshore DC terminal for the three given optimized FRT strategies.

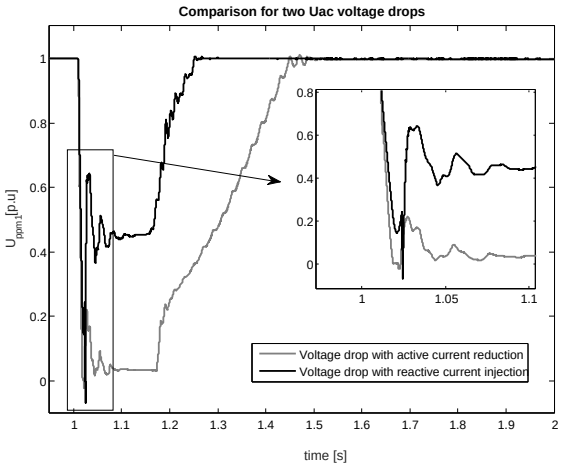

Figure 4.22: Comparison of the depth and duration of the AC voltage at the two power plants between the two subcases of the voltage drop strategy.

4.6. CONCLUSIONS

Large offshore wind power plants connected to the mainland AC grid utilizing VSC-HVDC transmission shall be fault ride through compliant. The classical chopper based fault ride through strategy increases the capital investment cost. New state of the art, coordinated control strategies are becoming nowadays more attractive. Moreover, since the VSC-HVDC link is mostly shared by different offshore wind power plants, the efficient estimation of the fault ride through control parameters for the wind plants and the HVDC link becomes an important task in order to ensure robust and stable compliance.

In this work, a method is presented for the optimal tuning of coordinated fault ride through compliance strategies which treats the VSC-HVDC link and the offshore wind plants as one power plant entity. The method is based on an iterative procedure that uses a sequence of electromagnetic transient type simulation runs of the complete plant (VSC-HVDC link and wind plant) driven by the mean variance mapping optimization (MVMO) algorithm. It is demonstrated that by optimizing the control parameters of coordinated FRT strategies, the dynamic response of the offshore wind power plants and the HVDC link is improved during AC grid faults. Moreover, the experienced electrical stresses and the tripping risk of the plant are minimized.

5

OPTIMIZATION OF THE COORDINATED FAULT RIDE THROUGH STRATEGIES FOR OFFSHORE HVDC GRIDS

5.1. INTRODUCTION

The development of future multi-terminal HVDC grids would evolve in stages [163],[164]. It will first start with the instalation of point-to-point connections and expand gradualy towards meshed HVDC schemes which would eventually interconnect different control areas and remote renewable energy resources (i.e offshore wind plants) [165].

Significant research effort has been made with respect to the modeling, the control and the analysis of HVDC grids [166]. Initially, AC/DC power flow algorithms are proposed [167]. Next, generic time average dynamic models have been introduced in [168], [169] first for two-level VSC-HVDC systems and recently extended for modular multilevel converter (MMC) HVDC technology. The main advantage of generic average value dynamic models is the reduced model complexity and the reduction of the computation time in grid connection studies. Moreover, generic models remove intellectual property concerns between transmission system operators and HVDC system vendors in grid code compliance studies [164, 169–171].

With reference to the latest ENTSO-E Network Code (NC)-HVDC [135], the Fault-ride-through capability (followed by the injection of reactive current) is a mandatory grid code article. Different coordinated FRT compliance schemes have been proposed in the literature, for the point-to-point [159] as well as the multiterminal DC (MTDC) connection [157] of the offshore wind power plants. However, for the MTDC grid case, the effect of the post fault ramping rate of the onshore converter station during the post fault period and the influence of different operating states (snapshots) of the MTDC grid

(inversion and rectification) have not been investigated in detail. The selection of the post-fault ramping rate affects the dynamic behavior of the direct voltage in the MTDC grid and the response of offshore collector grid, when coordinated FRT strategies are applied. Furthermore, dynamic interactions between the offshore converter station, the onshore converter station and the wind power power plants during the FRT period might lead to a trip of the HVDC grid.

In that context, this chapter evaluates the proposed EMT-enabled iterative procedure as it is presented in chapter 4 for the MTDC grid connection case of the offshore wind power plants. This chapter aims to provide insights on the FRT compliance of MTDC grids and demonstrate the adequacy of the tuning methodology presented in chapter 4 for ensuring robust and optimal FRT compliance of the wind plants in MTDC grid connection with general grid code requirements.

5.2. TEST SYSTEM

A three-terminal, meshed, VSC-Based HVDC grid is used in this study with rated direct voltage at +/-250kV. It includes two grid side converters (each rated at 200MVA) and one wind park converter (at 500MVA) which connects two large offshore wind power plants. The wind plants (200MVA and 300MVA each) are connected to the offshore HVDC hub by means of HVAC offshore cables, as shown in figure 5.1. The two HVAC cables have lengths 3 km and 5 km respectively and their rated voltage is 150kV. A 110kV/150kV transformer is used to interface the offshore HVDC converter to the HVAC cables. The collector grid of the wind power plant is assumed 33kV.

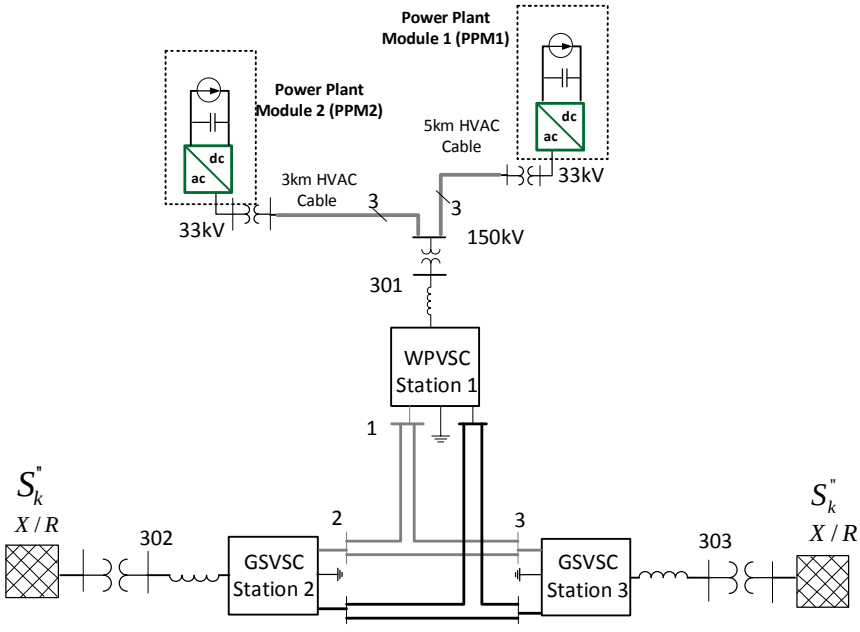

Figure 5.1: One-line diagram of the MTDC Grid test system used in this chapter.

Different snapshots of the MTDC grid are evaluated in this chapter as shown in figure 5.2. In the case a, the offshore wind plant is operated in point-to-point connection. Of course the generated offshore wind power corresponds to the capacity of the onshore HVDC station (GSVSC2). In the case b, the generated offshore wind power is dispatched between the two onshore VSC stations (station GSVSC 2 and 3). The two onshore stations apply direct voltage control at their DC terminal (using a power based droop controller). In the case c, the GSVSC2 operates in constant active power control mode whilst, GSVSC3 in direct voltage control mode. For the cases b and c the offshore wind power is flowing radially from the wind plants (Offshore HVDC station) to the onshore grids (onshore HVDC station). The case d reflects a snapshot where the onshore HVDC station 2 (GSVSC2) is operating in rectification mode, transmitting power from the onshore grid 302 to the MTDC grid applying a constant power control. Finally, in the cases e and f, it is assumed that the wind power plants and the offshore converter station are completely disconnected and the 3-terminal MTDC grid operates as a point-to-point VSC-HVDC link connecting the two AC systems. All the above cases reflect either a variety of operating states or different development stages which will be simulated in order to compare the system performance.

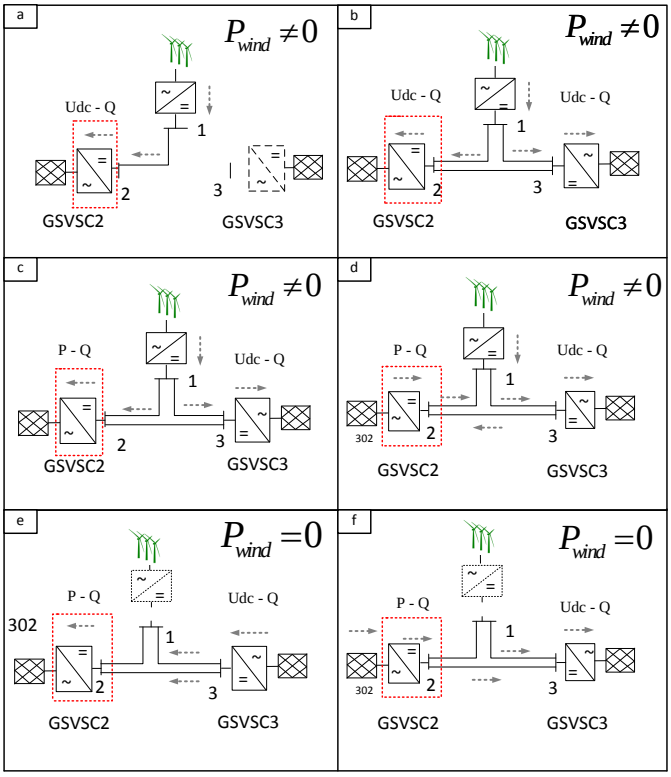

Figure 5.2: Operating cases of the MTDC grid (snapshots) which are studied in this chapter. With red colour we represent the converter station where the fault is applied at its AC terminals.

5.3. VSC-MTDC MODEL

5.3.1. VSC-HVDC STATION

We assume symmetrical-monopole VSC-HVDC configuration with two level converters for this paper analysis. A time average EMT model with detailed representation of inner current controller and the outer control loops is followed for the converters, as shown in chapter 4.

With reference to the outer control loops, typical PI-based control strategies are applied. The active current (i_d) loop is either in direct voltage control mode (using here power based droop control [169]) or in constant active power control mode using typical PI controller. The reactive current control loop (iq) provides voltage control during normal conditions and reactive short circuit current injection during AC system failures, as described in chapter 4.The model is developed in Matlab/Simulink in order to enable coupling with the Matlab optimization algorithms.

5.3.2. MODEL OF THE HVDC CABLES IN GRID CODE COMPLIANCE STUDIES

The common methodology to represent HVDC cables in power system stability time domain simulation studies is by applying lumped π-equivalent models mathematically given by state space differential equations in time domain [168]. A graphical overview of the MTDC grid transmission state space model is shown in figure 5.3. In the proposed state space generic form, the state vector (**x**) and the DC current input vector (**u**) are defined in (5.1) and (5.2) respectively. In this model, the information of the DC grid topology is included in the matrix A according to (5.3) where its submatrix vriables are given in (5.4) to (5.7). The input of the model is the DC current input vector **u**, while the output is equal to the state vector **x**. Vector **u**, includes the DC current in-feed as computed from the converters model by conservation of power at each node.

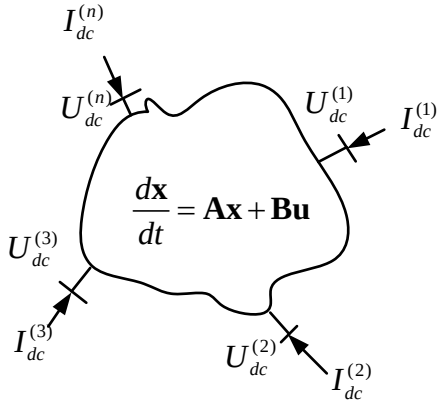

Figure 5.3: Graphical representation of the state space model used for the MTDC grid cables assuming π-section per branch.

A and B matrices are constant and are defined at the initialization stage of the dynamic model. For each DC cable section there are three states: two states referring to the DC voltage at the sending and receiving end, and one state referring to the direct current flowing through each HVDC cable section. The HVDC link could be bipolar on monopolar. In the case of bipolar, assuming that the AC system remains balanced during three phase faults in the AC side, the DC circuit remains also balanced. Hence, the dynamics of DC circuit in the bipolar configuration can be represented by a mono-polar circuit in power system stability studies with half the total current. It should be noted here that the DC capacitors of the VSC station are embedded in the DC capacitor of the HVDC cable model. If at a DC node there is no converter connected (i.e it is junction node), only the DC cable capacitance is used. Providing the state space model of each cable, it is possible to extend it to any DC grid topology by making use of the incidence matrix, which analytically describes the DC network topology.

$$\mathbf{x} = \begin{bmatrix} U_{dc}^{(1)} & U_{dc}^{(2)} & U_{dc}^{(3)} & \dots & U_{dc}^{(n)} I_{cable}^{(n+1)} & I_{cable}^{(n+2)} & I_{cable}^{(n+3)} & \dots & I_{cable}^{(n+m)} \end{bmatrix}^T_{1x(m+n)} \tag{5.1}$$

$$\mathbf{u} = \begin{bmatrix} I_{dc}^{(1)} & I_{dc}^{(2)} & I_{dc}^{(3)} & \dots & I_{dc}^{(n)} \end{bmatrix}^T_{1xn} \tag{5.2}$$

$$\mathbf{A} = \begin{bmatrix} \mathbf{a}_{nxn}^{(11)} & \mathbf{a}_{nxm}^{(12)} \\ \mathbf{a}_{mxn}^{(21)} & \mathbf{a}_{mxm}^{(22)} \end{bmatrix}_{(n+m)x(m+m)} \tag{5.3}$$

$$\mathbf{a}_{nxn}^{(11)} = [0]_{nxn} \tag{5.4}$$

$$\mathbf{a}_{nxm}^{(12)} = (\mathbf{M} * \mathbf{C})^T \tag{5.5}$$

$$\mathbf{a}_{mxn}^{(21)} = (\mathbf{L} * \mathbf{M}) \tag{5.6}$$

$$\mathbf{a}_{mxm}^{(22)} = diag(\frac{R_{cable,1}}{L_{cable,1}}, \frac{R_{cable,2}}{L_{cable,2}}, \dots, \frac{R_{cable,m}}{L_{calble,m}}) \tag{5.7}$$

$$\mathbf{C} = diag(-\frac{1}{C_{node,1}}, -\frac{1}{C_{node,2}}, \dots, -\frac{1}{C_{node,n}}) \tag{5.8}$$

$$\mathbf{L} = -diag(\frac{1}{L_{cable,1}}, \frac{1}{L_{cable,2}}, \dots, \frac{1}{L_{calble,m}}) \tag{5.9}$$

For a MTDC grid with n-nodes and m-branches, $R_{cable}i$ and $L_{cable}i$ with $i = ...m$, is the resistance and inductance of each DC cable section while C_{node},i is the sum of the converters and cable capacitance at each DC node. The incidence matrix, M for a DC grid with n number of nodes and m number of branches is a mxn matrix defined as:

$$M_{mxn}(i,j) = \begin{cases} 1, \ when\ branch\ current\ flows\ from\ i\ to\ j \\ -1, \ when\ branch\ current\ flows\ from\ j\ to\ i \\ 0, \ no\ branch\ between\ i\ and\ j \end{cases} \tag{5.10}$$

The B matrix is written as:

$$\mathbf{B} = \begin{bmatrix} \mathbf{b}_{nxn}^{(11)} \\ \mathbf{b}_{mxn}^{(21)} \end{bmatrix}_{(n+m)xn} \tag{5.11}$$

Where the sub-matrices are defined as:

$$\mathbf{b}_{nxn}^{(11)} = diag(\frac{1}{C_{node,1}}, \frac{1}{C_{node,2}}, \ldots, \frac{1}{C_{node,n}}) \tag{5.12}$$

$$\mathbf{b}_{mxn}^{(21)} = [0]_{nxn} \tag{5.13}$$

5.3.3. DIRECT VOLTAGE AND POWER CONTROL IN THE MTDC GRID

The direct voltage control is very important for the operation of any HVDC grid. Direct voltage variations are primarily affected by the active power balance between the converter stations during normal and fault conditions. The control of direct voltage in this chapter is performed by applying a power based, direct voltage droop controller as it is shown in figure 5.4. The power is measured at the PCC and the direct voltage variation at the DC side is used as input variable which regulates the active power reference of the onshore converter station. Practically it is a proportional controller applied to the power reference of the active power controller. There are also other alternatives of droop direct voltage control, either using as input the direct current measured in the DC side or applying the proportional controller on the active current component of the converter station.

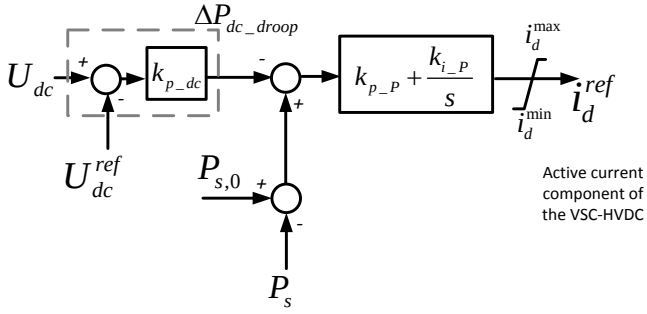

Figure 5.4: The power based droop controller used in this chapter as active current control loop.

5.3.4. EFFECT OF THE GRID CONNECTION POINT SHORT CIRCUIT POWER

Future power systems would host a large share of power electronic based generation capacity. The connection of a VSC-HVDC station to a grid connection point with very low short circuit power might lead to instabilities and a complete trip of the HVDC station during AC grid faults. The instability observed with weak connection points is primarily caused by the phase-lock loop (PLL) in conjugation with the poor dynamic performance of the inner current control loop. Different PLL configurations and as well as effective

tuning techniques have been studied in the literature in order to enable operation of the power converters even at very low short circuit power levels. The aim of this paragraph is to present the sensitivity of the grid connection point short circuit power to the VSC-HVDC station model used in this chapter. The short circuit ratio (SCR) is used here as grid connection point stiffness metric. The SCR is defined as the ratio of the short circuit power level at the grid connection point (without the connection of the VSC station) to the rated power of the GSVSC station (200MW here). Typical values for SCR at transmission level is ten. In this paragraph we will study and optimize the fault response of the VSC-HVDC grid to the lowest possible value of SCR that the VSC is stable. It is not the aim of this chapter to investigate the tuning of the PLL and the inner current controller for very low short circuit power levels.

Figure 5.5 presents the dynamic response of a point-to-point VSC-HVDC connection of figure 5.2 for three values of the SCR. The critical value of the SCR for the selected system parameters is 3. Above this critical SCR value the VSC station remains stable during a three phase fault at its terminal while providing grid code compliance. The response of the PLL frequency is plotted for different SCR values. The SCR value of five is adopted for the following simulations.

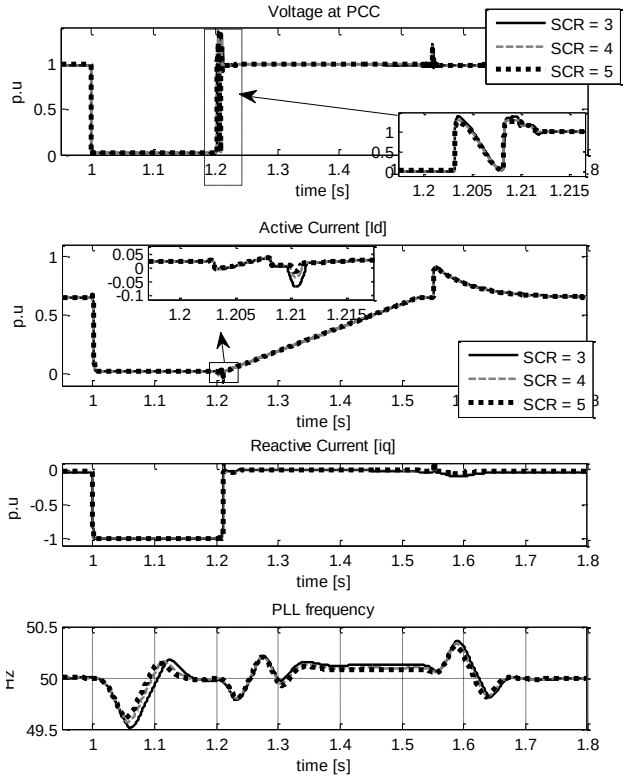

Figure 5.5: The effect of the SCR on the response of GSVSC2. From top to bottom the voltage amplitude at the PCC, the active current, the reactive current and the response of the PLL frequency.

5.3.5. FAULT-RIDE-THROUGH RESPONSE FOR THE GIVEN SNAPSHOTS OF THE MTDC GRID

The FRT response of the MTDC grid is assessed for the test system defined in figure 5.1 under the modelling assumptions presented in chapter 4 and 5. The six operating snapshots as defined in figure 5.2 are simulated for a 200ms self-cleared three phase fault at the GSVSC2. For those set of cases, the DC-chopper fault ride strategy is used (with choppers located at the onshore HVDC terminals). From the presented results in figure 5.6, it can be concluded that the reactive current injection of the onshore station is not affected by the state of the VSC operation (injection vs rectification). In addition, the activation of the DC chopper is performed only for the snapshots b and c. Since, the generated offshore wind power is higher than the capacity of the GSVSC3, the power which is injected to the AC grid by the GSVSC2 is dissipated by the chopper. Case B will be the focus of the following analysis as it represents the case where the FRT strategy need to be activated.

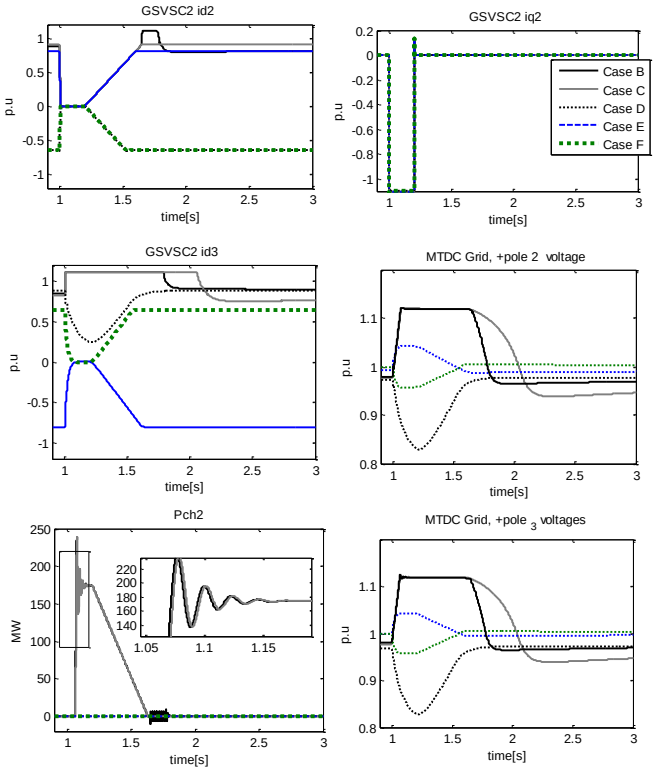

Figure 5.6: Simulation results for a three phase fault applied at the GSVSC2 terminal for the selected snapshots of the MTDC grid. The DC chopper FRT strategy is used.

The available over-current capacity of the GSVSC2 station (1.1 p.u) is provided as reactive current injection whilst the active current is reduced during the fault period to zero by the current limiter. The MTDC grid is balanced partially by the GSVSC2 chopper

(which dissipates the excess of power) and partially by the GSVSC 3, which being in direct voltage control mode automatically increases its active current component contributing in the power balancing of the MTDC converters. Furthermore, the amount of power injected from the MTDC grid to the un-faulted system (GSVSC3) depends on its pre-fault operating point and it is limited by the power capacity of GSVSC3.

When the fault is cleared, the GSVSC2 station ramps up its active current (hence its active power) back to the pre-fault value following a ramping rate of 2 p.u/s. From the simulation results it can be seen that the chopper solution is a robust FRT method with two clear advantages. First, it does not affect the response of the offshore island grid. Second, it enables the FRT compliance without triggering unwanted dynamics in the MTDC grid and/or the wind plants.

5.4. OPTIMALLY TUNED COORDINATED FRT SCHEMES

5.4.1. OPTIMAL TUNING OF THE VOLTAGE DROP FRT STRATEGY WITH REACTIVE CURRENT INJECTION BY THE OFFSHORE WIND PLANTS

The three coordinated FRT strategies as presented in chapter 4 are optimized using the EMT-enabled iterative procedure presented in chapter 4. First the iterative procedure is applied for the voltage drop FRT strategy. The same three terminal HVDC test system is used for the same applied fault at the grid side VSC terminal 2 (GSVSC2). It is assumed that the wind power plants inject reactive current during the imposed voltage drop in a similar way as they do for offshore AC faults. The mathematical formulation of the optimization problem is the same to the point to point connection presented in chapter 4 (paragraph 4.4.1). Similar to the point to point case, the direct over-voltage at the offshore DC terminal is minimized in conjugation with the applied voltage drop.

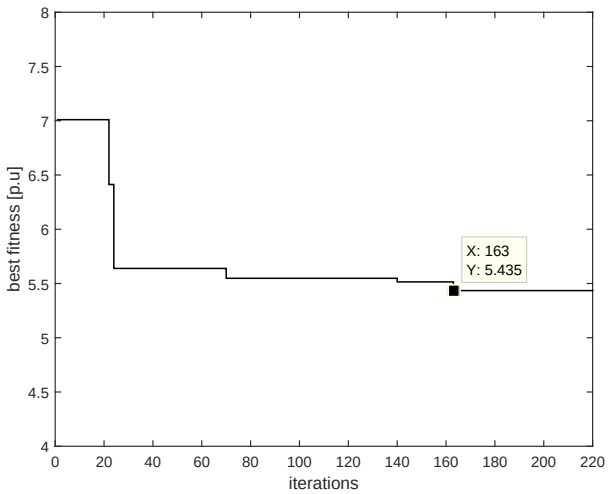

Figure 5.7: Evolution of the best fitness function.

Figure 5.7 presents the evolution of the best fitness function for the voltage drop strategy. As it can be seen the best fitness value has been detected nearly for 163 iterations. The iterations of the control variables are presented in figure 5.8. As it can be seen, after 100 iterations the reactive current boosting gains (K_{wt1}, K_{wt2}) for the PPM1 and PPM2 are concentrated around the optimal value. Similar is the evolution of the solution for the voltage drop gain of the offshore WPVSC station, Ku_{lvrt}.

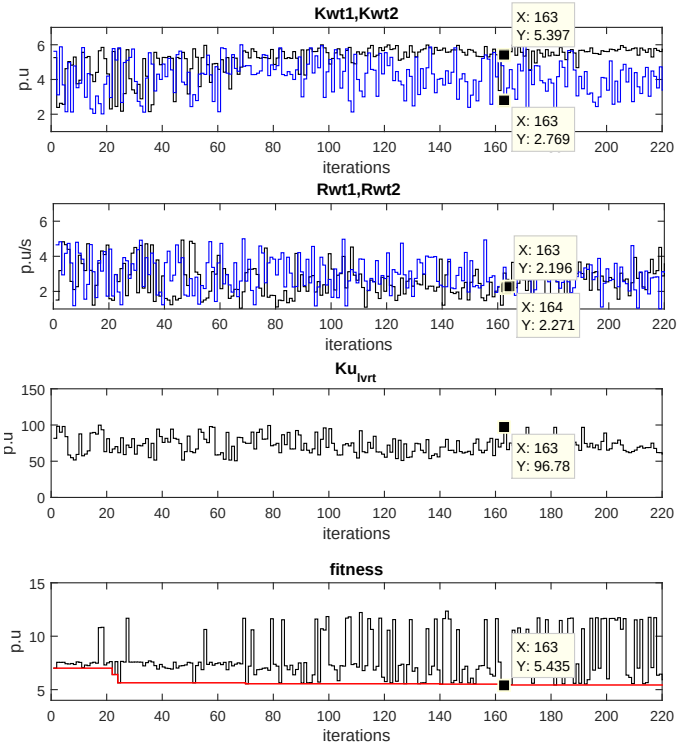

Figure 5.8: The iteration of the optimized control variables for the case of the voltage drop followed by reactive current injection by the offshore wind plants. With blue are variables referring to the wind power plant 2, PPM2.

Observing the time domain simulation of the MTDC grid in figure 5.9 for the optimized set of the control parameters, it can be seen that the applied voltage drop is above the selected 0.5p.u threshold where the ramping is applied (following the state machine of the wind turbines presented in chapter 4.3.6). We shall recall that for the point-to-point connection, the applied offshore voltage drop which ensures optimal FRT compliance is below 0.5 p.u value. In this region, the wind plant enters the FRT state injecting reactive current which as a result reduces to zero the active current. Contrary, for the MTDC connection the wind turbines do not enter their FRT state for the optimal set of values. The latter means that the ramping is not applied and obviously does not affect the dynamic response. The reason for the difference in the applied voltage drop is the

fact that in the MTDC connection, the MTDC grid power during the fault period is balanced additionally from the remote converter station (beside the FRT scheme). Hence, smaller amount of wind power needs to be reduced by the offshore converter station compared to the point to point connection case. Changing the voltage threshold of the state machine to values above the 0.5p.u would not achieve better response.

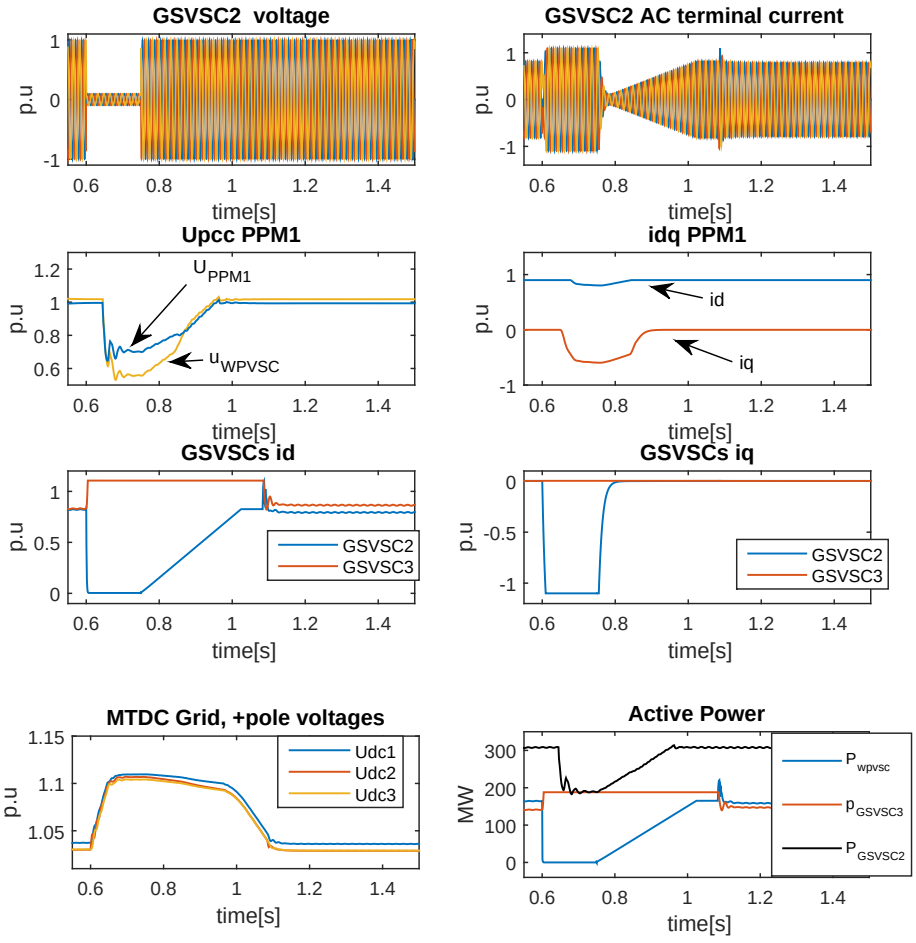

Figure 5.9: Time domain response of the wind power plants and the HVDC grid for the case that the optimal control parameters are applied.

5.4.2. OPTIMIZED FREQUENCY MODULATION FRT STRATEGY WITH ACTIVE CURRENT REDUCTION BY THE OFFSHORE WIND PLANTS

Next to the voltage drop strategy, the frequency modulation FRT technique is optimized. The frequency modulation strategy has been regarded as a rather slow in its dynamic response for being used as a FRT strategy. The advantage of the frequency modulation technique is that it is possible to be applied for longer than the fault-time periods.

This would give the ability to signal a reduction in the active power of the wind power plants (by adequate control) not only during the FRT period (usually 150ms) but extend it for other balancing reasons in the AC grid during primary frequency response or emergency power control. Emergency power control is considered valuable for cases of over-frequency events. The chopper itself cannot be applied in this case since it has a time duration operation limit (2sec).

The mathematical formulation of the optimization problem for the multi-terminal HVDC case is exactly the same as presented in the section 4.4.3. The evolution of the best fitness function is presented in figure 5.10. As it can be seen, the algorithm converges to the best fitness value for 195 iterations of total 200 iterations used. The best fitness value as defined in section 4.3.3 is 0.1325p.u and is close to the results found for the point to point connection in figure 4.19.

The iterations of the optimized control variables are presented in figure 5.11. It is worth to observe that the optimizer has converged to the result of the zero value for the gains T_2 (lag block time constant) in both wind plants, which means that the lag block of controller in figure 4.9 can be removed. The time constant T_1, associated with the lead block is different for the two plants. The gain of the frequency modulator at the offshore station (see figure 4.5), $K_{f,lvrt}$, is 1.6 which it is higher than in the point to point case (which is 1.0 as in (4.18)). This is because for the MTDC case, the rated direct voltage selected is 250kV (compared to the 320kV in the point to point case). Finally, the gains Kwt_{1f} and Kwt_{2f} of the controller in figure 4.9 have converted by the optimizer to high value similar to the the point-to-point connection case.

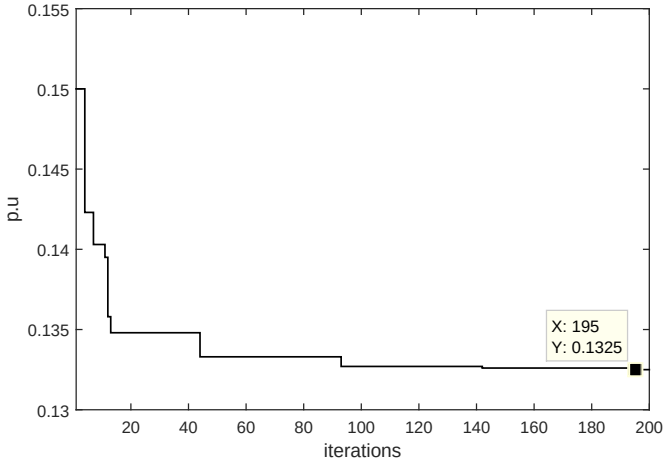

Figure 5.10: Best fitness evolution for the frequency modulation strategy.

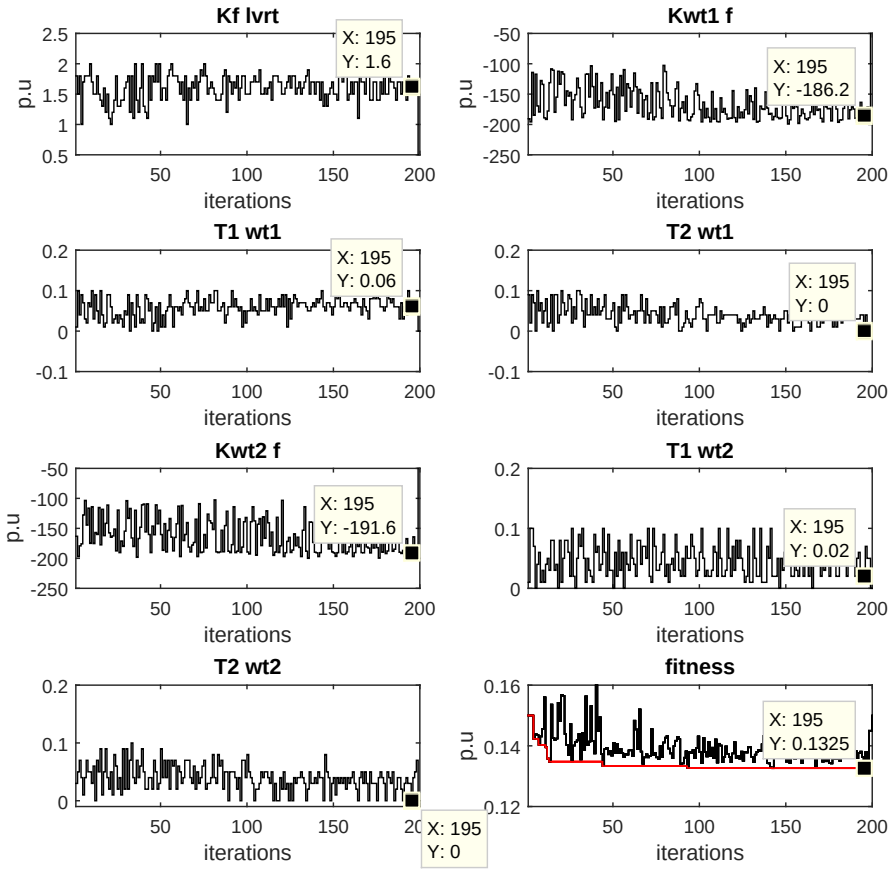

Figure 5.11: Iterations of the control variables during the solution of the optimization problem.

The time domain simulation of the complete plant and the HVDC grid for the optimized set of control parameters is given in figure 5.12. As it can be seen, the direct overvoltage in the three terminals is kept close to the 1.1p.u value as is the base case of the chopper. The remote converter which does experience the fault, provides its maximum power capacity during the fault and post-fault period in similar way as in the previous two strategies. Finally, it is worth to observe that the offshore frequency response for the optimized parameters does not deviate much from the 50Hz. The reason is that no dead-band in the frequency control is used for the sake of simplicity.

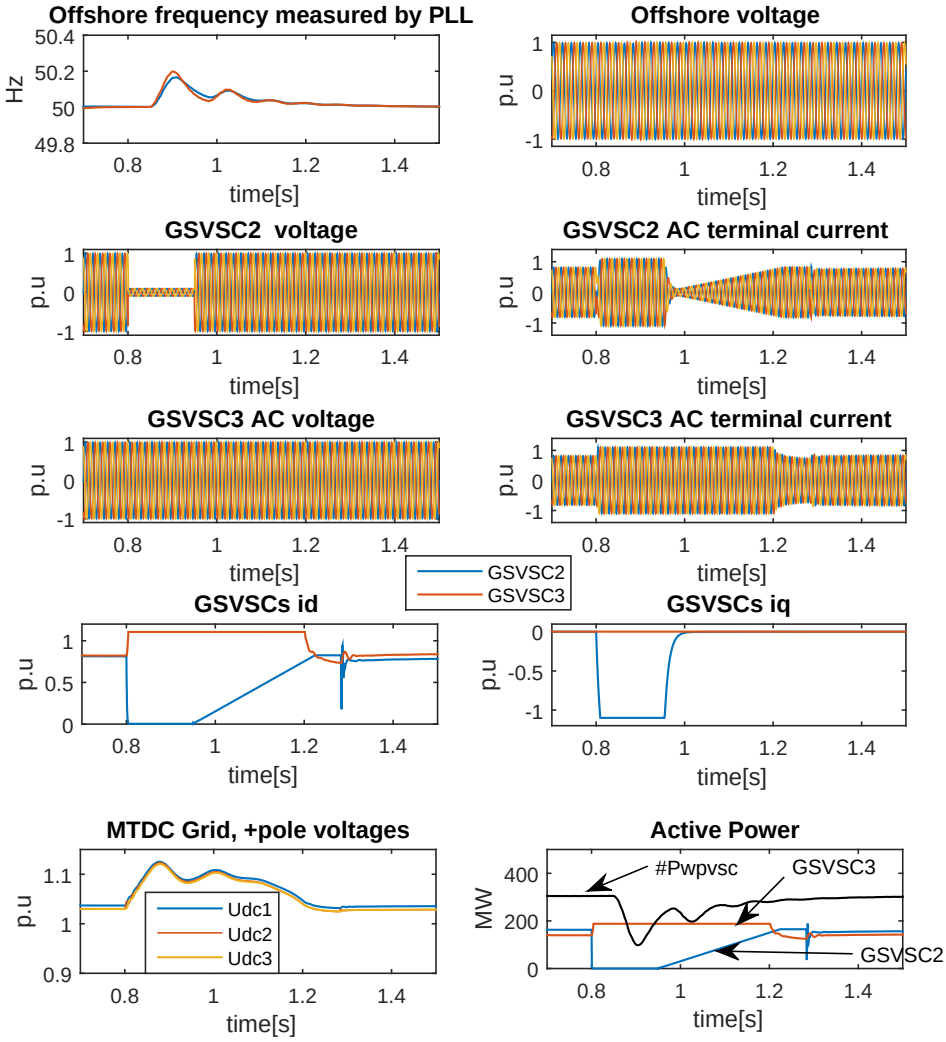

Figure 5.12: Time domain response of the MTDC grid and the wind plants connected for the case of the optimized frequency modulation strategy.

5.4.3. OPTIMIZED VOLTAGE DROP WITH ACTIVE CURRENT CURRENT REDUCTION BY THE OFFSHORE WIND PLANTS

Finally, the voltage drop strategy augmented by the active current reduction of the offshore wind plants is optimized (as shown in figure 4.9). The evolution of the best fitness function is presented in figure 5.13. whilst, the control parameters iterations are shown in figure 5.14.

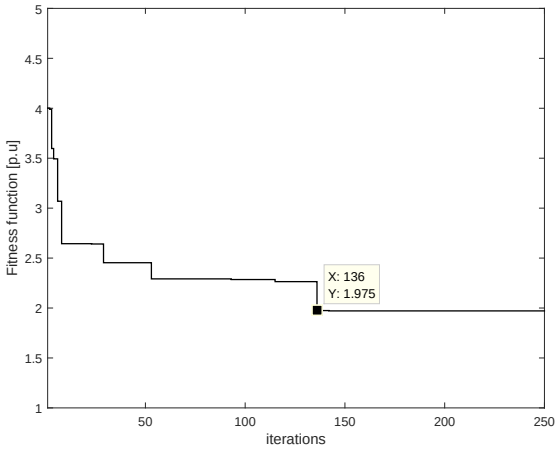

Figure 5.13: Best fitness function evolution for the case of the optimized voltage drop strategy with active current reduction by the wind plants.

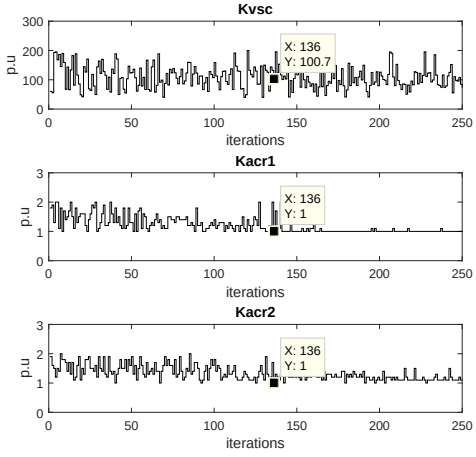

Figure 5.14: Iterations of the control variables by the iterative procedure for the case of the voltage drop strategy with active current reduction by the wind plants.

From the results, it takes 136 function evaluations (EMT simulation runs) before the best fitness function is obtained. It can be seen, that after 136 iterations, the gains K_{acr1} and K_{acr2} converge to the value 1. The same gain values are calculated also both for the the point to point (see figure 4.17) and for the multi-terminal HVDC connection case. The converged value of the offshore HVDC station voltage drop controller is different between the point to point and the multi-terminal connection, given the different DC voltage rated values between the test systems. Finally, the time domain response of the system for the best set of control variables is presented in figure 5.15. As it can be seen, a voltage drop of approximately 0.6p.u is applied offshore, which results in an active current reduction of 0.7p.u for both wind plats. The latter reduces the offshore HVDC station power to the same value as the maximum capacity of the un-faulted converter station.

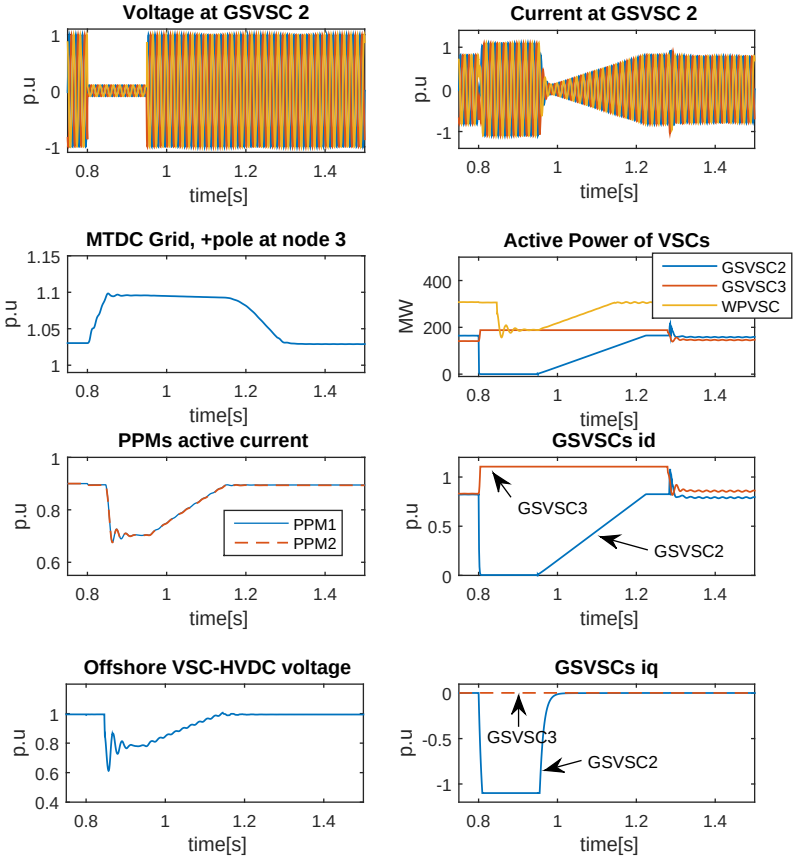

Figure 5.15: Time domain response of the MTDC grid and the wind plants connected for the case of the optimized voltage drop strategy followed by reduction of active current by the wind plants.

5.5. CONCLUSIONS

In this chapter, three different coordinated FRT strategies have been optimized for the multi-terminal HVDC connection of the offshore wind power plants. The chapter is an extension of chapter 4 for the multi-terminal HVDC connection. The first strategy refers to the case of the offshore voltage drop followed by the injection of reactive current by the wind plants. In this approach, it is shown that the injection of reactive current leads to the reduction of the active current which supports the power balance in the DC grid. In the second strategy, a different approach is followed for the voltage drop strategy. In this case, the active current is reduced by the wind plants when the offshore voltage drop is detected. Finally, as a third strategy, the frequency modulation method followed by the reduction of the active current at the offshore wind plants is studied. It has been shown that the obtained response of the HVDC grid and the wind plants is comparable to the DC chopper based scheme.

6

EFFECT OF THE FAULT RIDE THROUGH COMPLIANCE ON THE POWER SYSTEM TRANSIENT STABILITY

6.1. INTRODUCTION

The previous chapters have presented and optimized various coordinated control strategies which enable fault ride through compliance for the point-to-point and the multi-terminal HVDC connection of the offshore wind power plants. The research question to be addressed in this chapter is in which way does the reactive short circuit current injection from VSC-HVDC systems affects the short term voltage and rotor angle stability of the AC transmission systems during AC grid faults. Critical parameters are evaluated and their effect on the power system short term voltage and the rotor angle stability is assessed. Attention is paid to the following issues:

1. The effect of reactive current boosting gain applied to the onshore VSC station (known as 'k' gain or 'k' factor in most of the grid codes). This is a grid code related variable, which TSOs need to specify.

2. The choice of the current limitation strategy applied during the FRT period by the VSC-HVDC system. This is not explicitly defined in the grid codes and should be selected based on the power system needs.

3. The over-current capacity of the VSC-HVDC onshore converter station. The latter affects the voltage profiles and the rotor angle stability of the transmission system.

6.2. ASSESSMENT OF SHORT CIRCUIT CURRENT INJECTION USING LINEAR CIRCUIT ANALYSIS

Let us consider a VSC-HVDC onshore station that is connected to an equivalent grid as presented in figure 6.1 (a). A three phase symmetrical fault is applied at the grid connection point (PCC) and is represented by the reactance X_f as in figure 6.1 (b). $\underline{Z}_k^{"}$ is the short circuit impedance of the grid connection point and $\underline{U}_s^{"}$ the sub-transient voltage of the grid Thevenin equivalent during the fault. We assume, that the system remains symmetrical during the fault and the post-fault period so as it can be represented adequately by positive sequence components. Negative and zero sequence components are thus zero in this case. We assume that the active and the reactive power are positive when injected to the grid from the converter station. During the fault period, the fault current injection by the HVDC converter is saturated (limited) to the maximum current capacity $\underline{I}_{cm}$ (normally 1.1p.u) by the applied current limiting control module. The current injection of the converter during the fault period is controlled by the outer loop based on local measurements as presented in previous chapters. From the equivalent circuit of figure 6.1 (b), the fault current $\underline{I}_f^{"}$ is the sum of fault current contribution from the infinite grid and the fault-current injection from the VSC-HVDC converter station, as in 6.1.

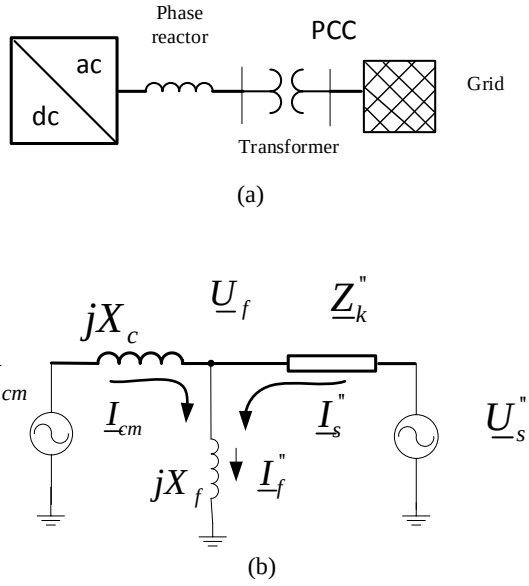

Figure 6.1: (a) Single line diagram of the VSC-HVDC station connected to an infinite grid, (b) equivalent circuit when fault is applied at the grid connection point.

$$\underline{I}_f^{"} = \underline{I}_{cm} + \underline{I}_s^{"}. \tag{6.1}$$

Reformulating the equation (6.1), the equation (6.2) is obtained as,

$$\underline{U}_f \left\{ 1 + \frac{jX_f}{Z_k^{"}} \right\} = jX_f \underline{I}_{cm} + j\frac{X_f}{\underline{Z}_k^{"}} \underline{U}_s^{"} \tag{6.2}$$

Given that the X/R ratio value is typically high at high voltage transmission system grid connection points, we can neglect the resistance of the short circuit impedance $Z_k^{"}$. Thus the short circuit impedance is now given by (6.3).

$$\underline{Z}_k^{"} = R_k + jX_k \simeq jX_k \tag{6.3}$$

Combining equations (6.2) and (6.3), the equation (6.4) is derived as:

$$\underline{U}_f = j \left\{ \frac{X_f X_k}{X_f + X_k} \right\} \underline{I}_{cm} + \frac{X_f}{X_f + X_k} \underline{U}_s^{"} \tag{6.4}$$

Let as define the reactance X_a and the per unit variable "b" such as:

$$X_a = \left\{ \frac{X_f X_k}{X_f + X_k} \right\} \tag{6.5}$$

$$b = \left\{ \frac{X_f}{X_f + X_k} \right\} \tag{6.6}$$

Substituting (6.5) and (6.6) into (6.4), we derive (6.7) as:

$$\underline{U}_f = jX_a \underline{I}_{cm} + b\underline{U}_s^{"} \tag{6.7}$$

From equation (6.7) it can be seen that the voltage phasor at the fault location $\underline{U}_f$ is affected by two terms. The first term depends on the external network voltage $\underline{U}_s^{"}$ multiplied by the voltage divider factor b. The variable b reflects the effect of the fault location since different values represent different voltage drops. The second term depends on the short circuit current injection phasor of the VSC-HVDC station. The short circuit current injection ($\underline{I}_{cm}$) provided by the converter consists of the active and the reactive current component. Depending on the current limitation control strategy applied, a different phasor $\underline{U}_f$ at the PCC can be observed. In order to quantify the effect of the grid connection point to the achieved voltage boosting by the converter, we rearrange (6.7) with $\underline{I}_k^{"}$ defined as the fault current provided by the equivalent grid when X_f is zero.

$$\underline{U}_f = \underline{U}_s^{"} b \left\{ 1 + j\frac{\underline{I}_{cm}}{\underline{I}_k^{"}} \right\} \tag{6.8}$$

Equation (6.8) defines the voltage support achieved at the grid connection point by means of the short circuit current injection from the onshore converter station of the VSC-HVDC transmission. From (6.8), it is worth to observe that the higher the short circuit current level at the grid connection point ($\underline{I}_k^{"}$), the smaller the voltage boosting

achieved by the converter station during the fault period. Furthermore, the variable b is also affecting the achieved voltage boosting. Let us now define the phasors as in (6.9) - (6.11).

$$\underline{U}_s^{"} = U_s^{"} \tag{6.9}$$

$$\underline{I}_{cm} = I_{cm} e^{j\theta} \tag{6.10}$$

$$\underline{I}_k^{"} = j I_k \tag{6.11}$$

Where θ is the angle of the converter current defined with reference to the grid voltage. It is important to note that this does not reflect any dq-frame since all the analysis is based on phasors. Substituting equation (6.9) - (6.11) into (6.8), the voltage boosting achieved during the fault period can be given by (6.12).

$$\eta = \frac{\underline{U}_f}{\underline{U}_s^{"}} = b\left\{1 + j\frac{\underline{I}_{cm}}{\underline{I}_k^{"}}\right\} = b\left\{1 + \frac{I_{cm}}{I_k^{"}} e^{j\theta}\right\} \tag{6.12}$$

Defining the short circuit ratio (SCR) as in (6.13), we finally obtain (6.14) from which we quantify the voltage boosting η as a function of the SCR for different values of b.

$$SCR = \frac{S_k^{"}}{S_{cm}} = \frac{I_k^{"}}{I_{cm}} \tag{6.13}$$

$$\eta = b\left\{1 + \frac{e^{j\theta}}{SCR}\right\} \tag{6.14}$$

6.3. THE EFFECT OF THE VSC CURRENT INJECTION ON VOLTAGE ANGLE STABILITY

In the previous section, it was shown how the fault current injection from the HVDC station affects the voltage boosting during faults. The present section investigates on the effect of the converter short circuit current on the voltage angle stability.

Let us assume a quasi-static symmetrical condition after the fault is applied in order to allow the drawing of the phasor diagram as it is presented in the figure 6.2. We assume that the variable “b” is non zero. From the equivalent circuit of figure 6.1, equation (6.15) is derived as:

$$\underline{U}_{cm} = \underline{U}_f + j\underline{X}_c\underline{I}_{cm} \tag{6.15}$$

From the geometry of the phasor diagram in figure 6.2, we can write equation (6.16). Next, by making use of common expressions for the active and the reactive power, equation (6.17) is derived, which accounts for the angle deviation between the phasor of the voltage at the fault location and the phasor of converter’s internal voltage (see figure 6.2).

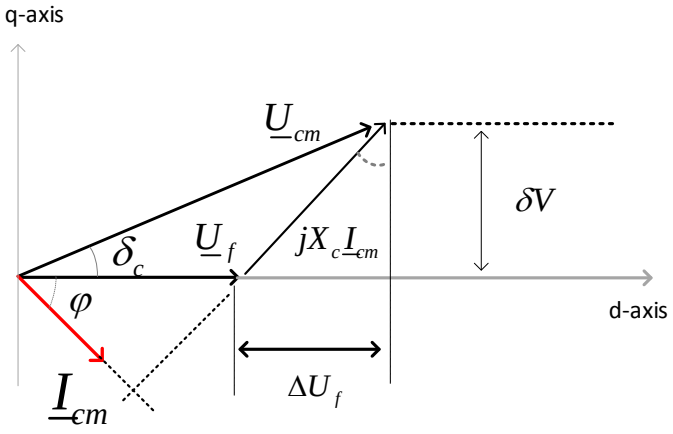

Figure 6.2: Phasor diagram of the equivalent circuit during the fault period under the assumption of quasi-static condition. The diagram adopts a generator convention, with the VSC delivering lagging current (injecting reactive power) to the faulted system (or else overexcited operation during the fault).

In equation 6.17, δV is not an angle but reflects the change of $\underline{U}_{cm}$ in the q-axis. By rewriting the active power (P) and the reactive power (Q) of the converter as a function of active (i_d) and reactive (i_q) component of $\underline{I}_{cm}$ in the dq reference frame, expressions (6.18) and (6.19) are obtained. In this way one can observe how the active (id) and the reactive current (iq) affect the internal angle δ_c during grid faults. This is not related at all to the equation 6.14. The angle we observe is between $\underline{U}_{cm}$ and $\underline{U}_f$. It is important to note that under the quasi steady state assumption, the d-axis is perfectly aligned with the voltage vector $\underline{U}_f$.

$$\underline{U}_{cm}^2 = \{U_f + X_c I_{cm} \sin\phi\}^2 + \{X_c I_{cm} \cos\phi\}^2 \tag{6.16}$$

$$\underline{U}_{cm}^2 = \left\{U_f + \frac{X_c Q}{U_f}\right\}^2 + \left\{\frac{X_c P}{U_f}\right\}^2 = \{U_f + \Delta U_f\}^2 + \{\delta V\}^2 \tag{6.17}$$

$$\delta V = \frac{X_c P}{U_f} = \frac{3 i_d X_c}{2} \tag{6.18}$$

$$\Delta U_f = \frac{X_c Q}{U_f} = \frac{-3 i_q X_c}{2} \tag{6.19}$$

Hence, from (6.18) and (6.19) it can be observed that by increasing the reactive current component i_q during the fault period, for the same active current component i_d, a high δV would be expected, increasing the angle δ_c between the voltage phasors $\underline{U}_f$ and $\underline{U}_s$. In this case, the variable ΔU_f defines the voltage support by the converter station during the fault period as a result of the reactive current injection. If during faulted conditions the voltage angle δ_c exceeds the well-known 90 degrees value, it will lead to local voltage angle instability.

Local voltage angle instability will trigger the loss of the PLL synchronization and would trip the converter. On the other hand, when the active current component i_d, is reduced during the fault period, for the same reactive current component i_q, the angle δ_c will be decreased while at the same time we would achieve higher voltage levels at the fault location. Hence, the active current reduction of the converter station during severe faults, decreases the tripping risk of the converter station during AC faults since it decreases the risk for local voltage angle instability. Such a case will be presented in the next paragraphs by means of time domain dynamic simulations. It is worth to recall that the reduction of active current has been also discussed for it's benefits during unbalanced grid faults.

6.4. EFFECT OF SHORT CIRCUIT RATIO ON THE ACHIEVED VOLTAGE BOOSTING

The voltage support (or voltage boosting) due to the effect of the fault current injection from the VSC-HVDC station for different short circuit ratio (SCR) values is estimated in this paragraph using equation 6.14 for the simple equivalent circuit of figure 6.1. Although this is a simplified case, it provides a good insight of the voltage support mechanism and the expected behavior of the voltage in real systems.

Figure 6.3 presents the calculated profile of the voltage support achieved as a function of the SCR value at the grid connection point. The b factor is equal to 0.5 for this case. In order to further simplify the analysis, it is assumed that the term $e^{j\theta}$ is equal to 1. Practically it means that an adequate current limitation strategy is used, which makes the angle θ zero. Of course this is hard to be achieved, but it serves here the purpose of presenting the best possible boosting. From the results, it can be observed that for typical 380kV transmission networks where the SCR is high (between 15 to 25), the achieved voltage support is smaller compared to a relevantly weak grid connection points where SCR is small.

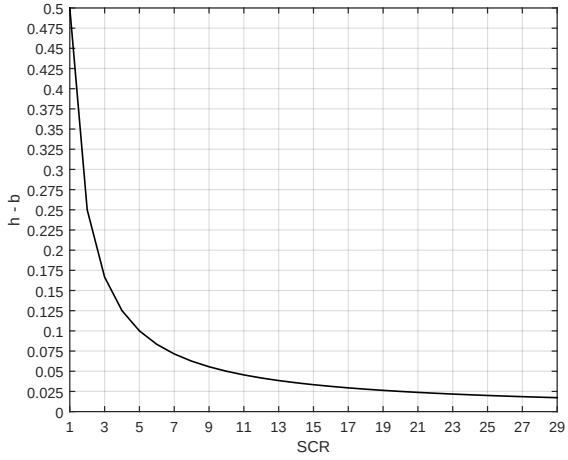

Figure 6.3: The effect of SCR on the voltage boosting by the onshore converter during faulted conditions.

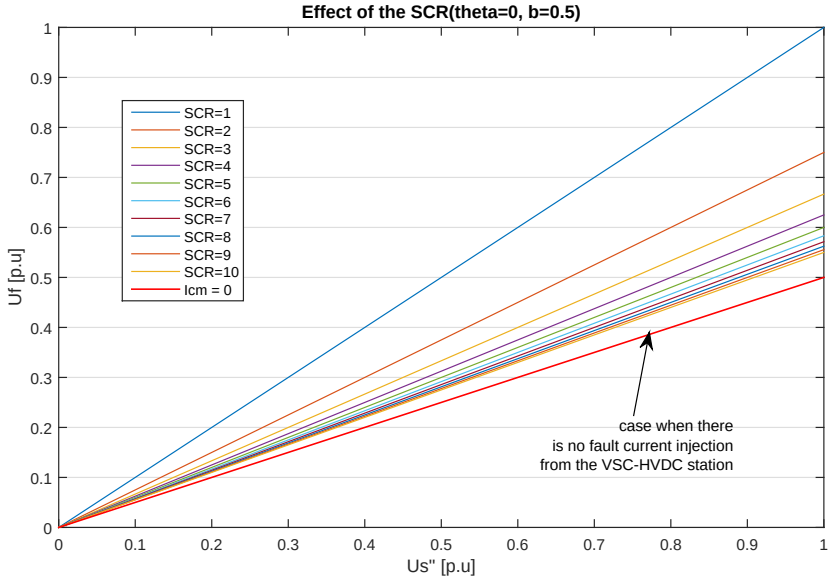

Figure 6.4: The effect of the SCR on the voltage drop at the grid connection point of the VSC-HVDC station for b=0.5.

Finally, figure 6.4 shows the voltage boosting for different values of the sub-transient voltage levels and SCR using equation 6.14. All the cases are compared to the base case where there is no fault current injection from the converter station (hence I_{cm} is zero).

It is important to mention that the graphs are calculated for the simple equivalent circuit of figure 6.1 under the assumption of quasi-steady state approach. In order to derive safe conclusions for multi-machine systems dynamic simulations are presented in following paragraphs.

6.5. VSC-HVDC CURRENT LIMITING STRATEGIES

Three are the common current limitation strategies applied for VSC-HVDC connections, namely: the active current priority, the reactive current priority and the equal current priority. In the active current priority, the active current is allowed to take any value between I_{max} and $-I_{max}$ while the reactive current is calculated so as the total current capacity I_{max} is not violated. In the reactive current priority, the reactive current is allowed to vary between Imax and -Imax while the active current is calculated accordingly. Finally, with the equal current priority the angle between the active and reactive current is kept constant, and the active and reactive currents are thus equally reduced.

6.6. THE EFFECT OF REACTIVE CURRENT BOOSTING GAIN

The provision of the reactive current by the onshore VSC-HVDC station is applied proportionally to the residual voltage at the PCC with a reactive current boosting gain "k". For different voltage drops at the AC terminal of the converter station, a different reactive current is injected. Figure 6.5 presents the influence of the reactive current boosting gain “k” on the active and the reactive current injections of the onshore converter station for different values of voltage drops as calculated by the presented analytical model. Reactive current priority is applied here. The phase reactor reactance X_c is assumed 0.15p.u for this analysis. The pre-fault operating point of the converter is assumed to be in zero reactive current injection and 1.0 p.u active current injection. Since, the over-current capacity is limited, the active current is reduced depending on the applied current limitation strategy.

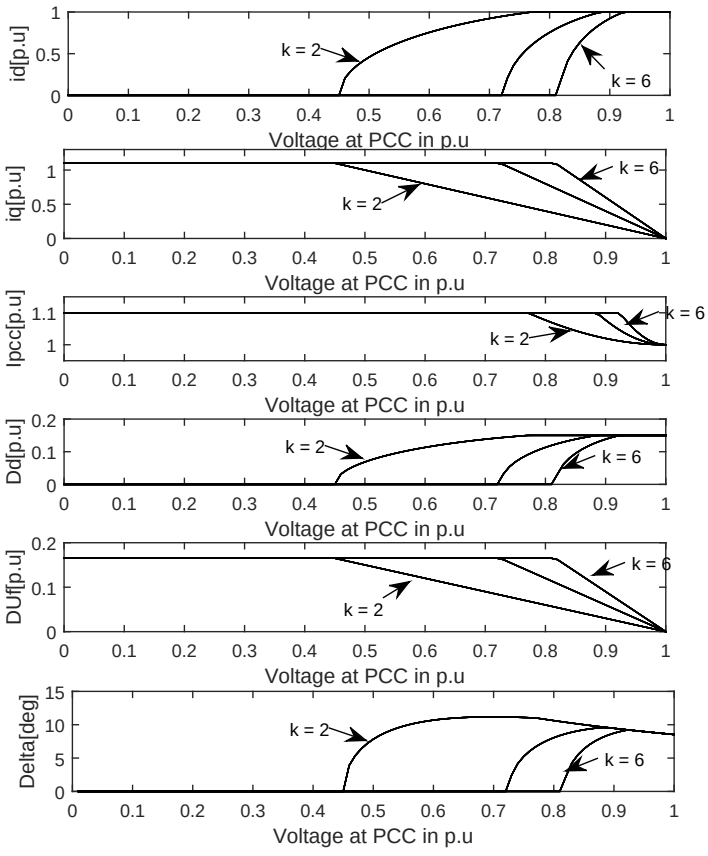

Figure 6.5: The influence of the reactive current boosting gain k on the active current (id), reactive current(iq), voltage drop across the phase reactor (ΔU_f) and the internal voltage angle of the converter for reactive current priority and for different voltage drops.

As it can be observed, an increased “k” value (k=6) will lead to high provision of reactive current by the converter station and the reduction of the active current component of the converter to zero value even for small voltage drops (i.e voltage levels of 0.8p.u). The active current reduction will reduce the internal converter voltage angle delta to zero. The drawback is that the fault ride through scheme will be triggered even at small voltage drops as the active current is reduced to zero. If we now assume that the active current is prioritized the results of figure 6.6 are derived. Active current priority although it is not common, it might be a choice for low inertia power systems where frequency stability is a concern.

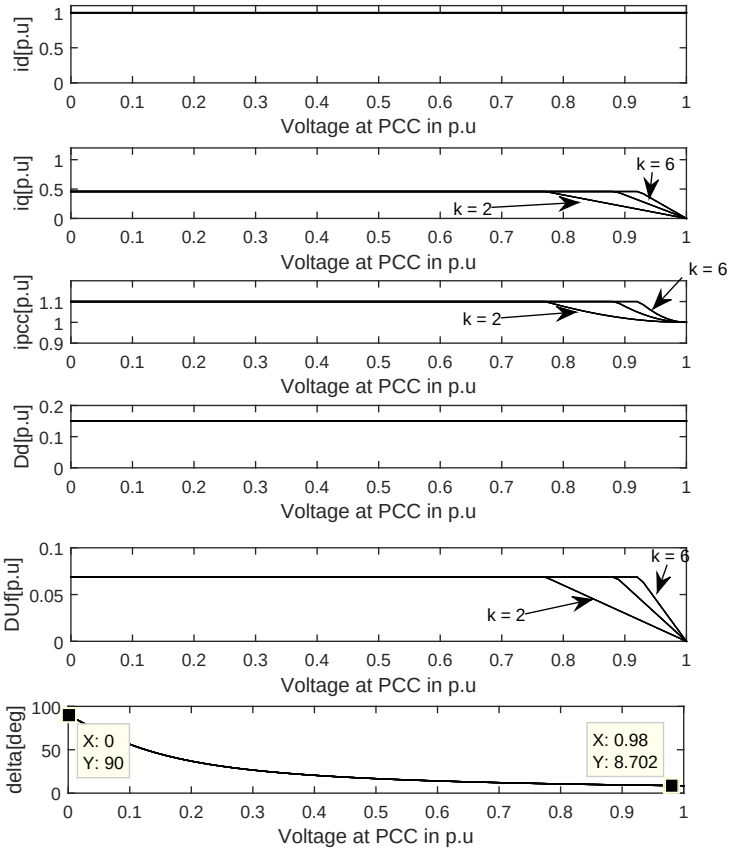

Figure 6.6: The influence of the reactive current boosting gain (k) on the active current, reactive current, voltage drop at the phase reactor and the internal voltage angle of the converter for active current priority.

From the calculations it can be observed, that by prioritizing the active current, the reactive current injection is limited to 0.5 p.u due to the limited converter capacity. Hence, the voltage support is "sacrificed" in order to provide active current injection. The most interesting point here is to observe the internal voltage angle value of the converter station in Figure 6.6 (bottom sub-figure). As it can be seen, the combined active and reactive current injection, leads to an increased internal voltage angle of the converter station. More specifically, when the PCC voltage reaches values close to zero, the internal angle reaches the critical point of 90 degrees which means that local voltage angle instability may occur if the voltage angle surpasses the 90 degrees threshold.

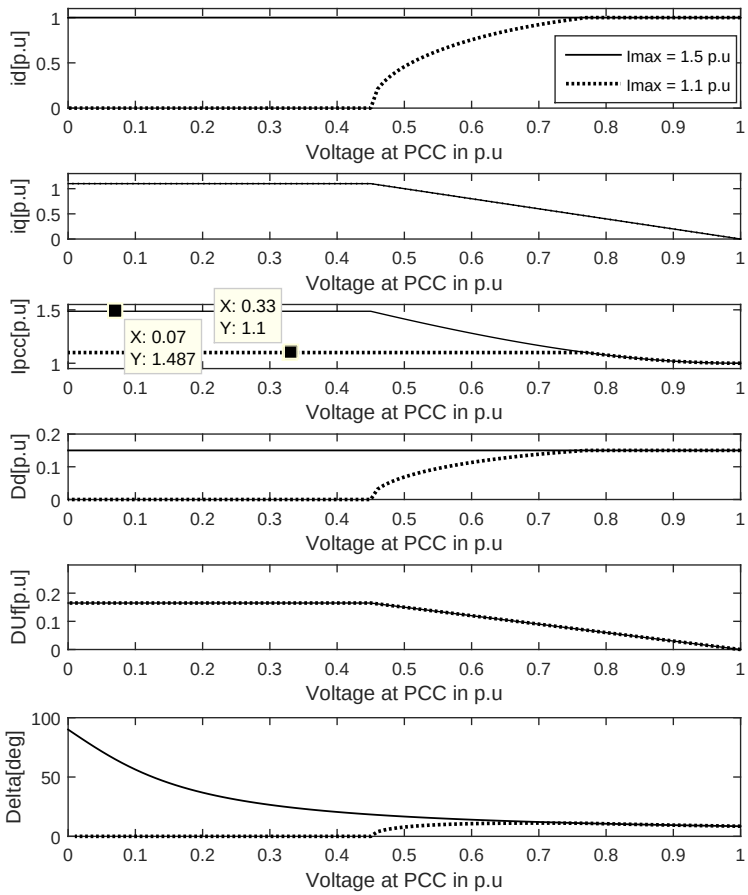

Figure 6.7: The influence of the I_{max} on the active current, reactive current, the voltage drop at the phase reactor and the internal voltage angle of the converter for reactive current priority.

6.7. THE EFFECT OF OVER-CURRENT CAPACITY

Finally, figure 6.7 demonstrates the effect of the over-current capacity of the converter station on the PCC voltage for the case of a k equal two. Two over-current capacities are selected, 1.1 and 1.5p.u respectively. The high over-current capacity of the converter is utilized with purpose to provide reactive current injection by the VSC-HVDC link during network disturbances without reducing the active current. However, as it can be seen from the response of the angle delta between the $\underline{U}_f$ and the internal converter voltage $\underline{U}_c$, high values of voltage angle delta are observed between the two selected capacities. The latter increases the risk of voltage angle instability. In order to avoid this, the increase in the over-current capacity of the converter station should be followed by an increase in the reactive current boosting gain k selected. In this way, when the reactive current priority is followed, it will reduce the active current and prevent reaching the instability limit.

6.8. DYNAMIC SIMULATIONS FOR POINT-TO-POINT VSC-HVDC CONNECTION

6.8.1. TEST SYSTEM

A modified version of the original IEEE 39-bus test system is used in this paragraph in order to demonstrate the effect of the VSC-Based HVDC systems on the short term voltage and rotor angle stability. It is presented in figure 6.8. The model is developed in PSS®E. Two offshore VSC-HVDC links are used, connected at buses 2 and 9 respectively. The models of the HVDC systems are developed in visual Fortan and integrated in the PSS®E simulation engine. The VSC-HVDC link models use identical control parameters and they apply the same control strategies. A step up transformer with short-circuit voltage u_k equal to 10% is used for the grid connection. Both onshore HVDC converters are rated at 650 MVA while the load flow operating point is 400 MW. The HVDC system in both cases is connecting two offshore wind power plants.

Furthermore, in order to increase the share of wind power generation in the IEEE 39 bus test system, two onshore wind power plants have been added at the buses 25 and 21 respectively. The onshore and offshore wind power plants are modelled following standard RMS models available in PSS®E. All synchronous generators have been modelled using IEEE standard models, using IEEE SEXS type excitation system and TGOV1 type governor with standard parameters. The total load in the test system is 7467.2MW with 5202.4MW generated by conventional units, 1600MW by onshore wind plants and 800MW by offshore wind plants. Different faults will be studied, namely faults at the terminals of the onshore VSC-HVDC stations, faults at the AC transmission system and faults at conventional generation units.

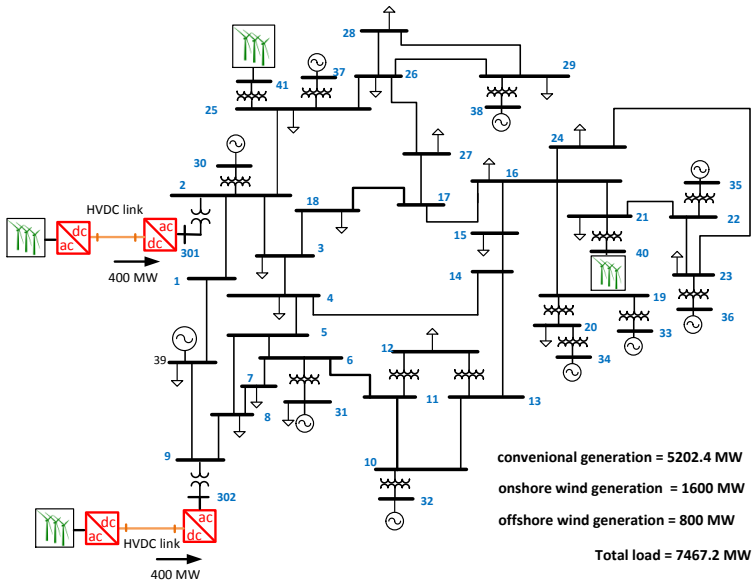

Figure 6.8: Modified IEEE 39-bus test system and the connected to it offshore wind plants with VSC-HVDC system in point-to-point connection.

6

6.8.2. RMS MODEL OF THE VSC-HVDC SYSTEM

A positive sequence, RMS modeling approach has been used to represent the dynamic response of the VSC-HVDC system in large system stability type studies [172]. The VSC-HVDC model used here is validated in [147] against EMT model. The test system is developed in the PSS®E simulation environment. Figure 6.9 presents the model of the onshore VSC-HVDC station and figure 6.11 the model of the offshore VSC-HVDC station. The time constants of the inner current controller are very small compared to the larger outer controller and AC system time constants. Moreover, since the rms value dynamic models are bounded by the 50Hz frequency of the phasors, larger frequency phenomena cannot be represented. The dynamics of the inner current controller could be neglected and replaced by algebraic equations. The outer controllers since they involve larger time constants are represented in detail. Figure 6.10 presents the active and reactive control loops as used here for the point to point and in the next section for the multi-terminal HVDC connection of the onshore HVDC converters. Finally, it has been assumed that the PLL can perfectly track the voltage angle at the point of common coupling (PCC)under the assumption of stiff grid connection point (short circuit ratio higher than 10) and X/R high.

The DC side of the converter is modelled as a DC current source, while the DC cables by a lumped pi section DC circuit. State space equations have been used to represent the dynamic behaviour of the DC cables as mathematically formulated in chapter 5. Figure 6.12 presents the model used. The necessity to represent DC cables with dynamic models is because of the need to represent the dynamic response of the DC voltage, especially under faulted conditions.

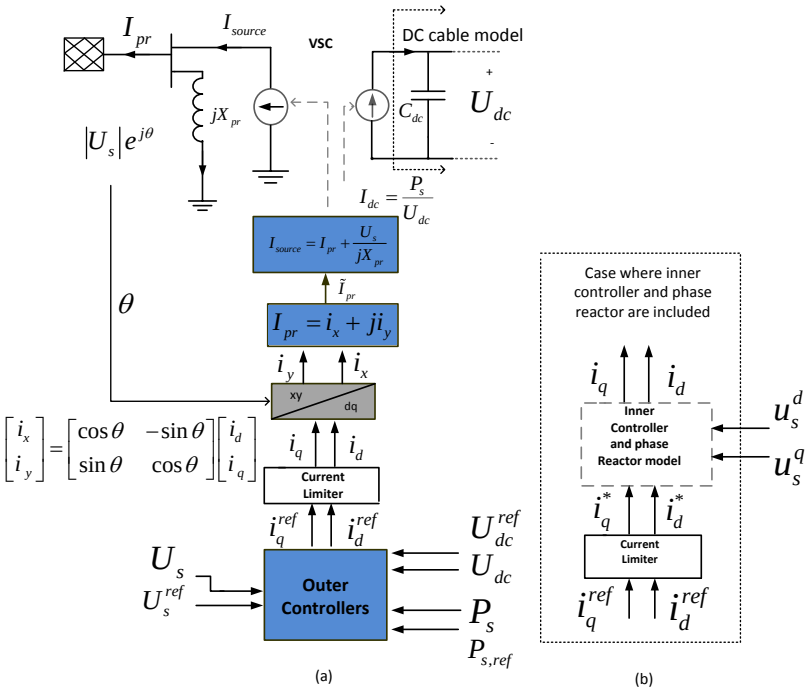

Figure 6.9: (a)The RMS model of the onshore VSC-HVDC station as used in this chapter dynamic simulations. (b) the part of the VSC dynamic model, which has been neglected.

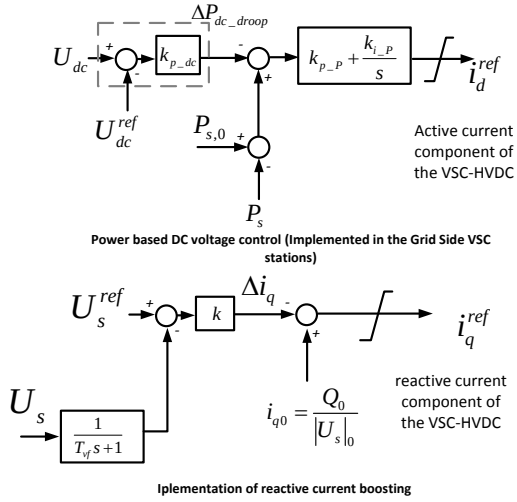

Figure 6.10: Outer control loops for the active and reactive current of the onshore converter station as used in this chapter analysis.

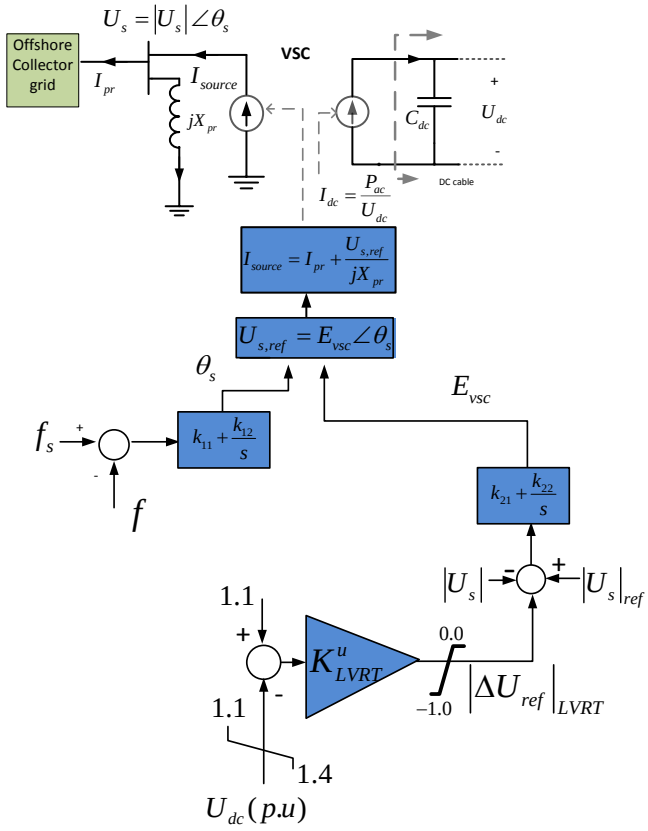

Figure 6.11: (a)The RMS equivalent model of the offshore VSC-HVDC station as used in this chapter.

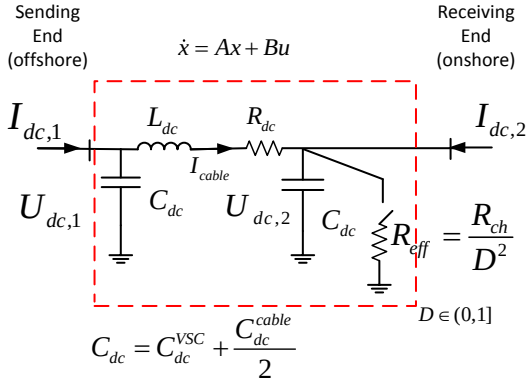

Figure 6.12: The HVDC cable model as used in this chapter analysis.

6.8.3. FAULT RIDE THROUGH COMPLIANCE USING A DC CHOPPER

A three phase fault is applied at the onshore VSC-HVDC station (bus 301). The response of the two VSC-HVDC links is presented in figure 6.13. The two onshore converters are using a reactive current boosting gain k equal to 2 (figure 6.10). During the fault period, the VSC station 301 injects all its fault current capacity as reactive current(i_q), reducing the active current (i_q) to zero since reactive current priority is followed. The fault current injection capacity of the station VSC 301 is 1.1 p.u. The voltage drop experienced by the VSC 302 is 0.8 p.u and the injected reactive current is 0.4 p.u. The dynamic response of the dq-current components and for the given voltage drop corresponds to the response estimated by the analytical equations of figure 6.5.

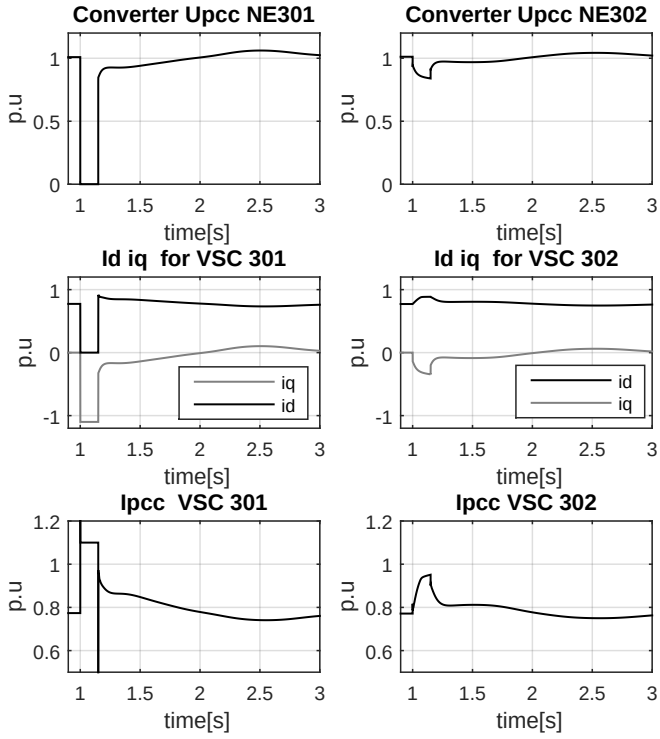

Figure 6.13: The response of key metrics for the two VSC-HVDC links for a fault applied at the VSC 301.

The onshore DC terminal voltage response for the same fault is presented in figure 6.14. The classical DC chopper fault ride through strategy is applied here. As it can be seen, for the fault at VSC 301, the power drops to zero and the DC chopper dissipates all the generated offshore wind power (400MW) during the fault period. The DC link 301 direct voltage is controlled at 1.15p.u. The DC link 302 power is not significantly affected due to the smaller AC voltage drop (0.8 p.u). The VSC 302 does not reach its over current capacity, although reactive current in injected. Finally the angle of selected generators defined from the reference generator (G39) in the modified IEEE 39-Bus system is pre-

sented in figure 6.15. As it can be seen, the system is transiently stable and returns to the pre-fault operating point. The following paragraphs will present the way that different values of the gain k affect the power system faulted response with the focus on the short term voltage and rotor angle stability.

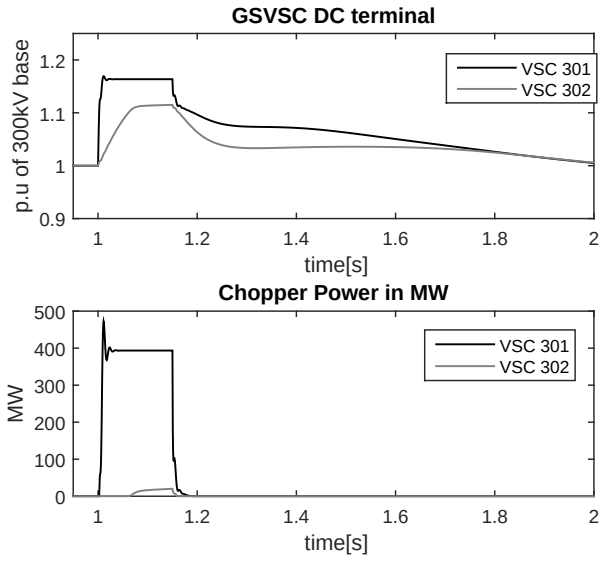

Figure 6.14: The time domain response of the DC link voltage and the dissipated power in the chopper of the two VSC-HVDC connections for a fault at bus 301.

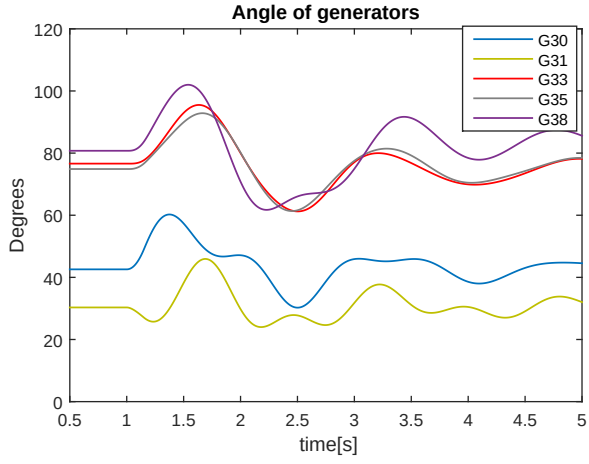

Figure 6.15: The response of selected generators in the IEEE 39-bus system for a fault at VSC 301. Angles difference from the reference generator G39.

6.8.4. THE EFFECT OF THE REACTIVE CURRENT BOOSTING GAIN K

Figure 6.16, shows the voltage profiles at buses 301 and 302 for a self cleared (150 ms) symmetrical three phase fault at bus 39. In this set of simulations no dead-band is applied at the reactive current boosting whilst reactive current limitation strategy is applied. From the voltage profiles at VSC 301, it can be observed that a relevantly high gain (k=6) leads to a lower voltage drop at the grid connection point, during the fault period. This is explained by the increased reactive current component of the HVDC converter station compared to the low gain (k equal two). However, the over-current capacity of the VSC-HVDC station is limited to 1.1 p.u. Thus, when the maximum over-current capacity is reached, the reactive current is saturated. This is the simulated case for VSC 302. As it has been presented in figure 6.5, for voltage drops below 0.45p.u, the converter output current is saturated to the maximum over-current capacity, Imax, and the same reactive current is injected between the gains 2 and 6. This means that no difference is observed for faults close to the converter station. Finally, figure 6.17 demonstrates the effect of the reactive current boosting gain k on the dissipated power by the DC choppers. In the high gain case, due to the reduction of the active current in the VSC 301 to zero, all the offshore wind power is dissipated.

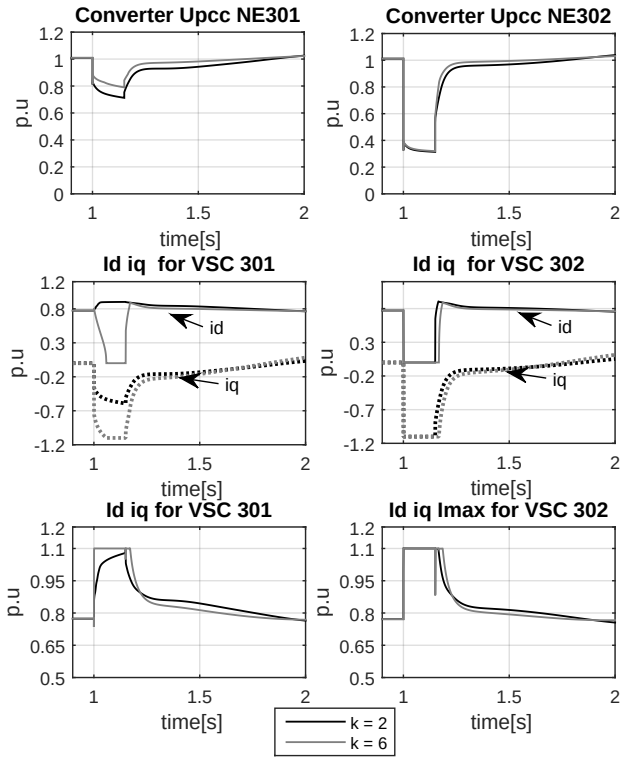

Figure 6.16: The simulation result for the IEEE 39-bus test system which shows the sensitivity of the k-factor on the onshore AC terminal of the VSC-HVDC station.

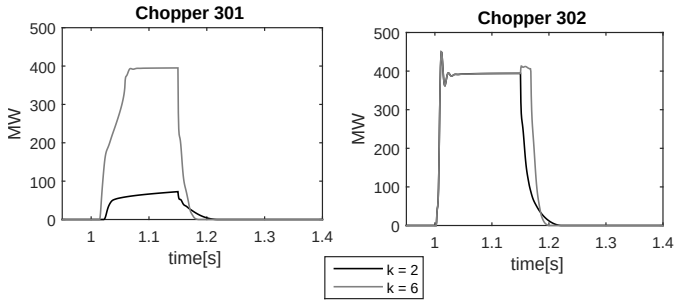

Figure 6.17: The effect of reactive current boosting gain k on the DC chopper response.

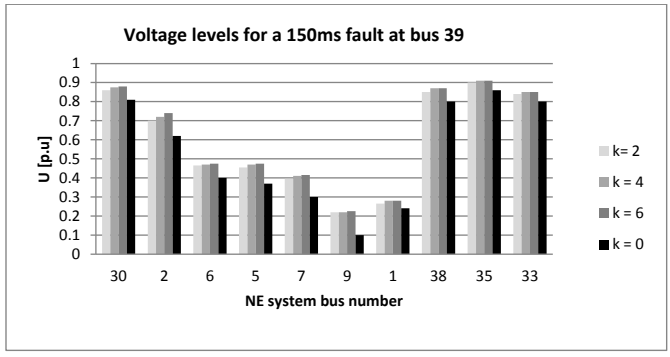

Figure 6.18: The effect of the reactive current boosting gain k on the voltage levels of the modified IEEE 39-Bus test system.

Furthermore, the test system is simulated for four values of the gain k in order to demonstrate its effect on the power system voltage response. Figure 6.18, summarizes the simulated voltage drop at selected buses. From the results, it can be concluded that an increased gain k leads to smaller voltage drops in the system (higher residual voltage) during faults especially at busses which are by means of large impedance remote from the fault location. The latter is derived from the higher injection of the reactive current. For k gains higher than 6, the injected fault current is saturated and no effect is observed on the voltage response. In general, it can be commented that for faults close to the HVDC stations, where the voltage drops below 0.45p.u, no difference is observed for values of k above 2.

In addition, the effect of the k gain on the critical clearing time (CCT) for two selected generators is demonstrated in figure 6.19. As it can be observed the short circuit current contribution of the VSC-HVDC system improves the rotor angle stability of the online synchronous generators in the test system. For each generator the CCT is defined by means of dynamic simulations for a symmetrical fault applied at the low voltage side terminal of the step up transformer of the generator unit. The observed improvement on the CCT is justified mainly by the improved post-fault voltage response and the smaller

rotor angle variation between the online generators. Finally, the results present the improvement in the power system dynamic response as a result of the grid code compliance compared to the no compliance case where no reactive current injection is applied (k=0).

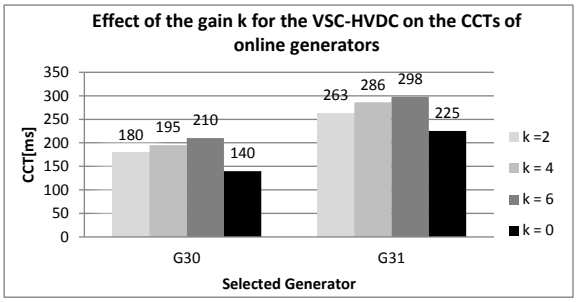

Figure 6.19: The effect of the selected reactive current boosting gain k applied at the two VSC-HVDC links on the CCTs of two selected generators.

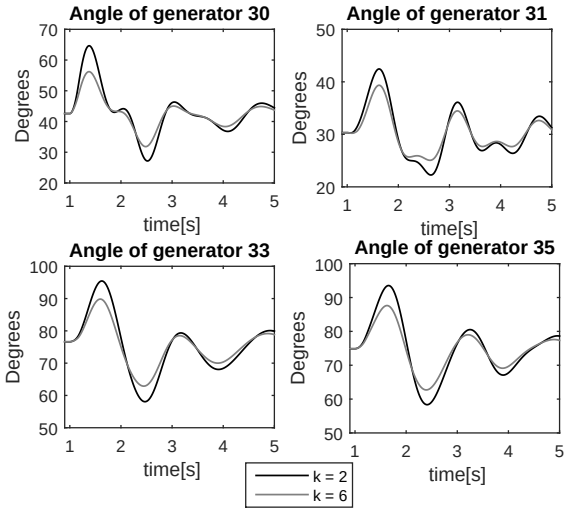

Figure 6.20: The effect of the selected reactive current boosting gain k at the two VSC-HVDC links on the angle response of selected generators. Angles difference from the reference generator G39.

Finally, figure 6.20 presents the simulated rotor angle response of four selected generators in the system. Two are the reasons for the improved rotor angle deviation. First, the higher residual voltages at the generator terminals during the fault. Second, the active current reduction from the VSC-HVDC stations which occurs due to the reactive current injection. Since, the loads in the simulated test system are static, the reduction of the injected active current from the VSC-HVDC links during the fault, reduces the gener-

ation and demand imbalance during the fault. Hence, it provides a damping effect in the speed of the generators, which also contributes to the improved rotor angle variation.

6.8.5. THE EFFECT OF THE CURRENT LIMITATION STRATEGY ON ROTOR ANGLE STABILITY

So far, reactive current priority has been followed by the VSC-HVDC stations. In this paragraph, the effect of the applied current limitation strategy on the dynamic response of the test system will be assessed for the same fault. The additional reactive current injection is applying a high gain (k=6). Such a high gain is selected in order both VSC-HVDC onshore converters to reach their maximum over-current capacity during the fault period and thus allowing for the current limitation strategy to be applied. No deadband is assumed for this analysis. The four current limitation strategies as presented are tested here. Figure 6.21 presents the rotor angle time domain response of the test system generators for the four current limitation strategies. All the examined cases are compared to the no reactive current injection case (k equal zero).

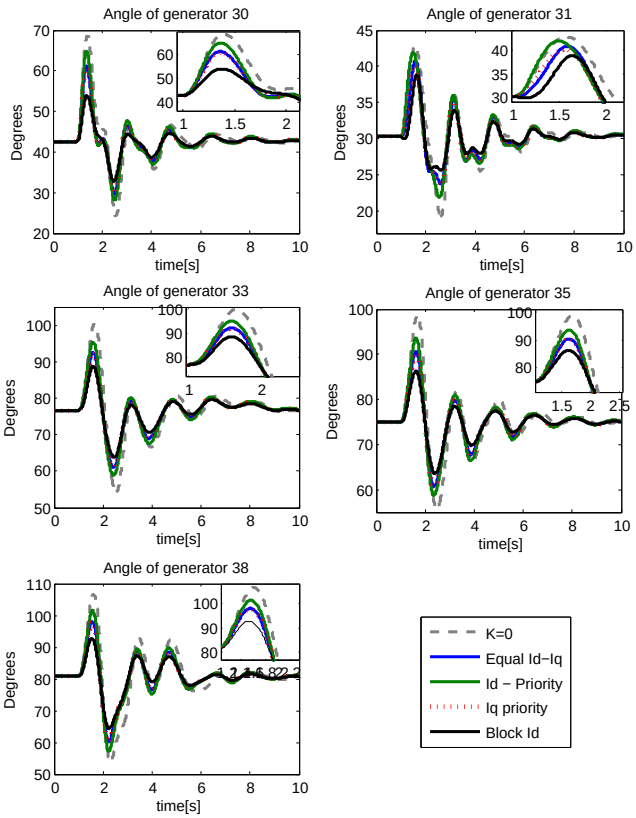

Figure 6.21: The effect of current limitation strategy priority on the rotor angle response of selected generatots. Angles difference from the reference generator G39.

From the simulation results, it can be observed that the worst rotor angle response is achieved in case of no reactive current injection by the VSC-HVDC links. The case of active current priority is the worst one out of the current limitation strategies. The reason of such a response is that an injection of the active current (active power) during the fault period by the VSC-HVDC links, would increase the imbalance between the generation and the load in the system, thus it will increase the speed deviation and the rotor angle during the fault period. On the contrary, for reactive current priority, since the active current is reduced as a result of limited fault current capacity, the power imbalance between the load and the generation is smaller, leading to a damping effect of the synchronous generators. The latter is further justified for the case of active current blocking. In this strategy, when the voltage drops below a certain level, the active current is set to zero. From the above results, it is demonstrated that the reactive current limitation priority during voltage sags leads to an improved AC system response both in terms of short term voltage stability but also rotor angle stability. It is worth to mention, that the loads are static in this test system. So voltage dependent dynamic loads, need to be added in the future work in order to examine their effect on the drawn conclusions. The later was out of this thesis scope.

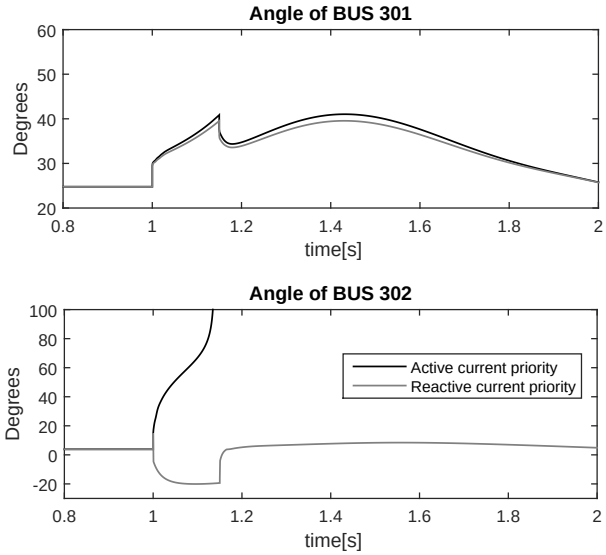

Figure 6.22: A simulation result of the voltage angle instability case for a fault applied at bus 9. This instability is not related to the generator but to the voltage angle separation between the converter voltage and the grid voltage. This result supports the analysis of section 6.3 where voltage angle stability is discussed.

6.8.6. THE RISK OF VOLTAGE ANGLE INSTABILITY

In paragraph 6.3 it has been discussed the risk of voltage angle instability when active current priority is applied at the onshore VSC-HVDC station. As presented in the figure 6.6, for faults close to the converter terminal, where the voltage becomes zero, the internal converter voltage angle drifts to values above the 90 degrees theshold. One such case is simulated in figure 6.22 for a fault applied at bus 9. As it can be seen, the injection of active and reactive current leads to the instability of the voltage angle. Contrary when reactive current priority is applied, the voltage angle is stable.

6.9. DYNAMIC SIMULATIONS FOR MULTI-TERMINAL VSC-HVDC CONNECTION

The contribution of this section is assessment of the influence of different grid code related control strategies on the short term voltage and rotor angle stability of a multi-machine power system as well as on the dynamic performance of the MTDC grids by using RMS type dynamic simulations. A five terminal high voltage MTDC grid connected to the modified New England test system is used as case study. Furthermore, the response of the MTDC grid itself is assessed and emphasis is given on the DC voltage variations and the response of the FRT strategy.

6.9.1. TEST SYSTEM USED

A five terminal VSC-Based MTDC grid is used as shown in figure 6.23 developed in PSS®E. In addition, the IEEE 39-bus tesst system (NE system) is connected via the MTDC offshore grid to a seven-generator benchmark power system with 60 GW generation installed capacity. The second 7-generator benchmark system was first used in [173] to represent the inter-area mode of 0.5 Hz of the Great Britain power system. All network parameters and dynamic parameters of the 7-generator system are taken from [173].

Same as in the previous paragraph, the modified version of the IEEE 39-bus (New England) system has been used for the purpose of this study, including both onshore and DC-connected offshore wind power plants. Round rotor 6th order model of synchronous generator equipped with SEXS type excitation system and TGOV1 governors are used. Standard models of the generators available in PSS®E are applied. Two onshore wind power plants each operating at 800MW have been added at bus 25 and 21 respectively using standard moldes [174]. This is done in order to increase the penetration level of wind power generation in the system. Each onshore wind power plant is modelled by an aggregate full converter direct drive wind turbine using standard dynamic models of PSS®E. The MTDC grid is used for the connection of three offshore wind power plants. In the load flow case studied, the total offshore wind generation is 1200 MW (400MW, 200MW and 600MW). The HVDC system is monopolar rated at 250kV. The HVDC grid is meshed as it is shown in figure 6.23. DC choppers are installed at the onshore HVDC stations. The two onshore HVDC converters connected at IEEE 39-bus system inject a total of 800MW generation in the evaluated load flow case. The third converter is connected to the second system as shown figure 6.23. The total generation becomes 7.6 GW (with a share of 21% onshore, 10.5% offshore wind, and 68% conventional generation). Finally, the total load is scaled to 7.47 GW in this modified New England test system. The three

onshore HVDC stations utilize the power based direct voltage droop control using the outer control loops as it is shown in figure 6.10. The AC and the DC grid are initialized using a DC grid load flow. Another study for the interested reader using the same model can be found in [175].

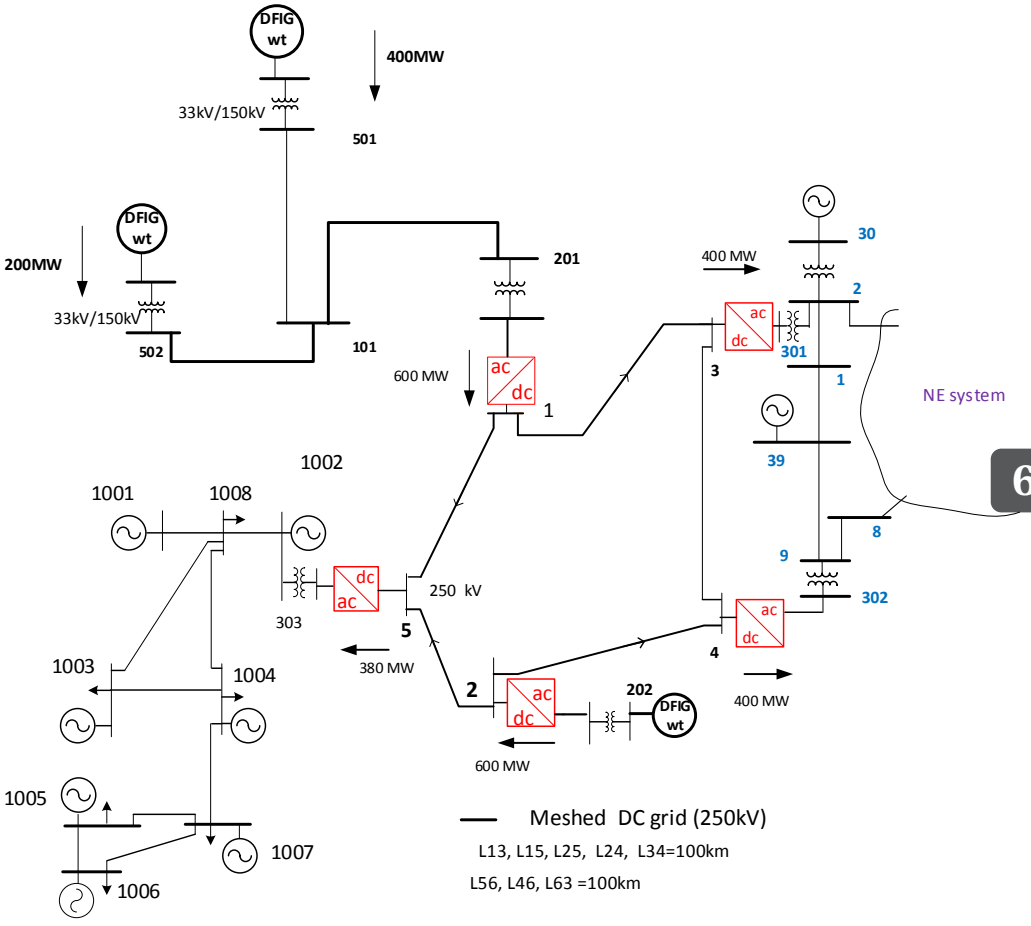

Figure 6.23: Single Line diagram of the modified IEEE 39-bus test system connected to the multi-terminal HVDC grid test system.

6.9.2. FAULT RIDE THROUGH COMPLIANCE OF THE MTDC GRID

A 150ms three-phase self cleared fault is applied at the AC terminal of the VSC-HVDC station 301. Figure 6.24 presents the results of the HVDC grid converters. The VSC-HVDC station 301, experiences a severe voltage drop since the fault is applied at its terminal. It provides its fault current capacity (1.1 p.u) as reactive current injection (iq), reducing the active current (id) to zero. The results of the MTDC grid case with respect to the AC voltage response are similar to the point to point case presented in figure 6.13. It is worth to observe the active current injection at the remote terminal 303 due to the response of the DC voltage droop controller.

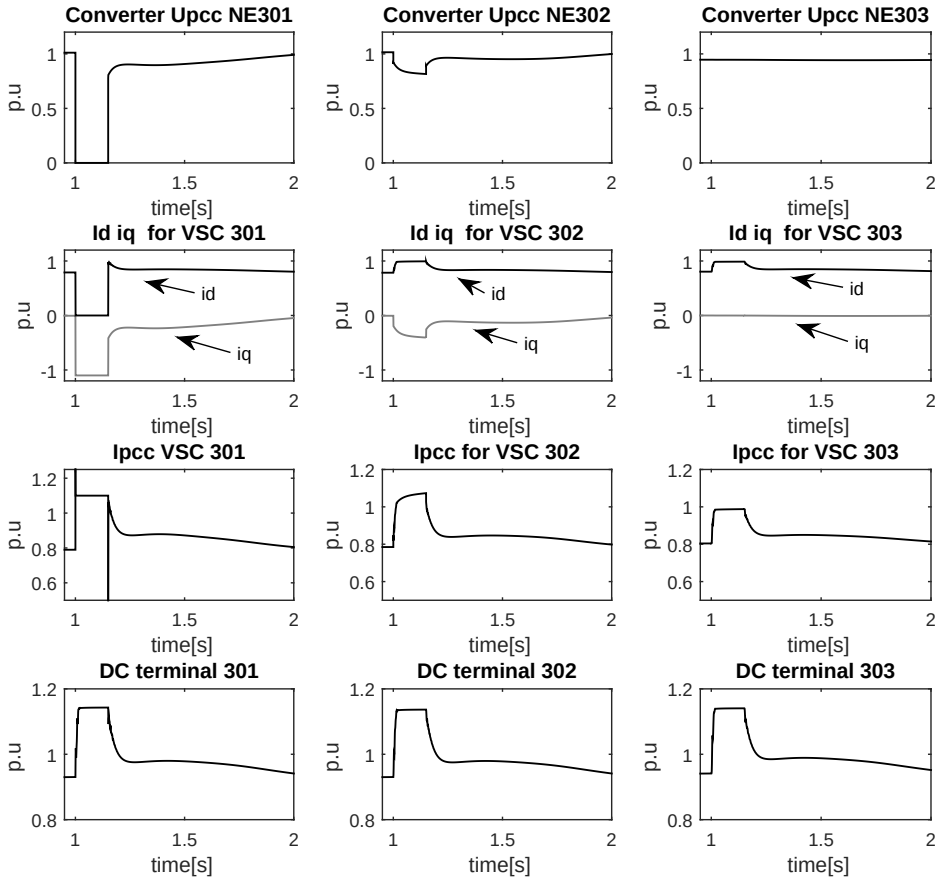

Figure 6.24: FRT compliance of the offshore MTDC grid for fault at the onshore VSC 301 connected to the IEEE 39-bus system. From up to down, the RMS voltages at the onshore converters, the dq-currents, the PCC current and direct voltages.

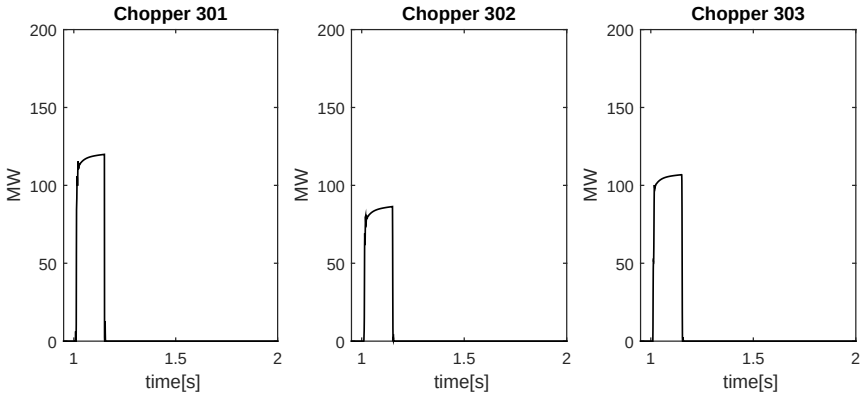

Figure 6.25: Dissipated power in the choppers as a result of the FRT compliance of the MTDC grid.

Finally, for the fault case on the VSC301, the response of the three DC choppers in the HVDC grid is presented in figure 6.25. As it can be seen 300MW of power is dissipated in the chopper out of 400MW that VSC301 is injecting to the grid. The remaining power is injected in the VSC302 and VSC303 as can be seen from the response of the active current (id) for the VSC 302 and 303 in figure 6.24. It is worth to observe that by means design principle, the active current is not allowed to go above 1.0p.u value. This is why the id (hence Ipcc) is 1.0 and not 1.1p.u. As a result the maximum active power that can be injected in the remote un-fault system is the rated power of the converter.

6.9.3. THE EFFECT OF THE FAULT RIDE THROUGH STRATEGY

In this paragraph, the effect of the applied fault ride through (FRT) strategy on the response of the MTDC grid system is assessed using RMS time domain simulations. In the analysis presented in chapter 5, the voltage drop strategy is discussed and optimized. It is shown that the injection of reactive current is not affected by the applied FRT strategy as long as the direct voltage is maintained between given well defined boundaries. Figure 6.26 and 6.27 presents the response of the MTDC grid for the case where the voltage drop FRT strategy is applied. As it can be seen in 6.27, the fault at VSC301 has triggered the reduction of the offshore voltage by the offshore station to 0.7p.u. The latter has reduced the power injected by the wind plants to the DC grid (and the power of the VSC 201 and 202. The remaining of the power is balanced by the VSC station 303. Figure 6.26 presents the active power response of the onshore, and the offshore stations. As it can be observed, the HVDC station VSC303 in the un-faulted system providing balancing of the MTDC grid during the fault period.

Finally, figure 6.28 compares the active power profiles of the three onshore stations for the chopper and voltage drop FRT strategy. As it can be observed, during the fault period the almost identical response is observed when DC chopper or offshore AC voltage drop FRT is used. During the post-fault period, there is a slight difference mainly due to the dynamics which are associated with the wind turbines.

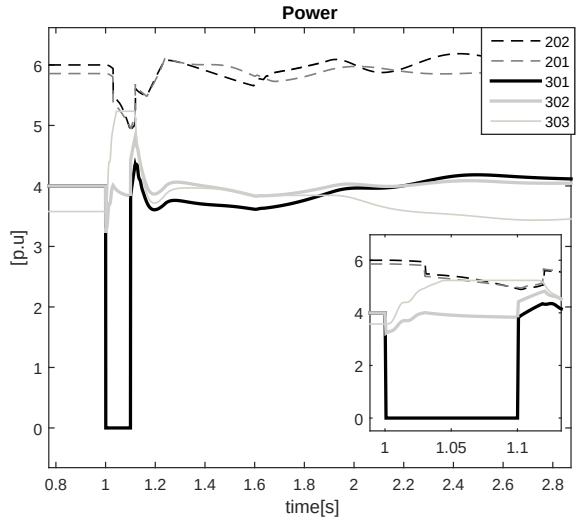

Figure 6.26: The response of the active power in the onshore and the offshore HVDC stations. Case with the voltage drop strategy. Sb=100MVA.

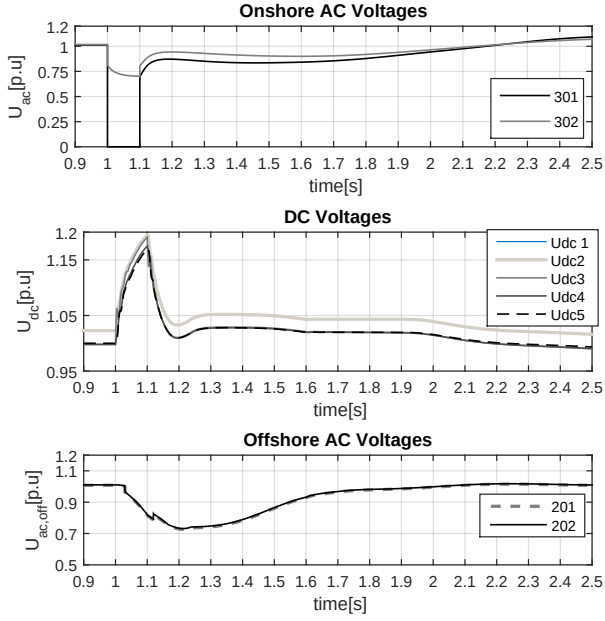

Figure 6.27: AC and DC voltages at the onshore and offshore terminals of the MTDC grid. Case with the offshore AC voltage drop strategy.

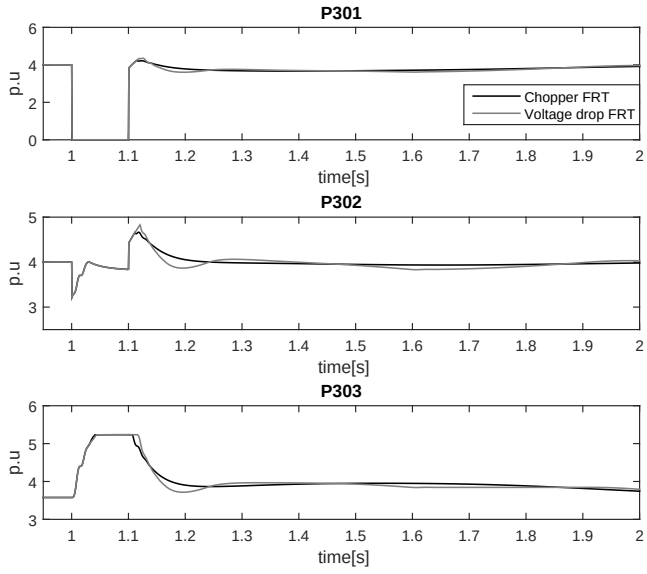

Figure 6.28: The impact of fault ride through strategy on the active power response of the onshore stations. Comparison between chopper and voltage drop strategy. Sb=100MVA.

6.9.4. THE IMPACT OF THE REACTIVE CURRENT BOOSTING GAIN ON THE AC-DC TRANSMISSION

Similar to the point to point connection, let us observe the dynamic behaviour of the New England test system for a 150ms symmetrical three phase fault at bus 39. Figure 6.29 demonstrates the voltage and current phasors of the converters measured at their grid connection point. The active and reactive current components i_{dq} of the VSC-HVDC stations 301 and 302 demonstrate the same dynamic response between the point-to-point and the MTDC connection. Since the VSC302 has reached its current saturation for both cases k equal to 2 and 6, the voltage response is the same. For VSC 301, the voltage drop is improved since in the case of k equal 6, higher amount of reactive current is injected.

Observing the MTDC grid metrics (direct voltage and power dissipated by the choppers), it can be concluded that when a small reactive current boosting gain is used (k=2), the power dissipated by the choppers is significantly lower compared to the case of (k=6). This occurs due to the reduction of the active current component (id). Hence, in the multi-terminal connection case, the increase of reactive boosting gain would lead to the higher balancing effort from the DC chopper.

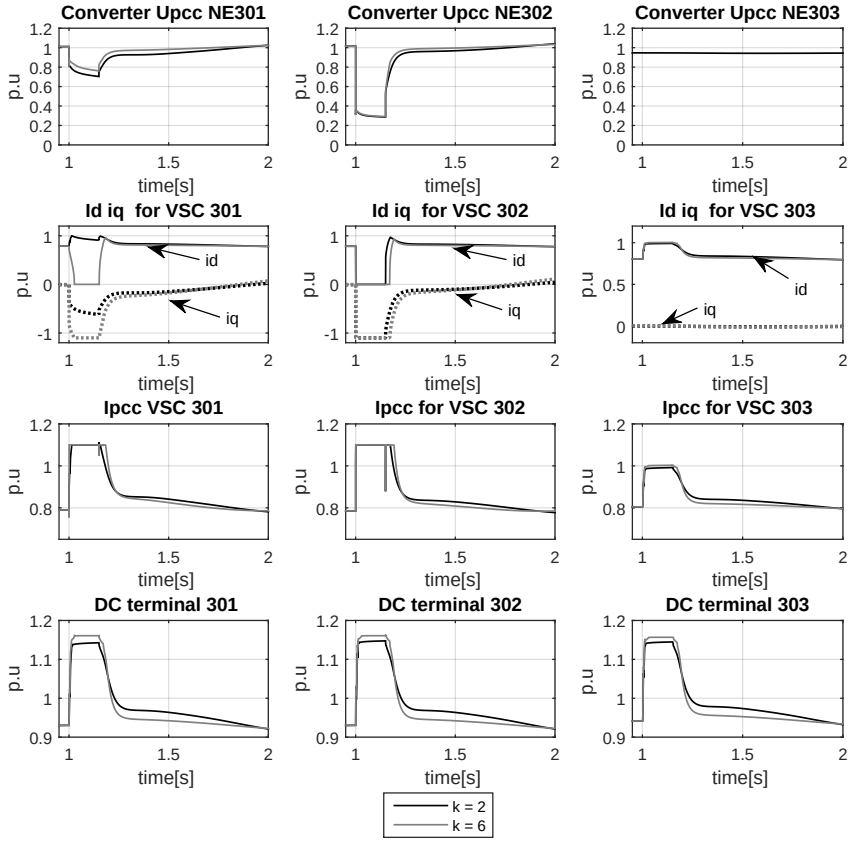

Figure 6.29: The effect of reactive current boosting gain on the MTDC grid metrics, including AC and DC voltages of the onshore converters.

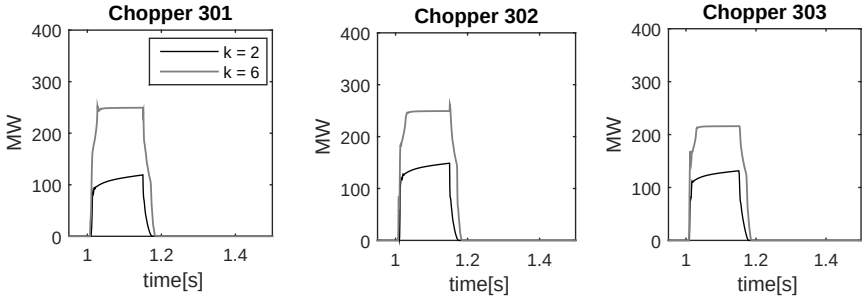

Figure 6.30: The effect of reactive current boosting gain on the choppers of the MTDC grid.

6.10. CONCLUSIONS

This chapter studies the effect of the short circuit current injection from VSC-HVDC systems connecting large offshore wind plants on the AC power system voltage and rotor angle stability. The main conclusions drawn are summarized as follows:

1. During AC grid faults, the injection of additional fast reactive short circuit current proportionally to the residual voltage at the grid connection point has improved the voltage and the rotor angle stability of the examined test system. The increase of the proportional reactive current boosting gain k to values above 2 (possibly 6), would enhance the voltage and rotor angle stability of the system under the condition that reactive current priority is followed. Both the CCTs and the voltage levels achieved are enhanced. The drawback from the use of increased reactive current boosting gain k is the higher electrical stresses on the HVDC link and the more frequent activation of the FRT strategy. Finally, the chapter has analyzed the effect of the short circuit ratio (SCR) on the voltage boosting. It was shown that for grid connection points with SCR above 15, the voltage boosting (or voltage support) achieved is marginal compared to lower SCR cases (5-10).

2. During severe voltage drops, the combined active and reactive current injection from the onshore HVDC converter station increases the risk of local voltage angle instability. The injection of reactive current during voltage drops shall be followed by the reduction of the active current component. In this frame, reactive current priority is advised for the onshore VSC-HVDC converter station during AC faults.

3. With regard to the selection of the over-current capacity of the VSC-HVDC onshore station, it is shown that the applied values above 1.1p.u should be followed by an increase of the reactive current boosting gain k and the extension of the reactive current profiles above 1 p.u value. The latter would increase the voltage support and improve the rotor angle stability of the onshore power system. The increase of the over-current capacity could create risk for voltage angle instability when both active and reactive currents are injected simultaneously.

4. In the multi-terminal HVDC grid connection, there is a wide area effect during the FRT period but also during post-fault period. The application of higher reactive current boosting gains places an additional burden to the FRT control scheme and the effect on the MTDC grid dynamic response. Finally, the applied FRT strategy (i.e chopper solution versus the offshore voltage drop) has limited effect on the rotor angle stability of the system.

7

CONCLUSIONS AND RECOMMENDATIONS

The focus of this thesis was the modeling and fault analysis of offshore wind power plants with VSC-HVDC transmission assuming state of the art grid code compliance strategies. The topic has been assessed using Elecro-magnetic transient (EMT) and RMS simulation models. Three phase balanced as well as un-balanced grid faults at the onshore and the offshore AC terminals were studied. Coordinated fault-ride through control schemes were introduced and optimally tuned. Finally, the thesis provided insights on the effect of VSC-HVDC connected wind power plants on the voltage and rotor angle stability of the AC transmission grids assuming typical grid connection requirements.

The general conclusion that could be drawn is that the compliance with typical fault ride through grid connection requirements enhances the fault response of the transmission grid boosting the voltage profiles and the rotor angle stability in the transmission system. Moreover, optimally tuned coordinated fault-ride through schemes could improve the dynamic response of the offshore wind power plants and the VSC-HVDC station during AC grid faults. Furthermore, the offshore wind plants and the VSC-HVDC transmission can be regarded in this case as unified power plant entity where specific grid code requirements could be imposed at the onshore VSC-HVDC system terminals. With respect to unbalanced faults, the decoupled control of the positive and the negative sequence current could enhance the unbalanced power system faulted response. As far as faults at the offshore AC island grid were considered, it was shown that adequate control schemes could ensure fault-ride through capability even for severe faults applied at the offshore VSC-HVDC station terminals. In addition, given the small size of the offshore AC island system, it is recommended that grid codes for offshore grids should not be too strict providing the opportunity to the vendors for the best and cost effective offshore system design.

7.1. SCIENTIFIC CONTRIBUTIONS

7.1.1. OPTIMAL TUNING OF THE COORDINATED FRT STATEGIES

Power system stability and security with high penetration levels of wind power is influenced by the ability of the wind power plants and their HVDC transmission system to provide power system support functionality. Fault ride-through (FRT) is nowadays a mandatory requirement for all offshore wind power generation units. So far in the literature, advanced coordinated fault ride-through strategies have been studied for point-to-point and for multi-terminal HVDC grid connection of offshore wind power plants. Although well reported, it has not been yet shown how to select the best set of grid code related control variables associated with the wind power plants and the HVDC transmission system which would enable optimal grid code compliance. The application of such coordinated methods would ensure optimal grid code compliance without the need of a DC chopper at the HVDC link but only by using the choppers available at the offshore wind turbines which are by default installed in state of the art wind turbines.

This thesis proposed an iterative procedure based on meta-heuristic optimization algorithms which enables the optimal tuning of coordinated fault ride-through (FRT) compliance strategies applied to offshore wind power plants with VSC-HVDC transmission. The optimal tuning is achieved using a sequence of electromagnetic transient (EMT) type simulation runs driven by a meta-heuristic optimization algorithm. Due to the highly non-linear nature of the problem, EMT time domain simulations are used in order to capture all the relevant dynamics and non-linearities of the HVDC transmission and the wind turbines. Analytical or theorerical approaches lack of this ability since they assume linearization of the system at a given operating point.

State of the art fault ride-through strategies have been assumed for this work, namely the controlled offshore voltage drop and the offshore frequency modulation technique. The objective function of the optimization problem aims at minimizing the electrical stresses experienced by the HVDC link during onshore AC grid faults (namely the experienced over-voltage of the HVDC link). The iterative procedure is solved for the point-to-point and for the multi-terminal HVDC connection case using the voltage drop and the frequency modulation fault-ride through strategy. The grid code fault ride through profiles at the onshore and at the offshore VSC-HVDC terminals and at the wind turbines is provided as input. The application of the optimally tuned control parameters have improved the dynamic response of the wind turbines and the VSC-HVDC system during the FRT and post-FRT period.

7.1.2. ENHANCED NEGATIVE SEQUENCE CURRENT CONTROL FOR OFFSHORE VSC-HVDC LINKS

The control of the VSC-HVDC transmission during unbalanced AC grid fault has gain importance in the last years as reflected by their insertion in national level grid codes in Europe. The second contribution of this thesis deals with the control of the VSC-HVDC system during unbalanced faults.

It was shown in this thesis that the negative sequence current suppression applied by the onshore VSC-HVDC station is beneficial for the protection of the power electronic components of the converter station from high unbalanced fault currents. It ensures that

the converter current is symmetrical for unbalanced grid voltages. On the other hand, the suppression of the negative sequence current by the onshore converter station leads to very low fault current levels during unbalanced grid faults. The later could create difficulties in the detection of line-to-line faults especially for weak grids with high grid impedance and high penetration of power converters. It was recommended in this thesis that the onshore converter station of the VSC-HVDC system injects a negative sequence current proportionally to the negative sequence voltage during unbalanced grid faults. This negative sequence current injection can be implemented in the same manner as the positive sequence reactive current injection (using a proportional controller). The constrain is that the positive and negative sequence current injections shall respect and not violate the maximum current capacity of the VSC-HVDC station. It was proposed in this thesis to apply current limiting scheme, with positive sequence current priority. In order to increase the share of the negative sequence current during unbalanced grid faults the latter current limiting scheme performs reduction of the positive sequence active current, leaving additional current space for the negative sequence reactive current.

7.2. ANSWERS TO THE MAIN RESEARCH QUESTIONS

1. *How do the reactive current boosting profiles applied at the onshore VSC-HVDC station affect the voltage and rotor angle stability of the power system. What is the effect on the VSC-HVDC system? What is the effect of the grid connection point?*

   Reactive current boosting is defined as the additional injection of reactive current (in the positive sequence) proportionally to the grid residual voltage during AC grid faults. Based on the modeling assumptions and the simulated test cases, it is shown that a reactive current boosting gain k (or k-factor) with values above 2 or even 6, followed with reactive current priority, is beneficial for the rotor angle and voltage stability of the transmission system. However, it has the drawback that it places additional electrical stresses to the VSC-HVDC station since the converter would reach its over-current capacity even at very small voltage drops (i.e 0.9 p.u). Moreover, the automatic reduction of the active current applied by the current limitation strategy would demand for additional balancing effort from the FRT scheme during small voltage drops. For VSC-Based HVDC connected wind power plants and embedded VSC-HVDC systems connected to the high voltage transmission system, a choice of reactive current boosting gain of 2 would be an adequate trade-off for the transient stability enhancement without over-engineering the HVDC link or the wind power plants.

   For very stiff grid connection points, with short circuit ratio (SCR) above 15, and for a high X/R ratio (above 10), the voltage boosting (or voltage support) which is achieved is marginal compared to lower SCR cases (5-10).

2. *Would an over-sized VSC-HVDC station enhance the power system stability during AC grid faults?*

   It has been shown that by increasing the AC fault-current capacity of the onshore VSC-HVDC station (above the 1.1p.u value) followed by an increase in the reactive current boosting gain k and the extension of the reactive current boosting profiles above 1 p.u value (with application of reactive current priority), would lead to improved transmission system faulted response.

3. *Could typical reactive current boosting grid code requirements lead to the trip of the VSC-HVDC link?*

   During severe voltage drops, where the residual voltage at the VSC-HVDC station terminals is very close to zero, the combined active and reactive current injection from the onshore VSC-HVDC station increases the potential risk of local voltage angle instability. This occurs due to the large angle separation between the internal converter voltage and the grid voltage. In that context, the injection of reactive current during voltage drops shall be always followed by the reduction of the active current component. In this way, the tripping risk of the VSC-HVDC system as a result of the grid code compliance can be eliminated.

4. *What are the observed differences between the point-to-point and the multi-terminal HVDC connection of the offshore wind power plants with regard to the FRT grid code compliance?*

   Based on the cases described in this thesis, the same fault ride-through and reactive current boosting profiles could be applied for onshore VSC-HVDC stations which are either in point-to-point or in MTDC grid connection. The application of higher reactive current boosting gains in the MTDC grid case places an additional burden to the FRT control scheme and effects the MTDC grid dynamic response. When the current capacity of HVDC stations is used as reactive current injection, additional measures need to be take to balance the DC grid power (i.e chopper or coordinated schemes). In the multi-terminal HVDC case, there is a DC side dynamic coupling of the converter stations. The later could propagate dynamics between AC grids coupled via HVDC grids or trigger small signal stability phenomena. With reference to the injection of reactive current during grid faults and its effect for the power system voltage and rotor angle stability, no difference are observed between the point to point and the multi-terminal HVDC connection.

5. *What undesired interactions and risks could be observed when coordinated fault-ride through strategies are applied to offshore wind power plants with VSC-HVDC transmission?*

   The application of coordinated fault-ride through strategies provides the advantage of the elimination of the need of the DC chopper at the HVDC link which would reduce the capital cost. The most common coordinated FRT schemes are the controlled offshore voltage drop and the frequency modulation of the offshore island grid followed by the active power reduction of the the wind plants.

However, the use of such FRT strategies involve risks of unwanted control interactions at the offshore side. The weak grid connection point offshore in conjugation with the presence of high concentration of power electronic based units (wind turbines and VSC-HVDC station), increase the instability risk. When coordinated FRT strategies are applied, the grid code compliance risks are associated with sustained activation of FRT strategy and unwanted interactions between the offshore VSC-HVDC station and the wind plants. In that frame, the application of coordinated schemes shall be applied with very careful assessment of the plant controllers.

6. *Could the dynamic response of the offshore wind power plants and the VSC-HVDC system be optimized such as reduced electrical stresses are observed during AC grids faults?*

   For offshore VSC-HVDC links, the compliance with fault ride though grid code articles (at the onshore terminals) leads to over-voltages in the DC link. Either by using a DC chopper or by means of coordinated fault-ride through control schemes, these over-voltages can be mitigated to the degree that they do not damage the power converter equipment. For the particular case of coordinated schemes, the selection of optimal control parameters could minimize the HVDC link over-voltages. The method presented in this thesis has enabled the estimation of the optimal parameters that ensure reduced over-voltages. The achieved over-voltages are comparable to the DC chopper case. Moreover, the methodology is tested not only for the point-to-point case but also for the multi-terminal HVDC connection, providing improved results.

7. *How does the negative sequence current control strategy applied to VSC-HVDC links affect the unbalanced fault response of transmission systems?*

   This thesis has presented that the injection of negative sequence current during unbalanced grid faults proportionally to the negative sequence voltage amplitude has two benefits. First, a higher in amplitude negative sequence current during line-to-line faults as measured at the point of common coupling. Second, a higher in amplitude zero sequence current components at the point of common coupling during single line to ground faults. A proportional controller similarly applied as for the positive sequence reactive current injection would be adequate control scheme. Moreover, the reduction of the positive sequence active current and the injection of only negative sequence reactive current during unbalanced faults is considered as the best approach for future implementation in grid codes for VSC-HVDC links.

8. *Is it meaningful to apply fault ride-through and fault current injection grid code requirements at offshore AC islands formed by wind power plants and the offshore VSC-HVDC station?*

   The offshore AC island grid formed by the offshore VSC-HVDC station and the offshore wind power plant, constitutes a weak grid connection point with potentially zero inertia. Based, on the proposed in chapter 3 grid forming control scheme applied to the offshore HVDC station, it is possible for the offshore VSC-HVDC station and the wind turbines to provide fault ride-through capability and short

circuit current injection. The injection of reactive short circuit current by the wind turbines and potentially by the VSC-HVDC station could have a twofold benefit. It could maintain the residual voltage in the offshore AC island grid to higher levels during the fault period. The latter would allow for the better synchronization of the wind turbines phase-lock loops (PLL). Secondly, it could help the protection schemes to detect and isolated permanent offshore AC grid faults.

7.3. RECOMMENDATIONS FOR FUTURE RESEARCH WORK

7.3.1. UPGRADE OF THE RMS MODEL TO MMC-HVDC TOPOLOGY

In this thesis two level VSC-HVDC topology has been assumed. As a result, the RMS model of the HVDC grid is developed based on this assumption. Future work could upgrade the existing RMS models for MMC-HVDC topology investing potential differences and limitations. Furthermore, the effect of the phase-lock loop (PLL) has not been included in the RMS model, assuming instantaneous synchronization. Finally, in the thesis, the DC circuit is modeled assuming a pi-section represented with differential equations in state space form. Future work could examine the effect of this assumptions in the presented results.

7.3.2. VSC-HVDC LINKS WITH GRID FORMING CONTROL SCHEMES

The main assumption of this thesis is that the onshore VSC-HVDC station and the wind turbines apply current control schemes (grid following operation) synchronized to the grid voltage via phase-lock loops (PLL). Although, such grid following schemes present certain advantages, they are prone to unstable operation in weak grids or systems with no conventional generation at all. As a follow up of chapter 3, future research work could investigate the feasibility of grid forming control schemes, especially for MMC-HVDC links connecting large wind plants to the main transmission grid.

The application of grid forming control to the onshore converter MMC-HVDC station would enable stable operation with 100% converter based generation. Such case is realistic during cases of system split. The fault ride-through capability of grid forming control schemes needs to be investigated thoroughly in future research considering MMC converter topology which is not done in this thesis. Current limiting is an additional concern in such control schemes and more research is needed.

7.3.3. ASSESSMENT OF THE TRANSIENT STABILITY OF AC-DC TRANSMISSION USING CO-SIMULATION OF PSSE AND PSCAD

In this thesis the effect of grid code compliance on the power system stability is addressed using offline RMS time domain dynamic simulations. The use of RMS time domain simulation models is an effective way for the assessment of the transient stability of the power system.

The use of detailed EMT type models for large scale power system studies has the drawback of very high computation time and difficulty to initialize at a given power system operating point (load flow case). In that direction, future research work could investigate on the development of a co-simulation environment which could efficiently solve these bottlenecks. In that platform, the large scale grid (i.e the European network) could

be simulated in PSSE while the HVDC transmission in PSCAD.

7.3.4. ASSESSMENT OF SUB-SYNCHRONOUS TORSIONAL INTERACTIONS IN AC-DC TRANSMISSION GRIDS

In this thesis the interactions of VSC-HVDC stations with the AC grid is performed under the transient stability time frame of interest (phenomena between 0.1-1.2Hz). Another topic which needs to be investigated thoroughly and has not been addressed in this thesis is sub-synchronous torsional interactions between generator units and HVDC links. Torsional interactions refer to the interactions between electrical systems and the turbine/generator torsional mechanical modes of oscillations. These vibrations triggered by the electrical characteristic of the power systems might cause cumulative fatigue damage to the turbine/generator when they exceed the material fatigue limits. A known electrical environment that can trigger such Torsional interactions is the presence of series capacitors in transmission lines in combination with the presence of MMC-HVDC converters stations or other power electronic interfaced renewable generation plants. Although the topic is well studied in the 70s for LCC-HVDC systems, it becomes again important in future grids dominated by converter based MMC-HVDC generation and transmission.

BIBLIOGRAPHY

[1] M. Bhattacharya, S. R. Paramati, I. Ozturk, and S. Bhattacharya, "The effect of renewable energy consumption on economic growth: Evidence from top 38 countries," *Applied Energy*, vol. 162, pp. 733–741, 2016.

[2] A. Cherp, J. Jewell, V. Vinichenko, N. Bauer, and E. De Cian, "Global energy security under different climate policies, gdp growth rates and fossil resource availabilities," *Climatic Change*, vol. 136, no. 1, pp. 83–94, 2016.

[3] H.-f. Lu, D. E. Campbell, M. Sagisaka, H. Ren, *et al.*, "Interactions among energy consumption, economic development and greenhouse gas emissions in japan after world war ii," *Renewable and Sustainable Energy Reviews*, vol. 54, pp. 1060–1072, 2016.

[4] J. Chow, R. J. Kopp, and P. R. Portney, "Energy resources and global development," *Science*, vol. 302, no. 5650, pp. 1528–1531, 2003.

[5] H. Geman, "Commodities and commodity derivatives," *Modeling and Pricing for Agriculturals, Metals and Energy, Chichester (Grande-Bretagne): Wiley Finance*, 2005.

[6] N. Heidari and J. M. Pearce, "A review of greenhouse gas emission liabilities as the value of renewable energy for mitigating lawsuits for climate change related damages," *Renewable and Sustainable Energy Reviews*, vol. 55, pp. 899–908, 2016.

[7] A. Robbins, "How to understand the results of the climate change summit: Conference of parties21 (cop21) paris 2015," *Journal of public health policy*, vol. 37, no. 2, pp. 129–132, 2016.

[8] W. D. Nordhaus, "After kyoto: alternative mechanisms to control global warming," *The American economic review*, vol. 96, no. 2, pp. 31–34, 2006.

[9] A. Foley and A. G. Olabi, "Renewable energy technology developments, trends and policy implications that can underpin the drive for global climate change," 2017.

[10] M. A. M. M. van der Meijden, "A sustainable and reliable electricity system," tech. rep., Delft University of Technology, 02 2012.

[11] S. Jacobsson, A. Bergek, D. Finon, V. Lauber, C. Mitchell, D. Toke, and A. Verbruggen, "Eu renewable energy support policy: Faith or facts?," *Energy policy*, vol. 37, no. 6, pp. 2143–2146, 2009.

[12] Y. Kumar, J. Ringenberg, S. S. Depuru, V. K. Devabhaktuni, J. W. Lee, E. Nikolaidis, B. Andersen, and A. Afjeh, "Wind energy: Trends and enabling technologies," *Renewable and Sustainable Energy Reviews*, vol. 53, pp. 209–224, 2016.

[13] A. Colmenar-Santos, J. Perera-Perez, D. Borge-Diez, *et al.*, "Offshore wind energy: A review of the current status, challenges and future development in spain," *Renewable and Sustainable Energy Reviews*, vol. 64, pp. 1–18, 2016.

[14] R. Perveen, N. Kishor, and S. R. Mohanty, "Off-shore wind farm development: Present status and challenges," *Renewable and Sustainable Energy Reviews*, vol. 29, pp. 780–792, 2014.

[15] J. Stentoft, J. Stentoft, R. Narasimhan, R. Narasimhan, T. Poulsen, and T. Poulsen, "Reducing cost of energy in the offshore wind energy industry: The promise and potential of supply chain management," *International Journal of Energy Sector Management*, vol. 10, no. 2, pp. 151–171, 2016.

[16] R. Green and N. Vasilakos, "The economics of offshore wind," *Energy Policy*, vol. 39, no. 2, pp. 496–502, 2011.

[17] A. G. Gonzalez-Rodriguez, "Review of offshore wind farm cost components," *Energy for Sustainable Development*, vol. 37, pp. 10–19, 2017.

[18] M. Junginger, A. Faaij, and W. Turkenburg, "Cost reduction prospects for offshore wind farms," *Wind engineering*, vol. 28, no. 1, pp. 97–118, 2004.

[19] C. Perez-Collazo, D. Greaves, and G. Iglesias, "A review of combined wave and offshore wind energy," *Renewable and Sustainable Energy Reviews*, vol. 42, pp. 141–153, 2015.

[20] N. Kirby, M. Luckett, L. Xu, and W. Siepmann, "Hvdc transmission for large offshore windfarms," in *AC-DC Power Transmission, 2001. Seventh International Conference on (Conf. Publ. No. 485)*, pp. 162–168, IET, 2001.

[21] D. Elliott, K. R. W. Bell, S. J. Finney, R. Adapa, C. Brozio, J. Yu, and K. Hussain, "A comparison of ac and hvdc options for the connection of offshore wind generation in great britain," *IEEE Transactions on Power Delivery*, vol. 31, pp. 798–809, April 2016.

[22] J. De Decker and A. Woyte, "Review of the various proposals for the european offshore grid," *Renewable energy*, vol. 49, pp. 58–62, 2013.

[23] H. Iswadi, R. J. Best, and D. J. Morrow, "Irish power system primary frequency response metrics during different system non synchronous penetration," in *PowerTech, 2015 IEEE Eindhoven*, pp. 1–6, IEEE, 2015.

[24] N. Miller, M. Shao, S. Venkataraman, C. Loutan, and M. Rothleder, "Frequency response of california and wecc under high wind and solar conditions," in *Power and Energy Society General Meeting, 2012 IEEE*, pp. 1–8, IEEE, 2012.

[25] F. D. Bianchi, J. L. Domínguez-García, and O. Gomis-Bellmunt, "Control of multiterminal hvdc networks towards wind power integration: A review," *Renewable and Sustainable Energy Reviews*, vol. 55, pp. 1055–1068, 2016.

[26] W. Winter, D. Chan, M. Norton, E. Haesen, and A. Szekely, "Towards a european network code for hvdc connections and offshore wind integration," in *Power Engineering Conference (UPEC), 2015 50th International Universities*, pp. 1–6, IEEE, 2015.

[27] C. Feltes, H. Wrede, F. W. Koch, and I. Erlich, "Enhanced fault ride-through method for wind farms connected to the grid through vsc-based hvdc transmission," *Power Systems, IEEE Transactions on*, vol. 24, no. 3, pp. 1537–1546, 2009.

[28] P. Moran, J. Goggins, and M. Hajdukiewicz, "Super-insulate or use renewable technology? life cycle cost, energy and global warming potential analysis of nearly zero energy buildings (nzeb) in a temperate oceanic climate," *Energy and Buildings*, vol. 139, pp. 590–607, 2017.

[29] M. Pacesila, S. G. Burcea, and S. E. Colesca, "Analysis of renewable energies in european union," *Renewable and Sustainable Energy Reviews*, vol. 56, pp. 156–170, 2016.

[30] A. Beyer and S. Fischer, "Transatlantic energy security: On different pathways?," 2016.

[31] P. Aalto, *The EU-Russian energy dialogue: Europe's future energy security*. Routledge, 2016.

[32] A. Herranz-Surrallés, "An emerging eu energy diplomacy? discursive shifts, enduring practices," *Journal of European Public Policy*, vol. 23, no. 9, pp. 1386–1405, 2016.

[33] R. Inglesi-Lotz, "The impact of renewable energy consumption to economic growth: A panel data application," *Energy Economics*, vol. 53, pp. 58–63, 2016.

[34] A. Markandya, I. Arto, M. González-Eguino, and M. V. Román, "Towards a green energy economy? tracking the employment effects of low-carbon technologies in the european union," *Applied Energy*, vol. 179, pp. 1342–1350, 2016.

[35] J. Abrell and S. Rausch, "Cross-country electricity trade, renewable energy and european transmission infrastructure policy," *Journal of Environmental Economics and Management*, vol. 79, pp. 87–113, 2016.

[36] J. Huenteler, C. Niebuhr, and T. S. Schmidt, "The effect of local and global learning on the cost of renewable energy in developing countries," *Journal of Cleaner Production*, vol. 128, pp. 6–21, 2016.

[37] J. Riesz and B. Elliston, "Research and deployment priorities for renewable technologies: Quantifying the importance of various renewable technologies for low cost, high renewable electricity systems in an australian case study," *Energy Policy*, vol. 98, pp. 298–308, 2016.

[38] H. C. Gils, Y. Scholz, T. Pregger, D. L. de Tena, and D. Heide, "Integrated modelling of variable renewable energy-based power supply in europe," *Energy*, vol. 123, pp. 173–188, 2017.

[39] R. Redlinger, P. Andersen, and P. Morthorst, *Wind energy in the 21st century: Economics, policy, technology and the changing electricity industry*. Springer, 2016.

[40] I. Boie, C. Kost, S. Bohn, M. Agsten, P. Bretschneider, O. Snigovyi, M. Pudlik, M. Ragwitz, T. Schlegl, and D. Westermann, "Opportunities and challenges of high renewable energy deployment and electricity exchange for north africa and europe–scenarios for power sector and transmission infrastructure in 2030 and 2050," *Renewable Energy*, vol. 87, pp. 130–144, 2016.

[41] T. Brown, P.-P. Schierhorn, E. Tröster, and T. Ackermann, "Optimising the european transmission system for 77% renewable electricity by 2030," *IET Renewable Power Generation*, vol. 10, no. 1, pp. 3–9, 2016.

[42] R. Martin, I. Lazakis, S. Barbouchi, and L. Johanning, "Sensitivity analysis of offshore wind farm operation and maintenance cost and availability," *Renewable Energy*, vol. 85, pp. 1226–1236, 2016.

[43] N. Ederer, "Evaluating capital and operating cost efficiency of offshore wind farms: A dea approach," *Renewable and Sustainable Energy Reviews*, vol. 42, pp. 1034–1046, 2015.

[44] K. Samoteskul, J. Firestone, J. Corbett, and J. Callahan, "Changing vessel routes could significantly reduce the cost of future offshore wind projects," *Journal of environmental management*, vol. 141, pp. 146–154, 2014.

[45] D. E. Gernaat, D. P. Van Vuuren, J. Van Vliet, P. Sullivan, and D. J. Arent, "Global long-term cost dynamics of offshore wind electricity generation," *Energy*, vol. 76, pp. 663–672, 2014.

[46] T. Ashuri, M. B. Zaaijer, J. R. Martins, G. J. Van Bussel, and G. A. Van Kuik, "Multidisciplinary design optimization of offshore wind turbines for minimum levelized cost of energy," *Renewable Energy*, vol. 68, pp. 893–905, 2014.

[47] J. Voormolen, H. Junginger, and W. van Sark, "Unravelling historical cost developments of offshore wind energy in europe," *Energy Policy*, vol. 88, pp. 435–444, 2016.

[48] A. Keyhani, *Design of smart power grid renewable energy systems*. John Wiley & Sons, 2016.

[49] M. Morjaria, D. Anichkov, V. Chadliev, and S. Soni, "A grid-friendly plant: The role of utility-scale photovoltaic plants in grid stability and reliability," *IEEE Power and Energy Magazine*, vol. 12, no. 3, pp. 87–95, 2014.

[50] M. Hossain, N. Madlool, N. Rahim, J. Selvaraj, A. Pandey, and A. F. Khan, "Role of smart grid in renewable energy: An overview," *Renewable and Sustainable Energy Reviews*, vol. 60, pp. 1168–1184, 2016.

[51] L. E. Jones, *Renewable energy integration: practical management of variability, uncertainty, and flexibility in power grids*. Academic Press, 2014.

[52] B. Johansson, "Security aspects of future renewable energy systems–a short overview," *Energy*, vol. 61, pp. 598–605, 2013.

[53] B. V. Mathiesen, H. Lund, D. Connolly, H. Wenzel, P. A. Østergaard, B. Möller, S. Nielsen, I. Ridjan, P. Karnøe, K. Sperling, *et al.*, "Smart energy systems for coherent 100% renewable energy and transport solutions," *Applied Energy*, vol. 145, pp. 139–154, 2015.

[54] I. Mason, S. Page, and A. Williamson, "Security of supply, energy spillage control and peaking options within a 100% renewable electricity system for new zealand," *Energy Policy*, vol. 60, pp. 324–333, 2013.

[55] S. Spiecker and C. Weber, "The future of the european electricity system and the impact of fluctuating renewable energy–a scenario analysis," *Energy Policy*, vol. 65, pp. 185–197, 2014.

[56] M. Sencar, V. Pozeb, and T. Krope, "Development of eu (european union) energy market agenda and security of supply," *Energy*, vol. 77, pp. 117–124, 2014.

[57] N. Jaalam, N. Rahim, A. Bakar, C. Tan, and A. M. Haidar, "A comprehensive review of synchronization methods for grid-connected converters of renewable energy source," *Renewable and Sustainable Energy Reviews*, vol. 59, pp. 1471–1481, 2016.

[58] M. Bollen, J. Meyer, H. Amaris, A. M. Blanco, A. G. de Castro, J. Desmet, M. Klatt, L. Kocewiak, S. Ronnberg, and K. Yang, "Future work on harmonics-some expert opinions part i-wind and solar power," in *Harmonics and Quality of Power (ICHQP), 2014 IEEE 16th International Conference on*, pp. 904–908, IEEE, 2014.

[59] H. Liu and J. Sun, "Voltage stability and control of offshore wind farms with ac collection and hvdc transmission," *IEEE Journal of Emerging and selected topics in Power Electronics*, vol. 2, no. 4, pp. 1181–1189, 2014.

[60] J. B. Glasdam, V. Gevorgian, C. L. Bak, J. Hjerrild, and L. H. Kocewiak, "Harmonic stability studies in vsc-hvdc grid connected offshore wind power plants," *IEEE Transactions on Power Delivery*, 2017.

[61] S. Zhang, S. Jiang, X. Lu, B. Ge, and F. Z. Peng, "Resonance issues and damping techniques for grid-connected inverters with long transmission cable," *IEEE Transactions on Power Electronics*, vol. 29, no. 1, pp. 110–120, 2014.

[62] A. Bayo-Salas, J. Beerten, J. Rimez, and D. Van Hertem, "Analysis of control interactions in multi-infeed vsc hvdc connections," *IET Generation, Transmission & Distribution*, vol. 10, no. 6, pp. 1336–1344, 2016.

[63] J. Sun, "Impedance-based stability criterion for grid-connected inverters," *IEEE Transactions on Power Electronics*, vol. 26, no. 11, pp. 3075–3078, 2011.

[64] X. Wang, F. Blaabjerg, M. Liserre, Z. Chen, J. He, and Y. Li, "An active damper for stabilizing power-electronics-based ac systems," *IEEE Transactions on Power Electronics*, vol. 29, no. 7, pp. 3318–3329, 2014.

[65] L. Yutian, F. Rui, and V. Terzija, "Power system restoration: a literature review from 2006 to 2016," *Journal of Modern Power Systems and Clean Energy*, vol. 4, no. 3, pp. 332–341, 2016.

[66] K. Meng, H. Yang, Z. Y. Dong, W. Guo, F. Wen, and Z. Xu, "Flexible operational planning framework considering multiple wind energy forecasting service providers," *IEEE Transactions on Sustainable Energy*, vol. 7, no. 2, pp. 708–717, 2016.

[67] R. Li, C. Booth, A. Dys, A. Roscoe, H. Urdal, J. Zhu, *et al.*, "A systematic evaluation of network protection responses in future converter-dominated power systems," 2016.

[68] A. G. Phadke, W. Peter, D. Lei, and V. Terzija, "Improving the performance of power system protection using wide area monitoring systems," *Journal of Modern Power Systems and Clean Energy*, vol. 4, no. 3, pp. 319–331, 2016.

[69] P. T. Manditereza and R. Bansal, "Renewable distributed generation: The hidden challenges–a review from the protection perspective," *Renewable and Sustainable Energy Reviews*, vol. 58, pp. 1457–1465, 2016.

[70] S. Mirsaeidi, D. M. Said, M. W. Mustafa, M. H. Habibuddin, and K. Ghaffari, "Fault location and isolation in micro-grids using a digital central protection unit," *Renewable and Sustainable Energy Reviews*, vol. 56, pp. 1–17, 2016.

[71] S. Swain and P. K. Ray, "Ride-through capability improvement of a grid-integrated dfig based wind turbine system using a new protection design," in *Power Systems (ICPS), 2016 IEEE 6th International Conference on*, pp. 1–5, IEEE, 2016.

[72] A. Zidan, M. Khairalla, A. M. Abdrabou, T. Khalifa, K. Shaban, A. Abdrabou, R. El Shatshat, and A. M. Gaouda, "Fault detection, isolation, and service restoration in distribution systems: State-of-the-art and future trends," *IEEE Transactions on Smart Grid*, 2016.

[73] A. Saleem, R. Arshad, and D. Khan, "Wide area protection and monitoring in smart-power-grid," *Journal of Electronic Systems Volume*, vol. 6, no. 3, p. 89, 2016.

[74] A. Egea-Alvarez, S. Fekriasl, F. Hassan, and O. Gomis-Bellmunt, "Advanced vector control for voltage source converters connected to weak grids," *IEEE Transactions on Power Systems*, vol. 30, no. 6, pp. 3072–3081, 2015.

[75] A. A. A. Radwan and Y. A.-R. I. Mohamed, "Improved vector control strategy for current-source converters connected to very weak grids," *IEEE Transactions on Power Systems*, vol. 31, no. 4, pp. 3238–3248, 2016.

[76] J. A. Suul, S. D'Arco, P. Rodríguez, and M. Molinas, "Impedance-compensated grid synchronisation for extending the stability range of weak grids with voltage source converters," *IET Generation, Transmission & Distribution*, vol. 10, no. 6, pp. 1315–1326, 2016.

[77] M. Ashabani and Y. A.-R. I. Mohamed, "Integrating vscs to weak grids by nonlinear power damping controller with self-synchronization capability," *IEEE Transactions on Power Systems*, vol. 29, no. 2, pp. 805–814, 2014.

[78] P. Mitra, L. Zhang, and L. Harnefors, "Offshore wind integration to a weak grid by vsc-hvdc links using power-synchronization control: A case study," *IEEE Transactions on Power Delivery*, vol. 29, no. 1, pp. 453–461, 2014.

[79] M. Liserre, R. Cardenas, M. Molinas, and J. Rodriguez, "Overview of multi-mw wind turbines and wind parks," *IEEE Transactions on Industrial Electronics*, vol. 58, no. 4, pp. 1081–1095, 2011.

[80] D. Y. Leung and Y. Yang, "Wind energy development and its environmental impact: A review," *Renewable and Sustainable Energy Reviews*, vol. 16, no. 1, pp. 1031–1039, 2012.

[81] M. Tsili and S. Papathanassiou, "A review of grid code technical requirements for wind farms," *IET Renewable Power Generation*, vol. 3, no. 3, pp. 308–332, 2009.

[82] P. W. Carlin, A. S. Laxson, and E. Muljadi, "The history and state of the art of variable-speed wind turbine technology," *Wind Energy*, vol. 6, no. 2, pp. 129–159, 2003.

[83] G. J. Herbert, S. Iniyan, E. Sreevalsan, and S. Rajapandian, "A review of wind energy technologies," *Renewable and sustainable energy Reviews*, vol. 11, no. 6, pp. 1117–1145, 2007.

[84] J. Conroy and R. Watson, "Low-voltage ride-through of a full converter wind turbine with permanent magnet generator," *IET Renewable Power Generation*, vol. 1, no. 3, pp. 182–189, 2007.

[85] J. F. Conroy and R. Watson, "Frequency response capability of full converter wind turbine generators in comparison to conventional generation," *IEEE transactions on power systems*, vol. 23, no. 2, pp. 649–656, 2008.

[86] S. I. Gkavanoudis and C. S. Demoulias, "A combined fault ride-through and power smoothing control method for full-converter wind turbines employing supercapacitor energy storage system," *Electric Power Systems Research*, vol. 106, pp. 62–72, 2014.

[87] T. Knüppel, J. N. Nielsen, K. H. Jensen, A. Dixon, and J. Østergaard, "Power oscillation damping capabilities of wind power plant with full converter wind turbines considering its distributed and modular characteristics," *IET Renewable Power Generation*, vol. 7, no. 5, pp. 431–442, 2013.

[88] J. Ekanayake, L. Holdsworth, and N. Jenkins, "Control of dfig wind turbines," *Power Engineer*, vol. 17, no. 1, pp. 28–32, 2003.

[89] J. Ekanayake and N. Jenkins, "Comparison of the response of doubly fed and fixed-speed induction generator wind turbines to changes in network frequency," *IEEE Transactions on Energy conversion*, vol. 19, no. 4, pp. 800–802, 2004.

[90] A. D. Hansen and G. Michalke, "Fault ride-through capability of dfig wind turbines," *Renewable energy*, vol. 32, no. 9, pp. 1594–1610, 2007.

[91] D. Xie, Z. Xu, L. Yang, J. Østergaard, Y. Xue, and K. P. Wong, "A comprehensive lvrt control strategy for dfig wind turbines with enhanced reactive power support," *IEEE Transactions on Power Systems*, vol. 28, no. 3, pp. 3302–3310, 2013.

[92] M. Edrah, K. L. Lo, and O. Anaya-Lara, "Impacts of high penetration of dfig wind turbines on rotor angle stability of power systems," *IEEE Transactions on Sustainable Energy*, vol. 6, no. 3, pp. 759–766, 2015.

[93] D. Ochoa and S. Martinez, "Fast-frequency response provided by dfig-wind turbines and its impact on the grid," *IEEE Transactions on Power Systems*, 2016.

[94] A. G. Abd-Elkader, D. F. Allam, and E. Tageldin, "Islanding detection method for dfig wind turbines using artificial neural networks," *International Journal of Electrical Power & Energy Systems*, vol. 62, pp. 335–343, 2014.

[95] X. Sun, D. Huang, and G. Wu, "The current state of offshore wind energy technology development," *Energy*, vol. 41, no. 1, pp. 298–312, 2012.

[96] J. Jonkman, S. Butterfield, W. Musial, and G. Scott, "Definition of a 5-mw reference wind turbine for offshore system development," *National Renewable Energy Laboratory, Golden, CO, Technical Report No. NREL/TP-500-38060*, 2009.

[97] S. Heier, *Grid integration of wind energy: onshore and offshore conversion systems*. John Wiley & Sons, 2014.

[98] B. Byrne and G. Houlsby, "Foundations for offshore wind turbines," *Philosophical Transactions of the Royal Society of London A: Mathematical, Physical and Engineering Sciences*, vol. 361, no. 1813, pp. 2909–2930, 2003.

[99] G. Van Bussel, A. Henderson, C. Morgan, B. Smith, R. Barthelmie, K. Argyriadis, A. Arena, G. Niklasson, and E. Peltola, "State of the art and technology trends for offshore wind energy: operation and maintenance issues," in *Offshore Wind Energy EWEA special topic conference*, 2001.

[100] N. Boccard, "Capacity factor of wind power realized values vs. estimates," *energy policy*, vol. 37, no. 7, pp. 2679–2688, 2009.

[101] R. J. Barthelmie, S. Pryor, S. T. Frandsen, K. S. Hansen, J. Schepers, K. Rados, W. Schlez, A. Neubert, L. Jensen, and S. Neckelmann, "Quantifying the impact of wind turbine wakes on power output at offshore wind farms," *Journal of Atmospheric and Oceanic Technology*, vol. 27, no. 8, pp. 1302–1317, 2010.

[102] M. B. Christiansen and C. B. Hasager, "Wake effects of large offshore wind farms identified from satellite sar," *Remote Sensing of Environment*, vol. 98, no. 2, pp. 251–268, 2005.

[103] L. Hirth and S. Müller, "System-friendly wind power: How advanced wind turbine design can increase the economic value of electricity generated through wind power," *Energy Economics*, vol. 56, pp. 51–63, 2016.

[104] P. D. Lund, J. Lindgren, J. Mikkola, and J. Salpakari, "Review of energy system flexibility measures to enable high levels of variable renewable electricity," *Renewable and Sustainable Energy Reviews*, vol. 45, pp. 785–807, 2015.

[105] F. Díaz-González, M. Hau, A. Sumper, and O. Gomis-Bellmunt, "Participation of wind power plants in system frequency control: Review of grid code requirements and control methods," *Renewable and Sustainable Energy Reviews*, vol. 34, pp. 551–564, 2014.

[106] A. D. Hansen, M. Altin, and F. Iov, "Provision of enhanced ancillary services from wind power plants–examples and challenges," *Renewable Energy*, vol. 97, pp. 8–18, 2016.

[107] V. Y. Singarao and V. S. Rao, "Frequency responsive services by wind generation resources in united states," *Renewable and Sustainable Energy Reviews*, vol. 55, pp. 1097–1108, 2016.

[108] H. Holttinen, A. Ivanova, and J. L. Dominguez, "Wind power in markets for frequency support services," in *European Energy Market (EEM), 2016 13th International Conference on the*, pp. 1–5, IEEE, 2016.

[109] T. Soares, P. Pinson, T. V. Jensen, and H. Morais, "Optimal offering strategies for wind power in energy and primary reserve markets," *IEEE Transactions on Sustainable Energy*, vol. 7, no. 3, pp. 1036–1045, 2016.

[110] A. E. Leon, G. Revel, D. M. Alonso, and G. E. Alonso, "Wind power converters improving the power system stability," *IET Generation, Transmission & Distribution*, vol. 10, no. 7, pp. 1622–1633, 2016.

[111] M. Cui, J. Zhang, H. Wu, and B.-M. Hodge, "Wind-friendly flexible ramping product design in multi-timescale power system operations," *IEEE Transactions on Sustainable Energy*, 2017.

[112] M. Fischer, S. Engelken, N. Mihov, and A. Mendonca, "Operational experiences with inertial response provided by type 4 wind turbines," *IET Renewable Power Generation*, vol. 10, no. 1, pp. 17–24, 2016.

[113] T. Xu and N. Zhang, "Coordinated operation of concentrated solar power and wind resources for the provision of energy and reserve services," *IEEE Transactions on Power Systems*, 2016.

[114] J. Van de Vyver, J. D. De Kooning, T. L. Vandoorn, B. Meersman, and L. Vandevelde, "Comparison of wind turbine power control strategies to provide power reserves," in *Energy Conference (ENERGYCON), 2016 IEEE International*, pp. 1–6, IEEE, 2016.

[115] T. Xu, W. Jang, and T. Overbye, "An economic evaluation tool of inertia services for systems with integrated wind power and fast-acting storage resources," in *System Sciences (HICSS), 2016 49th Hawaii International Conference on*, pp. 2456–2465, IEEE, 2016.

[116] L. Petersen, F. Kryezi, and F. Iov, "Design and tuning of wind power plant voltage controller with embedded application of wind turbines and statcoms," *Iet Renewable Power Generation*, 2016.

[117] G. Lalor, A. Mullane, and M. O'Malley, "Frequency control and wind turbine technologies," *IEEE Transactions on Power Systems*, vol. 20, no. 4, pp. 1905–1913, 2005.

[118] L. Ruttledge, N. W. Miller, J. O'Sullivan, and D. Flynn, "Frequency response of power systems with variable speed wind turbines," *IEEE transactions on Sustainable Energy*, vol. 3, no. 4, pp. 683–691, 2012.

[119] M. Kayikçi and J. V. Milanovic, "Dynamic contribution of dfig-based wind plants to system frequency disturbances," *IEEE Transactions on Power Systems*, vol. 24, no. 2, pp. 859–867, 2009.

[120] G. Ramtharan, N. Jenkins, and J. Ekanayake, "Frequency support from doubly fed induction generator wind turbines," *IET Renewable Power Generation*, vol. 1, no. 1, pp. 3–9, 2007.

[121] J. Morren, J. Pierik, and S. W. De Haan, "Inertial response of variable speed wind turbines," *Electric power systems research*, vol. 76, no. 11, pp. 980–987, 2006.

[122] X. Yingcheng and T. Nengling, "Review of contribution to frequency control through variable speed wind turbine," *Renewable Energy*, vol. 36, no. 6, pp. 1671–1677, 2011.

[123] D. Gautam, L. Goel, R. Ayyanar, V. Vittal, and T. Harbour, "Control strategy to mitigate the impact of reduced inertia due to doubly fed induction generators on large power systems," *IEEE Transactions on Power Systems*, vol. 26, no. 1, pp. 214–224, 2011.

[124] C. Huang, "Studies of uncertainties in smart grid: Wind power generation and wide-area communication," 2016.

[125] D. Alahakoon and X. Yu, "Smart electricity meter data intelligence for future energy systems: A survey," *IEEE Transactions on Industrial Informatics*, vol. 12, no. 1, pp. 425–436, 2016.

[126] P. Bresesti, W. L. Kling, R. L. Hendriks, and R. Vailati, "Hvdc connection of offshore wind farms to the transmission system," *IEEE Transactions on energy conversion*, vol. 22, no. 1, pp. 37–43, 2007.

[127] L. Xu and B. R. Andersen, "Grid connection of large offshore wind farms using hvdc," *Wind Energy*, vol. 9, no. 4, pp. 371–382, 2006.

[128] L. Xu, L. Yao, and C. Sasse, "Grid integration of large dfig-based wind farms using vsc transmission," *IEEE Transactions on Power Systems*, vol. 22, no. 3, pp. 976–984, 2007.

[129] L. Fan, Z. Miao, and D. Osborn, "Wind farms with hvdc delivery in load frequency control," *IEEE Transactions on Power Systems*, vol. 24, no. 4, pp. 1894–1895, 2009.

[130] N. Flourentzou, V. G. Agelidis, and G. D. Demetriades, "Vsc-based hvdc power transmission systems: An overview," *Power Electronics, IEEE Transactions on*, vol. 24, no. 3, pp. 592–602, 2009.

[131] K. Bell, D. Cirio, A. M. Denis, L. He, C.-C. Liu, G. Migliavacca, C. Moreira, and P. Panciatici, "Economic and technical criteria for designing future off-shore hvdc grids," in *Innovative Smart Grid Technologies Conference Europe (ISGT Europe), 2010 IEEE PES*, pp. 1–8, IEEE, 2010.

[132] C. Meyer, M. Hoing, A. Peterson, and R. W. De Doncker, "Control and design of dc grids for offshore wind farms," *IEEE Transactions on Industry applications*, vol. 43, no. 6, pp. 1475–1482, 2007.

[133] E. Prieto-Araujo, F. D. Bianchi, A. Junyent-Ferre, and O. Gomis-Bellmunt, "Methodology for droop control dynamic analysis of multiterminal vsc-hvdc grids for offshore wind farms," *Power Delivery, IEEE Transactions on*, vol. 26, no. 4, pp. 2476–2485, 2011.

[134] A. Egea-Alvarez, J. Beerten, D. Van Hertem, and O. Gomis-Bellmunt, "Hierarchical power control of multiterminal hvdc grids," *Electric Power Systems Research*, vol. 121, pp. 207–215, 2015.

[135] "ENTSOE, network code on hvdc connections." https://www.entsoe.eu/major-projects/network-code-development/high-voltage-direct-current/Pages/default.aspx. Accessed: 10-9-2016.

[136] H.-s. Song and K. Nam, "Dual current control scheme for pwm converter under unbalanced input voltage conditions," *IEEE transactions on industrial electronics*, vol. 46, no. 5, pp. 953–959, 1999.

[137] A. Yazdani and R. Iravani, "A unified dynamic model and control for the voltage-sourced converter under unbalanced grid conditions," *IEEE Transactions on Power delivery*, vol. 21, no. 3, pp. 1620–1629, 2006.

[138] K. Ma, W. Chen, M. Liserre, and F. Blaabjerg, "Power controllability of a three-phase converter with an unbalanced ac source," *IEEE Transactions on Power Electronics*, vol. 30, no. 3, pp. 1591–1604, 2015.

[139] C. Ng, L. Ran, and J. Bumby, "Unbalanced grid fault ride-through control for a wind turbine inverter," in *Industry Applications Conference, 2007. 42nd IAS Annual Meeting. Conference Record of the 2007 IEEE*, pp. 154–164, IEEE, 2007.

[140] S. Engelhardt, J. Kretschmann, J. Fortmann, F. Shewarega, I. Erlich, and C. Feltes, "Negative sequence control of dfg based wind turbines," in *2011 IEEE Power and Energy Society General Meeting*, pp. 1–8, IEEE, 2011.

[141] T. Neumann, T. Wijnhoven, G. Deconinck, and I. Erlich, "Enhanced dynamic voltage control of type 4 wind turbines during unbalanced grid faults," *IEEE Transactions on Energy Conversion*, vol. 30, no. 4, pp. 1650–1659, 2015.

[142] I. Erlich, T. Neumann, F. Shewarega, P. Schegner, and J. Meyer, "Wind turbine negative sequence current control and its effect on power system protection," in *Power and Energy Society General Meeting (PES)*, pp. 1–5, 2013.

[143] L. Xu, B. R. Andersen, and P. Cartwright, "Vsc transmission operating under unbalanced ac conditions-analysis and control design," *IEEE transactions on Power Delivery*, vol. 20, no. 1, pp. 427–434, 2005.

[144] S. K. Chaudhary, R. Teodorescu, P. Rodriguez, P. C. Kjaer, and A. M. Gole, "Negative sequence current control in wind power plants with vsc-hvdc connection," *IEEE Transactions on Sustainable energy*, vol. 3, no. 3, pp. 535–544, 2012.

[145] A. Moawwad, M. S. El Moursi, and W. Xiao, "A novel transient control strategy for vsc-hvdc connecting offshore wind power plant," *IEEE Transactions on Sustainable Energy*, vol. 5, no. 4, pp. 1056–1069, 2014.

[146] L. Xu, L. Yao, and C. Sasse, "Grid integration of large dfig-based wind farms using vsc transmission," *IEEE Transactions on Power Systems*, vol. 22, no. 3, pp. 976–984, 2007.

[147] A. A. van der Meer, M. Ndreko, M. Gibescu, and M. A. M. M. van der Meijden, "The effect of frt behavior of vsc-hvdc-connected offshore wind power plants on ac/dc system dynamics," *IEEE Transactions on Power Delivery*, vol. 31, pp. 878–887, April 2016.

[148] S. I. Nanou, G. N. Patsakis, and S. A. Papathanassiou, "Assessment of communication-independent grid code compatibility solutions for vsc–hvdc connected offshore wind farms," *Electric Power Systems Research*, vol. 121, pp. 38–51, 2015.

[149] P. Mitra, L. Zhang, and L. Harnefors, "Offshore wind integration to a weak grid by vsc-hvdc links using power-synchronization control: A case study," *IEEE Transactions on Power Delivery*, vol. 29, no. 1, pp. 453–461, 2014.

[150] J.-W. Moon, J.-W. Park, D.-W. Kang, and J.-M. Kim, "A control method of hvdc-modular multilevel converter based on arm current under the unbalanced voltage condition," *IEEE Transactions on Power Delivery*, vol. 30, no. 2, pp. 529–536, 2015.

[151] Q. Tu, Z. Xu, Y. Chang, and L. Guan, "Suppressing dc voltage ripples of mmc-hvdc under unbalanced grid conditions," *IEEE Transactions on Power Delivery*, vol. 27, no. 3, pp. 1332–1338, 2012.

[152] M. Guan and Z. Xu, "Modeling and control of a modular multilevel converter-based hvdc system under unbalanced grid conditions," *IEEE Transactions on Power Electronics*, vol. 27, no. 12, pp. 4858–4867, 2012.

[153] S. Li, X. Wang, Z. Yao, T. Li, and Z. Peng, "Circulating current suppressing strategy for mmc-hvdc based on nonideal proportional resonant controllers under unbalanced grid conditions," *IEEE Transactions on Power Electronics*, vol. 30, no. 1, pp. 387–397, 2015.

[154] S. K. Chaudhary, R. Teodorescu, P. Rodriguez, and P. Kjar, "Chopper controlled resistors in vsc-hvdc transmission for wpp with full-scale converters," in *Sustainable Alternative Energy (SAE), 2009 IEEE PES/IAS Conference on*, pp. 1–8, IEEE, 2009.

[155] A. A. van der Meer, R. L. Hendriks, and W. L. Kling, "A survey of fast power reduction methods for vsc connected wind power plants consisting of different turbine types," *EPE wind energy*, pp. 23–24, 2009.

[156] L. Xu, L. Yao, and C. Sasse, "Grid integration of large dfig-based wind farms using vsc transmission," *Power Systems, IEEE Transactions on*, vol. 22, no. 3, pp. 976–984, 2007.

[157] B. Silva, C. Moreira, H. Leite, and J. Lopes, "Control strategies for ac fault ride through in multiterminal hvdc grids," *Power Delivery, IEEE Transactions on*, vol. 29, no. 1, pp. 395–405, 2014.

[158] S. I. Nanou, G. N. Patsakis, and S. A. Papathanassiou, "Assessment of communication-independent grid code compatibility solutions for vsc–hvdc connected offshore wind farms," *Electric Power Systems Research*, vol. 121, pp. 38–51, 2015.

[159] I. Erlich, C. Feltes, and F. Shewarega, "Enhanced voltage drop control by vsc–hvdc systems for improving wind farm fault ridethrough capability," *Power Delivery, IEEE Transactions on*, vol. 29, no. 1, pp. 378–385, 2014.

[160] M. Ndreko, A. M. Bucurenciu, M. Popov, and M. A. M. M. van der Meijden, "On grid code compliance of offshore mtdc grids: modeling and analysis," in *PowerTech, 2015 IEEE Eindhoven*, pp. 1–6, June 2015.

[161] S. Filizadeh, A. M. Gole, D. A. Woodford, and G. D. Irwin, "An optimization-enabled electromagnetic transient simulation-based methodology for hvdc controller design," *Power Delivery, IEEE Transactions on*, vol. 22, no. 4, pp. 2559–2566, 2007.

[162] J. L. Rueda and I. Erlich, "Testing mvmo on learning-based real-parameter single objective benchmark optimization problems," in *Evolutionary Computation (CEC), 2015 IEEE Congress on*, pp. 1025–1032, IEEE, 2015.

[163] O. Gomis-Bellmunt, J. Liang, J. Ekanayake, R. King, and N. Jenkins, "Topologies of multiterminal HVDC-VSC transmission for large offshore wind farms," *Electric Power Systems Research*, vol. 81, no. 2, pp. 271 – 281, 2011.

[164] F. D. Bianchi, J. L. Domínguez-García, and O. Gomis-Bellmunt, "Control of multiterminal HVDC networks towards wind power integration: A review," *Renewable and Sustainable Energy Reviews*, vol. 55, pp. 1055 – 1068, 2016.

[165] T. K. Vrana, J. Beerten, R. Belmans, and O. B. Fosso, "A classification of DC node voltage control methods for HVDC grids," *Electric Power Systems Research*, vol. 103, pp. 137 – 144, 2013.

[166] J. Beerten, O. Gomis-Bellmunt, X. Guillaud, J. Rimez, A. van der Meer, and D. Van Hertem, "Modeling and control of HVDC grids: A key challenge for the future power system," in *Power Systems Computation Conference (PSCC), 2014*, pp. 1–21, Aug 2014.

[167] J. Beerten, S. Cole, and R. Belmans, "Generalized steady-state vsc mtdc model for sequential ac/dc power flow algorithms," *IEEE Transactions on Power Systems*, vol. 27, no. 2, pp. 821–829, 2012.

[168] S. Cole, J. Beerten, and R. Belmans, "Generalized dynamic vsc mtdc model for power system stability studies," *Power Systems, IEEE Transactions on*, vol. 25, no. 3, pp. 1655–1662, 2010.

[169] J. Beerten, O. Gomis-Bellmunt, X. Guillaud, J. Rimez, A. van der Meer, and D. Van Hertem, "Modeling and control of hvdc grids: a key challenge for the future power system," in *Power Systems Computation Conference (PSCC), 2014*, pp. 1–21, IEEE, 2014.

[170] J. Beerten and D. Van Hertem, "Analysis of power redispatch schemes for HVDC grid secondary voltage control," in *Power Energy Society General Meeting, 2015 IEEE*, pp. 1–5, July 2015.

[171] R. Pinto, P. Bauer, S. Rodrigues, E. Wiggelinkhuizen, J. Pierik, and B. Ferreira, "A novel distributed direct-voltage control strategy for grid integration of offshore wind energy systems through MTDC network," *IEEE Transactions on Industrial Electronics*, vol. 60, pp. 2429–2441, June 2013.

[172] S. Liu, Z. Xu, W. Hua, G. Tang, and Y. Xue, "Electromechanical transient modeling of modular multilevel converter based multi-terminal hvdc systems," *IEEE Transactions on Power Systems*, vol. 29, no. 1, pp. 72–83, 2014.

[173] T. Knüppel, J. N. Nielsen, K. H. Jensen, A. Dixon, and J. Østergaard, "Small-signal stability of wind power system with full-load converter interfaced wind turbines," *IET Renewable Power Generation*, vol. 6, no. 2, pp. 79–91, 2012.

[174] M. Asmine, J. Brochu, J. Fortmann, R. Gagnon, Y. Kazachkov, C.-E. Langlois, C. Larose, E. Muljadi, J. MacDowell, P. Pourbeik, *et al.*, "Model validation for wind

turbine generator models," *IEEE Transactions on Power Systems*, vol. 26, no. 3, pp. 1769–1782, 2011.

[175] M. Ndreko, A. A. van der Meer, M. Gibescu, and M. A. van der Meijden, "Impact of dc voltage control parameters on ac/dc system dynamics under faulted conditions," in *PES General Meeting| Conference & Exposition, 2014 IEEE*, pp. 1–5, IEEE, 2014.

GLOSSARY

LIST OF ABBREVIATIONS

AC	Alternating current
CAPEX	Capital expenditude
CCT	Critical clearing time
DEVEX	Development expenditure
DC	Direct current
DG	Distributed Generation
DSO	Distribution System Operator
ENTSO-E	European Network of Transmission system Operators for Electricity
EHV	Extra-High Voltage (380/220kV in NL)
EMT	Electro-magnetic transient
FD	Feeder
GSVSC	Grid Side Voltage Source Converter
FRT	Fault Ride Through
HV	High Voltage (150/110kV in NL)
HVAC	High-Voltage Alternating Current
HVDC	High-Voltage Direct Current
IGCT	Integrated Gate Commutated Thyristors
LVRT	Low Voltage Ride-Through
LCC	Line commutated Converter
MTDC	Multi-terminal direct current
NSVD	Negative sequence voltage dependent
NF	Notch filters
MMC	Modular multilevel converter
MF	Membership function
NC	Network Code
OPEX	Operation expenditure
PV	Photovoltaic
PV	Proportional Integral
PPM	Power Plant Module
PLL	Phase-lock loop
PSVD	Positive sequence voltage dependent
RMS	Root mean square
RES	Renewable Energy Sources
SCR	Schort circuit ratio
RfG	Requirements for Generators
PCC	Point of common coupling
SRF	Synchronous reference frame
TSO	Transmission System Operator

TGOV	Turbine Governor
VSC	Voltage Source converter
WPVSC	Wind plant Side Voltage Source Converter

SYMBOLS OF CHAPTER 2

T_{fault}	Time the fault is applied
T_{clear}	Time the fault is cleared
T_{rec}	Time the voltage has recovered
T_{blc}	Time the converter is allowed to be blocked
U_{fault}	Voltage at the time the fault is applied
U_{clear}	Voltage when the fault is cleared
U_{rec}	Voltage level at time of recovery
U_{blc}	Voltage level that blocking is allowed
U	Voltage during the fault
U_0	Pre-fault voltage level
U_N	Rated voltage of the system
I_b	Reactive current bousting
I_N	Rated current
I_b0	Reactive current before the fault
P	Active power
Q	Reactive power
P_{max}	Maximum active power

SYMBOLS OF CHAPTER 3

Onshore converter model:

i_{pcc}	Instantaneous value of the three phase current at the PCC

i_{grid}	Instantaneous value of the three phase current at the infinite grid
i_{vsc}	Instantaneous value of the three phase current at the phase reactor of the VSC
u_f	Instantaneous value of the three phase voltage at the onshore VSC filter
u_c	Instantaneous value of the three phase converter voltage at the onshore station
$i_{(dq^+)}$	Positive sequence reference frame dq current components
$i_{(dq^-)}$	Negative sequence reference frame dq current components
$u_{(dq^+)}$	Positive sequence reference frame dq voltage components
$u_{(dq^-)}$	Negative sequence reference frame dq voltage components
$u^+_{f(abc)}$	Instantaneous positive sequence value of the filter voltage
$u^-_{f(abc)}$	Instantaneous negative sequence value of the filter voltage
$u_{f(dq^+)}$	Positive sequence reference frame dq filter voltage components
$u_{f(dq^-)}$	Negative sequence reference frame dq filter voltage components
$u_{c(dq^+)}$	Positive sequence reference frame dq components of the converter internal voltage
$u_{c(dq^-)}$	Negative sequence reference frame dq components of the converter internal voltage
U^+_{dc}	Direct voltage at the positive pole of the HVDC link converter terminal
U^-_{dc}	Direct voltage at the negative pole of the HVDC link converter terminal
U^{ref}_{dc}	Direct voltage reference of the HVDC link converter terminal
U_f	Measured filter voltage
U^{ref}_f	Reference of the filter voltage
I_{max1}	Maximum positive sequence current

	capacity of the converter station
I_{max2}	Maximum negative sequence current capacity of the converter station
i_{vsc}^{+}	Instantaneous positive sequence value of the phase reactive current
i_{vsc}^{-}	Instantaneous negative sequence value of the phase reactive current
i_{d+}^{ref}	Positive sequence reference of the d-axis current component
i_{q+}^{ref}	Positive sequence reference of the q-axis current component
$k_{p,U_{dc}}$	Proportional gain of the PI-based direct voltage controller
$T_{i,U_{dc}}$	Time constant of the PI-based direct voltage controller
$k_{p,U_{ac}}$	Proportional gain of the PI-based AC voltage controller
$T_{i,U_{ac}}$	Time constant of the PI-based AC voltage controller
i_{q+}^{LVRT}	Positive sequence reactive current boosting during AC faults
i_{d-}^{ref}	Negative sequence reference of the d-axis current component
i_{q-}^{ref}	Negative sequence reference of the q-axis current component
f_s	Frequency of the system
I_{VSC}^{1}	Positive sequence current amplitude of the onshore converter station
I_{VSC}^{2}	Negative sequence current amplitude of the onshore converter station

Offshore HVDC converter model:

$u_{c,ref}^{d}$	d-axis positive sequence internal converter voltage of the offshore station
$u_{c,ref}^{q}$	q-axis positive sequence internal converter voltage of the offshore station
u_{fd}^{ref}	d-axis voltage reference of the offshore converter station

u_{fq}^{ref}	q-axis voltage reference of the offshore converter station
u_{fd}	d-axis filter voltage of the offshore converter station
u_{fq}	q-axis filter voltage reference of the offshore converter station
m_{abc}	q-axis filter voltage reference of the offshore converter station
i_{cd}^{ref}	d-axis current reference of the offshore converter station
i_{cq}^{ref}	q-axis current reference of the offshore converter station
i_{cd}	d-axis current of the offshore converter station
i_{cq}	q-axis current of the offshore converter station

Full converter wind turbine model:

I_{dc}	DC current of the wind turbine DC terminal
U_{dc}	DC voltage of the wind turbine DC terminal
$u_{c,abc}$	Instantaneous value of the wind turbine internal voltage
$u_{s,abc}$	Instantaneous value of the grid connection of the wind turbine
$i_{s,abc}$	Instantaneous value of the wind turbine current at grid connection point
m_{abc}	Total modulation index of the grid side inverter of the wind turbine
m_{abc+}	Positive sequence modulation index of the grid side inverter of the wind turbine
m_{abc-}	Negative sequence modulation index of the grid side inverter of the wind turbine
m_{d+}	d-axis component of the positive sequence modulation index
m_{q+}	q-axis component of the positive sequence modulation index
m_{d-}	d-axis component of the positive sequence modulation index
m_{q-}	q-axis component of the negative modulation index
u_{sd+}	d-axis component of the positive sequence grid voltage

u_{sq+}	q-axis component of the positive sequence grid voltage
u_{sd-}	d-axis component of the positive sequence grid voltage
u_{sq-}	q-axis component of the pnegative modulation grid voltage
i_{sd+}	d-axis component of the positive sequence current at the grid connection point
i_{sq+}	q-axis component of the positive sequence current at the grid connection point
i_{sd-}	d-axis component of the negative sequence current at the grid connection point
i_{sq-}	q-axis component of the negative sequence current at the grid connection point
T_i	Time constant of the PI regulator
G	Proportional gain of the PI regulator
k_1	Positive sequence reactive current boosting gain
Δi_q	Positive sequence reactive current boosting
θ	Angle of the PLL

SYMBOLS OF CHAPTER 4 AND 5

k_{wt1}	Reactive current boosting gain of the wind power plant 1
k_{wt2}	Reactive current boosting gain of the wind power plant 2
R_{wt1}	Post fault ramping rate of the wind power plant 1
R_{wt2}	Post fault ramping rate of the wind power plant 2
k_u^{LVRT}	Proportional gain at the offshore HVDC station which applies the voltage reduction
k_{acr}	Gain which enables the voltage dependent active current reduction at the wind plants

$k_{wt,f}$	Gain which enables the frequency dependent active current reduction at the wind plants
T_1	Lead block time constant
T_2	Lag block time constant
T_f	Time the fault is applied
$T_{duration}$	duration of the EMT simulation
U_{ppm}^{off}	The voltage at the offshore wind power plant terminal
U_{offsh}^{lim1}	The voltage threshold that the offshore wind power plants enters the LVRT mode
U_{offsh}^{lim2}	The voltage threshold that the offshore wind power plants enters the FRT mode

SYMBOLS OF CHAPTER 6

I_{cm}^{*}	Reference of the converter current amplitude
I_{cm}	Converter current amplitude
$I_f^{''}$	Fault current amplitude
X_c	Converter phase reactor
X_f	Reactance which simulates the fault
$Z_k^{''}$	Grid complex impedance
$U_s^{''}$	Norton equivalent grid voltage
U_f	Voltage amplitude at the fault location
δ_c	voltage angle between converter and fault location voltage

List of Figures

List of Publications

Journal Papers

1. **M. Ndreko**, J. Rueda, M. Popov, M. Mart A. M. M van der Meijden. *Optimal FRT Compliance of Offshore Wind Power Plants with VSC-HVDC Connection by Meta-heuristic Based Tuning. Electrical Power Systems Research,* 2017 April 30, 145, 99-111.

2. **M. Ndreko**, M. Popov, M. Mart A. M. M van der Meijden. *Study on FRT compliance of VSC-HVDC connected offshore wind plants during AC faults including requirements for the negative sequence current control. International Journal of Electrical Power & Energy Systems,* 2017 Feb 28, 85, 97-116..

3. A. van der Meer, **M. Ndreko**, M. Gibescu , M. A. M. M van der Meijden. *The Effect of FRT Behavior of VSC-HVDC-Connected Offshore Wind Power Plants on AC/DC System Dynamics. IEEE Transactions on Power Delivery.* Volume:31, Issue: 2, April 2016.

Conference Papers

1. A. Theologi, **M. Ndreko**, J. Rueda, M. Mart A. M. M van der Meijden, F. González-Longatt. *Optimal management of reactive power sources in far-offshore wind power plants. Proc. PowerTech, 2017 IEEE Manchester,* 2017/6/18, 1-6.

2. **M. Ndreko**, J. Rueda, M. Popov, M. Mart A. M. M van der Meijden. *Optimal FRT compliance of offshore wind power plants in VSC-HVDC connection based on genetic algorithms. Proc. Power Systems Computation Conference (PSCC), IEEE,* 2016 Jun 20 (pp. 1-7).

3. **M. Ndreko**, M. Popov, M. Mart A. M. M van der Meijden. *The effect of the offshore VSC-HVDC connected wind power plants on the unbalanced faulted behavior of AC transmission systems.*
Proc. IEEE International Energy Conference (ENERGYCON) 2016, IEEE. Apr 4 (pp. 1-6).

4. A. Hariadi, **M. Ndreko**, M. Popov, M. Mart A. M. M van der Meijden. *Investigation on different negative sequence current control options for MMC-HVDC during single line to ground AC faults. Proc. PES Innovative Smart Grid Technologies Conference Europe (ISGT-Europe), 2016 IEEE,* 2016/10/9, 1-6.

5. A. Agbemuko, **M. Ndreko**, M. Popov, M. Mart A. M. M van der Meijden. *A Knowledge-Based Approach to Voltage and Power Control in HV-MTDC Grids. Proc. PES Innovative Smart Grid Technologies Conference Europe (ISGT-Europe), 2016 IEEE,* 2016/10/9, 1-6.

6. A. van der Meer, **M. Ndreko**, J. Bos , M. Gibescu , M. A. M. M van der Meijden, W. Kling . *Stability assessment of VSC-HVDC connected large-scale offshore wind power: A North-Sea region case study. Proc. PowerTech, 2015 Eindhovel,* 2017/6/18, 1-6.

7. **M. Ndreko**, M. Popov, J. Rueda, M. Mart A. M. M van der Meijden. *Impact of offshore wind and conventional generation outages on the dynamic performance of AC-DC transmission systems. Proc. PowerTech, Eindhoven 2015, IEEE,.* Jun 29 (pp. 1-6).

8. **M. Ndreko**, A. Bucurenciu, M. Popov, M. Mart A. M. M van der Meijden. *On grid code compliance of offshore mtdc grids: modeling and analysis. Proc. PowerTech, Eindhoven 2015, IEEE,.* Jun 29 (pp. 1-6).

9. A. Bucurenciu, **M. Ndreko**, M. Popov, M. Mart A. M. M van der Meijden. *Frequency response using MTDC grids: A comparative study of common methods. Proc. PowerTech, Eindhoven 2015, IEEE,.* Jun 29 (pp. 1-6).

10. **M. Ndreko**, M. Popov, M. Mart A. M. M van der Meijden. *Short Circuit Current Contribution from MTdc Grids to the ac Power System under ac System Faulted Conditions. Proc. AC and DC Power Transmission, 11th IET International Conference.* 2015 Feb 10 (pp. 1-8). IET.

11. **M. Ndreko**, M. Popov , J. C. Boemer , M. A. M. M van der Meijden. *Sensitivity analysis on short-circuit current contribution from VSC-HVDC systems connecting far and large offshore wind power plants. Proc. Innovative Smart Grid Technologies Conference Europe (ISGT-Europe), 2014 IEEE PES.* 12-15 Oct. 2014.

12. **M. Ndreko**, A. van der Meer , M. Gibescu , B. G. Rawn , M. A. M. M van der Meijden. *Impact of DC voltage control parameters on AC/DC system dynamics under faulted conditions. Proc. IEEE PES GM, 27-31.* July. 2014 (pp. 1-5).

13. **M. Ndreko**, A. van der Meer , M. Gibescu , B. G. Rawn , M. A. M. M van der Meijden. *Damping Power System Oscillations by VSC-Based HVDC Networks: A North Sea Grid Case Study. Proc. 12th International Workshop on Large-scale Integration of Wind Power into Power Systems as well as on Transmission Networks for Offshore Wind Power Plants.* Oct. 2013 (pp. 1-5).

14. **M. Ndreko**, A. van der Meer , J. Bos , M. Gibescu , B. G. Rawn , K. PJ Jansen , M. A. M. M van der Meijden. *Transient stability analysis of an onshore power system with multi-terminal offshore VSC-HVDC transmission: A case study for the Netherlands. Proc. IEEE PES GM, 21-25.* July. 2013 (pp. 1-5).

ACKNOWLEDGEMENTS

I am grateful to a number of people who have been instrumental in getting this thesis to completion.

First of all, I need to express my special gratitude to my promotor prof. M.A.M.M van der Meijden who gave me the great opportunity to conduct my research. Mart, thank you so much for the positive attitude and the deep conversations on my research project. Thank you for supporting my dreams especially in hard times. A special gratitude goes to my daily supervisor and co-promotor, Dr. M.Popov. Marjan, thank you very much for the guidance and supervision. Thank you for encouraging my research and for allowing me to grow as a research scientist.

I would like to thank all the members of my doctoral examination committee for their effort to improve the quality of my Phd thesis. Thank you all so much for providing a valuable and highly appreciated feedback.

This thesis was developed in the context of Far and Large Offshore Wind Farm (FLOW) project and the support of TenneT TSO B.V. Special thanks to Kees Jansen and Jorrit Bos for our excellent cooperation within the FLOW project. I would to thank Dr. M. Gibescu for her supervision during the first year of my Ph.D thesis. My special thanks to Dr. C.Feltes, for the very fruitful discussions in the context of the FLOW project. I am grateful to Dr. W.Winter and all my colleagues at TenneT TSO GmbH who supported my efforts for the final completion of this thesis during the last year.

I am specially thankful to my fellow Ph.D candidates and the IEPG academic staff, for their cooperation and friendship during the last four years in Delft. First of all, my office mates, Swasti Khuntia, Bart Tuinema, and Kaikai Pan many special thanks. Mr. Swasti, thank you so much for the great time in the office. It has been my great pleasure to share the office with you my friend. Bart, I mostly admire your kindness. Kai-kai, we spent only a few months together, but still it was enough to become good mates. Hossein, I always enjoyed our discussions and share of thoughts. Thank you Gent! Matija, you were a great colleague and you are a good friend. Romain I am grateful for the relaxing moments that we shared in our free time in Delft. Arcadio, thank you for sharing your passion and ideas with me on MMC-HVDC transmission. Shahab, Ana, Nakisa, Lian, Rishabh, Arun, Claudio, Vinaj, Ilya and all the other IEPG colleagues, thank you so much for the fantastic working environment. I would like to acknowledge Dr. Jose Rueda for his support and cooperation during my research work. Specially, I would like to thank Dr. Arjen van der Meer for our nice cooperation during my years at TU Delft. Thank you also for introducing me to the HVDC world through my M.Sc project. Finally, I would like to express my gratitude to the very sweet ladies of the secretariat, Ellen, Illona and Sharmila for their daily support.

To my good friend Andreas Theocharis and his wife Theoni, many thanks for the great hospitality in Delft. I want to thank my very good friend Theodoris Tsiourakis for the nice friendship during the past years in Delft.

Special thanks to my dear Eleni, for her support and patience she showed to me all these years. I would have never managed to overcome all the hard situations and difficulties of this Ph.D thesis without you by my side. Thank you for listing my queries and for being a true friend and partner in my life. Last, but definitely not least, many thanks to my parents for their encouragement to complete this thesis. Words cannot express how grateful I am for what your have given to me.

Thank you all!
Mario Ndreko

Bayreuth, 7-11-2017

CURRICULUM VITÆ

Mario Ndreko was born in Albania in October 1985. At the age of four he moved with his family to Athens, Greece. In 2004 he received a University scholarship for his performance during the Panhellenic examinations. He received the Diploma degree in electrical and computer engineering (with M.Sc. in Electrical Power Engineering) from the National Technical University of Athens, Greece, in 2009. His thesis was on the modeling and control analysis of a direct drive permanent magnet full converter wind turbine. During his diploma studies, he performed an internship at the electromechanical service department of the Lavrion-Keratea power plant 1572MW. The assignment was related to the installation of a modern UPS system for the gas substation unit. In 2010 he moved to the Netherlands, where in 2012, he obtained the M.Sc. degree in Sustainable Energy Technology from the Delft University of Technology, Delft, the Netherlands. During his M.Sc, he ran an internship at TenneT TSO B.V. where he investigated the tuning of power system stabilizers for a real case power plant in the Netherlands. After the successful completion of his internship, he conducted his M.Sc. graduation project also within Tennet TSO B.V. on the modeling and transient stability analysis of a multi-terminal HVDC grid connected to the Dutch transmission system. In November 2012 he joined the power systems group at Delft University of technology as Ph.D candidate. His research topic was the analysis of grid connection requirements for large offshore wind power plants with voltage source converter high voltage direct current (VSC-HVDC) transmission. His research interests include power system modeling, power system control and stability and grid connection of offshore wind power plants through VSC-HVDC. He is member of the Greek Technical Chamber since 2010 and IEEE student member. Since January 2017 he works for TenneT TSO GmbH in Bayreuth, Germany, at the grid planning department as HVDC specialist. His main topics include investigation of new control schemes for future power systems running with high penetration of converter based generation units and analysis of high frequency interactions between HVDC converters and the grid. He is also involved in the Kopernikus ENSURE project in Germany and in ENTSOE working group on the topic of power system security and stability.